The Development of Chemical Probes for Detecting and Modulating NAPE-PLD Activity

By

Jonah Elliot Zarrow

Dissertation

Submitted to the Faculty of the

Graduate School of Vanderbilt University

in partial fulfillment of the requirements

for the degree of

DOCTOR OF PHILOSOPHY

in

Chemical and Physical Biology

May 12, 2023

Nashville, Tennessee

Approved:

Gary A. Sulikowski, Ph.D.

Jerod S. Denton, Ph.D.

Claus Schneider, Ph.D.

Charles R. Flynn, Ph.D.

Sean S. Davies, Ph.D.

Dedicated to the family, friends, and dogs that I love

and

To myself, for persevering.

# ACKNOWLEDGEMENTS

**TABLE OF CONTENTS**

**Page**

# LIST OF TABLES

# LIST OF FIGURES

# LIST OF ABBREVIATIONS

| Abbreviation | Definition |
|---|---|
| 95% CI | 95% confidence interval |
| *A. oryzae* | *Aspergillus oryzae* |
| ABCA1 | ATP-binding cassette subfamily A member 1. |
| ABHD4 | Alpha/beta hydrolase domain-containing protein 4 |
| AEA | Anandamide |
| ANOVA | Analysis of variance |
| ApoA1 | Apolipoprotein AI |
| ApoE | Apolipoprotein E |
| AUDA | 12-[[(tricyclo[3.3.1.13,7]dec-1-ylamino)carbonyl]amino]-dodecanoic acid |
| αvβ3 integrin | Integrin composed of integrin alpha V and integrin beta 3 |
| Bith | Bithionol; Inh2 |
| BMDM | Bone marrow-derived macrophage |
| BME | β-mercaptoethanol |
| BODIPY | 4,4-Difluoro-5,7-dimethyl-4-bora-3a,4a-diaza-*s*-indacene |
| BODIPY FL $C_5$ | 4,4-Difluoro-5,7-dimethyl-4-bora-3a,4a-diaza-*s*-indacene-3-pentanoic acid |
| BODIPY-PA | BODIPY bound to phosphatidic acid |
| BT-PSP | Benzothiazole-phenyl-sulfonamide |
| C16-NAPE | 1,2-dioleoyl-*sn*-glycero-3-phosphoethanolamine-*N*-palmitoyl |
| C17:0 NAPE | 1,2-dipalmitoyl-*sn*-glycero-3-phosphoethanolamine-*N*-heptadecanoyl |
| CAD | Coronary artery disease |
| CCR7 | C-C chemokine receptor type 7 |
| CD36 | Cluster of differentiation 36 |
| CD86 | Cluster of differentiation 86 |

- CRC          Concentration-response curve
- CXC3Cl1      Fractalkine
- Δ47          Recombinant human NAPE-PLD with the first 46 amino acids removed
- DCA          Deoxycholic acid
- DHA          Docosahexaenoic acid
- DMEM         Dulbecco's modified eagle medium
- DMSO         Dimethyl sulfoxide
- DNP          2,4-Dinitrophenyl
- DNP-NAE      DNP bound to NAE
- *E. coli*      *Escherichia coli*
- $EC_{50}$          Half-maximal effective concentration
- $E_{max}$          Maximum activity that can be induced by a compound
- EPO          Erythropoietin
- Ex/em        Excitation/emission
- FAAH         Fatty acid amide hydrolase
- Fas          *F*S-7-associated surface antigen
- flame-NAPE   fluorogenic amide NAPE analog
- Gas6         Growth arrest specific 6
- GDE          Glycerophosphodiester phosphodiesterase
- GDE1         Glycerophosphodiester phosphodiesterase 1
- GDE4         Glycerophosphodiester phosphodiesterase 4
- GDE7         Glycerophosphodiester phosphodiesterase 7
- GLP-1        Glucagon-like peptide 1
- GP-NAE       Glycerophospho-NAE
- GPR119       G protein-coupled receptor 119
- GTPase       guanosine triphosphate hydrolase
- HBSS         Hank's balanced saline solution
- HI-FBS       Heat-inactivated fetal bovine serum
- HTS          High-throughput screening

- IC$_{50}$         Half-maximal inhibitory concentration
- IC$_{95}$         95% of maximal inhibitory concentration
- ICAM-1         Intercellular adhesion molecule 1
- IL-4            Interleukin 4
- IL-6            Interleukin 6
- IL-10           Interleukin 10
- IPTG            Isopropyl β-ᴅ-1-galactopyranoside
- K$_{1/2}$         Concentration of substrate that produces a half-maximal enzyme velocity
- K$_I$           The concentration required to produce half-maximal inhibition
- K$_M$           Michaelis constant
- LC/MS           Liquid chromatography-mass spectrometry
- LC/MS/MS        Liquid chromatography with tandem mass spectrometry
- LCA             Lithocholic acid
- LEA             Linoleoylethanolamide
- LRP1            Low density lipoprotein receptor-related protein 1
- Lyso-PC         Lysophosphatidylcholine
- m/z             Mass-to-charge ratio
- MBP             Maltose-binding protein
- MD              Molecular dynamics
- MerTK           Proto-oncogene tyrosine-protein kinase MER
- MFG-E8          Milk fat globule EGF factor 8 protein
- miR-21          microRNA 21
- MTT             Methylthiazoletetrazolium
- NAE             *N*-acylethanolamine
- NAFLD           Non-alcoholic fatty liver disease
- NAPE            *N*-acylphosphatidylethanolamine
- Nape-plc        *N*-acylphosphatidylethanolamine-hydrolyzing phospholipase C
- Nape-pld        *N*-acylphosphatidylethanolamine-hydrolyzing phospholipase D. Caps when in general or human-derived. Italics for the gene.

- NASH          Non-alcoholic steatohepatitis
- Native gel    Non-denaturing polyacrylamide gel electrophoresis
- NOG           $n$-Octyl-β-D-glucopyranoside
- NOPE          1,2-dihexanoyl-$sn$-glycero-3-phosphoethanolamine-$N$-oleoyl
- NPKO          NAPE-PLD knockout
- OD            Optical density
- OEA           Oleoylethanolamide
- PA            Phosphatidic acid
- PAGE          Polyacrylamide gel electrophoresis
- PC            Phosphatidylcholine
- PE            Phosphatidylethanolamine
- PEA           Palmitoylethanolamide
- PED-amide     flame-NAPE, without the methyl substitution on the amide group
- Phospho-NAE   $O$-phosphorylated NAE
- $PLA_1$       Phospholipase $A_1$
- $PLA_2$       Phospholipase $A_2$
- PLA2G4e       Phospholipase $A_2$ group IV-e
- PLAAT         Phospholipase A/ acyltransferase; HRASLS
- PLD           Phospholipase D
- PPAR-α        Peroxisome proliferator-activated receptor alpha
- PRM           Pro-resolving mediator
- PS            Phosphatidylserine
- PTPN22        Protein tyrosine phosphatase non-receptor type 22
- RFU           Relative fluorescence units
- RNA           Ribonucleic acid
- S1P           Sphingosine-1-phosphate
- SAR           Structure-activity relationship
- SD            Standard deviation
- SDS           Sodium dodecyl sulfate
- SDS-PAGE      Sodium dodecyl sulfate-polyacrylamide gel electrophoresis

- SEA — Stearoylethanolamide
- sEH — Soluble epoxide hydrolase
- SEM — Standard error of the mean
- SHIP1 — Src homology 2 domain containing inositol polyphosphate 5-phosphatase 1
- siRNA — Small interfering RNA
- SPM — Specialized pro-resolving mediator
- SR-BI — Scavenger receptor class B type 1
- SynCore — Vanderbilt University's Molecular Design and Synthesis Center
- T2D — Type 2 diabetes
- TAM — Tyro3-Ax1-MerTK family
- TG2 — Tissue transglutaminase
- TGF-β — Transforming growth factor beta
- THL — Orlistat; tetrahydrolipstatin
- TIM — T-cell/transmembrane-immunoglobulin-mucin family
- TLC — Thin-layer chromatography
- TPPU — N-[1-(1-oxopropyl)-4-piperidinyl]-N'-[4-(trifluoromethoxy)phenyl]-urea
- Tris-HCl — Tris(hydroxymethyl)aminoethane with hydrochloric acid
- $V_{max}$ — Maximum reaction rate
- WT — Wild-type
- Z' — Z-prime factor/ score

**CHAPTER 1**


**Introduction**


**1.1 Significance**

The goal of my project was to develop novel compounds to monitor and modulate *N*-acylphosphatidylethanolamine-hydrolyzing phospholipase D (NAPE-PLD), to aid in researching and potentially treating a variety of diseases in which this enzyme appears to be important. In order to understand the motivation behind this goal, one must first understand the largescale impacts that those diseases have. While the tools developed from my research could benefit our understanding of many diseases, I will focus primarily on cardiometabolic diseases, as their linkage to NAPE-PLD is the most well-established. Cardiometabolic diseases are a cluster of diseases including obesity, hypertension, type 2 diabetes, fatty liver disease, and heart disease that typically occur together and have shared pathophysiological aspects. Namely, they are characterized by inflammatory responses to an excess of energy substrates such as glucose and fatty acids, and an accompanying dysregulation of the transport and catabolism of those substrates.


1.1.1 Obesity

Approximately 13% of adults worldwide are obese (body mass index ≥ 30),[1] and an estimated 2 billion people, including children, are overweight (body mass index ≥ 25) or obese.[2] Obesity is also increasingly common among children: 124 million children aged 5-19 are obese, and 39 million under the age of 5 are overweight or obese.[1] With so many people afflicted by this condition worldwide, it is unsurprising that the global economic burden of obesity equals about 2.2% of global annual gross domestic product, or 1.92 trillion dollars per year.[3]

Given the prevalence of obesity, many remedies have been developed, including dietary changes, nutritional supplements, surgeries, and pharmacotherapies. Some of them have been beneficial, with particular promise among the glucagon-like peptide-1 receptor agonists,[4, 5] but it is clear from the high incidence of obesity worldwide that those treatments generally ineffective. In fact, less than 1% of people who use weight loss remedies return to a clinically normal body weight without undergoing bariatric surgery.[6] And even among those who do receive bariatric surgery, there is a strong chance of the obesity returning, though researchers seldom report on it.[7]

Some of the main impacts of obesity are psychological. Obesity represents an extreme psychosocial burden for people with and without it, and that burden is aggravated by the weight cycling that so often happens as people repeatedly attempt to lose weight.[8, 9] Additionally, having obesity increases the likelihood of developing a number of diseases.[1] For adults, those conditions include cardiovascular diseases, type 2 diabetes and non-alcoholic fatty liver disease (NAFLD), musculoskeletal disorders, and some cancers.[1, 10] For children, there is an increased risk of disability in adulthood, premature death, and early markers of the diseases seen in adults.[1] NAPE-PLD appears to endogenously combat the development of obesity and several of its concomitant cardiometabolic diseases.[11]

1.1.2 Type 2 Diabetes

One of those diseases is type 2 diabetes mellitus (T2D). About 6.3% of all people alive have T2D.[12] The annual global economic burden of all forms of diabetes, with T2D comprising about 90% of all diabetes cases,[13] is around 1.3 trillion dollars.[14] T2D is the 9th leading cause of death worldwide, causing 1 million deaths per year, not accounting for the other diseases that T2D induces.[12]

T2D, much like obesity, increases the likelihood of developing a number of other conditions. Those include NAFLD,[15, 16] cardiovascular diseases,[17] eye damage, kidney diseases, tooth diseases, neuropathy, delayed wound healing, skin problems, and hearing impairment.[13, 18-20] T2D itself, however, is quite mild at its onset, and often its

symptoms are not noticed until years after the disease has started.[13, 20] However, when the disease is allowed to progress untreated, its symptoms worsen and its concomitant diseases begin to arise.[13, 20] Fortunately, combinations of medications and lifestyle changes can, and often do, allow individuals to live normally.[20, 21] However, some patients' T2D still worsens even with medications.[22, 23] And due to socioeconomic health disparities, many patients are unable to access those resources, so their T2D worsens as well.[24]

1.1.3 Non-Alcoholic Fatty Liver Disease

NAFLD is a disease that is strongly associated with diabetes, obesity, and many other cardiometabolic diseases.[16] It affects some 30% of adults worldwide,[15, 25] and has been increasing in prevalence since 2005.[26] It causes a significant economic burden and decreases the quality of life for millions of people each year.[16] Like T2D, the progression of NAFLD is insidious. Initially, NAFLD symptoms are subtle and frequently go undetected.[10, 16, 27] Even when NAFLD is suspected, a liver biopsy is needed in order to conclusively diagnose it, which is a significant impediment for many people.[10, 27, 28] Eventually, the condition worsens and develops into one of the more severe stages of fatty liver disease, such as non-alcoholic steatohepatitis (NASH).[10, 27] This often leads to the development of particularly harmful phenotypes such as cirrhosis and hepatocellular carcinoma.[10, 27] And these more severe forms of NAFLD are common—about 20% of people with NAFLD will develop NASH.[16]

The mortality of NAFLD depends strongly on the stage of NAFLD in question: patients with cirrhosis or cancer more often die from those conditions, while those with only mild symptoms succumb to the cardiovascular diseases that typically accompany NAFLD.[16] Interventions, similarly, take two general routes. During the early stages of NAFLD, cases can be managed with lifestyle changes and medications.[16, 28, 29] Once the disease has progressed to a more severe stage, however, more extreme measures such as chemotherapy and liver transplantation are needed. This has made NASH the second most common reason for liver transplantation worldwide.[10] With liver donor-patient matches taking up to 5 years to find, patients with cirrhotic NASH can often die

before their surgeries.[30] Unfortunately, even with liver transplantation, NAFLD recurrence is common because there are so many other diseases, particularly cardiometabolic, that can contribute to the development of NAFLD.[27, 31]


1.1.4 Ischemic Stroke

Strokes are an incredibly common complication of cardiometabolic diseases. 1 in 4 adults will have a stroke in their lifetime, which amounts to 12.2 million strokes per year worldwide, or one stroke every 3 seconds.[32] Of those, approximately 80% are ischemic strokes, which arise from loss of blood flow to the brain, typically due to atherosclerosis.[14, 33] Strokes are the 2nd leading cause of death worldwide, and ischemic strokes alone account for some 3.3 million deaths globally per year.[32] Strokes also lead to debilitating complications such as paralysis, cognitive impairment, speech problems, emotional dysregulation, neuropathy, chronic idiopathic pain, motor control problems, and depression.[34] As a result, 63 million years of healthy life are lost each year due to ischemic stroke-related death and disability.[32] Unsurprisingly, this has made the total estimated worldwide cost of strokes fall between 450 and 700 billion dollars per year.[32, 35]

Currently, the only way to prevent this debilitating and prolific condition is to reduce one's risk factors.[34, 36] However, those risk factors are abundant and include common conditions such as heart disease, obesity, diabetes, atrial fibrillation, high blood pressure, high cholesterol, and lack of exercise.[34, 36] Fortunately, the complications of ischemic strokes can be reduced or eliminated by the timely administration of life-saving medications or surgeries. However, one has to receive intravenous thrombolytic medication within about 4 hours from the onset of an ischemic stroke in order for it to be effective.[34] Because strokes can go unnoticed at their onset and because many people lack access to intervention therapies, only 5% of ischemic stroke patients receive medical interventions in time and less than 1% receive mechanical thrombectomies in time.[33, 34] If the stroke proves to be non-fatal, unfortunately the outlook is still poor. 1 in 4 stroke survivors will have another stroke within 5 years, and there are currently about 101 million people worldwide who have

experienced a stroke and survived.[34, 35] On top of that, the recovery process is extremely difficult, expensive, and is not guaranteed to succeed.[36] As such, any research directed towards understanding or possibly reducing the prevalence of this devastating condition is of paramount importance.

1.1.5 Coronary Artery Disease

Cardiovascular disease causes even more deaths worldwide than strokes. There are many types of cardiovascular disease, but the one on which we focus is the most prevalent among them: coronary artery disease (CAD). CAD is also referred to as ischemic heart disease, coronary heart disease, atherosclerotic cardiovascular disease, and heart disease. CAD is the number one cause of death, disability, and years of healthy life lost in the world, and has been since 1990.[37] It affects about 1.72% of the world's population and has an associated financial burden of nearly a trillion dollars.[37]

A major reason for the prevalence of CAD is that only 2-7% of the world's population has no CAD risk factors.[37] Compounding the issue, more than 70% of people who have at least one risk factor for CAD have additional risk factors.[37] Importantly, those risk factors include cardiometabolic diseases, making CAD quite common among those with cardiometabolic disease.[38] Furthermore, not all of CAD's risk factors have effective treatments, and the accumulation of side-effects from those treatments can negate their benefits.[39]

Being the leading cause of death worldwide, CAD has many therapies specifically designed to prevent and treat it. Current treatments include statins, antiplatelet agents, vascular growth factors, and surgeries.[40] Despite clear reductions in mortality gained from CAD treatments, its overall mortality remains high and is expected to increase in the future.[37, 39]

**1.2 Atherosclerosis**

CAD and ischemic strokes share a primary underlying cause: atherosclerosis.[41-

[46] As those conditions are the top two causes of death worldwide, it is important to understand, and ideally prevent, their shared pathophysiology.

1.2.1 Biochemistry of Atherosclerosis

Atherosclerosis begins when modified lipoproteins accumulate in the subendothelial layer of arteries.[45-47] This is failure point number one, and it is the target of cholesterol-reducing drugs like the statins, as well as diet and exercise. Lipoprotein accumulation causes endothelial cell dysfunction, which causes the release of an inflammatory stimulus, which recruits leukocytes (particularly monocytes) into the arterial wall.[44-49] These subendothelial monocytes then differentiate into macrophages and internalize the cholesterol-laden lipoproteins, transforming the macrophages into dysfunctional foam cells.[44-46, 48, 49] Foam cells secrete chemical factors that promote the formation of more foam cells and cytokines that recruit additional immune cells to the area.[44, 46, 49] Eventually, the foam and immune cells die, often by apoptosis.[46, 47, 49] If these apoptotic cells are efficiently cleared by functional macrophages, in a process called efferocytosis, no further inflammation and damage occurs.[46, 47, 50] However, the ongoing accumulation of modified lipoproteins, reactive oxygen species, and inflammatory cytokines within the subendothelial space appears to dramatically impair the ability of macrophages to perform efferocytosis.[45-48, 51, 52] This is failure point number two, which our research aims to combat.

Without effective efferocytosis to clear them, apoptotic foam and immune cells undergo secondary necrosis, rupture, and trigger a strong inflammatory response.[46, 47, 51, 52] This response is characterized by the recruitment of additional immune cells, further impairment of efferocytosis, increased apoptosis, and buildup of necrotic cells into a "necrotic core" at the center of the lesion.[45-47, 49, 51, 52]  Next, vascular smooth muscle cells migrate to the lesion and form a collagen-rich fibrous cap between the lesion and the arterial lumen.[49, 51] This, again, keeps the plaque stable for a time.[49, 51, 53] However, the smooth muscle cells eventually succumb to the strongly inflammatory environment of the necrotic core—often becoming foam cells before they do so—and undergo apoptosis and secondary necrosis while the stabilizing collagen is degraded.[49,

[51, 53] This is failure point number three, which is difficult to prevent due to the strength and recursiveness of the inflammatory signals within the plaque.

At this point, the necrotic core is large and unstable, which is a pathological hallmark of advanced atherosclerosis.[45-47, 51] Furthermore, the only barrier between the growing plaque and the arterial lumen is a thin layer of endothelial cells undergoing continual damage from the inflammatory necrotic core.[51] Eventually, this barrier breaches and the plaque ruptures.[46, 51] Circulating clotting factors, fulfilling their duty to prevent blood loss, form a thrombus to cover the breach in the arterial wall.[46, 49, 51] However, due to the already large size of the plaque, addition of a thrombus occludes the arterial lumen, resulting in tissue hypoxia and damage.[46, 49, 51] This is failure point number four, and it is currently targeted by antiplatelet agents (to stop thrombosis), stents, bypass surgeries, and vascular growth factors (to bypass the blocked artery).[40] Due to their small size, arteries that supply the heart and the brain are more likely to become occluded by atherothrombosis, which causes myocardial infarction and strokes, respectively.[45-47, 49, 51]

## 1.2.2 Rescuing Efferocytosis

The impairment of efferocytosis is a key failure point in the progression of atherosclerosis. To find a way to prevent that failure, researchers have been interested in identifying and modulating biochemicals that endogenously enhance efferocytosis.

### 1.2.2.1 Pro-Resolving Mediators

Pro-resolving mediators (PRMs) include any protein or biochemical that promotes efferocytosis, healing, the resolution of inflammation, and/or macrophage M2 polarization. Many PRMs are factors that are directly involved in the performance of efferocytosis. On the macrophage side, those factors include MerTK, TAMs, TIMs, SR-BI, LRP1, Gas6, MFG-E8, TG2, $\alpha v \beta 3$ integrin, miR-21, ApoE, EPO, Rho-family GTPases, and CD36.[45-47, 50, 54-56] On the apoptotic cell side, those factors include PS, calreticulin, CX3CL1, Fas, Fas ligad, S1P, lyso-PC, and ICAM-1.[45-47, 50, 54, 56] Additionally, several PRMs have been shown to be pro-resolving by activating key

signaling cascades. These PRMs include IL-10, TGF-β, IL-4, IL-6, CD86, CCR7, ApoA1, and ABCA1 (acronyms from this paragraph are defined in the Abbreviations List on page xiv).[45-47, 50, 54, 56, 57]

*1.2.2.2 Lipid-Derived PRMs*

Within the class of PRMs, there is a sub-class of specialized pro-resolving mediators (SPMs). SPMs are signaling lipids derived from docosahexaenoic acid (DHA) and eicosapentaenoic acid (EPA),[58, 59] that have been proposed to exert pro-resolving effects including anti-inflammatory and pro-efferocytotic signaling in macrophages.[46, 58, 59] These findings remain highly controversial, as a consortium of researchers investigating SPMs found that they are synthesized at low levels, that their proposed receptors are not validated, and that their levels do not change as expected.[60] Furthermore, the researchers demonstrated that the most commonly used method for measuring SPMs cannot reliably quantify their levels.[60] Therefore, the benefits of SPMs to efferocytosis and the resolution of inflammation remain unclear. However, recent studies suggest that another family of signaling lipids may be important in regulating efferocytosis: *N*-acylethanolamines.

1.2.3 NAEs in Atherosclerosis

Recently, *N*-acylethanolamines (NAEs) have been identified as pro-efferocytosis, pro-resolving regulators of atherosclerosis.[53, 61] When bone marrow-derived macrophages (BMDMs) are polarized to the pro-resolving M2c phenotype, levels of the NAE palmitoylethanolamide (PEA) are increased, but they are decreased when the cells are polarized to the pro-inflammatory M1 phenotype.[53] Administering a different NAE, oleoylethanolamide (OEA), directly increased M1-to-M2 polarization.[61] Matching its effects on macrophage polarization, NAE administration to macrophages increased expression of efferocytosis effectors like MerTK and SR-BI, and enhanced both phagocytosis and efferocytosis by macrophages of all polarization states (though more strongly M2c).[53, 61]

As expected, NAE's ability to increase efferocytosis results in improved outcomes in atherosclerosis. NAE administration reduced plaque size and macrophage accumulation in early atherosclerotic lesions,[53] and in established lesions it increased plaque stability, decreased M1 and increased M2 polarization, reduced macrophage accumulation, decreased necrotic core size, and decreased the amount of apoptosis in the plaques.[53, 61] Based on these findings, it is logical to conclude that a treatment that increases NAE production would combat atherosclerosis via increased macrophage efferocytosis capacity.

## 1.2.4 NAPE-PLD in Atherosclerosis

The primary biosynthetic enzyme for NAEs is *N*-acylphosphatidylethanolamine-hydrolyzing phospholipase D (NAPE-PLD).[11, 62-64] Logically, if the products of NAPE-PLD are involved in increasing efferocytosis and hindering atherosclerosis, then NAPE-PLD itself is involved as well. And, indeed, initial evidence supports this notion. In cultured macrophages, M1 polarization caused a reduction in *Napepld* expression, matching the changes in NAE levels.[53] As atherosclerosis developed in mouse models of the disease, *Napepld* expression was progressively downregulated.[53] Even in humans, *NAPEPLD* expression was shown to be reduced in atherosclerotic plaques, particularly in unstable plaques, and specifically the macrophages within in those plaques expressed less *NAPEPLD*.[53] Conversely, increasing the levels of *N*-acylphosphatidylethanolamine (NAPE)—which NAPE-PLD hydrolyzes to create NAE—in mice with atherosclerosis reduced atherosclerotic lesion necrosis.[65] And, in unpublished experiments (described in Chapter 5), we have seen that BMDMs from *Napepld*^{-/-} mice efferocytose less. Based on this information, we hypothesized that by modulating NAPE-PLD, one could adjust NAE levels, which would change macrophage efferocytosis capacity, which would alter the progression of atherosclerosis.

**1.3 NAPE-PLD**

Based on the above information, investigations into NAPE-PLD's role in regulating efferocytosis and combatting atherosclerosis are warranted. Before addressing NAPE-PLD's many other biological roles, however, fundamental information about this enzyme should be detailed.

1.3.1 NAPE-PLD Fundamental Information

NAPE-PLD is a member of the zinc metallo β-lactamase family, class B.[66, 67] It is a membrane-bound protein, and it exists as a homodimer.[66-69] NAPE-PLD orthologs are found in mammals, fish, invertebrates, and yeast, suggesting highly conserved functions in normal physiology.[62, 70-72] The enzyme is expressed in a variety of tissues throughout the body, suggesting that it has significant physiological roles.[62, 67, 70, 71] NAPE-PLD's biochemical role is to hydrolyze NAPE into NAE and phosphatidic acid (PA), and unlike other PLDs, it cannot hydrolyze phosphatidylethanolamine (PE) or phosphatidylcholine (PC).[67, 70] Thanks to the elucidation of NAPE-PLD's structure using X-ray crystallography, the mechanism with which it hydrolyzes NAPEs has been predicted.

1.3.2 NAPE-PLD Catalysis

A likely catalytic mechanism for NAPE-PLD has been proposed based on its crystal structure,[68] and it has been represented graphically below (Figure 1). Seven residues coordinate the two catalytic $Zn^{2+}$ ions, which in turn interact with a free hydroxide ion and the oxygens of NAPE's phosphate group. At least three oxygens on the NAPE hydrogen bond with other residues of the enzyme to ensure substrate binding and, likely, selectivity. The zinc-stabilized hydroxide ion, possibly assisted by D189, performs a nucleophilic attack on the phosphorus. This dislodges the ethanolamine oxygen, which likely forms a stabilizing hydrogen bridge with H321. The glycerophospho oxygen is less likely to receive those electrons as it lacks a hydrogen bond/bridge donor. Throughout this transition state, the substrate is stabilized by its bonds to the

catalytic zincs and the coordinating side chains. Then, the two products—PA and NAE—leave the enzyme active site, though the mechanism for this release is not known. Meanwhile, a proton is abstracted from a free water molecule by either the NAE product or H321, creating a new hydroxide ion for the zinc ions to coordinate. Thus, NAPE-PLD converts one multifunctional molecule (NAPE) into two signalling molecules (NAE and PA).
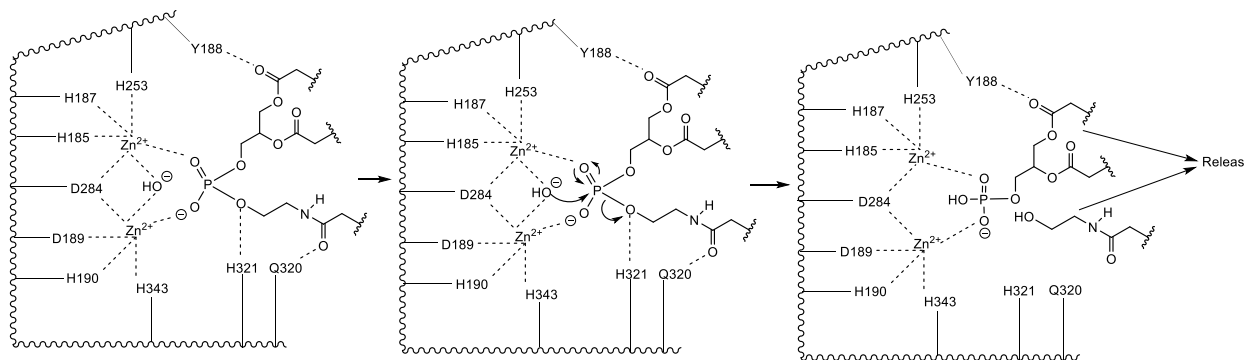


**Figure 1.** NAPE-PLD catalytic mechanism. Key active site residues (listed by amino acid and position in protein sequence) of NAPE-PLD (represented by wavy line) are shown bound to the catalytic zinc ions and to the NAPE substrate. Proposed mechanism is shown, with eventual release of PA and NAE products. This figure illustrates the findings of a previously published work (Magotti et al., 2015).

## 1.4 NAPE-PLD Substrates and Products

NAPE-PLD, by degrading NAPEs and creating NAEs and PAs, has many functions throughout the body. Due to the nature of NAPE-PLD's substrates and products, those functions include the biochemical regulation of several diseases.

### 1.4.1 Roles in Diseases

NAPE-PLD, NAEs, and particularly NAPEs play protective and healing roles in cells in response to cellular damage, stress, tissue degeneration, infection, and injury.[69, 70, 73-75] Due to their promotion of cell growth and proliferation,[73, 74, 76, 77] NAPE-PLD and its products are upregulated in some cancer cells,[76, 78, 79] though they are downregulated in others.[74, 80] As mentioned previously, macrophages express less NAPE-PLD and

produce less NAE when exposed to infection or inflammatory stimuli.[53, 73] And in inflammatory diseases such as colitis,[73, 81-83] celiac disease,[84] diabetic retinopathy,[62, 85] allergic reactions,[53, 86] and arthritis,[73] NAPE-PLD and NAEs appear to have protective, anti-inflammatory effects. Certain NAEs have also been shown to have analgesic effects, particularly in cases of chronic pain.[73, 86-89] Additionally, NAPE-PLD and NAEs are known to promote male and female fertility,[66, 74, 90-92] and are decreased in the tissues of miscarried placentae.[93, 94] Though, the roles of NAPE-PLD, NAPEs and NAEs have been best characterized in cardiometabolic diseases.

1.4.2 Roles in Cardiometabolic Diseases

*1.4.2.1 Obesity: Food Intake*

The actions of NAPE-PLD and NAEs combat obesity via two mechanisms: reducing food intake and decreasing adipogenesis.

Within the small intestine, NAPEs exert hypophagic effects that are mediated by their resultant NAEs.[95-98] In response to the ingestion of dietary fats, more NAPEs are synthesized in the small intestine.[87, 98-100] NAPE-PLD is also more active in the small intestine in response to food intake, converting those NAPEs into NAEs.[89, 99, 101] Those NAEs include OEA, PEA, SEA, and LEA. OEA induces satiety primarily by activating vagal afferent neurons in the proximal small intestine via peroxisome proliferator-activated receptor alpha (PPAR-α) activation, which then activate neurons in key regions of the brain to inhibit food intake.[89, 99, 102-109] PEA also decreases food intake, possibly by the same mechanism as OEA.[86, 105, 107] SEA (stearoylethanolamide) and LEA (linoleoylethanolamide) also seem to decrease food intake, though less strongly than either OEA or PEA, and their mechanisms are not yet established.[74, 87, 88, 99, 100, 109]

This overall mechanistic pathway and the role that it has in obesity have been confirmed by experimental interventions. The small intestines of fasted animals produce less NAPE,[74] have decreased Nape-pld activity,[89, 99, 101] and produce less NAE.[74, 100, 102, 104, 107] Animals that have been fed high-fat or high-sugar diets for as little as one week show reduced resting levels of NAEs in the small intestine, abrogated release of NAEs

12

in response to food intake, and reduced small intestinal Nape-pld expression.[88, 100, 110] When the feeding model is allowed to progress to diet-induced obesity, postprandial NAPE secretion in the small intestine is lost,[98, 100] resting NAE levels are decreased,[11, 99, 100] and NAEs are not produced in response to food intake.[11, 87, 100] When administered to the small intestines of lean animals, NAPEs, Nape-pld, and NAEs protect against diet-induced obesity,[87, 96-98, 103-105] while knockout of *Napepld* induces obesity.[11] When administered to obese animals, NAPE and NAE reduce food intake and body weight, and for NAPE, that effect is dependent upon Nape-pld activity.[96-98, 102, 104, 107, 111]

When taken together, these findings make it clear that small intestinal NAPE-PLD activity decreases food intake, and that its failure can cause obesity. Therefore, by modulating NAPE-PLD activity, one can externally regulate both food intake and obesity.

*1.4.2.2 Obesity: Adipogenesis*

The second mechanism by which NAPE-PLD combats obesity is by reducing adipogenesis.

Normal adipose tissue produces NAEs.[112] However, the adipose tissue of obese and high-fat-eating animals gain mass, lose NAE synthesis, and have reduced fatty acid metabolism gene expressions, all of which are partially a result of decreased Nape-pld activity.[11, 65, 89, 96, 97, 104, 112, 113] Conversely, when NAEs are administered to animals on a high-fat diet, they gain less weight primarily due to reduced gain in adipose mass.[65, 88, 96, 103, 104, 112]

In concurrence with this apparent role of NAPE-PLD, small intestinal and adipose-specific knockouts of *Napepld* both cause increased fat gain, decreased lipid catabolism, decreased basal metabolic rate, and obesity.[11, 112] Confirming the importance of NAPE-PLD in this process, when NAEs, but not NAPEs, are administered to mice with whole-body *Napepld* knockouts, those phenotypes are rescued.[96]

So, by both reducing food intake and increasing adipose lipid metabolism, NAPE-PLD combats obesity.

## 1.4.2.3 Non-Alcoholic Fatty Liver Disease

NAPE-PLD and NAEs play a role in regulating NAFLD, as well. Even though NAPE-PLD is not highly expressed in the liver,[63, 70, 96] it is thought that NAEs synthesized in the small intestine travel to the liver to exert protective effects.[65, 97, 108] Supporting this, knockout of *Napepld* in the small intestine causes hepatic steatosis.[11] Within the liver, NAEs reduce fat accumulation and inflammation, both before and after the onset of NAFLD.[65, 88, 89, 96, 97, 103, 113, 114] Therefore, compounds that increase NAE biosynthesis in the small intestine could protect against NAFLD.

## 1.4.2.4 Inflammation

Cardiometabolic diseases lead to chronic inflammation in a variety of tissues, which seems to be mediated by altered NAPE-PLD activity, NAE levels, and PPAR-α activity.[11, 73, 96, 100, 112, 113, 115] PEA acts as an endogenous anti-inflammatory agent by activating PPAR-α and possibly by other mechanisms.[11, 73, 86, 87, 104, 112, 116] OEA and SEA may be anti-inflammatory as well.[11, 73, 86, 87, 100, 104, 113, 116] NAPE-PLD activity itself is anti-inflammatory within adipose tissue,[96, 112] and the enzyme hydrolyzes pro-inflammatory phosphatidylethanolamine-modified isolevuglandins.[117] Based on the existing research, it seems that modulating NAE biosynthesis could be an effective means of researching and treating inflammation.

## 1.4.2.5 Type 2 Diabetes

NAPE-PLD, via its creation of NAEs, has multiple roles in protecting against the pathophysiology of T2D. OEA and possibly PEA activate G protein-coupled receptor 119 (GPR119) in small intestinal L-cells,[62, 88, 89, 95, 101, 118, 119] which causes the release of active forms of glucagon-like peptide 1 (GLP-1),[11, 62, 95, 101, 105, 118, 119] which plays a critical role in maintaining normal glycemic levels in response to food intake.[11, 88, 89, 95, 99, 100, 120] There is also evidence to show that the OEA produced in response to food/fat intake binds to newly-made GLP-1, travels with it to other tissues, and makes the receptor of GLP-1 more sensitive to the GLP-1.[100, 120] And, increasing GLP-1 levels, administering GLP-1 analogs, and increasing receptor sensitivity to GLP-1 are all

thought to be protective against T2D.[95, 100, 120] Together, these results suggest that NAPE-PLD's biosynthesis of NAEs protects against the development of T2D.

In people with diabetes, wound healing is impaired due to an abundance of bacterial biofilms and chronic inflammation.[121, 122] One of the reasons for the chronic inflammation in diabetic wounds is that the resident macrophages become dysregulated. They remain in the pro-inflammatory M1 polarization state in the absence of infection and have an impaired ability to perform efferocytosis,[56, 122, 123] thereby contributing to the inflammatory state and preventing healing. As discussed in section 1.2, NAPE-PLD activity appears to polarize macrophages to a pro-healing M2 state and to enhance efferocytosis, both of which help in wound healing.[122, 123] Therefore, activators of NAPE-PLD might be used to improve wound healing in diabetics.

## 1.5 Scope of the Dissertation

Based on all of the above information, we predicted that modulating NAPE-PLD activity could be an effective means of both studying and treating cardiometabolic diseases, particularly due to the enzyme's role in regulating efferocytosis. However, no NAPE-PLD activators and only a few potent NAPE-PLD inhibitors existed.[124-126]

### 1.5.1 Hypotheses and Goals

The primary goal of my project was to discover novel modulators of NAPE-PLD that could be used as research tools to determine the effect of NAPE-PLD modulation on efferocytosis, and that had the potential to be developed into therapeutics. We hypothesized that inhibiting NAPE-PLD activity or expression would decrease efferocytosis, and that activating NAPE-PLD would increase efferocytosis. Due to the potential health benefits of NAPE-PLD activators and the fact that any NAPE-PLD activator would be the first of its kind, we focused our efforts more heavily on activators.

This primary goal was accomplished in four steps. The first was identifying potential NAPE-PLD modulators by high-throughput screening. The second was

15

validating and characterizing the activities of those modulators. The third was developing a selective NAPE-PLD activity assay that worked in live cells. The fourth was demonstrating the modulators' ability to modulate NAPE-PLD activity in living cells safely and effectively, so that they could be used to test the hypothesis that NAPE-PLD activity regulates efferocytosis.

## 1.5.2 Experimental Overview

The experiments that we performed in order to accomplish those goals are summarized below. They have been separated into sub-sections, matching their chapters in the text of this dissertation.

### 1.5.2.1 Chapter 2: NAPE-PLD Modulator Identification

First, we performed experiments geared towards discovering novel NAPE-PLD modulators. This started with a pilot study to establish the methods that would be used. Then, I further optimized the modulator screening assay, which was performed cell-free using purified protein ("*in vitro*"). Next, I performed a high-throughput screening on nearly 40,000 molecules. I then performed a limited structure-activity relationship study around a selection of the hits to find the most promising modulator candidates. Finally, I determined the potency and efficacy of the members of our best class of candidate activators. By the conclusion of these experiments, we had identified a novel class of potent and efficacious NAPE-PLD activators.

### 1.5.2.2 Chapter 3: Compound Characterization

Next, we performed initial characterizations of our newfound NAPE-PLD activators. First, I validated their activation of NAPE-PLD. Next, we performed assays to characterize their mechanism of action. Finally, I assessed their selectivity for NAPE-PLD. By the conclusion of these experiments, we had validated that our newly discovered compounds were positive allosteric modulators of NAPE-PLD, and that they did so with an acceptable degree of selectivity.

*1.5.2.3 Chapter 4: Development of Flame-NAPE, a Selective Probe for Measurement of NAPE-PLD Activity*

Then, lacking a selective method for measuring NAPE-PLD in live cells, we synthesized a new, PLD-selective fluorogenic activity probe molecule and used it to develop an in-cell NAPE-PLD activity assay. To do this, we first synthesized the probe molecule, measured its fluorescence properties, and characterized its hydrolysis by Nape-pld. Next, we determined the selectivity of the probe molecule for hydrolysis by Nape-pld, both *in vitro* and in cells. Finally, I demonstrated the viability of this novel NAPE-PLD activity assay in four different cell types. By the conclusion of these experiments, we had developed a fluorescence-based method for selectively measuring PLD activity in cells, significantly improving upon existing assay methods.

*1.5.2.4 Chapter 5: Effects of NAPE-PLD Activators in Cells*

Finally, we utilized what we had discovered in the previous studies to determine whether the NAPE-PLD activators were safe and effective in cells, and to determine the effects of NAPE-PLD activity modulation on macrophage efferocytosis capacity. To do this, I first determined the cytotoxicity of the compounds in two types of cells. Then, I assessed how well they altered NAPE-PLD activity in those cells. Next, I validated their ability to activate NAPE-PLD. Lastly, we tested the hypothesis that pharmacological NAPE-PLD modulation is an effective means of regulating macrophage performance of efferocytosis. By the conclusion of these experiments, we had demonstrated that our novel NAPE-PLD activators had strong potential for use in research and *in vivo* settings, and that they could be used to enhance efferocytosis pharmacologically.

# CHAPTER 2

## NAPE-PLD Modulator Identification

Sections 2.1 and 2.7 include text from Symmetrically Substituted Dichlorophenes Inhibit *N*-acyl-phosphatidylethanolamine Phospholipase D that has been adapted to clarify individual contributions and have been reproduced with the permission of the publisher.[126] This research was originally published in the Journal of Biological Chemistry. Geetika Aggarwal, Jonah Zarrow, Zahra Mashhadi, C. Robb Flynn, Paige Vinson, C. David Weaver, and Sean S. Davies. Symmetrically Substituted Dichlorophenes Inhibit *N*-acyl-phosphatidylethanolamine Phospholipase D. J Biol Chem. 2020; 295(21):7289-7300. © the Authors. Author contributions: GA, CRF, PV, CDW, and SSD conceptualization; GA, PV, and SSD data curation; GA, JEZ, PV, and SSD formal analysis; GA, JEZ, and ZM investigation; GA, PV, CDW, and SSD methodology; GA, JEZ, and SSD writing—original draft; JEZ, CRF, PV, CDW, and SSD writing—review and editing; CRF and CDW resources; PV and SSD supervision and project administration; CDW software; SSD funding acquisition.

Sections 2.2-2.7 are adapted from Small Molecule Activation of NAPE-PLD Enhances Efferocytosis by Macrophages, published in bioRxiv, and has been reproduced with the permission of the publisher.[127] Authors: Jonah E. Zarrow, Abdul-Musawwir Alli-Oluwafuyi, Cristina M. Youwakim, Kwangho Kim, Andrew N. Jenkins, Isabelle C. Suero, Margaret R. Jones, Zahra Mashhadi, Kenneth P. Mackie, Alex G. Waterson, Amanda C. Doran, Gary A. Sulikowski, and Sean S. Davies. Author contributions: JEZ performed the majority of experiments, he also analyzed data, created figures, interpreted results, and assisted in writing of the initial manuscript. KK contributed to design of analogs. MAJ synthesized BT-PSP analogs. ZM assisted with conception of the project, and purification of enzyme. AGW contributed to molecular design and edited the manuscript. ACD assisted in conception of the project and assisted in writing the initial manuscript. GAS assisted with the conception of the project, molecular design of activator analogs, supervised the synthesis and characterization of compounds, provided guidance on the project, obtained financial

support, and edited the manuscript. SSD conceived and guided the overall project, supervised various studies, obtained financial support, oversaw interpretation of the data, created figures, and wrote the manuscript.

## 2.1 Pilot Study

In order to identify potential small-molecule modulators of NAPE-PLD, we first needed to clear three hurdles. The first was developing a rapid and reliable method for measuring NAPE-PLD activity. The second was using that assay to develop and test a high-throughput screening (HTS) methodology that could be used for a large-scale screening. And the third was demonstrating that each of the planned screening, characterization, and validation methodologies could work for our purposes. In order to accomplish this, Dr. Geetika Aggarwal led a pilot study in which we developed a NAPE-PLD activity assay, screened a small library of compounds for NAPE-PLD modulators, and performed appropriate follow-up tests on the hit compounds.[126] This pilot study was essential to the larger screening project because it established the methods that would be used and it demonstrated that the larger project was feasible.

### 2.1.1 PED-A1 Assay Development

An optimal HTS assay requires high reproducibility and sufficient dynamic range to reliably detect both activators and inhibitors. Fluorogenic substrates had been previously used successfully in high-throughput screenings for modulators of lipase activity,[128, 129] as well as NAPE-PLD.[124, 125] PED-A1 is a quenched fluorogenic NAPE analog that has previously been used to measure phospholipase $A_1$ (PLA$_1$) activity *in vitro* and in tissue samples,[130] and could theoretically serve as a substrate for NAPE-PLD.

To test if PED-A1 could be used as a substrate for NAPE-PLD, Dr. Aggarwal incubated PED-A1 with purified recombinant mouse Nape-pld and measured the appearance of fluorescence, adapting an existing NAPE-PLD activity assay.[124]

Incubation of active Nape-pld with PED-A1 resulted in a rapid rise in fluorescence, while incubation with Nape-pld that had been inactivated by boiling did not (Figure 2 A). The Michaelis constant ($K_M$) of recombinant mouse Nape-pld for PED-A1 (3±0.5 µM) was then determined by varying the concentration of PED-A1 incubated with 0.1 µM Nape-pld (Figure 2 B). Later experiments (Chapter 4) revealed a more accurate $K_M$ of 4.0±0.5 µM.
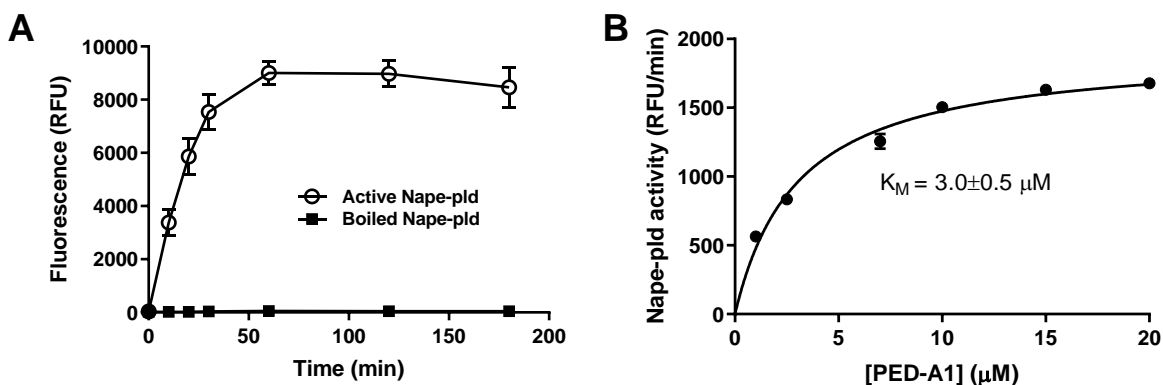


**Figure 2.** PED-A1 is a fluorogenic Nape-pld substrate. **A.** Incubation of PED-A1 with active recombinant mouse Nape-pld (open circles) resulted in rapid generation of fluorescence, while incubation with boiled Nape-pld (closed squares) did not. Data shown as mean ± standard error of the mean (SEM), n = 6 technical replicates. **B.** Recombinant Nape-pld (1 µM) was incubated with 0-20 µM PED-A1 and fluorescence (ex/em 488/535 nm) was measured to calculate Michaelis constant ($K_M$). Data shown as mean ± SEM, n = 9 technical replicates. Non-linear fit determined using Michaelis-Menten equation in GraphPad Prism 7.04

To ensure that this new assay could tolerate small variations in buffer composition, she then determined the concentration ranges of Nape-pld, N-octyl-β-D-glucoside (NOG, used to stabilize Nape-pld) and dimethyl sulfoxide (DMSO, vehicle component for PED-A1 and for screening compounds) where Nape-pld activity did not differ by more than 10% from its maximal activity. For NOG, this was 0.2–0.6% (w/v) and for DMSO this was 1.0–3.7% (v/v) (Figure 3). Based on these results, a final concentration of 0.1 µM Nape-pld, 0.4% NOG (w/v), and 1.6% DMSO (v/v) was used in all subsequent assays of the pilot study.
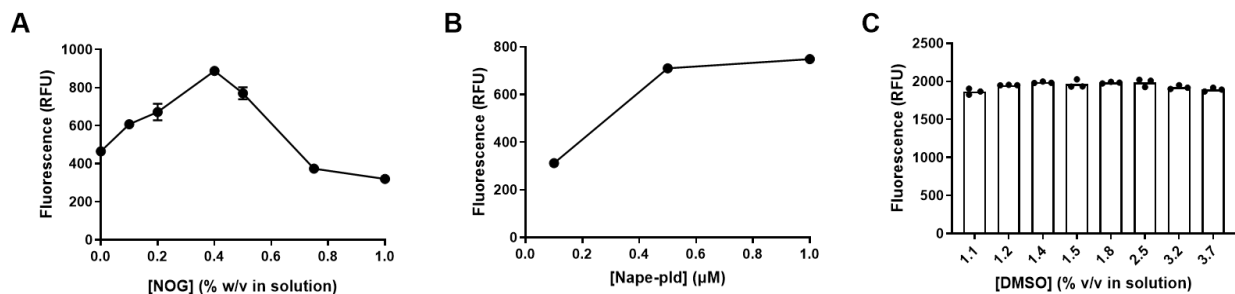
**Figure 3.** Assay component optimization. **A.** Optimization of NOG concentration. Enzyme at 0.5 µM, PED-A1 at 4 µM, DMSO at 1.14% (v/v). Points are mean ± SEM from two replicate experiments. **B.** Optimization of enzyme concentration. PED-A1 at 4 µM, DMSO at 1.14% (v/v), NOG at 0.4% (w/v). Points are mean ± SEM from two replicate experiments. **C.** Optimization of DMSO concentration. Enzyme at 0.15 µM, PED-A1 at 4 µM, NOG at 0.4% (w/v). Individual points from one experiment shown.

To assess the assay's ability to reproducibly distinguish between normal and inhibited signals across replicate wells in a 384-well plate (typically used for HTS), Dr. Aggarwal added 100 µM lithocholic acid (LCA) or vehicle in checkerboard fashion to a 384-well plate, and then determined initial rate of fluorescence change (t = 30-100 s) and steady state fluorescence (t = 419-420 s) (Figure 4). The calculated Z' (0.45-0.47) (used to quantify HTS assay quality) demonstrated that the signal windows were sufficiently separated to observe hits in the screen, regardless of plate position.[131] Therefore, we concluded that the PED-A1 assay was ready to be used in HTS.
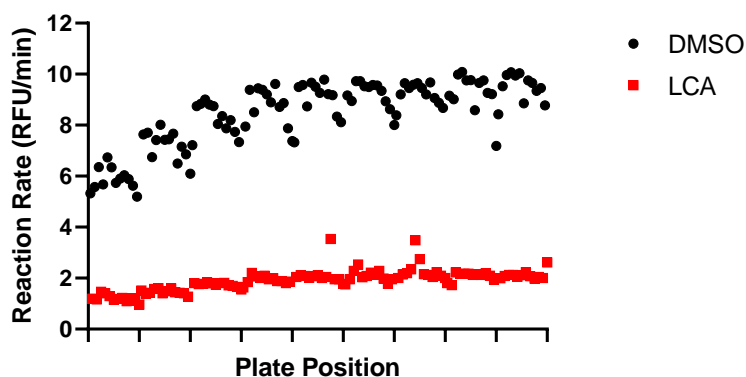


**Figure 4.** Pilot study checkerboard assay. Enzyme was treated with lithocholic acid (LCA) (100 µM) or vehicle (DMSO), in a checkerboard pattern across a 384-well plate. Enzyme activity reported as increase in fluorescence over time. Plate position shown to assess for location-dependent variability, ticks represent the end of a row. Z' was calculated to be 0.45 using WaveGuide software (WaveFront Biosciences), indicating sufficient signal separation.

    With guidance from members of the Vanderbilt University HTS Core, Dr.
Aggarwal screened 2,388 biologically active and structurally diverse compounds (the
Vanderbilt Spectrum Collection compound library) at a final concentration of 10 μM. For
all compounds, a B-score for both initial rate of fluorescence change and steady-state
fluorescence value was calculated (Figure 5),[132] but only initial rate B-scores were used
to identify hits. B-scores represent the number of standard deviations away from the
average a certain value is. Compounds with a B-score 3 or more standard deviations
above (activators) or below (inhibitors) the mean were classified as potential hits after
confirmation by manual inspection (Figure 6). Structures known to potentially interfere
with the assay due to fluorescence or quenching were eliminated from further study.
This yielded 14 inhibitor hits and 12 activator hits. She then re-assayed the compounds
to confirm the original findings. While all 14 of the potential inhibitors demonstrated
reproducible activity in the confirmation assay, none of the 12 potential activator
compounds did (data not shown).
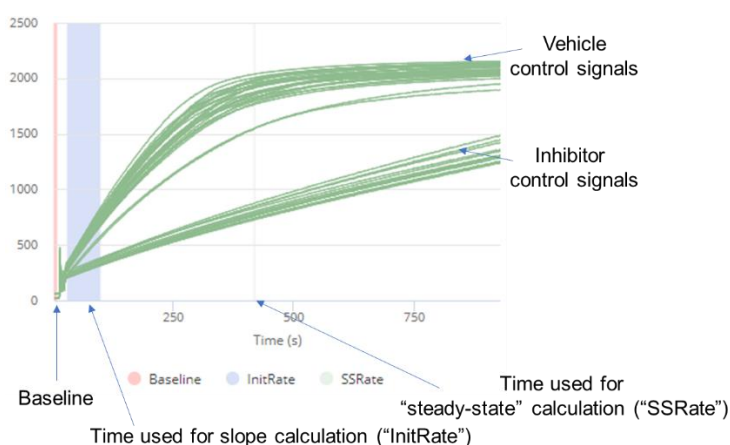


**Figure 5.** Representative high-throughput screening (HTS) assay curves. Labelled are key
time points used in calculations, as well as signals from vehicle and inhibitor control wells. Y-
axis is total fluorescence (RFU). Figure generated using WaveGuide software.
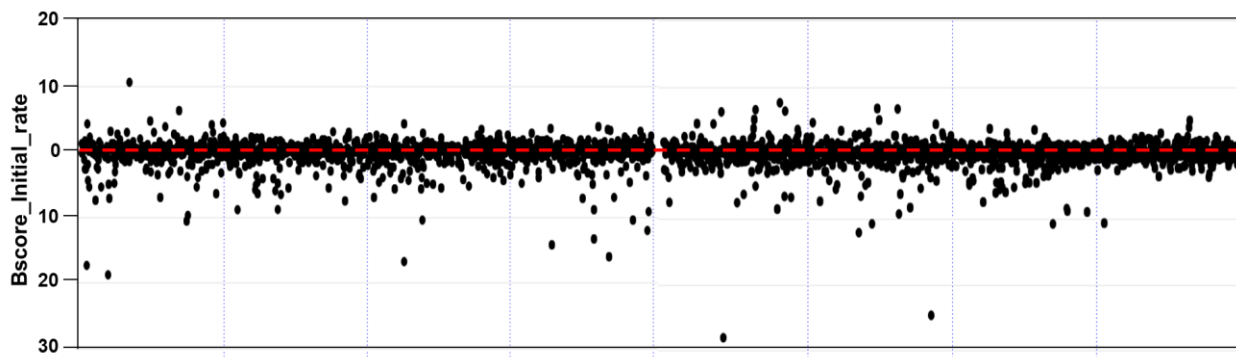
**Figure 6.** Pilot HTS results. B-scores (using initial rate) for all 2,388 compounds in the Vanderbilt Spectrum Collection. Compounds are distributed randomly along the X-axis. Values below the red dotted line represent reduced initial rate (inhibitors), points above the red dotted represent increased initial rate (activators).

2.1.3 Validation Assays

Dr. Aggarwal next determined whether the reduction in fluorescence by any of the 14 potential inhibitor compounds was due to direct quenching of fluorescence, rather than inhibition of Nape-pld. To test this, the compounds were incubated with BODIPY FL $C_5$, which bears the same fluorophore as PED-A1. For each compound, the fluorescence of BODIPY FL $C_5$ after treatment with 10 µM compound for 30 min was compared to vehicle treatment. None of the 14 hit compounds altered fluorescence by more than 10% (Figure 7), indicating they were genuine inhibitors of Nape-pld.
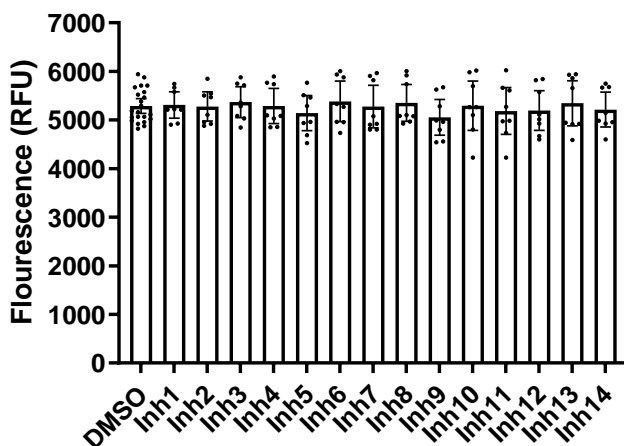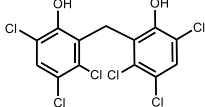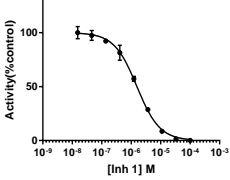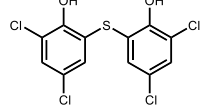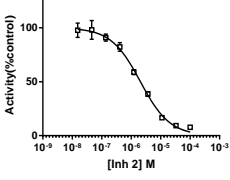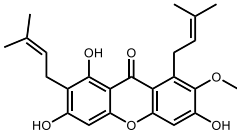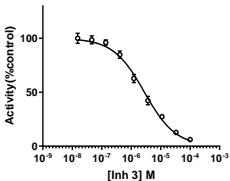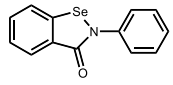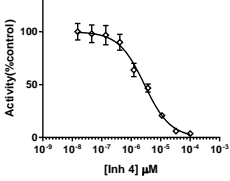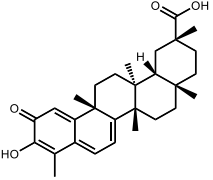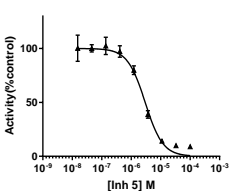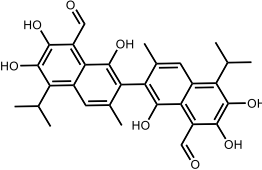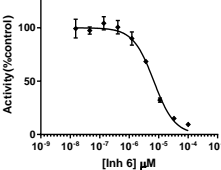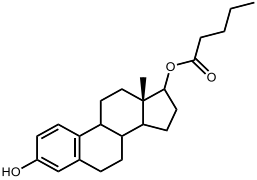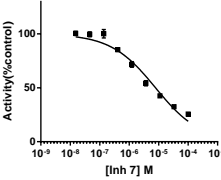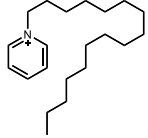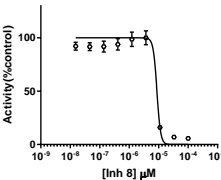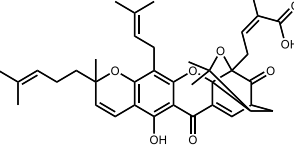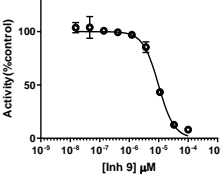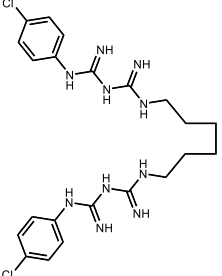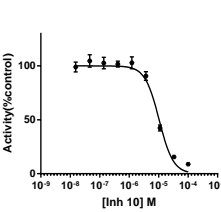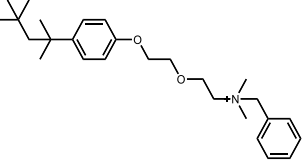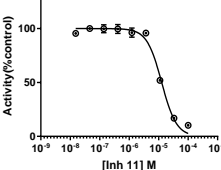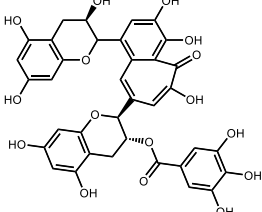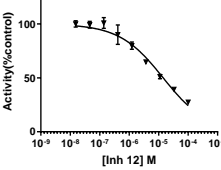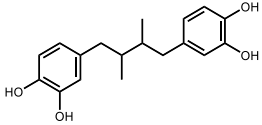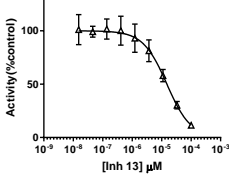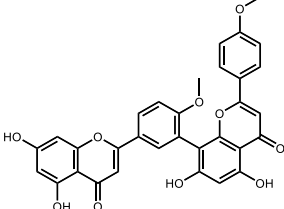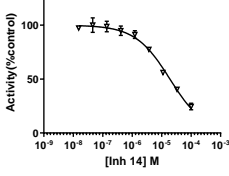


**Figure 7.** Putative Nape-pld inhibitors 1 through 14 (Inh1-14) do not directly quench BODIPY fluorescence. BODIPY FL $C_5$ was incubated with vehicle (DMSO) or 10 µM of each putative inhibitor for 30 min and then fluorescence measured (ex/em 488/535 nm). Individual results are shown, with mean ± 95% confidence interval (95% CI).

23

All 14 inhibitor compounds (Inh1-14) were then purchased from commercial sources to validate the screened compounds. Dr. Aggarwal did this by analyzing the purchased compounds with mass spectrometry to confirm their identity and purity. She then performed concentration-response curve (CRC) studies using the purchased stocks to establish potency. The half-maximal inhibitory concentrations ($IC_{50}$) of these compounds ranged from 1.6 µM to 19.1 µM, meaning that they were all more potent *in vitro* than best NAPE-PLD inhibitor at the time, ARN-19874 (Table 1).[124]

| Inhibitor # (common name) | Structure | Concentration-Response Curve | $IC_{50}$ (µM) (95% CI) |
|---|---|---|---|
| **Table 1.** Concentration-response curves (CRCs) of initial inhibitors from pilot screening. Shown are compound names, structures, results of CRCs, and calculated half-maximal inhibitory concentrations ($IC_{50}$) with 95% confidence intervals (95% CI) | | | |
| **Inh1** (Hexachlorophene) |  |  | 1.6 (1.4-1.7) |
| **Inh2** (Bithionol) |  |  | 2.1 (1.8-2.4) |
| **Inh3** (Mangostin) |  |  | 2.8 (2.5-3.2) |
| **Inh4** (Ebselen) |  |  | 2.8 (2.4-3.4) |
| **Inh5** (Tripterine) |  |  | 3.0 (2.5-3.5) |

| | | | |
|---|---|---|---|
| **Inh6**<br>(Gossypol) |  |  | 6.9<br>(5.9-8.0) |
| **Inh7**<br>(Estradiol valerate) |  |  | 7.8<br>(6.2 -10.0) |
| **Inh8**<br>(Cetylpyridinium) |  |  | 8.8<br>(6.8-10.0) |
| **Inh9**<br>(Gambogic acid) |  |  | 9.9<br>(8.8-11.1) |
| **Inh10**<br>(Chlorhexidine) |  |  | 10.4<br>(9.1-11.9) |
| **Inh11**<br>(Hyamine) |  |  | 12.7<br>(11.4-14.2) |
| **Inh12**<br>(Theaflavin<br>monogallates) |  |  | 14.3<br>(11.6-17.7) |

| | | | |
|---|---|---|---|
| **Inh13** (Nordihydroguaiaretic acid) |  |  | 15.1 (11.8-19.3) |
| **Inh14** (Dioxybenzone) |  |  | 19.1 (16.6-22.0) |

## 2.1.4 Kinetics Assay

Next, we wanted to assess the mechanisms by which the inhibitor hits modulated NAPE-PLD, so Dr. Aggarwal conducted a Michaelis-Menten kinetics test for the top two inhibitors. Inhibition of recombinant Nape-pld with Inh1 and Inh2 reduced the maximum reaction velocity ($V_{max}$) but did not increase $K_M$, consistent with a non-competitive mechanism of inhibition. The apparent $K_I$ for both Inh1 and Inh2 was ~2 µM (Figure 8).
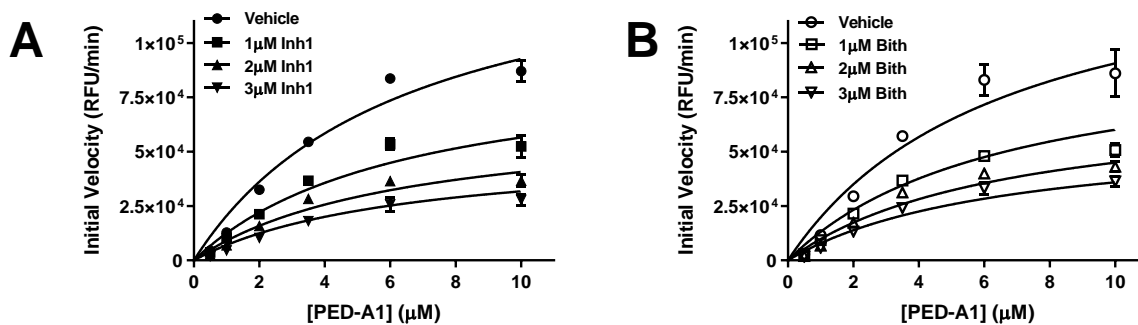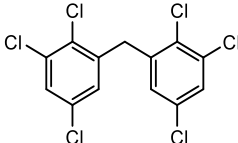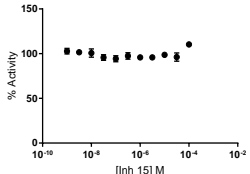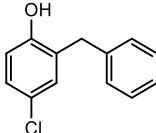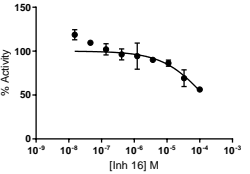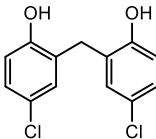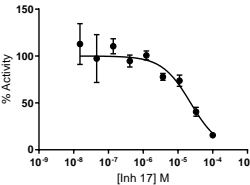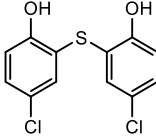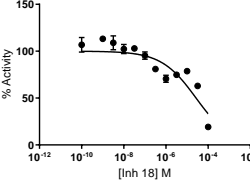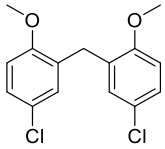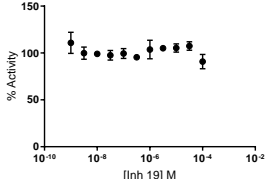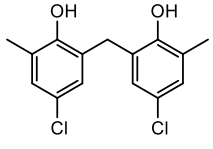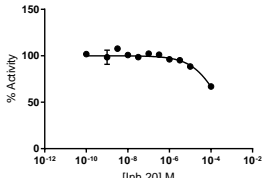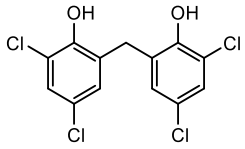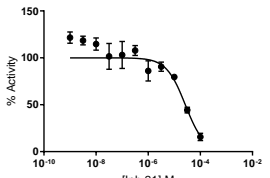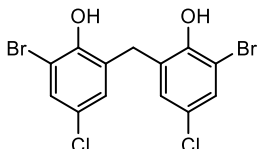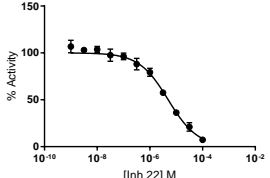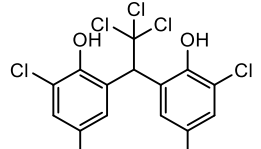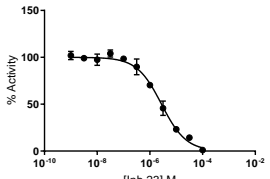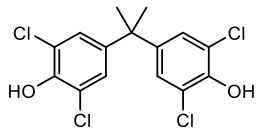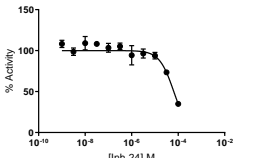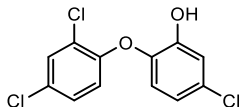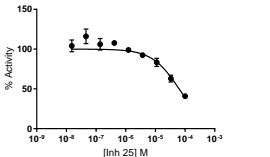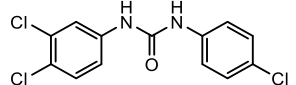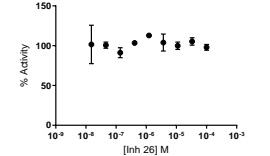


**Figure 8.** Mechanism of inhibition by Inh1 and Inh2 (bithionol, Bith). **A.** Recombinant mouse Nape-pld was incubated with 0-3 µM Inh1, 0-10 µM PED-A1 was added, and the initial velocity (t = 1-4 min) of PED-A1 hydrolysis determined for each. Non-linear best-fit curves (noncompetitive inhibition, least squares fit) are shown. Points are mean ± standard deviation (SD), n = 3 technical replicates. **B.** Same as A but using Bith.

## 2.1.5 Structure-Activity Relationships

The two most potent inhibitors, Inh1 (hexachlorophene) and Inh2 (bithionol, Bith), share a symmetrically substituted dichlorophene structure, with Bith having a thioether linker rather than an alkane linker, as well as lacking the 5/5'-chloro groups of Inh1 (Table 1). Since NAPE-PLD crystallizes as a homodimer,[68] the potency of these symmetrical compounds may arise from acting at the dimer interface (i.e., by binding to similar residues on both NAPE-PLD monomers). However, this idea alone was insufficient for us to understand the importance of the compounds' structural features for binding and activity. I therefore used commercially available dichlorophene analogs to carry out a limited structure-activity relationship (SAR) study.

**Table 2.** CRCs of compounds from pilot SAR study. Shown are compound names, structures, results of CRCs, and calculated $IC_{50}$ with 95% confidence intervals (95% CI). Compounds are arranged in an order to enhance understanding of the structure-activity relationship.

| Inhibitor # (common name) | Structure | Concentration-Response Curve | $IC_{50}$ (µM) (95% CI) |
|---|---|---|---|
| **Inh15** (CAS 2888-15-5) |  |  | No effect observed |
| **Inh16** (Chlorophene) |  |  | 132.9 (77.2-336.4) |
| **Inh17** (Dichlorophen) |  |  | 23.2 (15.8-34.2) |
| **Inh18** (Fenticlor) |  |  | 26.8 (18.2-41.6) |

| | | | |
|---|---|---|---|
| **Inh19**<br>(CAS 7569-57-5) |  |  | No effect observed |
| **Inh20**<br>(CAS 57693-35-3) |  |  | ~294.1<br>(198.0-512.4) |
| **Inh21**<br>(CAS 1940-43-8) |  |  | 26.5<br>(18.3-38.6) |
| **Inh22**<br>(CAS 15435-29-7) |  |  | 5.0<br>(4.2-5.9) |
| **Inh23**<br>(CAS 92167-59-4) |  |  | 2.8<br>(2.38-3.24) |
| **Inh24**<br>(CAS 79-95-8) |  |  | 64.7<br>(53.4-80.0) |
| **Inh25**<br>(Triclosan) |  |  | 62.9<br>(47.1-89.3) |
| **Inh26**<br>(Triclocarban) |  |  | No effect observed |

Replacement of Inh1's hydroxyl groups with chloro groups yielded a compound with no inhibitory activity (Inh15, Table 2), suggesting that the hydroxyl groups were critical for activity. Inh16 (chlorophene), with only a hydroxyl and a chloro group on one of the two aromatic rings, had only weak inhibitory activity, indicating that the substitutions around the rings were important for activity. Inh17 (dichlorophen) and Inh18 (fenticlor) have a hydroxyl and a chloro group on both aromatic rings, and both compounds were about 10-fold less potent than Inh1 and Bith, but more potent than Inh16. This showed, again, that the presence of functional groups on the aromatic rings was important for activity. Inh19, where both hydroxyl groups of Inh17 are replaced with methoxy groups, gave no measurable inhibitory activity, supporting the need for the hydroxyl groups. Symmetrical addition of methyl (Inh20), chloro (Inh21), or bromo groups (Inh22) at the 2- and 2'- position of Inh17 resulted in less, equal, or more potent inhibition of Nape-pld than with Inh17, respectively. This suggested that the addition of strong electronegative groups (at least at this position) enhances inhibitory activity. Addition of a trichloromethyl group to the carbon bridging the two aromatic rings of Inh21 (Inh23) increased potency about 10-fold, corroborating the importance of electronegative groups. Inh24, where the 1-/1'- hydroxyl groups of Inh17 are at the 3-/3'-position instead and there is dimethyl substitution on the carbon bridging the two aromatic rings, is about 3-fold less potent than Inh17. Inh25 (triclosan) also showed about 3-fold less potency than Inh17, while Inh26 (triclocarban) showed no inhibitory activity.

All together, these SAR results suggested that symmetrical halide substitution of the two phenolic groups is critical for potent inhibition. Additionally, the 1-, 1'- hydroxyl groups are critical for inhibition, and addition of electronegative groups to the structure typically increases potency. And, although Inh22 and Inh23 showed similar potency to Inh1 and Bith, they also showed significantly greater cytotoxicity in HEK-293 cells (data not shown), so we pursued further testing only with Inh1 and Bith.

## 2.1.6 Cell-Based Assays

We wanted to assess whether these compounds could be used to inhibit NAPE-PLD in live cells. As HEK-293 cells endogenously express NAPE-PLD, are easily cultured cells, and have been extensively used as a model cell type,[117, 124] we used them to assess the cellular activities of our candidate inhibitors.

First, Dr. Aggarwal determined the effects of our inhibitors on cell viability in order to determine whether they could be safely used to inhibit NAPE-PLD in live cells. Inh1-14 were each tested at a concentration equal to 5 times that of their own calculated $IC_{50}$ ($5xIC_{50}$). At these concentrations, six of the fourteen compounds gave cell viability >70%: Inh1, 2, 4, 7, 12, and 14 (Figure 9 A). As Inh1 and Bith (Inh2) had become the focus of our studies, she then determined the maximum concentrations of Inh1 and Bith that could be used for cellular inhibition studies without causing severe cytotoxicity. HEK-293 cells were treated with 0-100 μM compounds and cytotoxicity was measured as before. Both inhibitors showed high cytotoxicity at 100 μM (Figure 9 B-C), so 20 μM was chosen as the maximum concentration for inhibition studies.
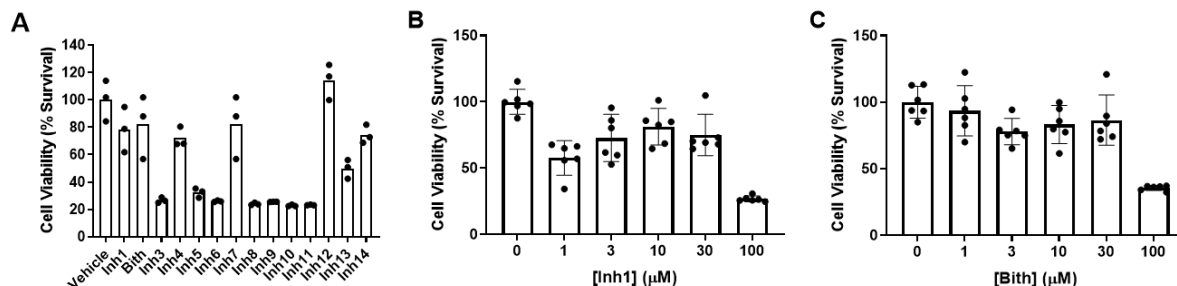


**Figure 9.** Effect of inhibitors on cell viability. **A.** HEK-293 cells were incubated for 24 h with a concentration of inhibitor representing 5x the $IC_{50}$ for recombinant Nape-pld for that compound. Resulting cell viability was measured by MTT assay and normalized to that of vehicle-treated cells. Three replicate wells of 24-well plate were used for each compound. Mean and individual points are shown for each treatment. **B-C.** The same method was used to measure the cytotoxicity of Inh1 and Bith at a range of concentrations, 6 replicate wells per dose. Mean ± 95% CI shown.

To measure NAPE-PLD inhibition in live cells, I treated HEK-293 cells with 0-20 μM of each inhibitor for 30 min, followed by administration of PED-A1. Inh1 and Bith inhibited cellular NAPE-PLD activity with $IC_{50}$s of 9.8 μM and 10.7 μM, respectively (Figure 10). This indicated that both compounds could be used to modulate NAPE-PLD

in cells, albeit less potently than *in vitro*. By the conclusion of the pilot study, we had established a set of methods that could be used for a larger screening of potential NAPE-PLD modulators. And we established that finding potent and selective modulators of NAPE-PLD using these methods was possible.
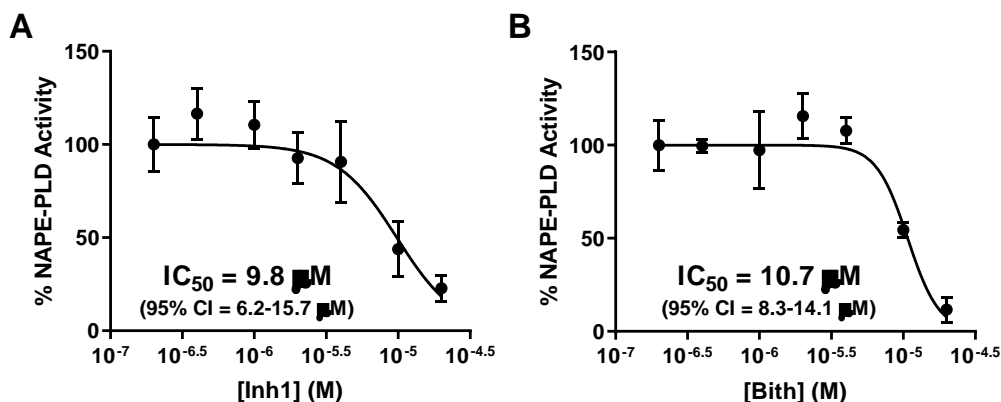


**Figure 10**. Inh1 and Inh2 inhibit the NAPE-PLD activity of HEK-293 cells. 0-20 µM of Inh1 (**A**) or Bith (**B**) were added to confluent wells of HEK-293 cells plated in 96-well plates and incubated for 30 min. PED-A1 was then added and NAPE-PLD activity determined by change in fluorescence (ex/em 488/530 nm) over 25 min and then normalized to control. Points represent mean ± SEM, n = 6 (3 wells on two replicate days). $IC_{50}$ and 95% confidence interval calculated using log(inhibitor) vs. normalized response-variable slope analysis.

## 2.2 Assay Development

While the HTS method developed by Dr. Aggarwal was effective, proven, and reliable, it had two weaknesses that we wanted to address before conducting our larger HTS for NAPE-PLD modulators. The first problem was that, since we planned to screen many more compounds than in the pilot screening, it would be simpler to test more compounds in each plate. To accomplish that, we attempted to use 1,536-well plates instead of 384-well plates. The second problem was that PED-A1 is an expensive compound, and each assay plate used a lot of it. Therefore, I also sought a way to dilute the PED-A1 without compromising the reliability of its signal. Then, after pursuing those modifications, I finalized the HTS assay protocol and assessed its reliability with a checkerboard assay.

## 2.2.1 1,536-Well Plate Trials

Using 384-well plates, Dr. Aggarwal was able to test 320 compounds at a time to screen a total of 2,388 compounds. With a screening library of 100,000 total compounds, we sought to quadruple the number of compounds tested per plate by using 1,536-well plates. However, after several attempts with the help of Dr. Paige Vinson, we determined that the Agilent Bravo robotic liquid handlers could not precisely pipette the same volume into each of the wells on the plate (data not shown). This was likely due to the fact that the robot was designed for use on 96- or 384-welll plates, not 1,536. Therefore, we decided to proceed using a 384-well plate-based method.

## 2.2.2 PED-A1 Dilution

PED-A1 is an expensive substrate, costing around $200 for 100 µg. While the PED-A1 assay was developed using a benchtop-grade plate reader, the camera used in the HTS assay (Panoptic, WaveFront Biosciences) is of much higher quality and can detect much weaker fluorescence signals than a simple plate reader. Therefore, we reasoned that we could dilute the PED-A1 while increasing the gain settings of the Panoptic instrument and still observe the same signal quality. I did not simply dilute the PED-A1 in a larger amount of buffer, however. The concentration of 4 µM PED-A1 was specifically chosen because it was approximately equal to the substrate's $K_M$ with Nape-pld, thereby allowing the detection of both activators and inhibitors. So, when reducing the amount of PED-A1 administered, I replaced it with 1,2-dioleoyl-*sn*-glycero-3-phosphoethanolamine-*N*-palmitoyl (C16-NAPE), an optically inactive NAPE-PLD substrate with a $K_M$ around that of PED-A1.[70, 133] This allowed me to reduce the amount of PED-A1 used while maintaining a constant total amount of substrate available to the enzyme.

Determining the degree to which we could dilute PED-A1 while maintaining assay quality happened in three steps, all performed with consultation from Dr. Vinson. First, I created conditions that replicated the endpoints of Nape-pld hydrolysis of four different concentrations of PED-A1, using the same buffers as in the HTS assay and

using BODIPY FL C$_5$ + C16-NAPE to mimic the planned doses of PED-A1 + C16-NAPE (BODIPY FL C$_5$ has the same fluorescence properties as hydrolyzed PED-A1).[126, 133] Then, using simple trial and error, I identified camera settings that gave a robust signal for each concentration of fluorophore. I found that even when diluting the fluorophore 10-fold, I could still detect a robust signal.

However, the PED-A1 assay is not an endpoint assay—it relies on signals from early time-points. So, in the second experiment, I expanded the set of BODIPY FL C$_5$ dilutions to include three doses that were chosen to mimic periodic time points in the reactions of each PED-A1 dilution (12 total conditions, 3 doses per dilution). I again tuned the camera's settings to capture strong signals for each of the different surrogate time-points of a particular BODIPY FL C$_5$ dilution. This yielded four sets of camera settings that could detect the hydrolysis of four doses of PED-A1 over time.

I then tested these camera settings in a third and final test to determine if diluting the PED-A1 would be viable. For each of four dilutions of PED-A1 (still with C16-NAPE to replace the lost PED-A1), I tested three conditions using the Nape-pld activity assay: vehicle-treated, LCA-treated, and enzyme-free. Each PED-A1 dilution was tested separately, as the camera settings for each were different. Then, I compared the differences in signal between the three treatment conditions for each PED-A1 dilution. I found that in all dilutions, the different conditions could be reliably differentiated based on their signals (Figure A1 in Appendix). Since diluting the PED-A1 10-fold would be the least expensive option and it yielded signals as robust as those with undiluted PED-A1, we proceeded using the 10-fold dilution and its associated camera settings.


2.2.3 High-Throughput Screening Method

*2.2.3.1 Checkerboard Assay*

In order to verify that this updated assay could reliably detect modulator hits anywhere on the plate, I next performed a checkerboard assay with help from Corbin Whitwell and Dr. Vinson of the Vanderbilt University HTS Core.[126] In it, we administered DMSO and LCA to Nape-pld in a checkerboard pattern across a 384-well plate to

determine how well their signals could be differentiated. Also, one column of wells contained PED-A1 with no enzyme, and another contained enzyme with no PED-A1. The former showed us how much signal bleeding we would see between neighboring wells, while the latter allowed us to be sure that the enzyme and buffers would not create significant background signal. As in the pilot HTS, the time used to calculate Nape-pld activity was the 30-100 second initial slope range. From this checkerboard assay, we could see that there was no meaningful signal bleeding or background fluorescence (data not shown). We could also see qualitatively that the DMSO and LCA signals were differentiable (Figure 11). Quantitatively, the plate's Z' score was 0.676, which indicated that the assay could reliably differentiate hits and non-hits.[131]
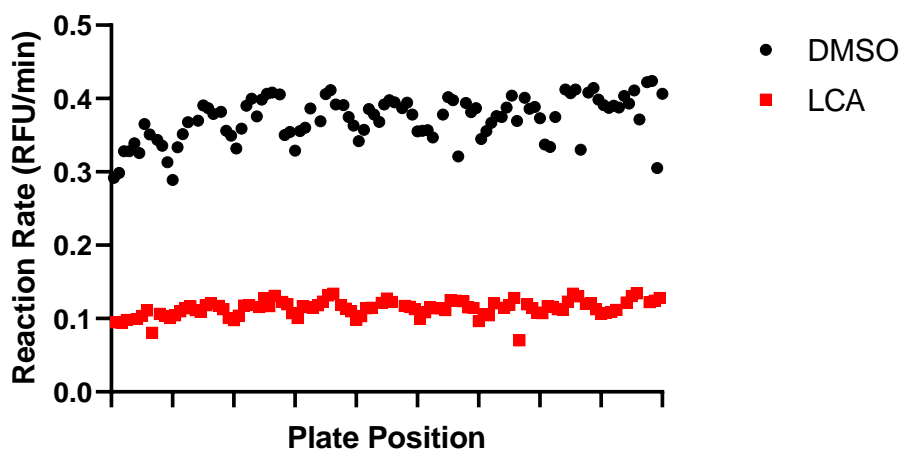


**Figure 11.** HTS checkerboard assay. Enzyme was treated with LCA (100 µM) or vehicle (DMSO), in a checkerboard pattern across a 384-well plate. Enzyme activity reported as increase in fluorescence over time during the steady-state period. Plate position shown to assess for location-dependent variability, ticks represent the end of a row. Z' was calculated to be 0.676 using WaveGuide software (WaveFront Biosciences), indicating robust signal separation.

*2.2.3.2 Screening Method*

In its final form, I performed the HTS method as follows, with assistance and consultation from the Vanderbilt University HTS Core. 40 µL of Nape-pld (0.1 µM final) and NOG (0.4% w/v final) in 50 mM Tris-HCl buffer (pH = 8.0) were administered to the central 320 wells of a 384-well plate. Columns 1, 2, 23, and 24 received a checkerboard pattern of either that same Nape-pld mixture, or a solution with buffer in place of Nape-

pld—these columns were used as control wells. In parallel, Corbin Whitwell administered 35 nL of test compounds (10 µM final), vehicle controls (DMSO), and inhibitor controls (Bith, 10 µM final) to appropriate wells of a black-walled, clear-bottom, 384-well test plate using an Echo acoustic liquid handler. Next, a Bravo robotic liquid handler transferred 30 µL of the contents of each well of the enzyme solution-containing plate to the test plate and pipetted three times to mix. The test plate was incubated at 37 °C for 1 h and the enzyme plate was discarded.

During this incubation, 30 µL of PED-A1 (diluted as explained previously) was added to each well of another 384-well plate (enough volume to test four plates of compounds). This plate was sealed, kept on ice, and kept in the dark until it was needed, to prevent degradation of the substrate and evaporation of the ethanol in its vehicle. Also during the incubation, the WaveFront Panoptic instrument was prepared for use (camera cooled, testing chamber heated to 37 °C, robotic liquid handlers primed, and protocols prepared).

After the 1 h incubation, the test plate was moved to the Panoptic instrument, where another Bravo robot transferred 5 µL of PED-A1 into all wells of the plate. Fluorescence excitation/emission (ex/em) of 482/536 nm was read over the course of 4 min. The data for that plate were extracted and the next plate was run.


## 2.3 High-Throughput Screening

Using this assay, I tested a total of 39,328 compounds for Nape-pld modulation. Compounds were a structurally diverse set selected from the Vanderbilt Discovery Collection (High-Throughput Screening Core, Vanderbilt University), which is a library of compounds that are lead-like and unlikely to cause pan-assay interference.

## 2.3.1 Hit Selection Information
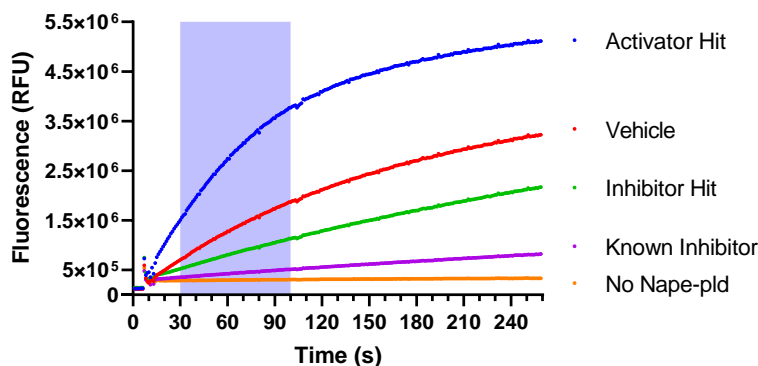


**Figure 12.** Sample fluorescence kinetics curves from high-throughput screening. One example well for each type of control used and hit observed are graphed as labelled. All five curves come from the same test plate. Region highlighted in blue is the initial slope region, used to calculate B-scores. Curves are comprised of individual fluorescence readings (ex/em 482/536 nm), measured every second.

HTS data were analyzed using WaveGuide software (WaveFront Biosciences). For each kinetic curve (Figure 12), the initial slope was calculated as the slope between the 30 s and 100 s timepoints. Initial slopes were used as that is the region where the concentration of substrate is approximately constant, and because at later timepoints the signals of activator hits could have already begun to plateau and so show a misleadingly small difference from controls. Using the 64 total vehicle, enzyme-free, and inhibitor controls on each plate, B-scores were calculated for each compound-containing well.[132] As B-scores represent the number of standard deviations away from the mean a particular value is,[132] hits were defined as compounds with absolute B-scores of 3 or higher.

## 2.3.2 HTS Results

A total of 1,404 hits were identified, of which 1,005 were inhibitors and 399 were activators (Figure 13, Table 3). This represented an overall hit rate of 3.6%. A Z' score was calculated for each screening plate to ensure that hits could be reliably detected in each one (Z' ≥ 0.5),[131] and the average Z' across all of the screening plates was 0.52.
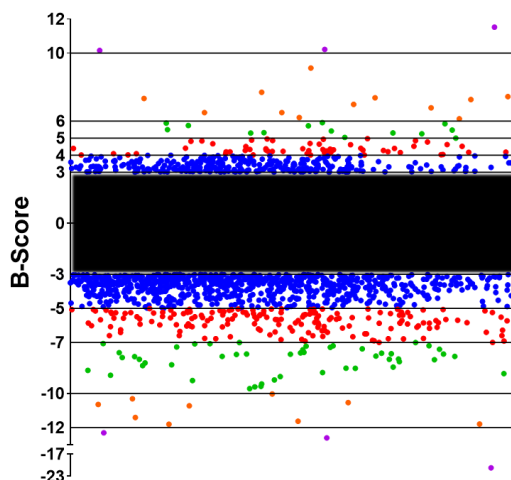
**Figure 13.** Results of high-throughput screening. B-scores of each hit are shown as individual points. Non-hits are represented by the rectangle in the center. Compounds are separated by their B-scores, as shown by both lines and colors. Compounds with B-scores ≥ 3 were considered to be activator hits, compounds with B-scores ≤ -3 were considered to be inhibitor hits.

| B-Score Range | Number of Hits |
|:---:|:---:|
| 12 to 10 | 3 |
| 10 to 6 | 12 |
| 6 to 5 | 14 |
| 5 to 4 | 56 |
| 4 to 3 | 314 |
| 3 to -3 | 37,924 |
| -3 to -5 | 770 |
| -5 to -7 | 174 |
| -7 to -10 | 49 |
| -10 to -12 | 9 |
| -12 to -21 | 3 |

**Table 3.** Summary of HTS results. Shows total numbers of compounds scoring within given B-score ranges. Compounds with B-scores ≥ 3 were considered to be activator hits, compounds with B-scores ≤ -3 were considered to be inhibitor hits.

## 2.3.3 Re-Run Samples

Certain plates and compounds had to be tested a second time. Entire plates were re-run if their Z' scores were below 0.5. And if that plate contained compounds with potential fluorescent properties (identified manually), then those compounds were replaced with vehicle controls. Individual compounds were also re-run if the

experimenter or any of the robotic liquid handlers logged an error in its preparation (for example, if not enough of the compound was added to the well). The results of these re-run samples were incorporated into the data presented above, replacing their data from the initial assessments.

## 2.4 Replication and Structure-Activity Relationships

Next, I re-ran the HTS assay on the most promising compounds, to determine whether their previously strong performances were replicable. In the process, I also tested new compounds whose structures were similar to those of the top inhibitor and activator hits. The method used for these assays was the same as in the high-throughput screening, except each compound was tested in triplicate and more control wells were included.

### 2.4.1 Compound Selection

While it could have been beneficial to replicate the activities of all of the compounds tested, doing so was not feasible and did not meet our needs. Instead, we focused on the most promising compounds: those with the highest and lowest B-scores, and their structural analogs. So, for the replication assay, I tested the compounds that most strongly changed Nape-pld activity in the initial screening (B-scores above 3.8 and below -4.8). We also identified several hundred compounds in the Vanderbilt chemical libraries with similar structures to the best hits with the help of Dr. Ian Romaine and tested those as well. In both categories of compounds, we favored potential activators, as no other NAPE-PLD activators existed, and they have the highest therapeutic potential. Therefore, ~75% of the compounds tested in this assay were potential activators.

Of the 562 compounds tested, 15 were strong activators and 6 were strong inhibitors (Figure 14). The compounds have been organized by their compound identification numbers to make it apparent that compounds with similar structures (and, therefore, similar identification numbers) had similar activities. At the conclusion of this assay, we had a selection of promising candidate modulators.
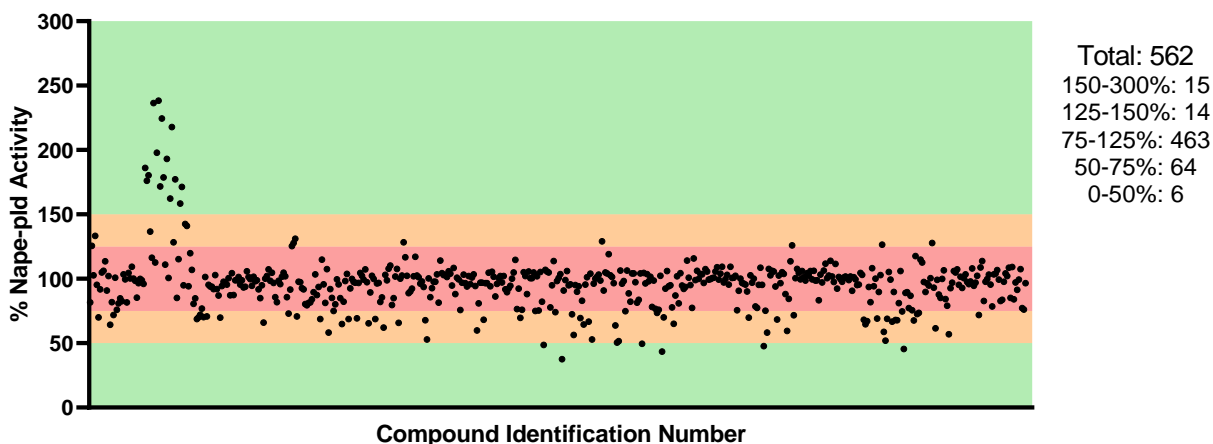


**Figure 14.** Replication and SAR results. Average Nape-pld activity (RFU/min) normalized to vehicle controls for each compound (n = 3 replicate wells) are plotted against compound identification number. Compounds in the red region (75-125%) were non-modulators. Compounds in the orange regions (50-75% and 125-250%) were weak modulators. Compounds in the green regions (0-50% and 150-300%) were strong modulators. Total numbers of compounds in each region are shown. Compounds with similar identification numbers are similar in structure. All compounds were tested at 10 µM.

## 2.5 Concentration-Response Curves

We had identified many promising modulator candidates, but we did not know how potent they were and to what extent they could change Nape-pld's activity. Therefore, I performed concentration-response curves using the same activity assay as in the HTS but testing each compound at a graded range of concentrations.

## 2.5.1 Initial Concentration-Response Curve Results

The results of this experiment are summarized in Table 4 and the full curves are presented in Figure A2 (in Appendix). I identified several strong Nape-pld inhibitors and many potent Nape-pld activators. All of the best activators were of the same structural class, which prompted me to do a second round of CRCs. In this follow-up experiment, I tested all remaining compounds in the Vanderbilt chemical library with similar structures to the top activators. I also tested two compounds with structures similar to our top inhibitors, and one with a structure similar to a different activator hit. These results are summarized in Table 5 and the full curves are presented in Figure A3 (in Appendix). This experiment demonstrated that the structural class of our top activators was robust, as it contained many potent and efficacious Nape-pld activators.

**Table 4.** Summary of initial Nape-pld CRC results. $EC_{50}$ is concentration required to produce half-maximal activity for that specific compound. $E_{max}$ is the maximum amount of Nape-pld activity elicited by that specific compound. Values were calculated from non-linear curve fits using log(compound) vs. response, variable slope.

| Inhibitors | | | Activators | | | |
|---|---|---|---|---|---|---|
| Compound Identification Number | $IC_{50}$ (µM) | $IC_{50}$ 95% CI (µM) | Compound Identification Number | $EC_{50}$ (µM) | $EC_{50}$ 95% CI (µM) | $E_{max}$ |
| VU0617254 | 5.213 | 4.21 to 6.44 | VU0506534 | 0.2677 | 0.113 to 0.425 | 201.3 |
| VU0643207 | 6.505 | 4.77 to 8.91 | VU0506517 | 0.7665 | 0.533 to 1.04 | 195.3 |
| VU0614378 | 8.711 | 6.99 to 10.9 | VU0506575 | 0.9519 | 0.659 to 1.31 | 219.1 |
| VU0625283 | 12.21 | 10.3 to 14.5 | VU0506605 | 1.038 | 0.801 to 1.23 | 160.8 |
| VU0613571 | 13.16 | 11.7 to 14.6 | VU0506536 | 1.543 | 0.773 to 2.77 | 223.9 |
| VU0642955 | 14.70 | 12.8 to 16.9 | VU0506542 | 2.132 | 0.105 to 7.01 | 175.9 |
| VU0535890 | 15.02 | 11.5 to 20.0 | VU0506539 | 2.375 | 1.47 to 3.66 | 167.3 |
| VU0643006 | 15.35 | 13.0 to 18.2 | VU0644762 | 8.334 | 5.39 to 14.9 | 139.7 |
| VU0613570 | 15.63 | 12.9 to 18.9 | VU0533641 | N/A | N/A | <120 |
| VU0628477 | 16.09 | 14.4 to 18.0 | VU0534491 | N/A | N/A | <120 |
| VU0611271 | 16.65 | 12.0 to 23.9 | VU0620581 | N/A | N/A | <120 |
| VU0644470 | 16.92 | 14.5 to 19.7 | VU0496613 | N/A | N/A | <120 |
| VU0604956 | 17.30 | 13.3 to 23.0 | VU0545679 | N/A | N/A | <120 |
| VU0643305 | 18.07 | 14.0 to 23.8 | VU0611881 | N/A | N/A | <120 |
| VU0522028 | 18.62 | 14.4 to 24.5 | VU0636960 | N/A | N/A | <120 |
| VU0630638 | 18.77 | 12.8 to 29.0 | VU0519825 | N/A | N/A | <120 |
| VU0643011 | 20.52 | 17.4 to 24.3 | VU0519827 | N/A | N/A | <120 |
| VU0613568 | 20.55 | 17.6 to 24.0 | VU0533614 | N/A | N/A | <120 |
| VU0619032 | 20.59 | 17.9 to 23.7 | VU0302900 | N/A | N/A | <120 |

| | | | | | | |
|---|---|---|---|---|---|---|
| VU0643164 | 21.58 | 17.2 to 27.8 | VU0494051 | N/A | N/A | <120 |
| VU0643170 | 22.74 | 18.6 to 28.2 | VU0521234 | N/A | N/A | <120 |
| VU0643169 | 23.13 | 16.6 to 34.0 | VU0619943 | N/A | N/A | <120 |
| VU0534990 | 23.40 | 21.5 to 25.6 | VU0642673 | N/A | N/A | <120 |
| VU0497392 | 23.75 | 20.4 to 28.0 | VU0509082 | N/A | N/A | <120 |
| VU0532188 | 25.10 | 18.0 to 36.8 | VU0519824 | N/A | N/A | <120 |
| VU0525353 | 25.92 | 21.8 to 31.2 | VU0613198 | N/A | N/A | <120 |
| VU0546159 | 26.82 | 19.9 to 37.7 | VU0630726 | N/A | N/A | <120 |
| VU0640175 | 27.83 | 22.0 to 36.2 | VU0643245 | N/A | N/A | <120 |
| VU0511527 | 28.27 | 25.5 to 31.5 | VU0643296 | N/A | N/A | <120 |
| VU0526103 | 31.17 | 23.3 to 43.8 | | | | |
| VU0640191 | 32.02 | 24.2 to 44.2 | | | | |
| VU0610885 | 32.02 | 26.3 to 39.8 | | | | |
| VU0640185 | 33.22 | 25.6 to 44.8 | | | | |
| VU0514333 | 34.13 | 29.0 to 40.7 | | | | |
| VU0643233 | 36.62 | 27.1 to 52.5 | | | | |
| VU0625294 | 38.80 | 27.6 to 58.8 | | | | |
| VU0528508 | 39.62 | 33.7 to 47.4 | | | | |
| VU0541105 | 40.08 | 35.1 to 46.3 | | | | |
| VU0519850 | 40.43 | 36.8 to 44.6 | | | | |
| VU0526442 | 41.18 | 34.3 to 50.4 | | | | |
| VU0611121 | 44.06 | 35.0 to 56.5 | | | | |
| VU0528012 | 45.77 | 38.3 to 55.9 | | | | |
| VU0529510 | 47.17 | 37.9 to 61.0 | | | | |
| VU0641984 | 48.92 | 35.5 to 73.1 | | | | |
| VU0610704 | 49.21 | 42.8 to 56.9 | | | | |
| VU0543974 | 58.64 | 43.7 to 84.9 | | | | |
| VU0648659 | 154.7 | 105. to 337. | | | | |
| VU0608714 | N/A | N/A | | | | |

| Table 5. Summary of follow-up Nape-pld CRC results. Values calculated from non-linear curve fits, using log(compound) vs. response, variable slope. | | | | |
|---|---|---|---|---|
| Compound Identification Number | $EC_{50}$ (µM) | $EC_{50}$ 95% CI (µM) | $E_{max}$ | Structure |
| VU0506488 | 0.387 | 0.13 to 0.71 | 135.5 | |
| VU0506486 | 0.441 | 0.2 to 0.86 | 167.9 | |
| VU0506601 | 1.06 | poor fit | 171.2 | |
| VU0506484 | 2.56 | 1.97 to 3.14 | 161.5 | |
| VU0506541 | 3.30 | 2.52 to 5.95 | 152.6 | |
| VU0506485 | 29.0 | poor fit | 231.6 | |
| VU0506572 | N/A | N/A | <120 | |
| VU0522368 | N/A | N/A | <120 | |
| VU0644767 | N/A | N/A | <120 | |
| VU0649732 | N/A | N/A | <120 | |

## 2.5.2 BT-PSP Scaffold Investigation

### 2.5.2.1 Selection of Scaffold

Based upon that information, the lack of existing NAPE-PLD activators, and the importance of increasing NAPE-PLD activity in cardiometabolic diseases, we decided to limit our research into the new NAPE-PLD inhibitors and instead make this newly discovered activator scaffold the focus of our research. It was named the benzothiazole-phenyl-sulfonamide class (BT-PSP) after its defining structural moieties (Figure 15).
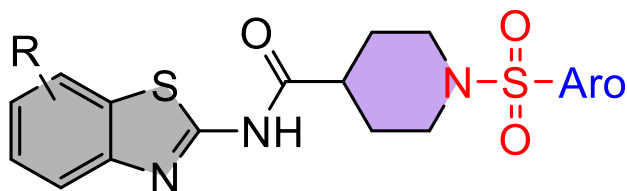


**Figure 15.** BT-PSP scaffold diagram. Structural groups responsible for the name of the BT-PSP scaffold are shaded (benzothiazole group in gray, piperidine in lilac, sulfonamide in red, and phenyl in blue). R groups are substituted around the 6-membered ring portion of the benzothiazole group and include various numbers and arrangements of methyl and methoxy groups. Aromatic rings (blue) are typically phenyl groups with mono-halogen substitutions.

### 2.5.2.2 Testing of New Compounds and Batches

To expand our selection of BT-PSPs, Dr. Margaret Jones, Dr. Kwangho Kim, and the Vanderbilt University Molecular Design and Synthesis Center (SynCore) made 9 additional compounds. Also, to control for batch effects, all other BT-PSPs were either re-synthesized by Dr. Kim of the SynCore or were re-ordered from the original vendor by the Vanderbilt HTS Core. Two BT-PSPs were not included in this process: VU0506572 and VU0506541. The former because it showed poor activity but could not be considered inactive, and the latter because we had difficulty obtaining a new stock of it. I performed CRCs on all new stocks of compounds, and then replicated those results one or more times. The results are summarized in the next sub-section, and the synthetic mechanisms for the synthesized compounds are provided in the original publication of their discovery.[127]

At the same time as the BT-PSPs, I performed CRCs on several other compounds. I replicated the CRCs of 5 of the top inhibitor hits, confirming their activities

(Figure 16 A-E). I tested two published NAPE-PLD inhibitors: ARN-19874 and LEI-401,[124, 125] because I had previously seen a lack of efficacy from ARN-19874 and wanted to replicate that result and see if it also applied to LEI-401. ARN-1974's lack of efficacy was confirmed and is still unexplained (Figure 16 F), though may be due to poorer quality of the commercially available product compared to the original synthesized product. LEI-401 was considerably less potent than had been reported in its original publication (Figure 16 G),[125] but it is possible that our different experimental design and our use of mouse rather than human NAPE-PLD were responsible for that. Finally, to assist in testing our novel fluorogenic NAPE-PLD substrate (Chapter 4), I tested two inhibitors of enzymes with phospholipase $A_1$ activity to see if they would interfere with our results by modulating Nape-pld (Figure 16 H and I). Neither compound modulated Nape-pld to a meaningful extent.
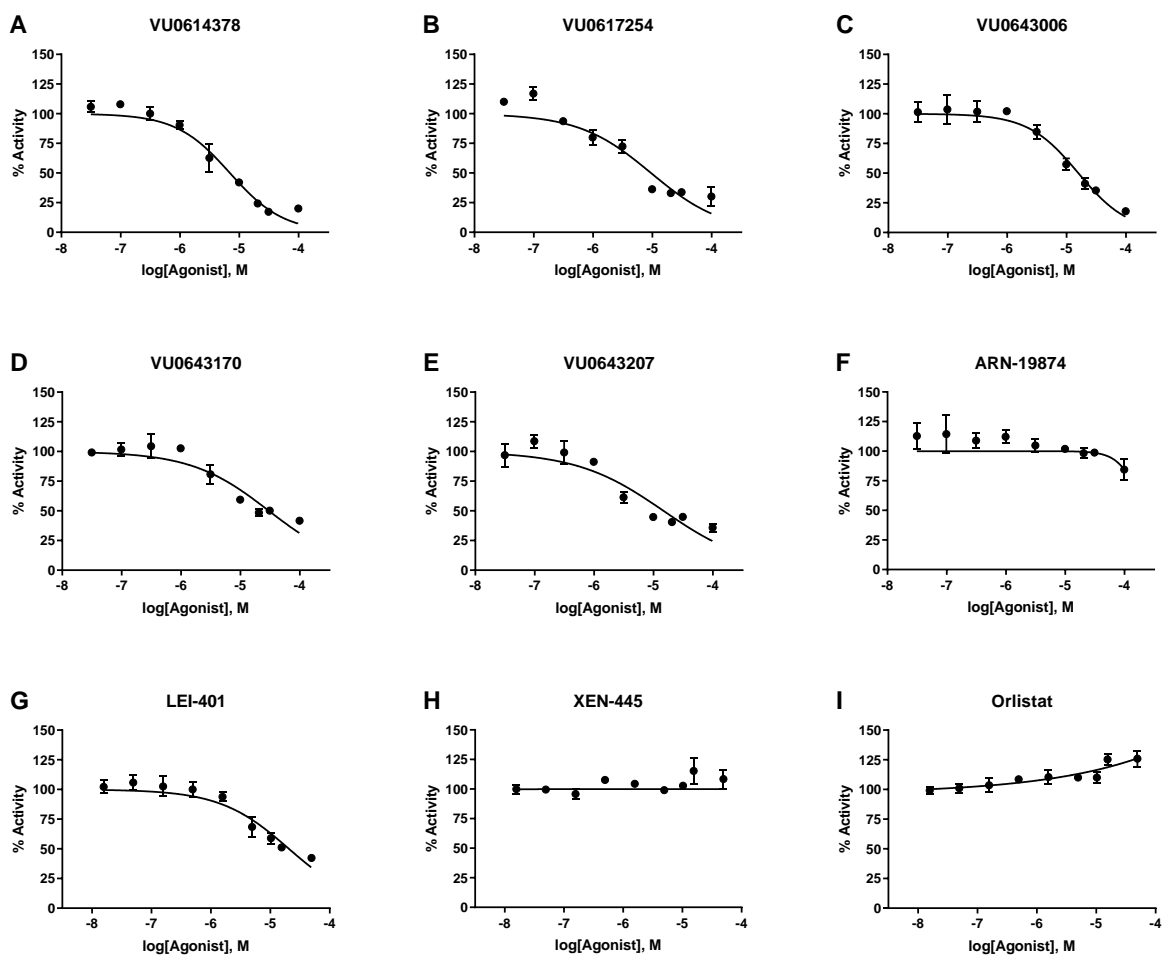
**Figure 16.** Nape-pld CRCs of miscellaneous compounds. Individual points are mean ± SD from 3 replicate wells. Inhibitor curves were calculated using log(inhibitor) vs. normalized response, variable slope in GraphPad Prism 9. Activator curve (I) was calculated using log(agonist) vs. response, variable slope (four parameters) in GraphPad Prism 9. Graphs with flat curves did not show sufficient dose-dependent activity changes to generate a well-fitting curve.

### 2.5.2.3 BT-PSP CRC Results

The final summary results of the BT-PSP CRCs using either re-ordered or re-synthesized compound batches are shown in Table 6 (the full CRC curves are in Figure A4 in Appendix). In total, we identified twenty promising NAPE-PLD activators with low-micromolar or high-nanomolar potencies that strongly increased Nape-pld activity. Two additional analogs had little to no effect on Nape-pld despite having similar structures to the other compounds, which made them especially useful for comparing the effects of NAPE-PLD activation to the effects of the BT-PSP scaffold itself.

**Table 6.** Summary of BT-PSP Nape-pld CRC results. Compounds were either purchased from commercial source or prepared in house by chemical synthesis, each CRC was performed on two or more replicate days. Values calculated using non-linear curve fits (log(agonist) vs. response, variable slope—four parameters). $EC_{50}$ is concentration needed for 50% maximal activator effect, expressed in µM. $E_{max}$ is maximal efficacy expressed as fold-increase in Nape-pld activity versus vehicle only. [a] 95% CI for $EC_{50}$ and $E_{max}$ indeterminant due to poor curve fit. [b] Not active.

| Compound Identification Number | Structure | $EC_{50}$ (95% CI) | $E_{max}$ (95% CI) | Compound Identification Number | Structure | $EC_{50}$ (95% CI) | $E_{max}$ (95% CI) |
|---|---|---|---|---|---|---|---|
| VU0506484 | | 2.3 (1.8-3.1) | 2.1 (2.0-2.2) | VU05060601 | | 0.94 (0.71-1.2) | 1.8 (1.8-1.9) |
| VU0506485 | | 12.0 (7.3-85.9) | 2.0 (1.8-4.0) | VU0506605 | | 0.74 (0.50-1.22) | 2.1 (2.0-2.2) |
| VU0506486 | | 0.32 (0.15-0.58) | 1.8 (1.7-1.9) | VU0934231 | | 1.1[a] | 2.0[a] |
| VU0506488 | | 3.3 (2.7-4.2) | 1.7 (1.6-1.8) | VU0934205 | | N/A[b] | <1.2 |
| VU0506539 | | 0.74 (0.46-1.1) | 1.7 (1.6-1.8) | VU0934212 | | 2.5 (1.8-3.3) | 1.6 (1.5-1.6) |
| VU0506542 | | 0.95 (0.66-1.36) | 1.9 (1.9-2.0) | VU0934233 | | N/A[b] | <1.2 |
| VU0506517 | | 1.1 (0.9-1.4) | 2.0 (2.0-2.1) | VU0934209 | | 3.5 (2.4-5.4) | 1.9 (1.8-2.1) |
| VU0506534 | | 0.30 (0.17-0.47) | 2.1 (2.0-2.2) | VU0934227 | | 4.1 (2.6-9.1) | 1.7 (1.6-1.9) |
| VU0506533 | | 0.30 (0.16-0.44) | 2.6 (2.6-2.8) | VU0934210 | | 1.8 (1.3-2.3) | 2.4 (2.3-2.6) |
| VU0506536 | | 1.1 (0.7-1.6) | 2.3 (2.2-2.4) | VU0934203 | | 4.8 (3.2-7.4) | 1.8 (1.7-2.0) |
| VU0506575 | | 0.57 (0.34-0.92) | 2.4 (2.3-2.5) | VU934211 | | 1.4 (1.0-1.9) | 2.1 (2.0-2.2) |

## 2.6 Conclusions

In order to better study the role of NAPE-PLD in cardiometabolic diseases, we needed new small-molecule modulators of its activity—ideally activators. To find such molecules, Dr. Aggarwal and the Davies Lab first developed a NAPE-PLD activity assay and used it to identify and characterize 14 new NAPE-PLD inhibitors. Next, I further optimized the activity assay and used it to screen nearly 40,000 compounds for NAPE-PLD modulators. This yielded 1,404 hits, for a total hit rate of 3.6%. After replicating our

results and conducting some limited SAR, we discovered that all of our best activators shared a common core structure. We named this the BT-PSP scaffold, and then evaluated a series of BT-PSPs for modulation of Nape-pld activity. We observed that the BT-PSPs are a potent and efficacious class of Nape-pld activators.

The experiments described in this chapter yielded a suite of Nape-pld activators with sufficiently low $EC_{50}$ (half-maximal effective concentration) and sufficiently high $E_{max}$ (maximum inducible activity) to be considered useful research tools. On top of that, we discovered the first true NAPE-PLD activators (with reasonable potency and replicable activity[69]). As discussed previously, NAPE-PLD activators have the potential to dramatically change the landscape of NAPE-PLD research, cardiometabolic disease research, and cardiometabolic disease treatments. However, at this point, the BT-PSPs were not yet ready to be used by others. We first needed to validate their ability to modulate NAPE-PLD, characterize their activity, and determine how selective they were for NAPE-PLD.

**2.7 Methods**

2.7.1 Pilot Study

*2.7.1.1 Reagents*

Recombinant hexahistidine-tagged mouse Nape-pld was expressed and purified as described previously.[117] *N*-((6-(2,4-DNP)amino)hexanoyl)-1-(BODIPY™ FL C$_5$)-2-hexyl-*sn*-glycero-3-phosphoethanolamine (PED-A1) and BODIPY™ FL C$_5$ were purchased from Thermofisher scientific, USA. Rabbit anti-NAPE-PLD primary antibody was obtained from Abcam. Human embryonic kidney 293 (HEK-293) cells were purchased from American Type Culture Collection (Manassas, VA). The fourteen hit inhibitor compounds used for confirmation were purchased from MicroSource Discovery Systems, Inc. Dulbecco's modified Eagle's medium (DMEM medium), optiMEM (1X) reduced serum medium and heat-inactivated fetal bovine serum (HI-FBS) were from

Gibco chemicals. Lithocholic acid and 3-(4,5-dimethylthiazol-2-yl)-2,5-diphenyltetrazolium bromide (MTT) were purchased from Millipore-Sigma. N-octyl-β-D-glucoside (NOG) was obtained from Cayman Chemicals (Ann Arbor, MI). Standard protein molecular weight marker was purchased from Invitrogen. Nickel nitrilotriacetic acid-agarose was from GE Healthcare. The Spectrum Collection compound library was provided by the Vanderbilt University High Throughput Screening Core facility and was originally obtained from MicroSource (Gaylordville, CT). The collection includes a wide range of biologically active and structurally diverse compounds consisting of active drugs (50%), natural products (30%) and other bioactive components (20%).

*2.7.1.2 Boiled Nape-pld Activity Assay*

Recombinant mouse Nape-pld or boiled Nape-pld was diluted in assay buffer containing 50 mM Tris-HCl, pH 8.0 and 1% NOG to a final concentration of 1.0 µM and incubated with 10 µM PED-A1. Fluorescence (ex/em 488/530 nm, fixed bandwidth 16 nm) was measured at 1-minute time points for 2 h in 96-well plate reader (Synergy H1 Hybrid Multi-Mode Reader, BioTeK).

*2.7.1.3 NAPE-PLD Activity Assay Optimization*

The $K_M$ for PED-A1 hydrolysis by recombinant mouse Nape-pld was determined by enzyme kinetics. Briefly, Nape-pld was diluted in assay buffer to a final concentration of 4.5 µg mL$^{-1}$ and enzyme kinetics was performed in a 384-well plate using 0–20 µM PED-A1. Fluorescence (excitation 482±18 nm; emission 536±20 nm) was measured for 15 min using a Wavefront Panoptic kinetic imaging plate reader.

The effect of varying the concentration of NOG (0–1%) concentration was measured using final concentration of 4 µM PED-A1 and 4.5 µg mL$^{-1}$ Nape-pld. For the DMSO tolerance test, DMSO (35 nL–900 nL) was transferred onto an empty 384-well plate using an Echo liquid handler. Then, 30 µL of 4.5 µg mL$^{-1}$ enzyme diluted in assay buffer containing 0.4% NOG (w/v) was dispensed into the DMSO-containing plate using a Bravo liquid handler robot, followed by 5 µL PED-A1 (final concentration 4 µM) and fluorescence kinetics (ex/em 482/536 nm) measured for 15 min.

The consistency of replicates across the 384-plate was determined using the final optimized concentrations of DMSO (1.6%, v/v), NOG (0.4%, w/v), and 4.5 µg mL$^{-1}$ Nape-pld, with replicates of the NAPE-PLD inhibitor, lithocholic acid (LCA), dispersed in checkerboard pattern across the plate ("Checkerboard Assay"), and then 5 µL PED-A1 (4 µM final concentration) added. The Z' score for LCA inhibition across the plate was calculated as Z' = 1 – [3(X + X')/(Y – Y')], where Y and Y' are the mean values of PED-A1 produced fluorescence in the absence and presence, respectively, of LCA as a control inhibitor at initial rate of reaction. X and X' are standard deviation of PED-A1 produced fluorescence.

*2.7.1.4 Pilot Screening*

Screening was performed on 2,388 compounds. 35 nL of 10 mM test compounds and 140 nL of 100% DMSO were combined in black-walled, clear bottom 384-well plates using an Echo Acoustic liquid handler, resulting in a final compound concentration of 10 µM for the primary screen. 175 nL of 20 mM LCA or 175 nL of DMSO were added to control wells as inhibited and uninhibited signal controls, respectively. 30 µL of 4.5 µg mL$^{-1}$ Nape-pld enzyme in buffer solution with 0.4% NOG (w/v) was dispensed in each well using an Agilent Bravo robotic liquid handler. Plates were incubated at 37 °C for 1 h. The assay was initiated by the Panoptic instrument's internal Bravo robotic liquid handler when it dispensed 5 µL of PED-A1 (4 µM final) in buffer solution (1.6% DMSO final, v/v) to each well. Changes in fluorescence (ex/em 482/536 nm) were measured for 15 min. Initial slope measurements used slope from t = 30-100 s.

To assess effect of compounds on BODIPY fluorescence, 4 µM of BODIPY FL C$_5$ was incubated with or without 10 µM of each compound in total 80 µL of 50 mM Tris-HCl (pH = 8.0) in a 96-well plate and fluorescence (ex/em 482/536 nm) measured for 30 min using a Biotek Synergy H1 plate reader.

Screening and most CRC experiments were performed in the Vanderbilt High-Throughput Screening (HTS) Core Facility with assistance provided by Dr. Paige Vinson and Corbin Whitwell. The Spectrum Collection was distributed by the Vanderbilt HTS

Core. The WaveFront Biosciences Panoptic kinetic imaging plate reader is housed and managed within the Vanderbilt HTS Core Facility, an institutionally supported core.

## 2.7.1.5 Concentration-Response Curves

The $IC_{50}$ for each hit compound was determined using similar conditions as for screening except that concentration of inhibitor was varied from 0 to 200 µM. The averaged initial slope measurements for Nape-pld activity in the absence of inhibitor were set as 100% activity and the normalized % activity calculated by dividing the initial slope observed with each concentration of inhibitor by this value. Fitting of the response curve and calculation of the $IC_{50}$ and 95% confidence interval (95% CI) was performed using log(inhibitor) vs. normalized response -variable slope analysis in GraphPad Prism version 7.04.

## 2.7.1.6 Cytotoxicity

The effects of the compounds on the viability of HEK-293 cells were determined using MTT assay to measure changes in cellular redox state. Briefly, $10 \times 10^4$ HEK-293 cells/well were seeded in 24-well plates for 24 h. Cells were treated with a concentration of each compound that represented 500% of the $IC_{50}$ concentration determined in the CRC assay ($5 \times IC_{50}$) prepared in opti-MEM reduced serum media containing 1% HI-FBS for 24 h (Gibco 21985-070). After treatment, media was removed, and 300 µL of 0.5 mg mL$^{-1}$ MTT solution was added. After 3 h, the media was removed, the purple crystals dissolved in 100 µL of DMSO, and 80 µL transferred to 96-well plate, and absorbance measured at 590 nm. Percent viability was normalized to cells treated with vehicle (DMSO) only.

## 2.7.1.7 Cellular NAPE-PLD Activity

HEK-293 cells in DMEM buffer containing 4.5 g L$^{-1}$ glucose, 4 mM L-glutamine, 1 mM sodium pyruvate, phenol red and supplemented with 10% HI-FBS were seeded at ~20,000 cells/well in tissue culture-treated, clear-bottom, black-walled, 96-well plates. After reaching ~95% confluency (48 h), the medium was removed and replaced with similar DMEM buffer (70 µL per well) except without phenol red or HI-FBS. 5 µL of inhibitor or vehicle solutions were then added to each well to generate final

concentrations of inhibitors of 0.2–20 μM. 30 min after addition of inhibitors, 5 μL of 56 μM PED-A1 was added to each well (3.5 μM final concentration), and fluorescence signal (ex/em 488/530 nm) was recorded every minute for 25 min in Synergy H1 plate reader. NAPE-PLD activity was measured as the increase in fluorescence from time = 1-25 min and normalized to average activity found in absence of inhibitor. For each concentration of inhibitor, 3 replicate wells on two separate days were measured (n = 6 wells total) and mean ± SEM (standard error of the mean) determined.

## 2.7.2 Modulator Identification

### 2.7.2.1 HTS Method and Modifications

Starting with the final assessment of the PED-A1 dilution, all remaining assays in this chapter utilized a variation of the HTS method described in *2.2.3.2*. Therefore, I will detail those variations here. Each assay will be preceded by a letter, to help separate them from each other. (A) For the final PED-A1 dilution assay, the wells used are described alongside the results (all other wells were left empty). The camera settings that worked best for the dilution that was used in the HTS assay were: camera temperature of -70 °C, exposure 30 ms, emission gain of 111, pre-gain of 1, 1x1 binning, 1000 ms cycle time, no flat field correction, no well mask. (B) The modifications to the HTS method used in the checkerboard assay are described in the main text. (C) In the replication assays, the only modification to the HTS method was in compound plating. Wells A3-22 and P3-P22 were left empty; inhibitor (10 μM Bith) controls were in wells A1, A2, P1, P2, A23, A24, P23, and P24; vehicle controls were in columns, 2, 6, 10, 14, 18, 22, and 23 (excluding the top and bottom rows); in columns 1 and 24 were alternating enzyme-free and vehicle controls, reversed in order between them, and excluding the top and bottom rows. Test compounds were plated in triplicate in the remaining wells of the plate, and were arranged so as to minimize any location-based differences in signal. (D) In the concentration-response curve (CRC) assays, columns 1, 2, 23, and 24 were the same as in the replication assays, except the inhibitor control wells were left empty. Rows A and P were completely empty. Columns 3-22 of rows B,

F, J, and N contained vehicle-treated controls, as did rows B-O of columns 12 and 13. Columns 3-11 and 14-22 of row O contained the same doses of Bith as were used for the test compounds; this was included as a control to confirm assay viability for each plate. Finally, the remaining wells contained graded concentrations of test compounds, in triplicate, arranged for ease of compound distribution.

*2.7.2.2 Materials*

Initial stocks of candidate modulators were purchased from Life Chemicals and provided by the Vanderbilt University HTS Core. After the replication assay, candidate modulator compounds were repurchased from the same manufacturer or were synthesized by the SynCore, to check for batch effects. The results of the CRCs and all subsequent assays using BT-PSPs were performed using the re-ordered or re-synthesized stocks of the compounds. BT-PSP synthesis information can be found in the paper from which these results have been adapted.[127] *N*-palmitoyl-dioleoyl-PE (C16-NAPE) was purchased from Avanti Polar Lipids. PED-A1 was purchased from Millipore-Sigma, and BODIPY FL $C_5$ was purchased from ThermoFisher Scientific.

The method for expression and purification of recombinant mouse Nape-pld was performed as follows. *Escherichia coli* (*E. coli*) DH5α cells bearing a pQE80L1 plasmid conferring ampicillin resistance and expression of recombinant wild-type mouse *Napepld* with a C-terminus hexahistidine tag was used for mouse Nape-pld expression.[126] Bacteria were grown in 2 L of media (Luria Broth with 100 µg/mL ampicillin) at 37 °C, expression was induced using isopropyl β-D-1-thiogalactopyranoside (IPTG) (Sigma I5502) when $OD_{600}$ = 0.5-0.8 (optical density at 600 nm), and expression was carried out at 28 °C for 16 h. Pelleted cells were lysed using both probe sonication and lysozyme (MP Biomedicals 100834), and purified using cobalt affinity beads according to manufacturer specifications (Cytiva Life Sciences 28957499). After elution from the column with 250 mM imidazole, protein was pooled and dialyzed in Hank's balanced saline solution (HBSS) with 6-8 kDa molecular weight cutoff dialysis tubing (Spectra/Por 1). During cell lysis and in all subsequent steps until dialysis, protease inhibitors were present (Sigma 04693132001). Following dialysis, the pooled protein was concentrated using 10 kDa molecular weight cutoff centrifuge tubes

(Millipore-Sigma). Protein concentration was determined using a Bradford assay (Bio-Rad).

### 2.7.2.3 Analyses

All statistical analyses and non-linear regression analyses were performed using GraphPad Prism 9 software, except for calculation of B-scores and initial fluorescence slopes, which were calculated using WaveGuide software (WaveFront Biosiences). All chemical structures were generated using ChemDraw Professional 22.0 software (PerkinElmer Informatics). Unless stated otherwise, all experiments were replicated two or more times on separate days, normalized to same-day controls, and combined for analysis.

### 2.7.2.4 HTS Core Acknowledgement

Screening and CRC experiments were performed in the Vanderbilt High-Throughput Screening (HTS) Core Facility with assistance provided by Dr. Paige Vinson, Dr. Joshua Bauer, and Corbin Whitwell. The Discovery Collection was distributed by the Vanderbilt HTS Core. The WaveFront Biosciences Panoptic kinetic imaging plate reader is housed and managed within the Vanderbilt HTS Core Facility, an institutionally supported core.

# CHAPTER 3

## Compound Characterization

Having discovered a series of first-in-class NAPE-PLD activators, we next performed experiments designed to characterize their activities. We did this by verifying their modulation of NAPE-PLD, characterizing their mechanism of action on NAPE-PLD, and determining their selectivity for NAPE-PLD. In addition to determining how the BT-PSPs work, these experiments would test their usefulness in future research efforts.

Calcutt and Brian Hachey. Allison Pickens also assisted with LC/MS assay development. Drs. Raymond Blind and Alex Waterson assisted with conceptualization of target engagement assays. Experiments performed in the laboratory of Dr. D. Borden Lacy were conducted with the help of Dr. Heather Kroh.

## 3.1 Validation Assays

Thus far, we had only tested our compounds in one type of assay: PED-A1-based. While PED-A1 is a close analog of native NAPEs, the two are not identical. Therefore, we needed to perform orthogonal assays in order to validate our compounds' ability to modulate Nape-pld's hydrolysis of NAPEs.

### 3.1.1 Fluorescence Interference Test

To determine whether our hits were identified simply because they augmented or inhibited the fluorescence of our reporter molecule, I conducted a fluorescence interference assay on the HTS hits with the best B-scores (non-BT-PSPs included). The format of this assay was the same as the Nape-pld activity replication assay (section 2.4), but with BODIPY FL $C_5$ in place of PED-A1. Under these conditions, only one of the tested compounds significantly altered fluorescence (Figure 17), and it was a compound bearing a known fluorophore (VU0549410). As the other compounds did not either enhance or diminish BODIPY fluorescence, we concluded that they did not score as hits simply due to this form of assay interference.
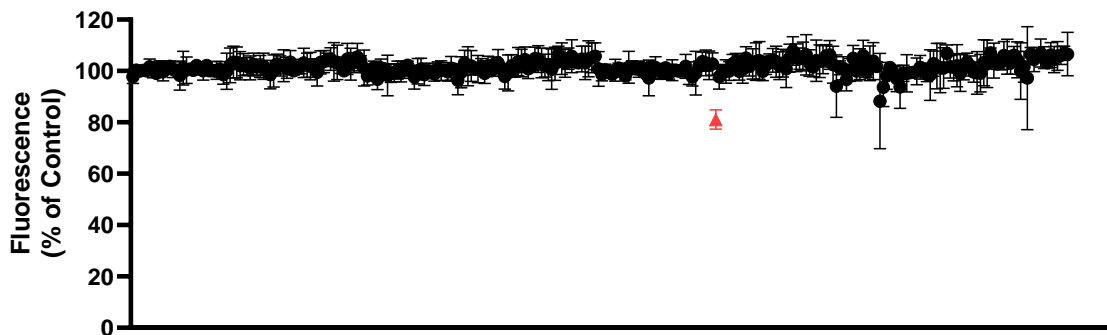
**Figure 17.** Top HTS hits did not interfere with fluorescence. Effect of candidate modulators on BODIPY FL $C_5$ fluorescence (ex/em 482/536 nm), normalized to vehicle-treated controls. Each point represents the mean ± SD of 3 technical replicates of one compound. Within each test plate (four total), an ordinary one-way ANOVA with Dunnett's multiple comparisons test was run. The compound shown as a red triangle significantly differed from control ($p<0.0001$) and was eliminated from further evaluation. All other compounds did not significantly differ from control.

### 3.1.2 *In Vitro* LC/MS Assay Development

In order to assess whether the BT-PSPs would affect NAPE-PLD's hydrolysis of genuine NAPEs, we first needed to establish an assay that directly measured the NAPE substrates and the NAE products of NAPE-PLD hydrolysis. A liquid chromatography-mass spectrometry (LC/MS)-based assay was perfectly suited to these needs. Over the course of nearly two years, members of the Davies lab (Dr. Sean Davies, Allison Pickens, Isabelle Paz, Andrew Jenkins, and myself) troubleshot various components of the assay until we discovered a set of parameters that would allow us to measure the conversion of NAPEs to NAEs *in vitro*. The full methods are detailed in section 3.5, but the most impactful alteration was using *N*-acylated dihexanoyl-PEs as our NAPE species. This helped the NAPEs remain in solution and, therefore, be available to the Nape-pld for hydrolysis. The use of hexanoyl chains in the non-reacting positions of lipids is well-established practice in lipid research, as it helps to overcome this common hydrophobicity problem.[134-137]

### 3.1.3 *In Vitro* LC/MS Test

Using this method, Andrew Jenkins and I were able to test whether or not our best BT-PSPs would modulate Nape-pld's hydrolysis of true NAPEs. Recombinant mouse Nape-pld was pre-treated with VU0506534 (activator), VU0506533 (activator), VU0934233 (neutral), or vehicle for 30 min, then 1,2-dihexanoyl-*sn*-glycero-3-phosphoethanolamine-*N*-oleoyl (NOPE) was added and the reactions were incubated at 37 °C for 90 min. Then, the levels of unreacted NOPE and produced OEA were measured by LC/MS. Both VU0506534 and VU0506533 significantly increased the OEA/NOPE ratio, while VU0934233 had no significant effect (Figure 18). These results validated our compounds' ability to modulate Nape-pld (or not modulate, in the case of VU0934233), as their activity using NAPE as a substrate matched their activity when using a fluorogenic substrate.
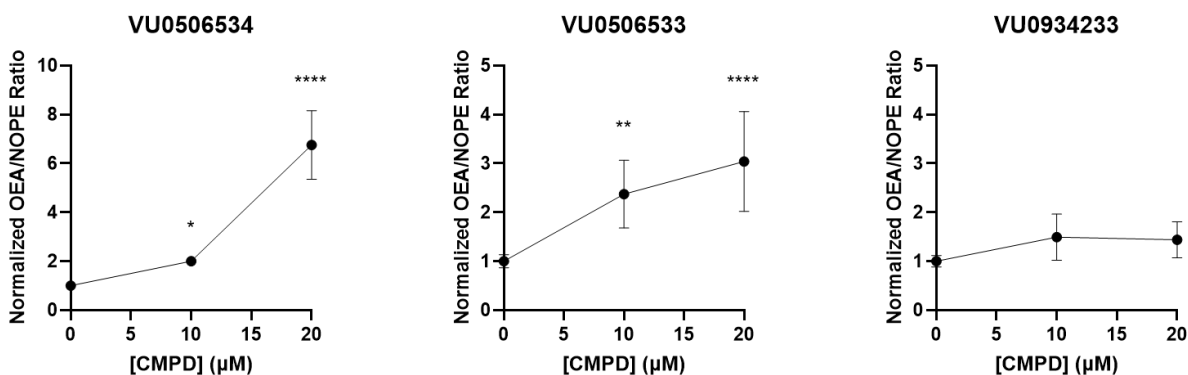


**Figure 18.** BT-PSP effects validated by LC/MS assay *in vitro*. Activity of recombinant mouse Nape-pld using N-oleoyl-phosphatidylethanolamine (NOPE) as substrate, with measurement of NOPE and resulting OEA by LC/MS/MS. Ratio of OEA to NAPE was normalized to 0 µM compound control. Points represent mean ± SD from 6 replicates (two days, 3 replicates per day). The assays of VU0506534 and VU0934233 were performed using the same 0 µM compound replicates, as they were run on the same days. 1-way ANOVA for VU0506534 and VU0934233 $p=0.0243$, and for VU0506533 $p<0.0001$. Results from Dunnett's multiple comparison test for individual compounds are represented by *$p=0.0374$, **$p=0.0029$, ****$p<0.0001$.

## 3.2 Activity Characterization

Small-molecule enzyme modulators operate through a variety of mechanisms. Some of these mechanisms rely on the molecule upregulating the transcription of the

enzyme ("inducers"). In other mechanisms, the small molecule binds to a ligand or substrate and ensures that it reaches the enzyme ("chaperones"). And in still other mechanisms, the molecule binds to the enzyme itself to modulate its activity. To this point, we had been measuring compound-induced changes in Nape-pld activity using purified enzyme. So, we would be unable to see a change in activity if the compounds were inducers. But if they served as chaperones, that would be a problem because they would potentially not do so when outside of the confines of our *in vitro* assay. Therefore, we performed studies designed to characterize the nature of the interaction between our compounds and NAPE-PLD, and to determine whether their effects were due to direct engagement of NAPE-PLD or to effects on its substrates.

### 3.2.1 Competition Assays

Some of these studies were competition assays. I conducted the first such assay *in vitro* using three compounds of interest: a NAPE-PLD inhibitor (LEI-401),[125] a BT-PSP NAPE-PLD activator (VU0506534), and an inactive BT-PSP compound (VU0934233). When administered alone, LEI-401 dose-dependently decreased PED-A1 hydrolysis down to nearly 0 activity at the highest dose (Figure 19 A). In the presence of VU0506534, LEI-401 again dose-dependently decreased activity, but up until the highest dose (where the ratio of LEI-401 to VU0506534 was five to one) there was still increased activity from VU0506534. This was consistent with VU0506534 behaving as a positive allosteric modulator, whose effects can still be seen when adding an inhibitor until so much inhibitor is present that any activation is ineffectual. When the data were normalized to either vehicle alone (for LEI-401 doses without VU0506534) or to VU0506534 alone (for LEI-401 doses with VU0506534), we could see that LEI-401 inhibited Nape-pld to the same extent at each dose, with or without VU0506534 present (Figure 19 B). This indicated that LEI-401 and VU0506534 do not affect each other's ability to modulate the enzyme. In total, these data were consistent with VU0506534 acting as a positive allosteric modulator of NAPE-PLD, and binding to a different site than LEI-401.
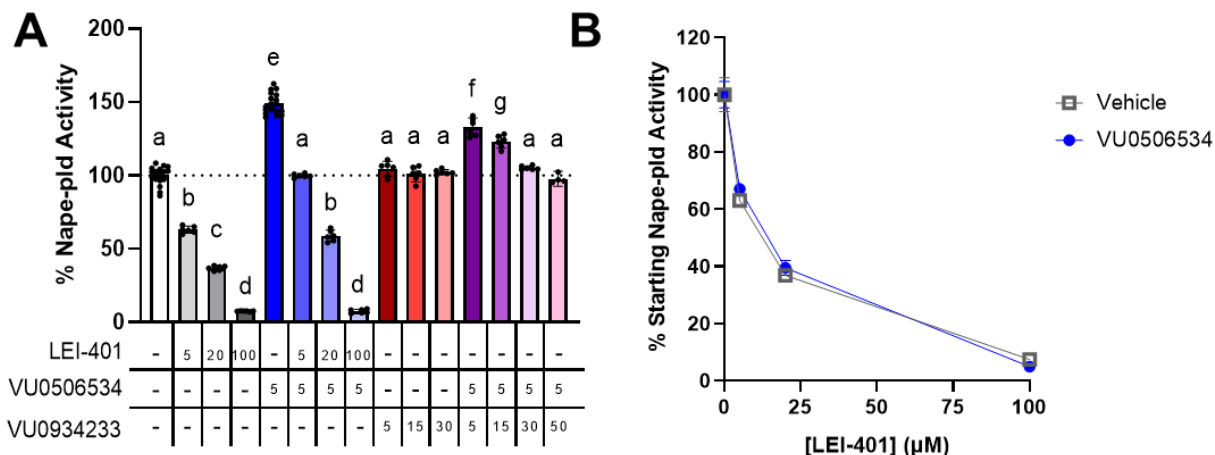
**Figure 19.** VU0506534 competes with analog but not LEI-401 for Nape-pld binding *in vitro*. **A.** Effects of compounds on PED-A1 hydrolysis by recombinant mouse Nape-pld, normalized to vehicle-only controls. Compound concentrations are listed in µM (- means 0 µM). Bars show mean ± 95% CI. Ordinary one-way ANOVA, $p<0.0001$. Tukey multiple comparisons test was run to compare all groups with each other, groups sharing letters did not significantly differ from each other ($p>0.05$). **B**. Data from same competition assay data, re-normalized to either 0 µM LEI-401 + 5 µM VU0506534 for all samples containing VU0506534 ("VU0506534" line), or to 0 µM LEI-401 + 0 µM VU0506534 for all samples without VU0506534 ("Vehicle" line). Samples treated with the same concentration of LEI-401, with or without VU0506534 present, did not significantly differ, according to Šídák's multiple comparisons test. Points are mean ± SD.

I also utilized the inactive BT-PSP, VU0934233, in this competition assay. At every dose tested, VU0934233 alone had no effect on Nape-pld activity (Figure 19 A). When in the presence of VU0506534, however, VU0934233 dose-dependently eliminated the augmentative effects of VU0506534. This was not an inhibitory effect that only manifested when the two compounds could interact, as a dose of VU0934233 well above that needed to completely eliminate VU0506534-enhanced activity caused no significant reduction in activity from the next-lowest dose. Instead, it appeared that VU0506534 and VU0934233 bind to Nape-pld at the same site—which made sense given their structural similarities—but that VU0506534 caused an allosteric change that increases enzyme activity while VU0934233 did not. And as more VU0934233 was added, less VU0506534 could bind to their shared binding site and so the activity returned to that seen when only VU0934233 was present. Again, these data were consistent with VU0506534 acting as a positive allosteric modulator of NAPE-PLD.

I also performed a competition assay in cultured cells, which is detailed in Chapter 5 (section 5.3.2). The relevant conclusions from this assay were that VU0506534 modulated PED-A1 hydrolysis in cells by acting on Nape-pld, and that Bith and VU0506534 did not affect each other's ability to modulate the enzyme. These data further indicated that VU0506534 and, by extension, the other BT-PSPs are positive allosteric modulators of NAPE-PLD.

### 3.2.2 Michaelis-Menten Kinetics

Another informative way of characterizing the nature of a modulator's effects on an enzyme is to construct a Michaelis-Menten kinetics curve. In this, reaction rate with and without the test compound present are plotted as a function of substrate concentration.
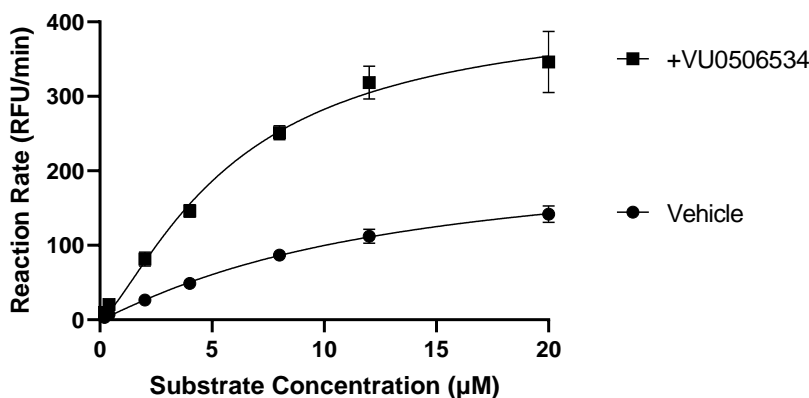


**Figure 20.** Michaelis-Menten kinetics of VU0506534. $K_{1/2}$ and $V_{max}$ for Nape-pld hydrolysis of flame-NAPE with vehicle (DMSO) were 12.9 µM and 227 RFU/min, respectively. $K_{1/2}$ and $V_{max}$ for hydrolysis with 10 µM VU0506534 were 5.9 µM and 421 RFU/min, respectively. Activity was measured as slope of fluorescence signal from recombinant mouse Nape-pld hydrolysis of fluorogenic substrate during the linear phase (1-4 min) of the reaction. Reaction kinetics values calculated using allosteric sigmoidal non-linear regression curves. Points are mean ± SD from 12 replicates (6 per experiment, two replicate days).

My results (Figure 20) indicated that VU0506534 increased Nape-pld activity both by increasing substrate affinity (decreasing $K_{1/2}$) and by increasing maximum reaction velocity ($V_{max}$). Had only the $K_{1/2}$ (concentration of substrate that produces a half-maximal enzyme response) changed, it would have been possible that VU0506534 was serving as a chaperone for the substrate. But since both $K_{1/2}$ and $V_{max}$ changed, it was

much more likely that VU0506534 binds to the enzyme and induces a conformation change that increases substrate binding and catalysis. This conclusion was corroborated by the fact that VU0934233 and VU0934205 had no effect on PED-A1 hydrolysis despite their structural similarities to the other BT-PSPs. While small structural differences can affect a compound's binding interactions on an enzyme, they are less likely to affect a compound's ability to chaperone a substrate to the enzyme.


3.2.3 Target Engagement

We next performed a series of experiments with the goal of validating the claim that BT-PSPs modulate NAPE-PLD by inducing conformational changes after binding directly to the enzyme.

3.2.3.1 Thermal Shift Assay

The first assay that Dr. D. Borden Lacy's laboratory at Vanderbilt University and I performed was differential scanning fluorimetry. When a protein binds to a molecule, its structure changes and becomes either more or less stable. This change in stability can be detected as a change in the temperature at which the protein loses structural integrity ("melts"). Therefore, the melting temperatures of purified, recombinant mouse Nape-pld with and without VU0506534 were measured using a Tycho NT.6 instrument (NanoTemper). Since our enzyme assay is normally conducted in the presence of a detergent, we also performed this experiment using our typical detergent (NOG) and a detergent often used by other groups (Triton X-100).[124, 126] However, under all conditions tested, the enzyme yielded low signals and misshapen curves (Figure 21).[138] As a result, this experiment was inconclusive. The only conditions where the curves appeared to be somewhat normal were in the presence of Triton X-100.
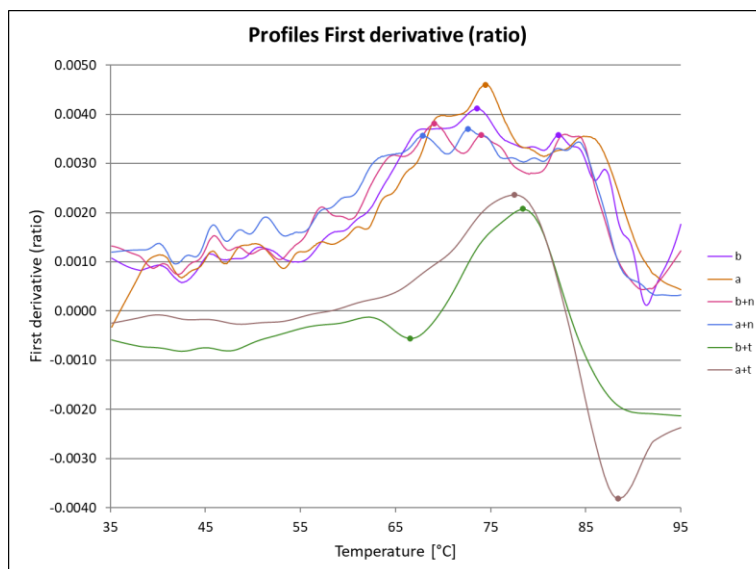
**Figure 21.** Thermal shift assay yields no conclusive information. b is Nape-pld + vehicle, a is Nape-pld + VU0506534 (33 µM), b+n is b with added NOG (0.4% w/v), a+n is a with added NOG (0.4% w/v), b+t is b with added Triton X-100 (0.1% v/v), and a+t is t with added Triton X-100 (0.1% v/v). The shapes, amplitudes, and texture of these curves indicated assay failure.

### 4.2.3.2 Detergent Assays

To further probe the effects of detergent on Nape-pld, I first tested Nape-pld activity in the presence of Triton X-100 (0.1% v/v). Compared with our typical detergent of NOG, the enzyme had much lower activity in the presence of Triton X-100 (Figure 22 A). This was somewhat surprising, as the thermal shift assay indicated that Nape-pld structure was more stable in the presence of Triton X-100. Despite the low overall enzyme activity, VU0506534 appeared to increase activity to a higher degree in the presence of Triton X-100 than NOG (5.3-fold vs. 2.2-fold), while Bith was equally potent under both conditions (Figure 22 B-C). The reasons for this cannot yet be determined, but it is noteworthy that even with VU0506534's increased maximal activity, a 5.3-fold increase in the Triton-stabilized activity was still approximately half as much total Nape-pld activity as a 2.2-fold increase in the NOG-stabilized activity.
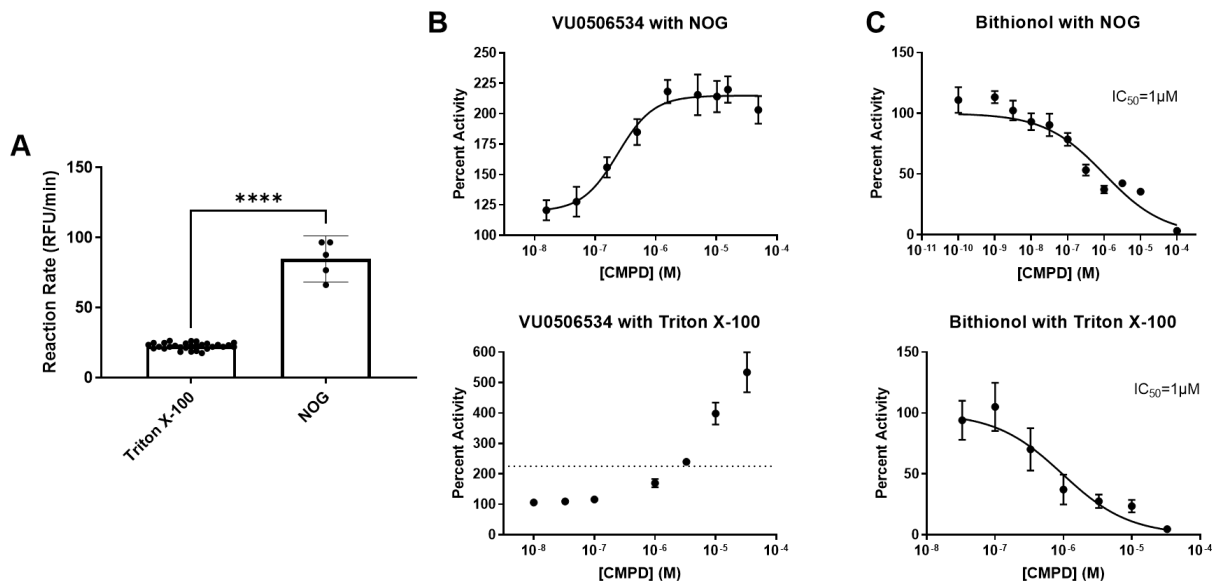
**Figure 22.** Triton X-100 and NOG differentially alter Nape-pld activity and modulation. **A.** Nape-pld reaction rate during the linear phase when solubilized by either NOG (0.4% w/v) or Triton X-100 (0.1% v/v). Two-tailed t-test, ****$p$<0.0001. Mean ± 95% CI shown. **B.** Top panel shows a sample CRC of VU0506534 with NOG used as the detergent (pulled from Chapter 2). Plotted is Nape-pld activity (RFU/min) normalized to vehicle controls. $E_{max}$ = 215%. Bottom panel shows CRC of VU0506534 with Triton X-100 used as the detergent. 215% activity shown as dotted line, maximal activity measured = 534%. All points are mean ± SD (n=3). **C.** Top panel shows a sample CRC of Bith with NOG used as the detergent (pulled from Chapter 2). Bottom panel shows a CRC of Bith with Triton X-100 used as the detergent (same non-linear regression used for both: log(inhibitor) vs. normalized response, variable slope). All points are mean ± SD (n=3).

Another detergent that I assessed was deoxycholic acid (DCA). DCA was used to help crystallize NAPE-PLD and high doses of it have been used to enhance NAPE-PLD activity in aqueous solutions.[68, 69] Therefore, we reasoned that DCA might stabilize our purified recombinant Nape-pld, and so make measuring its melting point easier. Before measuring this, I needed to determine whether VU0506534 activated Nape-pld in the presence of DCA, because if it did not then we would be unable to see an effect of VU0506534 in the thermal shift assay. Unexpectedly, I saw that DCA dose-dependently inhibited Nape-pld activity (Figure A5 A in Appendix). While VU0506534 was able to counteract this inhibition at certain doses (Figure A5 B in Appendix), the fact that DCA negatively impacted Nape-pld kinetics eliminated it from consideration as a detergent to use in thermal shift assays.

From these detergent tests, we concluded that Triton X-100 could work as the detergent when measuring Nape-pld melting temperatures, as both VU0506534 and Nape-pld behaved as expected in its presence. However, there was still the problem that the thermal shift assay signals were extremely low when we had attempted the experiment initially.

*3.2.3.3 Size-Exclusion Chromatography*

After each round of Nape-pld expression and purification, I ran an SDS-PAGE (sodium dodecyl sulfate-polyacrylamide gel electrophoresis) gel and performed either Coomassie staining or western blotting in order to confirm that I had, in fact, obtained Nape-pld. In every gel, it was apparent that I obtained several truncated forms of Nape-pld in addition to the desired full-length protein. The presence of these truncated, and likely misfolded and inactive, proteins could have contributed to the poor signals seen in the thermal shift assay. Therefore, the Lacy lab and I performed size-exclusion chromatography in an attempt to isolate full-length Nape-pld.[139]

Size-exclusion chromatography cannot be run if the protein is insoluble in aqueous solution, and it is incompatible with detergents. As NAPE-PLD is a membrane-bound enzyme and so is poorly soluble in aqueous solutions without a detergent present, we first had to remove all precipitated protein from the sample via centrifugation. We expected that this would also remove any large protein aggregates, leaving only free NAPE-PLD. An SDS-PAGE gel revealed that the size-exclusion column failed to isolate the full-length protein (Figure 23). Based on its size, the full-length protein was expected to elute in the range of fractions 6-9; instead, it eluted in fractions 3 and earlier. Those fractions contained large proteins, but no large proteins were seen in the SDS-PAGE gel. However, SDS-PAGE gels denature proteins and break up protein aggregates. Therefore, we concluded that the protein was present as large aggregates that were not broken up by the size-exclusion column. Non-denaturing (Native) PAGE gels, in which protein structures and superstructures remain intact, later confirmed this (sections *3.2.3.5* and *3.2.3.6*).
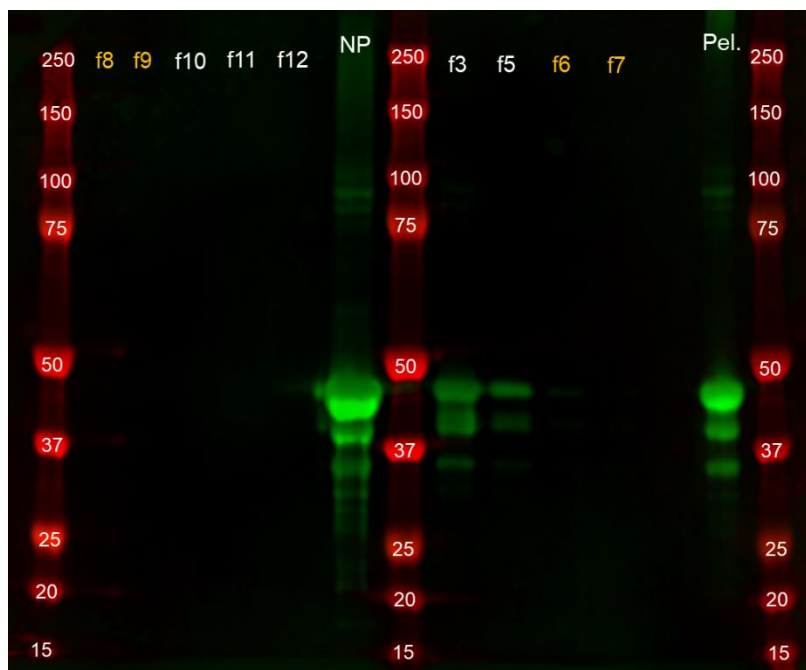
**Figure 23.** Size-exclusion chromatography western blot reveals Nape-pld present as large aggregates. f3-f12 are fractions from size-exclusion column, with lower numbers representing earlier fractions. Fractions in orange were where Nape-pld was expected to elute based on its size (46 kDa). Red bands are ladder, with molecular weights (in kDa) labelled. "NP" is crude purified recombinant Nape-pld. "Pel." is pellet of precipitate removed from the sample before it was put onto the column. Green is signal from secondary antibody.

*3.2.3.4 Denature-Renature*

We wanted to isolate full-length Nape-pld, but our protein was present as large aggregates, and we had seen that denaturing the protein with β-mercaptoethanol (BME) allowed for separation of the individual components of the aggregates. Therefore, my next experiment was to denature the aggregated Nape-pld using 8 M urea, pass it over an affinity column (the same type used to isolate the protein originally) to bind proteins with intact N-terminal hexahistidine tags, and then renature the protein by gradually removing the urea from solution. We predicted that this would not only de-aggregate the protein, but also help ensure that the protein would re-fold correctly without any other proteins surrounding it. The resulting protein had no measurable catalytic activity (data not shown), leading us to conclude that denaturing the protein would not be an effective means of de-aggregating it. As such, this line of inquiry was abandoned.

### 3.2.3.5 Native Binding

We knew that VU0506534 activated purified Nape-pld, even in its aggregated form. Therefore, if this binding induced a large conformational change to the enzyme, then it might travel differently on a non-denaturing (Native) gel. I tested this hypothesis and saw that VU0506534 may have slightly dimmed one of the aggregate bands, but this was not a robust effect (Figure A6 in Appendix). However, the lack of a clear result in this experiment did not mean that the compounds did not bind to and change the enzyme's structure—they may have done so, but I simply did not capture it with this particular assay. As such, this experiment was also inconclusive.

### 3.2.3.6 Reduced Expression Temperature

Again, to help us study full-length Nape-pld in the absence of aggregates, I attempted a modification to the way that I expressed and purified the protein, with consultation from Dr. Zahra Mashhadi. Previously, after inducing plasmid expression, I would incubate the transformed bacteria at 28 °C for ~16 h before beginning the purification process. In an attempt to reduce the amount of protein aggregation, I instead tested the effect of incubating the bacteria at 14 °C for ~25 h. We hypothesized that the slightly reduced temperature would allow the protein to remain in a thermodynamically favored state and not re-fold into a kinetically favored state. This method was effective at diminishing the aggregated protein bands in Native gels (Figure 24), and I therefore adopted it for all future NAPE-PLD purifications. However, not all of the aggregation was eliminated, so we were still unable to prepare Nape-pld in a way that would allow the truncated forms of the enzyme to be separated from the intact enzyme.
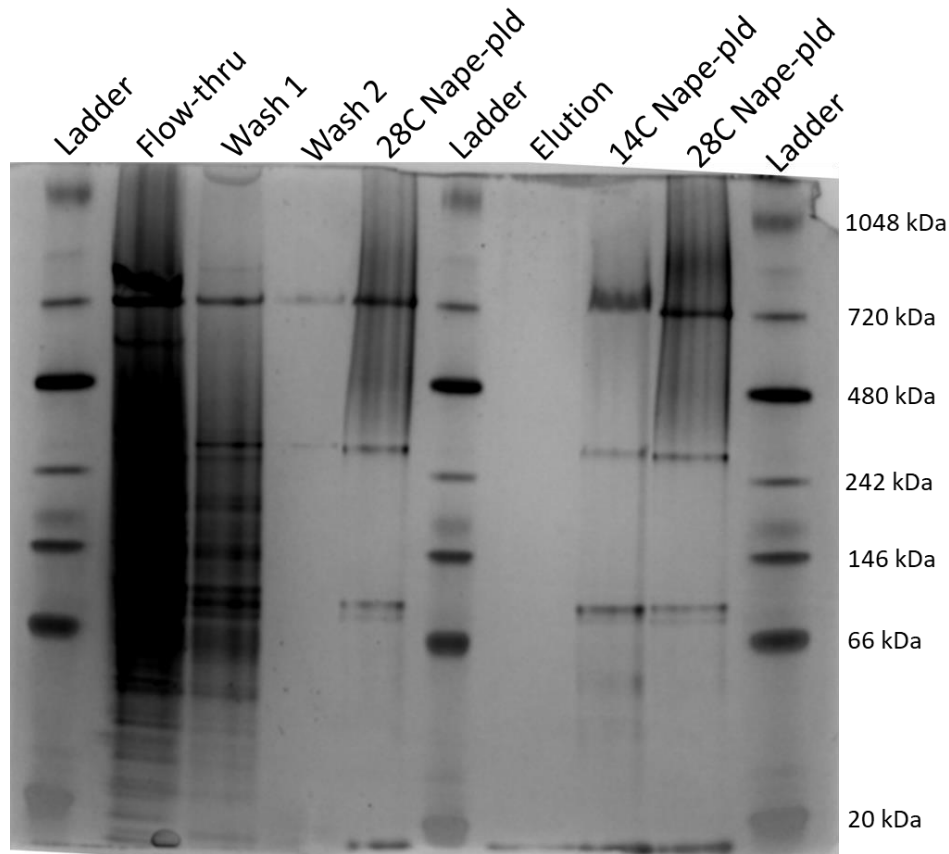
**Figure 24.** Reduced expression temperature yields reduced aggregation on non-denaturing (Native) PAGE, Coomassie stained. Lanes are labelled with their contents. Ladder molecular weights are indicated on the right. "Flow-thru" is contents of cell lysate that did not bind to the affinity column. "Wash 1" and "Wash 2" contain non-specific binders that were washed from the affinity column. "28C Nape-pld" is Nape-pld that was purified and dialyzed after being expressed at 28 °C. "Elution" is the crude product that eluted from the affinity column. "14C Nape-pld" is Nape-pld that was purified and dialyzed after being expressed at 14 °C. Nape-pld monomer is 46 kDa, homodimer is 92 kDa.

*3.2.3.7 Native Gel Activity Assay*

We next questioned whether the free intact enzyme (46 kDa on a Native gel) or the enzyme aggregates (150 kDa and above on a Native gel) were the active species in our enzyme activity assays. To attempt to answer this question, I treated the enzyme with either vehicle or VU0506534, separated the gross enzyme mixture by size using a Native gel, administered PED-A1 directly to the gel, and measured fluorescence over 50 min. I saw no change in fluorescence during the experiment, and quite a high fluorescence background signal (data not shown), suggesting that the PED-A1-based activity assay simply could not be used on protein bound in a Native gel. At this point,

67

we halted attempts to directly measure target engagement, and instead focused on alternative routes such as computational modeling (below), mutating the ligand binding site (below), kinetics assays (above), and competition assays (above).


<u>3.2.4 *In Silico* Modeling</u>

One potential means of identifying the binding site of the BT-PSPs on NAPE-PLD was by using computational (*in silico*) models. These models are imperfect in that they are limited to using the existing crystal structures of the enzyme, they do not perfectly model enzymes and their movements, and they cannot easily account for external factors like water and small molecules surrounding the enzyme. They can, however, be used to generate hypotheses as to where compounds bind, which we could then test using more definitive methods.

*3.2.4.1 Binding Site Identification*

In order to identify potential BT-PSP binding sites, Drs. Sean Davies and Alex Waterson performed modeling simulations using four different computational methods (Schrödinger Maestro SiteMap, SiteFinder, ProteinsPlus, and Python-Rx[140]). All four methods independently identified a large, druggable pocket in the NAPE-PLD homodimer interface where the BT-PSPs might bind (Figure 25 A). Subsequent docking simulations at this binding site (using Schrödinger Maestro GLIDEdock) identified a potential binding pose for VU0506534, with a favorable binding energy of -9.522±0.101 kJ/mol.
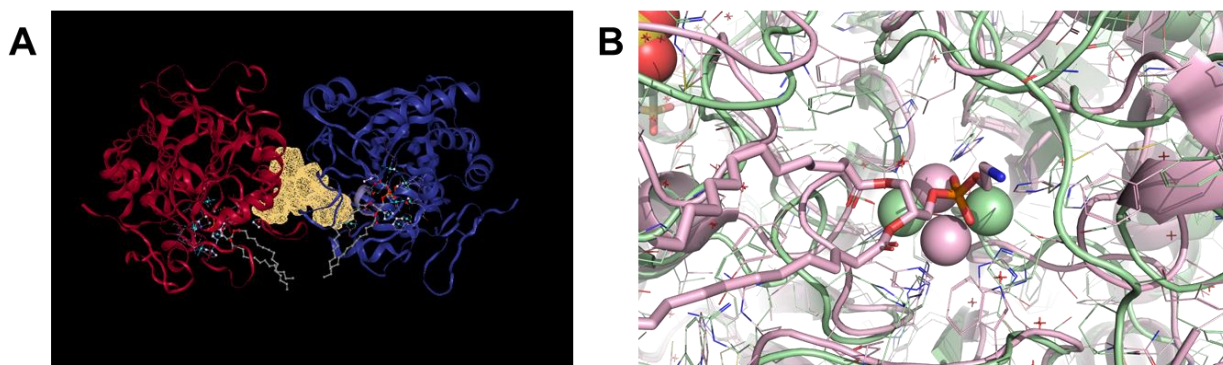
**Figure 25.** *In silico* binding simulations reveal potential allosteric BT-PSP binding site. **A.** Predicted binding site (yellow) identified by molecular modeling simulations (image from ProteinsPlus). Ribbon diagram: NAPE-PLD monomer A (red) and monomer B (blue). Ball-and-stick: NAPE. **B.** Active site architecture before (pink) and 50 ns after (green) VU0506534 binding, using molecular dynamics simulation. Ribbon: NAPE-PLD. Spheres: catalytic zinc ions. Ball-and-stick: PE (as surrogate for NAPE).

*3.2.4.2 Docking Simulation*

To further understand the specifics of BT-PSP binding and to determine what structural changes arise from binding at the identified site, Drs. Zeinab Haratipour and Raymond Blind performed a molecular dynamics (MD) simulation of NAPE-PLD's conformational changes after VU0506534 binding. This simulation showed that after VU0506534 binding, there was a large change in the structure of the active site: the secondary structures surrounding the active site shifted, and the catalytic zinc ions rotated 90 degrees within the active site (Figure 25 B). These conformational changes were in agreement with the notion that VU0506534 is an allosteric modulator of the enzyme. While this simulation did not prove that VU0506534 binds to NAPE-PLD at the predicted binding site, it provided confirmation that pursuing further studies on this potential binding site could be fruitful.

3.2.5 Mutagenesis

The *in silico* models of modulator binding provided us with an opportunity to demonstrate not only **whether** the BT-PSPs bind directly to NAPE-PLD to alter activity, but also **where** on the enzyme they do so. In order to accomplish this, we planned to

express and purify NAPE-PLD with mutations at selected residues in the predicted binding site, and then to test their activity with and without BT-PSP treatment.

### 3.2.5.1 Planned Mutations

Based on the MD simulation, I identified several possible interactions between VU0506534 and NAPE-PLD residues. These interactions are listed in Table AT1 (in Appendix) and are depicted in Figure 26. From those interactions, Drs. Raymond Blind, Sean Davies, and I chose three pairs of mutations to generate: R100A/R99A, S106F/K30D, and R99E/S106A. R100A/R99A would remove several strong interactions between the enzyme and VU0506534, as well as interactions that structure the binding pocket and that connect the two NAPE-PLD monomers. S106F/L30D would eliminate additional binding interactions and potentially occlude the binding site. R99E/S106A would eliminate a large number of potential hydrogen bonds and therefore hinder binding.
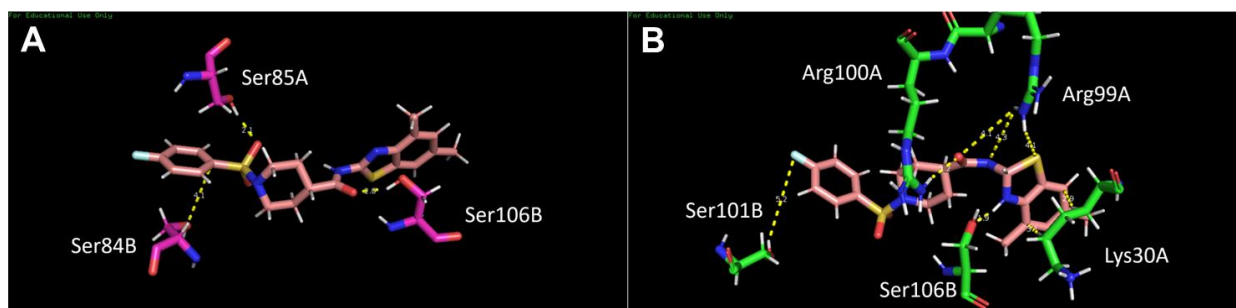


**Figure 26.** Potential BT-PSP binding interactions with NAPE-PLD. **A.** Residues that interacted with VU0506534 at the start of the molecular dynamics (MD) simulation. VU0506534 shown in salmon, NAPE-PLD in magenta, interactions are dotted yellow lines. **B.** Residues that interacted with VU0506534 at the end of the MD simulation. VU0506534 shown in salmon, NAPE-PLD in green, interactions are dotted yellow lines. Both images were generated using Pymol software (Schrödinger, Inc.).

### 3.2.5.2 Mutagenesis Scaffold

To date, there is only one crystal structure of NAPE-PLD, which was generated using a modified form of human NAPE-PLD.[68] Maltose-binding protein (MBP) was fused to the N-terminus of the protein, and a hexahistidine tag was added to the C-terminus. When the researchers first removed the MBP using Xa protease, they saw that the first 46 amino acids of NAPE-PLD were also susceptible to proteolysis. Therefore, they

removed the first 46 codons from *NAPEPLD* and fused MBP to the 47th for all subsequent purifications (MBP was still removed with Xa protease during purification).

This modified version of human NAPE-PLD is what was used to generate the only crystal structure of the enzyme and, therefore, it was used in our *in silico* binding models. Since we did not know how differently the enzyme would fold with the first 46 amino acids present and how this would affect BT-PSP binding, we concluded that the scaffold for our mutagenesis experiments needed to be human NAPE-PLD without the first 46 amino acids present (called Δ47 NAPE-PLD). We did not include the MBP fusion, however, as we suspected that it was unnecessary.

So, as a first step, I expressed Δ47 NAPE-PLD in bacteria and purified it using a cobalt-loaded histidine tag affinity column. The resulting protein had no catalytic activity (Figure A7 in Appendix). With help from Dr. Mashhadi, I then isolated and sequenced the expression plasmid to verify that I was expressing the correct protein. The sequence was confirmed to be correct. From this, we concluded that the MBP fusion was essential for the truncated enzyme to fold and function properly, but that MBP was not necessary when the enzyme was full-length. MBP is fused to proteins for three major reasons: it helps solubilize proteins, it functions as an affinity tag, and it aids in protein folding.[68, 141, 142] We suspected that our Δ47 NAPE-PLD did not fold properly without the aid of MBP and so it could not function properly. However, testing this hypothesis fell outside of the scope of this project, and therefore continuing the mutagenesis study did too.

### 3.2.5.3 Mutagenesis Future Directions

Future mutagenesis experiments in the Davies Lab can help to elucidate the nature of BT-PSP binding to NAPE-PLD. The first step would be to express, purify, and measure the activity of the same form of Δ47 NAPE-PLD used by the group that obtained its crystal structure. Assuming that this form of the enzyme shows activity as it has before,[68, 69, 124] we would then generate the mutants described above and test their activities with and without BT-PSP treatment.

## 3.2.6 Conclusions on Activity Characterization

Our efforts into understanding the binding and activity of the BT-PSPs were many, varied, and did not always yield meaningful results. As such, I will summarize our goals and our findings. We wanted to determine two things from these assays. Do the BT-PSPs directly engage NAPE-PLD to induce their effects? And if so, what is the nature of this binding—is it allostery or another mechanism, and where is the binding site?

The competition and Michaelis-Menten kinetics assays indicated that the BT-PSPs most likely bind directly to Nape-pld to induce their effects, with the Michaelis-Menten assay providing the additional detail that they likely do not serve as chaperones for the substrate. The remaining assays that we performed could not prove target engagement by the BT-PSPs, though the *in silico* models indicated that such binding was likely.

As for the nature of BT-PSP binding, the competition and kinetics assays indicated that this binding is most likely allosteric in nature. The competition assays also demonstrated that the BT-PSP binding site is not shared by LEI-401 or Bith, that the binding of those inhibitors does not affect BT-PSP binding, and that there is likely to be one shared binding site for all of the BT-PSPs. From the *in silico* models, we learned the locations of, key residues within, and conformational changes associated with potential binding sites. While these latter pieces of information were not conclusive, they will be informative for future experiments aimed at conclusively determining the location of BT-PSP binding.

From these results, it was safe to conclude that the BT-PSPs are positive allosteric modulators of NAPE-PLD. And, when combined with the validation assays, we could safely conclude that our compounds acted via NAPE-PLD. Future experiments will include continued troubleshooting of the thermal shift assay so that we can have absolute proof that the BT-PSPs bind to NAPE-PLD. Additionally, continued mutagenesis tests (as described above) will allow us to determine where and how the BT-PSPs bind to NAPE-PLD.

**3.3 Selectivity**

While it is easy to become myopic and only focus on the actions of one enzyme of interest, a small, drug-like molecule could well modulate one or more other enzymes. Also, a compound that has high efficacy on a mouse-derived enzyme could have no effect on the human ortholog. Of course, without tremendous resources, one cannot test the effects of a molecule on every pertinent enzyme and ortholog. Therefore, we selected three of the most important selectivity assays for our testing of the BT-PSPs.

3.3.1 Human NAPE-PLD

All of our assays so far had been performed using murine protein or mouse-derived cell lines. However, for the BT-PSPs to have any impact on human health, they needed to have efficacy on human NAPE-PLD. Therefore, my first test of selectivity was to repeat the CRCs of our BT-PSPs using purified, recombinant, full-length, human NAPE-PLD, with help from the Vanderbilt HTS Core. All of the compounds retained their activities with human NAPE-PLD (Figure 27). However, determining compound potency and maximal efficacy was difficult, as the activities tended to decline at higher concentrations. This was most likely due to solubility issues, and was not observed in earlier experiments possibly because the compound stocks were much newer at that time.[143, 144] Nevertheless, the compounds demonstrated a biologically relevant amount of activation of human NAPE-PLD, confirming their utility in human-directed research.
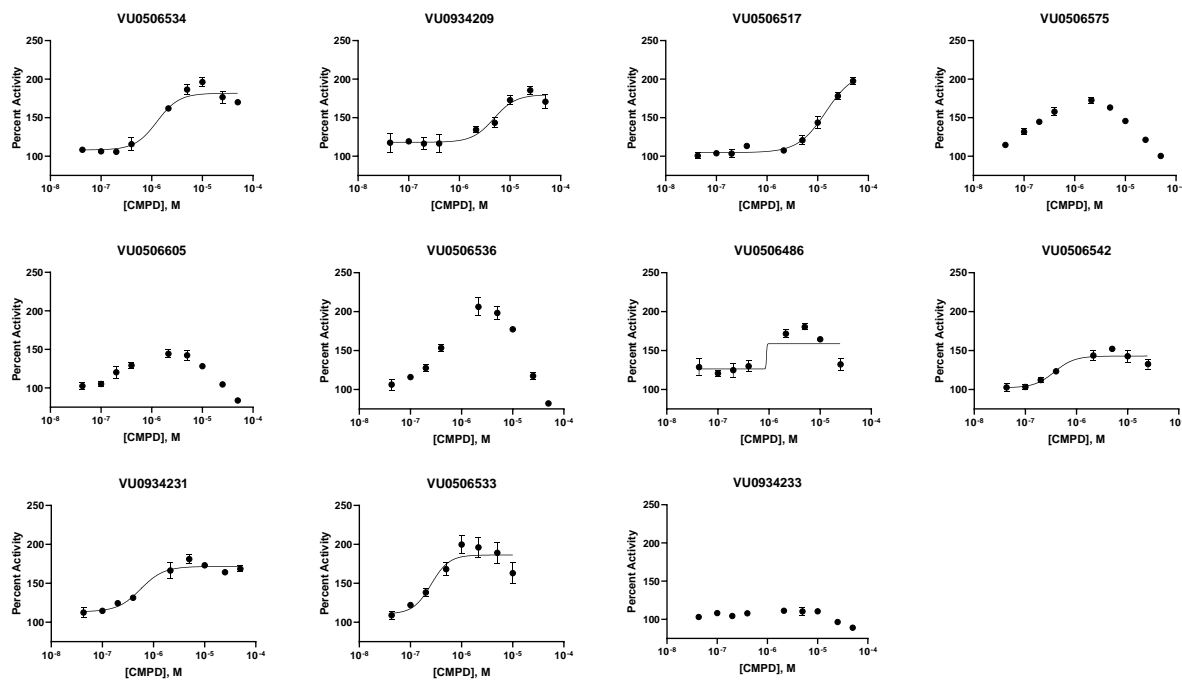
**Figure 27.** BT-PSPs activate human NAPE-PLD. Activity of purified recombinant human NAPE-PLD in the presence of graded concentrations of each BT-PSP compound was measured using PED-A1 and normalized to activity in absence of test compound. Each individual replicate was normalized to vehicle controls and then averaged (mean ± SD shown). A nonlinear curve fit with variable slope (four parameters) was used to generate each curve shown.

## 3.3.2 Fatty Acid Amide Hydrolase

Fatty acid amide hydrolase (FAAH) is an enzyme that catalyzes the conversion of NAEs to free fatty acids and ethanolamine, and it is one of the primary degraders of NAEs.[11, 62-64] As we intended to use our NAPE-PLD activators to investigate the effects of increasing NAE levels, it was crucial to know whether they had effects on FAAH. If a compound activated both NAPE-PLD and FAAH, it would be much less useful to researchers. A compound that activated NAPE-PLD but inhibited FAAH would be increasing NAE levels via two mechanisms and so could be more useful for studying NAE effects; however, it would also be a poorer candidate for *in vitro* studies. Bolstering this need to investigate the effects of our compounds on FAAH was the fact that a series of potent FAAH inhibitors with chemical structures strikingly similar to the BT-PSPs had been published.[145]

I used a commercially available FAAH modulation assay (Cayman 10005196) to determine whether our compounds affected FAAH activity. I found that at 33µM, most of the BT-PSPs had small effects on FAAH activity (Figure 28 A). Furthermore, I saw that there was no robust dose-dependence to the compounds' inhibition of FAAH (Figure 28 B), and that none of the compounds inhibited FAAH by at least 50% even at the highest dose tested (Figure 28 A-B). Therefore, we concluded that the BT-PSPs did not have enough FAAH-inhibitory activity to merit concern or additional investigatory experiments.
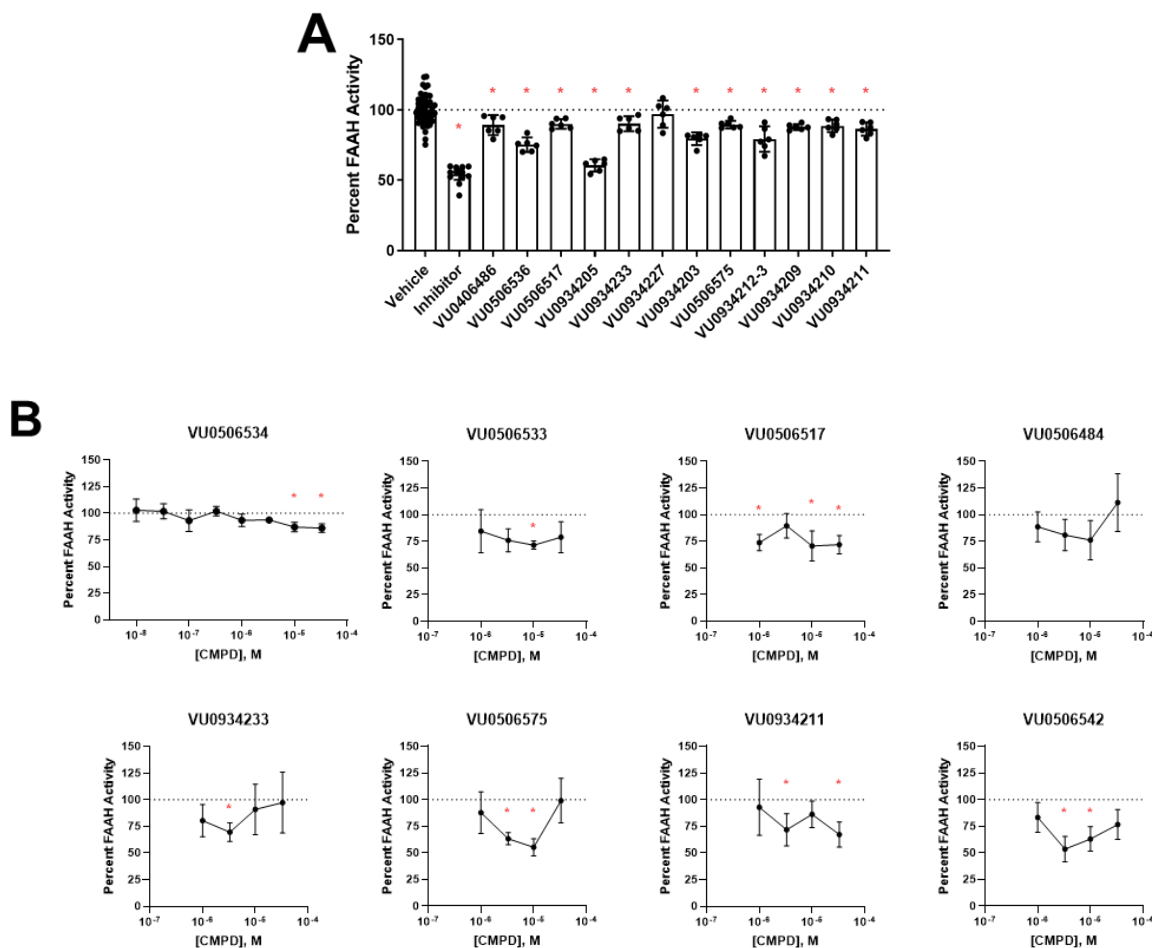


**Figure 28.** BT-PSP effects on FAAH activity. **A.** FAAH activity with BT-PSPs at 33 µM, normalized to vehicle controls. "Inhibitor" is JZL-195, a FAAH inhibitor. Ordinary one-way ANOVA, $p<0.0001$. Dunnett's multiple comparisons test, $*p<0.05$ vs Vehicle. Mean ± 95% CI shown. **B.** Concentration-response curves of FAAH activity (normalized to vehicle controls) with select compounds. CRC for VU0506534 was run as part of A, not B. Ordinary one-way ANOVA, $p<0.0001$. Dunnett's multiple comparisons test, $*p<0.05$ vs vehicle controls. Points are mean ± SD.

### 3.3.3 Soluble Epoxide Hydrolase

The published inhibitors that helped to instigate the FAAH modulation assay also inhibit soluble epoxide hydrolase (sEH).[145] sEH is an enzyme with important roles in cardiometabolic diseases and endocannabinoid signaling,[43, 59, 146-148] and it is involved in the synthesis of the SPMs.[59] So, it was important to investigate whether the BT-PSPs affected sEH, independent of the fact that they closely resembled known sEH inhibitors. To test this, I again employed a commercially available activity assay (Cayman 10011671) and saw that the compounds had some inhibitory activity against sEH (Figure 29 A). As with FAAH, the dose-dependence of this inhibition was not robust (Figure 29 B). Unlike with FAAH, several of the compounds inhibited sEH to a high degree (Figure 29 A). Therefore, we concluded that future medicinal chemistry efforts would be indicated in order to reduce this inhibition and, in the meantime, controls would be added to account for this mild off-target effect.
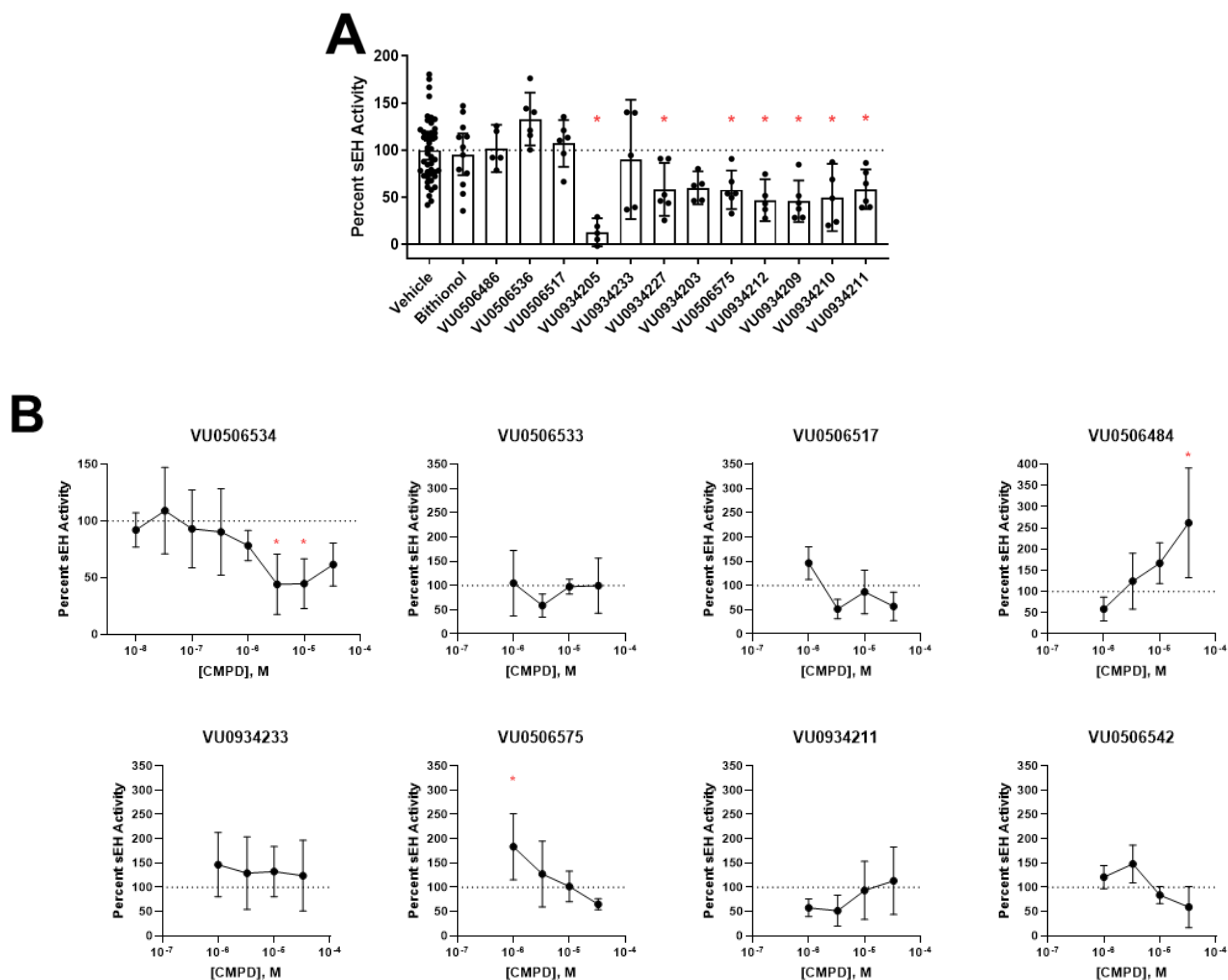
**Figure 29.** BT-PSP effects on sEH activity. **A.** sEH activity with BT-PSPs at 33 µM, normalized to vehicle controls. Ordinary one-way ANOVA, $p<0.0001$. Dunnett's multiple comparisons test, *$p<0.05$ vs Vehicle. Mean ± 95% CI shown. **B.** Concentration-response curves of sEH activity (normalized to vehicle controls) with select compounds. CRC for VU0506534 was run as part of A, not B. Ordinary one-way ANOVA, $p<0.0001$. Dunnett's multiple comparisons test, *$p<0.05$ vs vehicle controls. Points are mean ± SD.

## 3.4 Conclusions

Prior to the experiments detailed in this chapter, we had identified a series of compounds of the same structural class that strongly activated Nape-pld: the BT-PSPs. In order to validate these results, we tested their effects on the fluorophore used in the activity assay, and we demonstrated that their modulatory effects also apply to the hydrolysis of NAPE-PLD's actual substrate. We next performed experiments to

characterize the behavior of our compounds. While many of these experiments did not yield meaningful results, we were able to demonstrate that the BT-PSPs are positive allosteric modulators of NAPE-PLD. I then demonstrated that they modulated human NAPE-PLD in addition to mouse Nape-pld. And I demonstrated that they had weak effects on two important enzymes, sEH and FAAH. These off-target effects should not significantly interfere with the use of these compounds to probe the roles of NAPE-PLD activity, as long as *bona fide* inhibitors are also tested as controls.

Together, these results demonstrated that the BT-PSPs are true positive allosteric modulators of NAPE-PLD, that they are reasonably selective, and that they can be used as research tools. These results made the BT-PSPs the first class of verified NAPE-PLD activators ever published. However, to this point, all of our experiments had been performed *in vitro*. While *in vitro* studies are useful for building biochemical understanding, compounds that work in cells are much more widely useful in research settings. In order to test the effects of the BT-PSPs in live cells, however, we first needed to develop a NAPE-PLD activity assay that worked in cells.

## 3.5 Methods

### 3.5.1 General

#### 3.5.1.1 Materials

LEI-401, $[^2H_4]$OEA, and *N*-$[^2H_4]$palmitoyl-dioleoyl-PE were purchased from Cayman Chemicals. PED-A1 was purchased from ThermoFisher Scientific. Flame-NAPE was synthesized as previously described.[133] *N*-oleoyl-dihexanoyl-PE was synthesized using dihexanoyl-PE (Avanti Polar Lipids) and oleoyl chloride (Millipore-Sigma) as previously described.[127]

#### 3.5.1.2 NAPE-PLD Purification

For all assays that made use of purified, recombinant NAPE-PLD, the protocol for enzyme expression and purification is the same as in Chapter 2. For the full-length

human NAPE-PLD, the expression plasmid was pET, a hexahistidine tag was inserted at the C-terminus of the enzyme, and this expression plasmid was designed with and purchased from VectorBuilder. The same was true for Δ47 NAPE-PLD, with the added step of removing the nucleotides for the first 46 amino acids from the full-length human NAPE-PLD sequence.

*3.5.1.3 Analyses*

All statistical analyses were performed using GraphPad Prism 9 software. For human NAPE-PLD CRCs, slopes were calculated as described in Chapter 2 using WaveGuide software. Unless stated otherwise, all experiments with accompanying statistical analyses were replicated two or more times on separate days, normalized to same-day controls, and combined for analysis. All chemical structures were generated using ChemDraw Professional 22.0 software (PerkinElmer Informatics). Residues to mutate on Δ47 NAPE-PLD were identified by hand using Pymol software (Schrödinger, Inc.).

3.5.2 *In Vitro* LC/MS

For LC/MS assays, NOPE was added as substrate after 1 h pre-incubation with VU0506534, VU0506533, and/or VU0934233. 90 min after NOPE was added, the reaction was quenched by adding 3 volumes of ice-cold methanol containing [$^2$H$_4$]OEA and *N*-[$^2$H$_4$]palmitoyl-dioleoyl-PE and then 6 volumes of ice-cold chloroform.[149] The lower phase was dried under nitrogen gas and dissolved in 100 μL mobile phase A. High performance liquid chromatography was performed using a 2.1 mm C18 guard column (Phenomenex AJ0-8782), and a rapid gradient ramp. Mobile phase A was 5:1:4 (v/v/v) isopropanol: methanol: water, with 0.2% v/v formic acid, 0.66 mM ammonium formate and 3 μM phosphoric acid included as additives. Mobile phase B was 0.2% (v/v) formic acid in isopropanol. Initial column conditions were 5% mobile phase B, followed by gradient ramp to 95% B over 0.5 min, held at 95% B for 2 min, the returned to initial conditions (5% B) over 1 min. Flow rate throughout was 100 μL/min. Injection volume was 2 μL. The sample injector needle was washed before each injection using a strong

wash of methanol, and a weak wash of 1:1:1:1 (v/v/v/v) isopropanol: methanol: acetonitrile: water, with 0.2% formic acid, 0.3 mM ammonium formate, and 0.37 mM phosphoric acid included as additives. Multiple reaction monitoring for the following ions were monitored: OEA [M+H]$^+$: m/z 326.3→ m/z 62.1; [$^2$H$_4$]OEA [M+H]$^+$: m/z 330.3 → m/z 66.1; NOPE [M+NH$_4$]$^+$ : m/z 676.5 → m/z 308.3 (quantifier), m/z 693.5 → m/z 271.2 (qualifier); N-[$^2$H$_4$]palmitoyl-dioleoyl-PE [M+NH$_4$]$^+$: m/z 986.8 → m/z 286.3 (quantifier), m/z 1003.8 → m/z 603.5 (qualifier). The ratio of peak height for OEA to [$^2$H$_4$]OEA was used to calculate to amount of OEA generated and the ratio of peak height for NOPE to N-[$^2$H$_4$]palmitoyl-dioleoyl-PE was used to calculate the amount of NOPE remaining. These values were then used to calculate the OEA / NOPE ratio.

### 3.5.3 NAPE-PLD Activity Assays

#### 3.5.3.1 384-Well Plate Assay

For the CRCs in human NAPE-PLD, the same protocol as used in the mouse NAPE-PLD CRCs of Chapter 2 was followed, but with full-length human NAPE-PLD in place of mouse NAPE-PLD.

#### 3.5.3.2 96-Well Plate Assay

For all remaining NAPE-PLD activity assays in this chapter, the same base protocol was followed. Compounds (in DMSO for most, in deionized water for detergents) were pre-incubated with NAPE-PLD (final concentration 0.1 µM) and NOG (0.4% final, w/v) in 50 mM Tris-HCl buffer (pH = 8.0) for 1 h at 37 °C in black-walled, clear-bottom, non-treated, 96-well plates (volume of 70 µL during pre-incubation). Then, PED-A1 dissolved in 8% DMSO, 32% ethanol, 60% 50 mM Tris-HCl buffer was quickly added to the wells (10 µL added, 4 µM final concentration), the plate was immediately placed into a Biotek Synergy H1 plate reader, and fluorescence kinetics were read every minute for 50 minutes (ex/em = 488/530 nm). Activities were calculated as slope of fluorescence increase from 1-4 min.

<u>3.5.4 Gel Electrophoresis</u>

*3.5.4.1 Denaturing Gels*

Denaturing gels were run as follows. Samples were prepared in Laemmli SDS sample buffer (Bio-Rad 1610747), with added β-mercaptoethanol (Millipore-Sigma M6250) as denaturant. Samples were heated at 80 °C for 10 min before being loaded onto NuPAGE 4-12% Bis-Tris gels (ThermoFisher Scientific) and run using NuPAGE MOPS running buffer (ThermoFisher Scientific NP0001) for 50 min at a constant voltage of 200 V. For Coomassie staining, gels were then rinsed with deionized water (4 x 5 min), treated with Coomassie Blue stain (Bio-Rad 1710786) for 1 h, rinsed again with deionized water (3 x 15 min), and imaged using a Li-Cor EZreader blot imaging machine. For western blot staining, proteins were transferred onto nitrocellulose membranes using NuPAGE transfer (NP0006) containing 10% methanol; they were run for 75 min at a constant voltage of 30 V. Membranes were blocked using phosphate buffered saline (PBS)-based blocking buffer (Li-Cor 927-70001) for 1 h. Membranes were treated with a 1:500 dilution of primary antibody (abcam ab95397) in 1:1 blocking buffer: 0.1% Tween-20 (Millipore-Sigma) in PBS at 4 °C overnight. After washing the membranes with 0.1% Tween-20 in PBS (5 x 5 min), they were treated with a 1:10,000 dilution of secondary antibody (Li-Cor 926-311) in the same solvent as used for the primary antibody for 1 h. Membranes were then washed again and imaged using an Odyssey CLX gel imager.

*3.5.4.2 Non-Denaturing Gels*

For non-denaturing (Native) gels, the overall protocols followed were largely the same, with changes listed below. Sample buffer was NativePAGE gel-specific (ThermoFisher Scientific BN2003), running buffer was NativePAGE running buffer (ThermoFisher Scientific BN2001), samples were not heated before being loaded onto 4-16% Bis-Tris NativePAGE gels (ThermoFisher Scientific) and run for 100 min at a constant voltage of 150 V. Staining proceeded the same way as for denaturing gels.

### 3.5.5 Molecular Dynamics Simulation

To study how stable VU0506534 is in the binding site and how it affects the structure of the protein, 50ns MD simulation was performed on the complex of 4QN9-VU0506534. These complexes were then prepped for MD simulation using the CHARMM-GUI.[150] Briefly, the complex was solvated in an octahedral box of explicit TIP3P water with a 10-Å buffer around the protein complex. Potassium (K+) and Cl-ions were added to neutralize the protein and simulate physiologic conditions. All minimizations and 50 nanosecond MD simulations were performed with Amber17 employing the ff14SB, TIP3P, GAFF2 force field for proteins, ligand and water molecules, respectively.[151] All bonds between non-hydrogen atoms and hydrogens were fixed with the SHAKE algorithm. The simulation duration was 50ns using a 2fs time step with trajectories printed every 5000 ps to create 5000 frames. Analysis of the MD simulations was performed on 5000 frames using the CPPTRAJ module of AmberTools.[152] Root mean square deviation (RMSD) was calculated for all non-hydrogen atoms of protein residues for each frame in the trajectory using the initial structure as the reference, and root mean square fluctuations (RMSF) were calculated on the all non-hydrogen atoms of protein residues for each frame in the trajectory using the initial structure as the reference. RMSF is also calculated for all atoms of the compound for each frame in the trajectory using the initial structure as the reference.

### 3.5.6 Selectivity Assays

sEH and FAAH activity assays were performed and analyzed according to the manufacturer's specifications (Cayman 10011671 and 10005196).

## Development of Flame-NAPE, a Selective Probe for Measurement of NAPE-PLD Activity

This chapter is adapted from Selective Measurement of NAPE-PLD Activity via a PLA$_{1/2}$-Resistant Fluorogenic *N*-Acyl-Phosphatidylethanolamine Analog and has been reproduced with the permission of the publisher.[133] This research was originally published in the Journal of Lipid Research Methods Section. Jonah Zarrow, Jianhua Tian, Brendan Dutter, Kwangho Kim, Amanda C. Doran, Gary A. Sulikowski, and Sean S. Davies. Selective Measurement of NAPE-PLD Activity via a PLA$_{1/2}$-Resistant Fluorogenic *N*-Acyl-Phosphatidylethanolamine Analog. J Lipid Res. 2022; 63(1):100156. © the Authors. Author contributions: GAS and SSD conceptualization; JEZ, JT, BD, KK, GAS, and SSD methodology; JEZ validation; JEZ and SSD formal analysis; JEZ, JT, BD, KK, ACD, and SSD investigation; GAS and SSD resources and funding acquisition; SSD data curation; JEZ and SSD writing—original draft; JEZ, KK, ACD, GAS, and SSD writing—review and editing; GAS and SSD visualization and supervision; SSD project administration.

LC/MS experiments were conducted at the Vanderbilt Mass Spectrometry Research Core, with assistance from Dr. M. Wade Calcutt and Brian Hachey. The laboratory of Dr. Amanda Doran cultured the bone marrow-derived macrophages. Dr. Zahra Mashhadi assisted with culturing of the remaining cell types and with purification of recombinant Nape-pld.

### 4.1 Background

A means for selectively measuring NAPE-PLD activity in cultured cells was vital for testing the effectiveness of our candidate NAPE-PLD modulators. As discussed in Chapter 1, changes in NAPE-PLD activity may contribute to the progression of cardiometabolic diseases. So, measuring NAPE-PLD activity in cultured cells and

tissues could help to determine how changes in its activity contribute to pathophysiology.

However, existing methods for measuring NAPE-PLD activity were onerously time-consuming and/or lacked selectivity. The most common means of measuring NAPE-PLD activity was performed by adding radiolabeled NAPEs to the biological system of interest, followed by extraction and separation of resulting NAEs from their precursor NAPEs by thin-layer chromatography (TLC).[153] This assay is not particularly selective for NAPE-PLD activity because it is typically carried out using radiolabeled NAPEs bearing two *O*-acyl chains (diacyl-NAPEs). Diacyl-NAPEs are readily hydrolyzed by alternative enzymatic pathways (Figure 30), thereby yielding NAEs without using NAPE-PLD.[62, 64, 118]
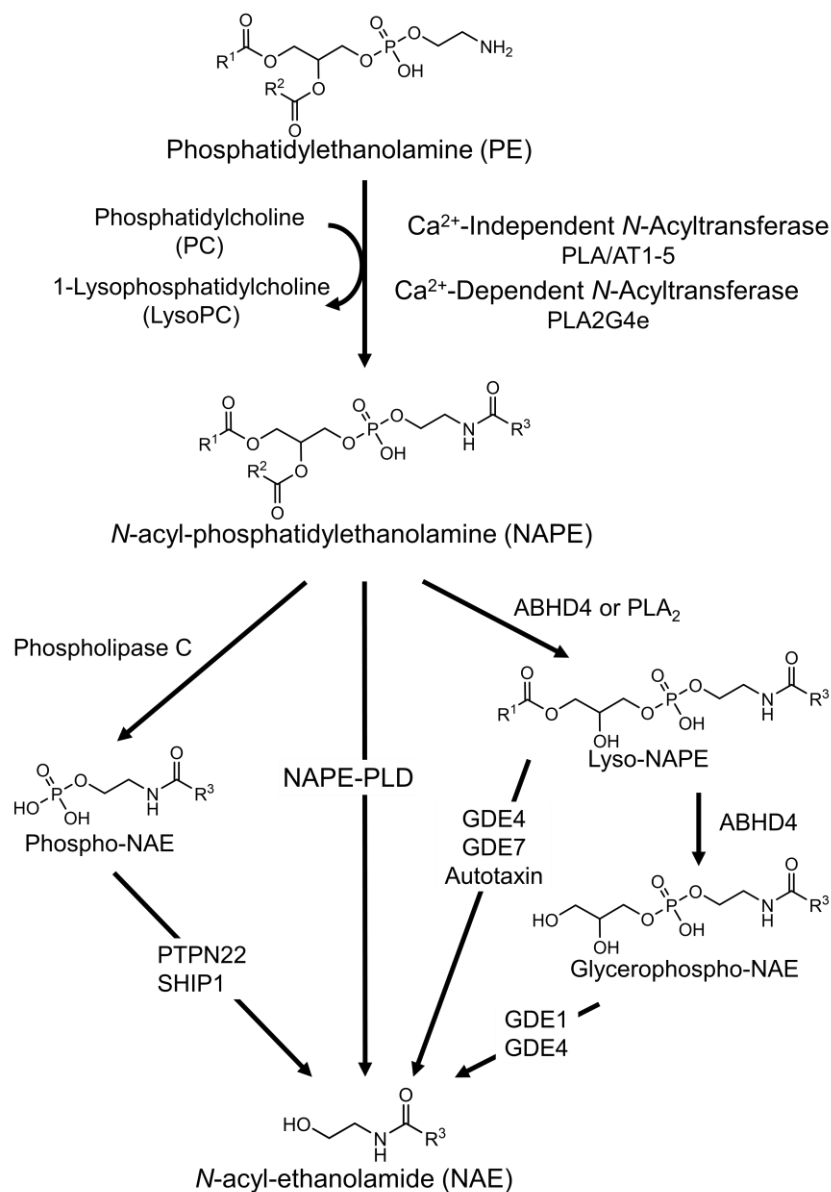
**Figure 30.** Pathways of *N*-acylethanolamide (NAE) biosynthesis from NAPE. $\alpha/\beta$-hydrolase domain-containing protein 4 (ABHD4), Glycerophosphodiester phosphodiesterase (GDE) -1, -4, -7, Phospholipase A/Acyltransferase (PLA/AT) 1-5, Phospholipase $A_2$ (PLA$_2$), PLA$_2$ group IV-e (PLA2G4e), Protein tyrosine phosphatase non-receptor type 22 (PTPN22), R1-3 (acyl chain substituents), SH-2 containing inositol 5' polyphosphatase 1 (SHIP-1).

For example, alpha/beta hydrolase domain-containing protein 4 (ABHD4) exerts both phospholipase $A_1$ and $A_2$ (PLA$_1$ and PLA$_2$)-type phospholipase activities to hydrolyze diacyl-NAPEs to glycerophospho-*N*-acyl-ethanolamides (GP-NAEs).[62, 64, 154] These GP-NAEs can then be hydrolyzed to NAEs by the actions of

glycerophosphodiester phosphodiesterases (GDEs) such as GDE1 and GDE4 [62, 154, 155]. In theory, this assay can be adapted to make it more selective for NAPE-PLD by using radiolabeled NAPEs whose *sn*-1 and *sn*-2 ester bonds have been replaced with ether bonds (diether-NAPE) to make them resistant to PLA$_{1/2}$-type phospholipases.[62, 64, 154] However, the results of diether-NAPE hydrolysis differ from those with diacyl-NAPE, indicating that the assay may not accurately replicate the hydrolysis of naturally occurring NAPEs.[110, 156, 157] Furthermore, regardless of which radiolabeled substrate is used, the use of radioisotopes requires specialized licensing, handling, and waste disposal, and TLC is labor-intensive and time-consuming.

Another widely used approach for measuring NAPE-PLD activity is to add non-radiolabeled *N*-C17:0-phosphatidylethanolamine (C17:0 NAPE) and then measure the resulting change in the ratio of C17:0 NAPE to its corresponding NAE product by LC/MS/MS (liquid chromatography with tandem mass spectrometry).[101, 125, 158] This LC/MS/MS assay is at least as labor-intensive, time-consuming, and expensive as the radioisotope method. And, unless diether-C17:0 NAPE is used as the substrate, it suffers from the same lack of selectivity for NAPE-PLD. Therefore, both of these approaches are too cumbersome for measuring NAPE-PLD activity in the large number of samples that are often needed for time-course studies or for screening the effects of various stimuli in cultured cells and tissues.

More recently, an alternative approach for measuring NAPE-PLD activity has become common. It utilizes PED-A1 or PED6, two commercially available fluorogenic compounds designed to measure PLA$_1$ and PLA$_2$ activity, respectively (Figure 31).[125, 126, 130, 159-165] These two NAPE analogs are designed so that their hydrolysis by the intended enzyme releases the 2,4-dinitrophenyl quencher moiety (DNP), thereby allowing detection of the BODIPY fluorophore. While both PED-A1 and PED6 allow for rapid and inexpensive measurement of NAPE-PLD activity *in vitro*, their sensitivity to PLA$_1$ or PLA$_2$ enzymes limits their effectiveness for selectively measuring NAPE-PLD activity in tissues and cultured cells, where all three types of enzyme are present.
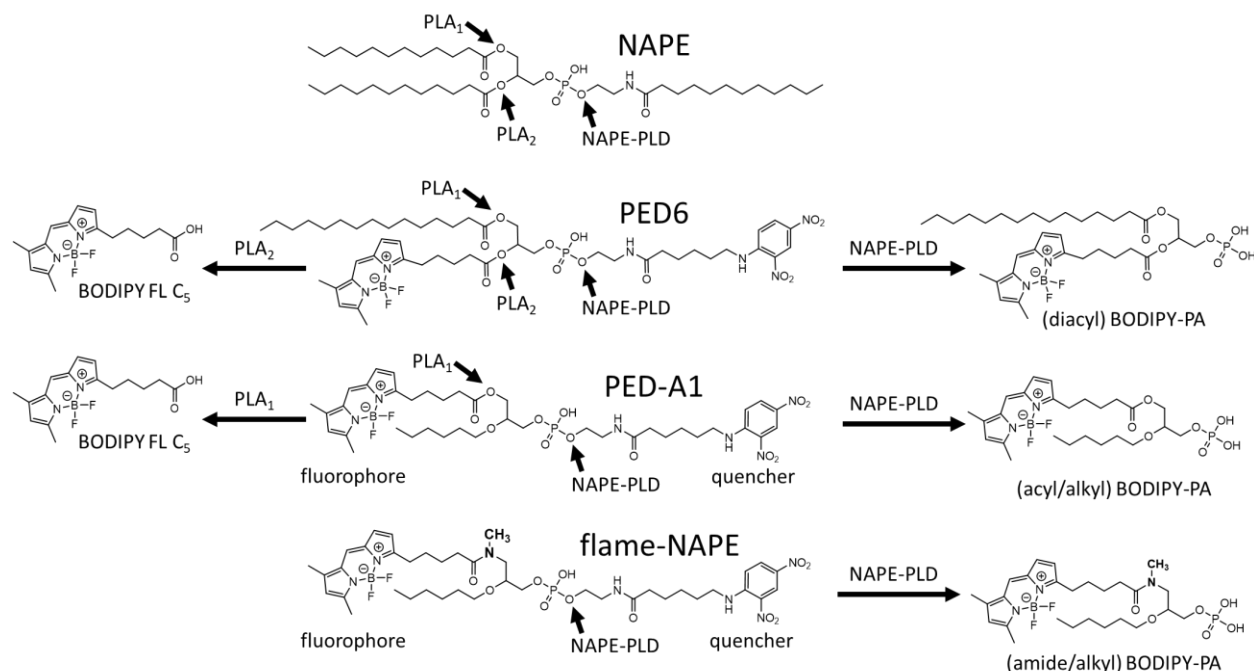
**Figure 31.** NAPE-PLD hydrolysis of its substrates. Endogenous NAPE can be hydrolyzed by various phospholipases, including $PLA_1$, $PLA_2$, and NAPE-PLD. PED6 is a fluorogenic NAPE analog where the dinitrophenol moiety of the *N*-acyl chain quenches the fluorescence of the BODIPY moiety on the *sn*-2 acyl chain. $PLA_2$ hydrolysis of PED6 releases the quencher moiety to generate a fluorescent fatty acid (BODIPY FL $C_5$), while NAPE-PLD hydrolysis generates a fluorescent phosphatidic acid (diacyl BODIPY-PA). $PLA_1$ hydrolysis of PED6 releases the *sn*-1 fatty acid chain but this does not generate fluorescence. PED-A1 is a fluorogenic NAPE where $PLA_1$ hydrolysis generates BODIPY FL $C_5$ and NAPE-PLD hydrolysis generates a fluorescent phosphatidic acid (acyl/alkyl BODIPY-PA). The ether bond of the PED-A1 *sn*-2 chain is resistant to $PLA_2$ hydrolysis. Flame-NAPE was designed to enable selective detection of NAPE-PLD by substituting an *N*-methyl amide bond for the *sn*-1 ester bond of PED-A1, thereby making it resistant to both $PLA_1$ and $PLA_2$ hydrolysis while retaining sensitivity to NAPE-PLD hydrolysis.

In order to overcome the selectivity issues of the fluorescence-based NAPE-PLD activity assays, reduction of ester groups to non-hydrolyzable ether groups was considered but eventually determined to be not chemically possible. Dr. Davies then requested that the SynCore generate an *sn*-1/*sn*-2 dialkyl analog of PED-A1. Although the SynCore was able to map out a chemical synthesis route for this analog, initial attempts at synthesis showed that the designed route was not likely to provide a sufficient yield of the desired compound. Members of the SynCore then proposed two alternative PED-A1 analogs. The first had an amide in place of the *sn*-1 ester of PED-A1. The second, which came to be called flame-NAPE (fluorogenic amide NAPE

analog), had an *N*-methyl amide bond at the *sn*-1 position (Figure 31). We anticipated that these substitutions would grant the probes resistance to PLA$_1$ hydrolysis (Figure 31), while retaining their ability to rapidly measure cellular NAPE-PLD activity.


## 4.2 Synthesis and Characterization of Flame-NAPE


<u>4.2.1 Synthesis</u>

Details on the synthesis of flame-NAPE are provided in the publication from which these results are adapted.[133] Briefly, commercially available (*R*)-glycerol acetonide was selectively functionalized and protected to provide the central amino diol. This enabled the sequential introduction of the *sn*-2 chain, the phosphate, the ethanolamine, the *N*-acyl chain, and the *sn*-1 chain. The final product was isolated by flash chromatography to >95% purity as indicated by LC/MS and nuclear magnetic resonance analysis. Flame-NAPE was synthesized by members of the Molecular Design and Synthesis Center of the Vanderbilt University Institute of Chemical Biology (Drs. Jianhua Tian, Brendan Dutter, Kwangho Kim, and Gary Sulikowski).


<u>4.2.2 Elimination of Amide Analog</u>

*4.2.2.1 Absorbance Scanning*

Before flame-NAPE, another analog of PED-A1 was synthesized by the SynCore. This compound bore an amide group at the position where flame-NAPE has an *N*-methyl amide (see Figure 31 for flame-NAPE structure). Upon receiving this compound, called PED-amide, I dissolved it in the same buffer as I would PED-A1 and to the same concentration, assuming 100% purity. Then, I performed an absorbance scan to determine its concentration relative to PED-A1, whose concentration was certain (Figure 32 A). This assay relied on the assumption that, if their structures were as predicted, PED-amide and PED-A1 would absorb light equally well at frequencies corresponding to their BODIPY and DNP groups. From this assay, I determined that the

PED-amide was approximately 4.5% as concentrated as PED-A1 when they were diluted the same way. This indicated that the PED-amide was only 4.5% pure. As the compound was synthesized and tested by a trustworthy and reputable laboratory, this was an unexpected result.
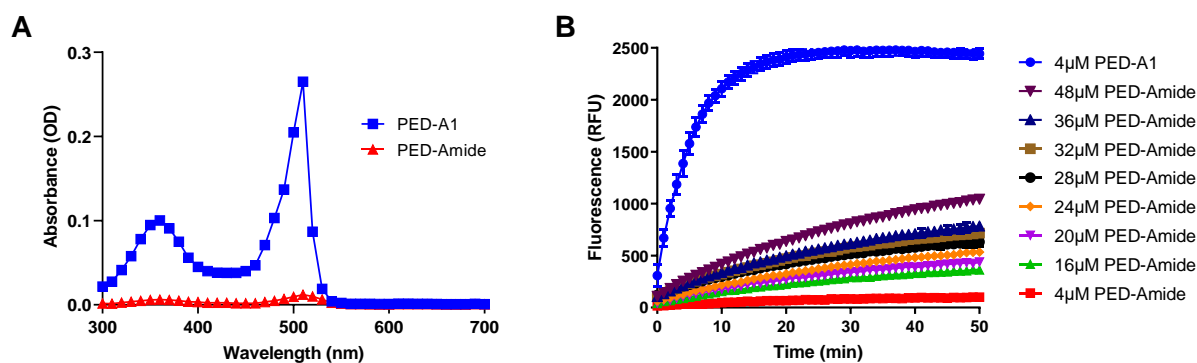


**Figure 32.** PED-amide characterization. **A.** Absorbance spectrum for PED-A1 and PED-amide, expressed as optical density (OD). Background (vehicle) signal has been subtracted and individual points are averaged across 6 technical replicates (± SD). **B.** Kinetics of PED-amide hydrolysis by Nape-pld, at graded concentrations. Individual points represent averaged replicate wells (±SD) (5 for each dose PED-amide, 8 for PED-A1). Fluorescence (ex/em 488/530 nm) is presented in relative fluorescence units (RFU).

### 4.2.2.2 $K_M$ Testing

Assuming that the determination of PED-amide's purity was accurate, I performed a dose-response test in order to characterize PED-amide hydrolysis by Nape-pld. I saw that, even adjusting for its low purity, PED-amide was scarcely hydrolyzed by Nape-pld (Figure 32 B). There were two likely explanations for this. The first was that the PED-amide genuinely was not a usable substrate for Nape-pld. As flame-NAPE, whose structure is highly similar to that of PED-amide, proved to be a usable substrate, this explanation is not particularly likely. The second possible reason was that the PED-amide was of poor quality. Under this explanation, the purity of the substrate was at or even lower than 4.5%, and when I adjusted for that during the activity experiment, I overestimated its degree of purity and/or the high amounts of impurities reduced the activity of the enzyme. Determining the reasons for Nape-pld's poor hydrolysis of PED-amide was not necessary, as an alternative substrate was synthesized soon thereafter: flame-NAPE.

<u>4.2.3 Characterization of Flame-NAPE</u>

*4.2.3.1 Substrate Scanning and $K_M$ Determination*

As with PED-amide, upon receipt of flame-NAPE I performed an absorbance scan to determine its concentration relative to PED-A1 (Figure 33 A). This showed that flame-NAPE was 86% as concentrated as PED-A1 when both were diluted the same way. All subsequent preparations of flame-NAPE were made proportionately more concentrated to account for this. I also performed scans with and without hydrolyzing the substrates, to further compare flame-NAPE and PED-A1 (Figure 33 B). These scans showed that flame-NAPE and PED-A1 had similar optical properties both when intact and after hydrolysis, as expected based on their chemical structures. This also demonstrated that flame-NAPE functioned as a Nape-pld substrate.

I then determined the $K_M$ of flame-NAPE at Nape-pld in order to compare it to that of PED-A1. I saw that PED-A1 had a $K_M$ of 4.0 μM with purified recombinant Nape-pld and a $V_{max}$ of 455 RFU/min (Figure 33 C), consistent with previous results.[126] Similarly, flame-NAPE had a $K_M$ of 9.2 μM and a $V_{max}$ of 525 RFU/min (Figure 33 C). From this, we concluded that flame-NAPE was a robust Nape-pld substrate, with sufficiently similar behavior to PED-A1 to be used as an alternative for measuring Nape-pld activity. What remained to be confirmed was whether flame-NAPE responded to PLD activity more selectively than PED-A1 did *in vitro* and in cells.
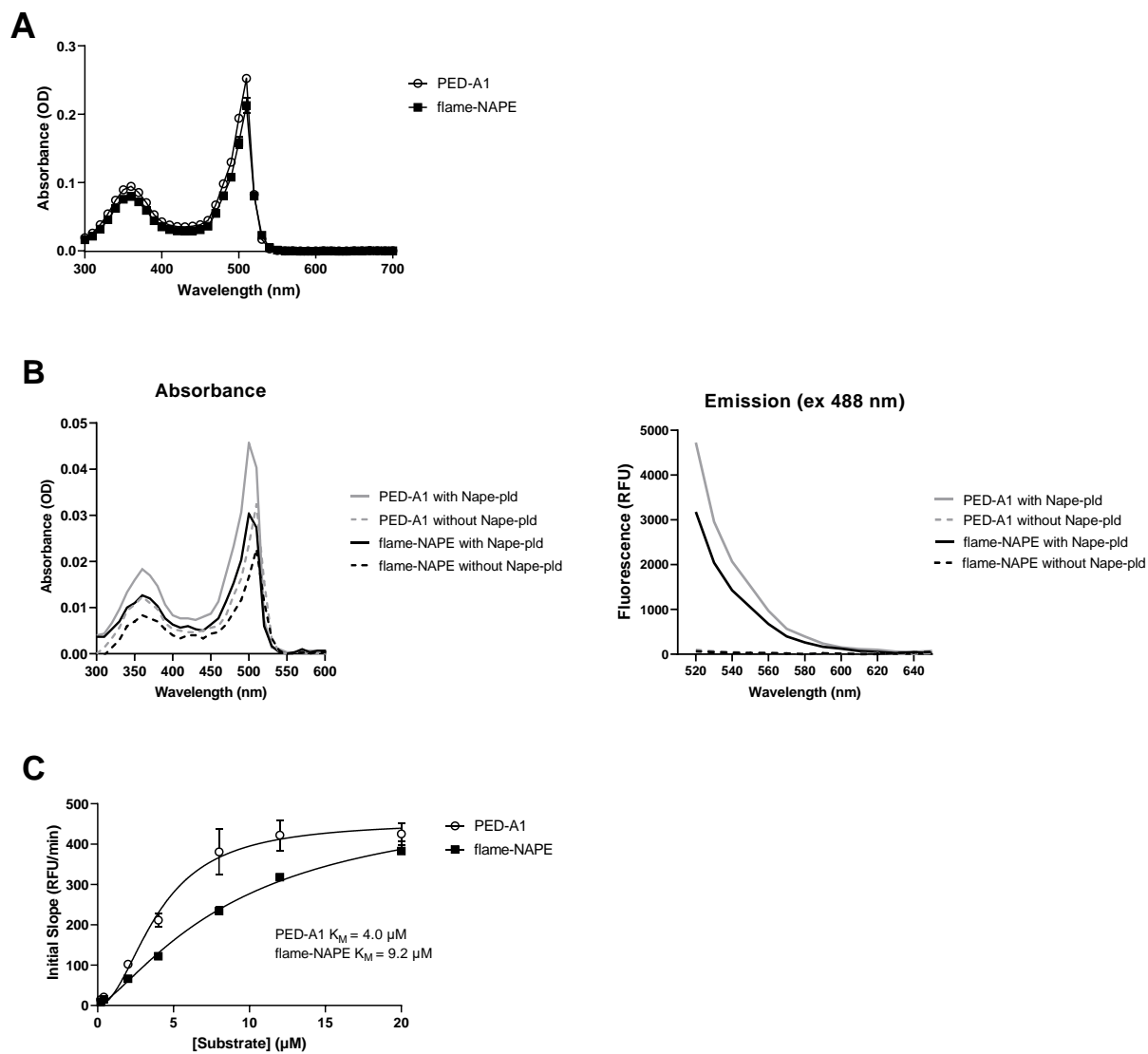
**Figure 33.** PED-A1 and flame-NAPE share similar spectrometric and NAPE-PLD utilization properties. **A.** Absorbance spectrum for PED-A1 and flame-NAPE, expressed as optical density (OD). Background (vehicle) signal has been subtracted and individual points are averaged across three technical replicates (± SD). **B.** UV/VIS absorbance (left panel) and fluorescence emission (right panel) spectra of PED-A1 and flame-NAPE with and without incubation with Nape-pld. Excitation at 488 nm was used to determine fluorescence emission spectrum. Lines are averaged across three technical replicates. **C.** Michaelis-Menten plot for hydrolysis of PED-A1 ($K_M$ = 4.0 µM) and flame-NAPE ($K_M$ = 9.2 µM) by recombinant murine Nape-pld (4.56 µg/mL). Fluorescence measured using ex/em of 488/530 nm. Each point is mean ± SD, n = 6 (two runs, 3 samples per run).

## 4.3 Selectivity of Flame-NAPE

<u>4.3.1 PLA$_1$ *in Vitro* Tests</u>

*4.3.1.1 PLA$_1$ Fluorescence Test*

Flame-NAPE being resistant to hydrolysis by enzymes with PLA$_1$ activity would represent a major advantage over the existing activity probe (PED-A1), which is why flame-NAPE was designed without the *sn*-1 ester bond necessary for it to undergo PLA$_1$ hydrolysis. To confirm this resistance, I tested the hydrolysis of flame-NAPE and PED-A1 by PLA$_1$ *in vitro*. As expected, PED-A1 was readily hydrolyzed to a fluorescent product (ex/em 488/530 nm) by 50 min incubation with either PLA$_1$ purified from *Aspergillus oryzae* (*A. oryzae*) or purified recombinant Nape-pld (Figure 34 A). In contrast, flame-NAPE could be hydrolyzed to a fluorescent product only by Nape-pld and not by PLA$_1$ (Figure 34 A).
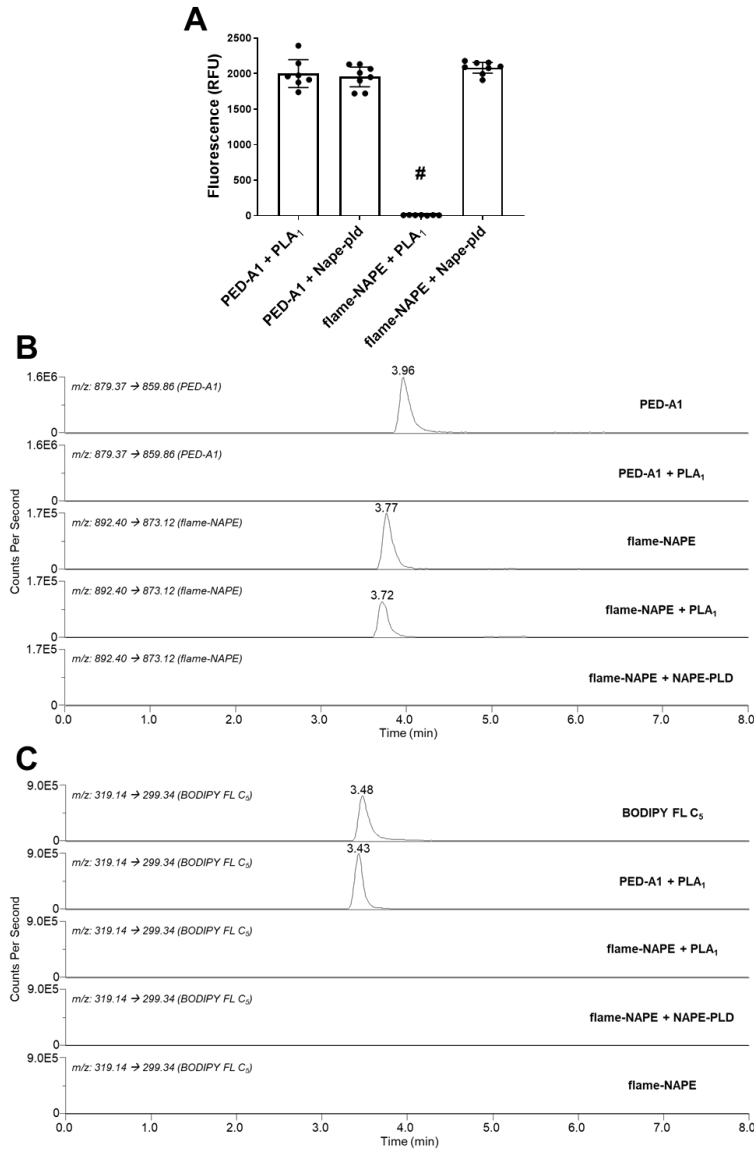
**Figure 34.** PED-A1 and flame-NAPE selectivity *in vitro*. PED-A1 and flame-NAPE were incubated *in vitro* with either purified $PLA_1$ from *Aspergillus oryzae* or recombinant murine Nape-pld, and the extent of hydrolysis was measured by fluorescence and by LC/MS/MS. **A.** Fluorescence (ex/em 488/530 nm) generated by phospholipase treatment with PED-A1 or flame-NAPE. Ordinary one-way ANOVA $p$=0.0310; Tukey multiple comparisons test, #$p$<0.0001 vs. each of the other treatments. Mean ± 95% CI shown. **B.** Representative multiple reaction monitoring chromatographs for unhydrolyzed PED-A1($m/z$ 879.1→ 859.9) and unhydrolyzed flame-NAPE ($m/z$ 892.4 → 873.1). **C.** Representative multiple reaction monitoring chromatographs for BODIPY FL $C_5$ ($m/z$ 319.1 → 299.3).

### 4.3.1.2 $PLA_1$ LC/MS Test

To confirm that the lack of fluorescence after incubation with $PLA_1$ was the result of flame-NAPE's resistance to hydrolysis, Dr. Davies and I developed an LC/MS/MS

93

multiple reaction monitoring method to measure intact PED-A1 (m/z 879.4 $\rightarrow$ m/z 859.9), flame-NAPE (m/z 892.4 $\rightarrow$ m/z 873.1), and the expected PLA$_1$ hydrolysis product of both (BODIPY FL C$_5$, m/z 319.1 $\rightarrow$ m/z 299.3) and used this method to analyze the products of the *in vitro* fluorescence experiment. Incubation of PED-A1 with purified *A. oryzae* PLA$_1$ for 50 min resulted in complete loss of LC/MS/MS signal for intact PED-A1 and the formation of a robust signal for BODIPY FL C$_5$ (Figure 34 B-C). In contrast, incubation of flame-NAPE with PLA$_1$ had little effect on the LC/MS/MS signal for intact flame-NAPE and failed to generate any signal for BODIPY FL C$_5$ (Figure 34 B-C). Incubation of flame-NAPE with recombinant Nape-pld resulted in a complete loss of signal for intact flame-NAPE and no formation of BODIPY FL C$_5$ (the PLA$_1$ hydrolysis product), consistent with flame-NAPE being a selective Nape-pld substrate.

From these results, we concluded that flame-NAPE was, in fact, a substrate for purified Nape-pld and not for purified *A. oryzae* PLA$_1$. What remained to be seen was whether this selectivity would withstand the addition of many more PLD and PLA$_1$ enzymes in a complex cellular milieu, as well as whether flame-NAPE could be used to measure NAPE-PLD activity in live cells.

## 4.3.2 PLA$_1$/NAPE-PLD Cellular Tests

### 4.3.2.1 Cellular Selectivity Test

In addition to their use in monitoring NAPE-PLD activity in living cells, PED-A1 and PED6 have also been used extensively to measure PLA$_1$ and PLA$_2$ activity in cells, respectively.[125, 126, 130, 159-165] Therefore, the fluorescence measured with these probes may reflect multiple phospholipase activities when administered to cells expressing many types of phospholipases. Flame-NAPE, on the other hand, might be able to overcome this weakness given its *in vitro* selectivity for Nape-pld over PLA$_1$.

HepG2 cells are a human hepatocellular carcinoma cell line that express both hepatic lipase (which has significant PLA$_1$-type activity) and NAPE-PLD. To determine if using flame-NAPE in place of PED-A1 would provide a more selective assay of NAPE-PLD activity in these cells, I investigated the sensitivity of the two substrates to inhibition

of PLA$_1$ and NAPE-PLD. Orlistat (THL) covalently reacts with the catalytic serines of a broad range of lipases, including PLA$_1$s such as endothelial lipase and hepatic lipase.[166-170] Because NAPE-PLD is a zinc metallohydrolase rather than a serine hydrolase, THL does not inhibit its activity (shown in Chapter 2). To inhibit NAPE-PLD, I used Bith, which the Davies lab had recently identified as a potent and selective NAPE-PLD inhibitor.[126]
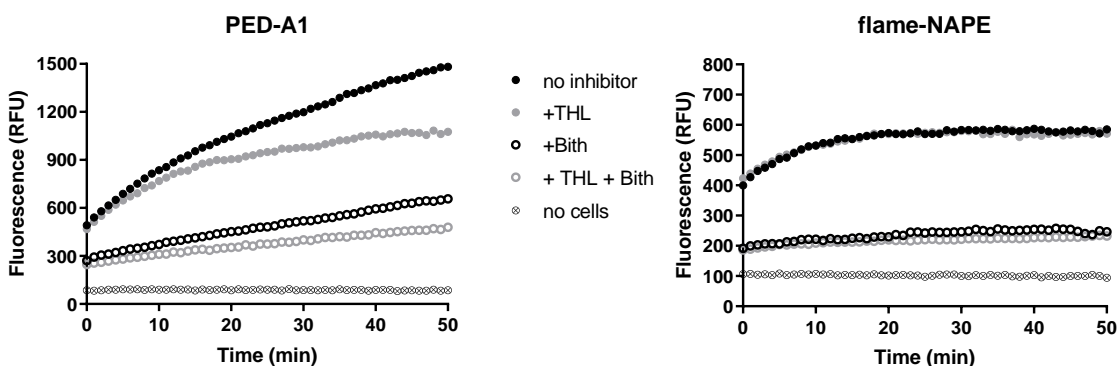


**Figure 35.** PED-A1 and flame-NAPE selectivity in cells. HepG2 cells in 96-well plates were treated with 10 μM tetrahydrolipstatin (THL, a pan-lipase inhibitor), and/or 15 μM bithionol (Bith, a NAPE-PLD inhibitor) prior to the addition of either PED-A1 or flame-NAPE (4 μM). Representative 50-minute fluorescence time course (1 read per minute) for each treatment. Similar time course obtained on two separate days. Symbols represent average of 6-8 replicate wells for each treatment.

In the absence of these PLA$_1$ and NAPE-PLD inhibitors, addition of either 4 μM PED-A1 or 4 μM flame-NAPE to HepG2 cells generated a robust time-dependent increase in cellular fluorescence (total fluorescence minus average fluorescence of substrate in media without cells), indicating phospholipase activity (Figure 35). The fluorescence measured at the 50 min timepoint using 4 μM PED-A1 was 2.9-fold greater than the fluorescence measured using 4 μM flame-NAPE, consistent with flame-NAPE being hydrolyzed by fewer enzymes than PED-A1. Treatment with the PLA$_1$ inhibitor, THL, decreased PED-A1 cellular fluorescence, particularly at time points greater than 10 minutes (Figure 35). Treatment with Bith also decreased PED-A1 cellular fluorescence, and co-treatment with THL and Bith further decreased PED-A1 cellular fluorescence (Figure 35). In contrast, while treatment with Bith markedly decreased flame-NAPE cellular fluorescence, treatment with THL had no effect on flame-NAPE

cellular fluorescence (Figure 35). These results were consistent with PED-A1 cellular fluorescence reporting both NAPE-PLD and $PLA_1$ activity, and flame-NAPE cellular fluorescence reporting NAPE-PLD but not $PLA_1$ activity. These results also suggested that using a relatively short timepoint (e.g., 10 min) as an endpoint makes PED-A1 cellular fluorescence signals more selective for NAPE-PLD activity than longer time points (e.g., 50 min) where $PLA_1$ activity more significantly contributed to the signal (Figure 35).

### 4.3.2.2 Residual Activity

The residual cellular fluorescence seen with flame-NAPE after 15 µM Bith treatment of the HepG2 cells (27% relative to vehicle-treated cells) likely reflected incomplete NAPE-PLD inhibition. The $IC_{95}$ (95% maximum inhibition concentration) for Bith using recombinant Nape-pld is 62.0 µM,[126] but I determined that Bith is cytotoxic to HepG2 cells at concentrations above 15 µM (Figure A8 in Appendix). In order to see the effects of complete NAPE-PLD inhibition on flame-NAPE hydrolysis, I administered combinations of NAPE-PLD inhibitors to HepG2 cells. Residual flame-NAPE cellular fluorescence when combining 15 µM Bith with LEI-401 (a NAPE-PLD inhibitor)[125] was only 10%, and only 6% when a third inhibitor was added (Figure 36). This result indicated that flame-NAPE was reporting exclusively NAPE-PLD activity. With help from Dr. Mashhadi, I attempted to corroborate this conclusion by eliminating NAPE-PLD activity using small interfering RNA (siRNA), but the efficiency of the siRNA transfection was too variable for that method to be relied upon (Figure A9 in Appendix). However, the results from combining NAPE-PLD inhibitors were sufficient confirmation that flame-NAPE was only reporting NAPE-PLD activity.
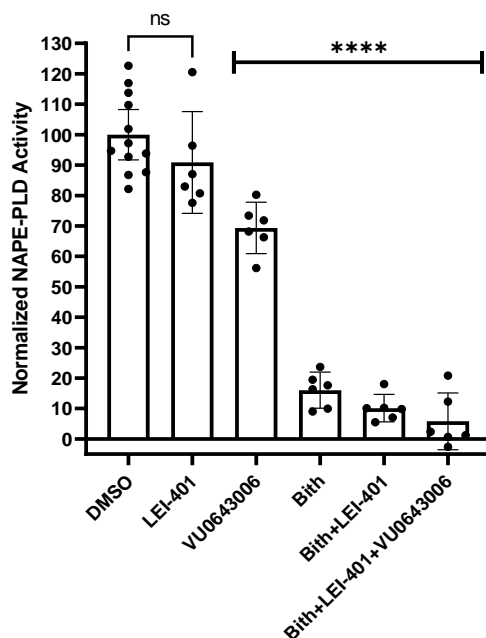
**Figure 36.** Near-complete inhibition of flame-NAPE cellular fluorescence signal by NAPE-PLD inhibitors. HepG2 cells were treated with vehicle (DMSO), 33 µM LEI-401, 33 µM VU0643006, 15 µM Bith, or a combination thereof, and cellular fluorescence with flame-NAPE was measured and normalized to vehicle controls. Ordinary one-way ANOVA $p<0.0001$, Tukey's multiple comparisons test ****$p<0.0001$. Mean ± 95% CI and individual values shown.

## 4.4 Cellular NAPE-PLD Activity Assay Viability

NAPE-PLD is proposed to play key roles in adipocytes, kidney epithelial cells, small intestinal enterocytes, and macrophages.[11, 53, 75, 96, 105, 112] Each of these cells expresses $PLA_1$s in addition to NAPE-PLD,[171-174] so we sought to determine if flame-NAPE would report NAPE-PLD activity in these cell types more selectively than PED-A1, as it did in HepG2 cells.

To determine this, I incubated PED-A1 and flame-NAPE with cultured HEK-293 cells (human kidney epithelial cells), 3T3-L1 cells (mouse preadipocyte cell line), mouse bone marrow-derived macrophages (BMDMs), and Caco-2 cells (human colon carcinoma cell line) that had been pre-treated with or without 15 µM Bith for 1 h, and cellular fluorescence was analyzed at the 10 min time point (Figure 37 A-D).

97
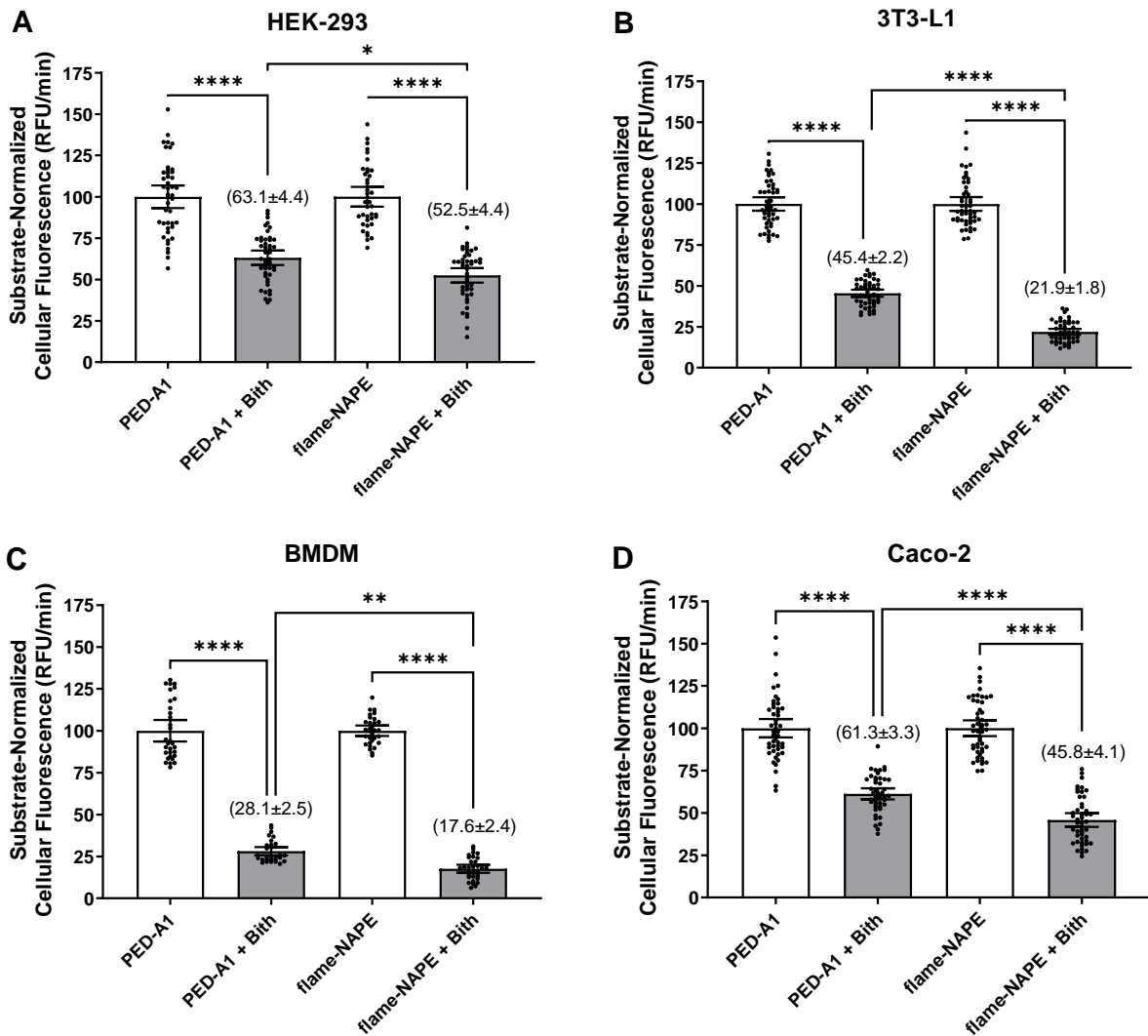
**Figure 37.** Phospholipase activity measured using flame-NAPE is more sensitive to NAPE-PLD inhibition than activity measured using PED-A1 in many cell types. Various cultured cell types were treated with or without 15 µM Bith prior to incubation with PED-A1 or flame-NAPE (4 µM). Bars represent average ± SEM, n = 31-48 with 7-16 replicates each for three separate experimental days. (**A**) HEK-293, (**B**) 3T3-L1, (**C**) BMDM (bone marrow-derived macrophage), and (**D**) Caco-2. 1-way ANOVA for each cell type $p<0.0001$, Tukey's multiple comparisons test, $*p<0.025$, $**p<0.0013$, $****p<0.0001$. Number in parentheses equals substrate-normalized cellular fluorescence for Bith-treated cells (mean ± 95% CI).

In all four cell types, Bith inhibited the flame-NAPE signal to a greater extent than the PED-A1 signal (47% vs 37% inhibition in HEK-293; 78% vs 55% in 3T3-L1; 82% vs 72% in BMDM; and 54% vs 39% in Caco-2). These results were consistent with flame-NAPE cellular fluorescence selectively reporting NAPE-PLD activity, and PED-A1

98

cellular fluorescence reporting the combined activity of NAPE-PLD and PLA$_1$s, even at a time point where PED-A1 was at its most selective for NAPE-PLD activity. These results also demonstrated that flame-NAPE can be used in a wide variety of cultured cells to measure NAPE-PLD activity selectively, rapidly, and easily.


## 4.5 Conclusions

Our results demonstrated that the use of flame-NAPE provides a facile method to assay NAPE-PLD activity selectively in a variety of cell types. Such an assay has long been needed to enable studies elucidating how various external stimuli and signaling pathways modulate NAPE-PLD activity and NAE biosynthesis. Understanding the control of NAE biosynthesis is critical because NAEs, including anandamide (AEA), PEA, and OEA, regulate a host of physiological processes such as feeding, nociception, leukocyte infiltration, insulin secretion, and macrophage polarization.[53, 62, 86, 102, 175-178] Therefore, altered activities of their biosynthetic enzymes may be important factors in diseases.

Understanding how NAE biosynthesis is regulated and why it becomes dysregulated under certain conditions has been challenging in part due to the lack of appropriate methods for measuring the activity of individual NAE-biosynthetic enzymes. In addition to NAPE-PLD, at least two other enzymatic pathways metabolize NAPEs into NAEs. ABHD4 acts as both a PLA$_1$ and a PLA$_2$ to convert NAPE to glycerophospho-*N*-acyl-ethanolamide (GP-NAE),[179] which can be converted to NAE by GDE1, GDE4, or other similar phosphodiesterases (Figure 30).[62, 154, 155] Another alternative pathway for NAE biosynthesis utilizes an as yet unidentified NAPE-hydrolyzing phospholipase C (NAPE-PLC) that hydrolyzes NAPE to diacylglycerol and phospho-*N*-acylethanolamine (phospho-NAE). Phospho-NAE can then be converted to NAE via phosphatases such as PTPN22 and SHIP1 (Figure 30).[180] Being able to measure the activity of the various members of these pathways selectively would greatly benefit investigations into the regulation of NAE biosynthesis. And the novel assay described herein will help in that process.

Fluorogenic activity assays have considerable advantages compared to methods such as TLC and LC/MS/MS in terms of reduced time and resource consumption, as long as the probes utilized selectively measure the desired activity. While the fluorogenic probes PED6 and PED-A1 have been used in high-throughput screenings to identify NAPE-PLD inhibitors *in vitro*,[125-127, 162] they are sensitive to hydrolysis by other phospholipases that are likely to be present in cells and tissues. PED6 was originally created as a probe for $PLA_2$ activity,[159] and PED-A1 was created as a probe for $PLA_1$ activity.[130] Since, for example, ABHD4 has both $PLA_1$ and $PLA_2$ activity, hydrolysis of PED-A1 or PED6 by NAPE-PLD is indistinguishable from hydrolysis by ABHD4 as measured by fluorimetry. Furthermore, many other $PLA_1$ or $PLA_2$ enzymes that can hydrolyze PED-A1 and PED6 are present in cells and tissues where measurement of NAPE-PLD activity is desired,[130, 181, 182] leading to additional interfering signals. In fact, our own studies with THL confirmed that a significant portion of PED-A1 hydrolysis in cultured cells resulted from phospholipases other than NAPE-PLD. Therefore, if PED-A1 (or PED6) is used to measure NAPE-PLD activity in cultured cells or tissues, THL (or another appropriate inhibitor) should be added prior to initiation of the assay to block signals from other enzymes.

The use of flame-NAPE to measure NAPE-PLD activity in our assay method overcame the major limitations of PED-A1 and PED6. The substitution of an *N*-methyl amide group for the *sn*-1 ester of PED-A1 made flame-NAPE completely resistant to hydrolysis by *A. oryzae* $PLA_1$. Flame-NAPE fluorescence was not inhibited by THL in HepG2 cells, supporting the notion that serine hydrolase-type phospholipases do not significantly contribute to flame-NAPE hydrolysis. Flame-NAPE fluorescence was, however, significantly inhibited by the NAPE-PLD inhibitor Bith in all of the cell-types that we tested and was reduced to nearly 0 when a combination of NAPE-PLD inhibitors was used. It is possible that in some cell types, a non-serine hydrolase-type phospholipase, such as the putative NAPE-PLC, contributes to flame-NAPE cellular fluorescence. One limitation of our validation studies was that the contribution of the putative NAPE-PLC to flame-NAPE fluorescence could not be tested directly because the enzyme has not been cloned or purified. However, significant NAPE-PLC contribution seems unlikely because this putative NAPE-PLC appears to prefer *N*-

arachidonoyl-PEs over NAPEs with shorter and more saturated *N*-acyl chains,[180] likely making flame-NAPE a poor NAPE-PLC substrate.

Although the method described herein was designed to measure NAPE-PLD activity in cultured cells, the previous use of PED6 in zebrafish embryos and larvae to image sites of active $PLA_2$ in the digestive tract suggest that flame-NAPE could be used in a similar manner for imaging NAPE-PLD activity *in vivo*.[161, 183] This might be particularly useful for examining the effects of diet and other environmental factors on intestinal, adipocyte, and macrophage NAPE-PLD activity. Imaging of flame-NAPE within cultured cells or tissues could also provide insight into NAPE-PLD localization.

In summary, flame-NAPE provides a rapid and straightforward method for measuring NAPE-PLD activity selectively both *in vitro* and in cultured cells. This assay has the potential to facilitate studies into factors that alter NAPE-PLD activity, the role of NAPE-PLD activity in controlling individual NAE levels, whether changes in NAPE-PLD activity contribute to disease, and the extent to which potential interventions rescue NAPE-PLD activity. And, of course, the flame-NAPE assay represents a simple and reliable means for measuring the effects of our novel NAPE-PLD modulators in cultured cells.

## 4.6 Methods

### 4.6.1 Acquisition of Absorbance and Emission Spectra

#### 4.6.1.1 Initial Absorbance Scans

NAPE-PLD substrates (PED-amide, PED-A1, and flame-NAPE) were prepared from dried stocks by dissolving in buffer containing 50 mM Tris-HCl pH 8.0, ethanol, and DMSO (60:32:8 v/v/v) and the absorbance spectrum from 300 to 700 nm recorded using an Eppendorf Biospectrometer kinetic UV/VIS spectrometer.

*4.6.1.2 Additional Scans*

PED-A1 (4 µM) and flame-NAPE (4 µM) were reacted with either Nape-pld or vehicle control according to the activity assay protocol described below. After allowing the reaction to reach completion (60 min), absorbance at 10 nm intervals from 300 to 700 nm was read using a BioTek Synergy H1 plate reader (at 37 °C). Also, emission was read using the same plate reader at 10 nm intervals from 510 to 700 nm (at 37 °C, excitation of 488 nm). For the absorbance spectra, background wells were included in order to eliminate background from the test wells.

## 4.6.2 *In Vitro* Activity Assays

Recombinant mouse Nape-pld was expressed in *E. coli* and purified as previously described.[126] Purified *Aspergillus oryzae* PLA$_1$ was purchased commercially (Sigma L3295). PED-A1 (ThermoFisher), flame-NAPE, and PED-amide were prepared in buffer containing 50 mM Tris-HCl pH 8.0, ethanol, and DMSO (60:32:8 v/v/v).

*4.6.2.1 $K_M$ Determination*

55 µL of 50 mM Tris-HCl buffer (pH = 8.0) and 5 µL of 7% (w/v) *N*-octyl-β-D-glucoside solution (Millipore 494459) was added to clear-bottom, black-walled, non-treated, 96-well plates (Thermo 265301), followed by 5 µL of 73 µg/mL Nape-pld (final concentration 4.56 µg/mL) or 5 µL of Tris-HCl buffer (for negative controls), and then 5 µL of test compound vehicle (1.6% DMSO (v/v) in Tris-HCl buffer) and incubated for 1 h at 37 °C. To initiate the activity assay, 10 µL of ice-cold substrate was added to every well with final concentration from 0 to 20 µM (6 replicates per condition). Fluorescence (ex/em 488/530 nm) was measured in a BioTek Synergy H1 plate reader at 37 °C. Reaction rate was measured as change in fluorescence from t = 1-4 min, n = 6, mean ± SEM. $K_M$ values for PED-A1 and flame-NAPE were calculated in GraphPad Prism 7.0 using nonlinear regression (allosteric sigmoidal) and software; there was evidence of an inadequate model for the flame-NAPE regression (F = 3.63, *p* = 0.0144).

*4.6.2.2 Determination of Enzyme Selectivity*

60 µL of Tris-HCl buffer was added to wells of a clear-bottom, black-walled, non-treated, 96-well plate, followed by 5 µL of Nape-pld (4.56 µg/ml final concentration), *A. oryzae* PLA$_1$ (34.6 U/mL final concentration), or Tris-HCl buffer (negative control). 5 µL of 7% (w/v) N-octyl-β-D-glucoside solution was added to the wells that received Nape-pld, and 5 µL of Tris-HCl buffer to wells that received PLA$_1$ or the negative control. After 1 h of incubation at 37 °C, 10 µL of ice-cold substrate was added (4 µM final concentration) and fluorescence was measured as above. Background fluorescence in absence of phospholipase was subtracted from all groups.

4.6.3 Cell-Based Assays

*4.6.3.1 Cell Culturing*

HepG2, HEK-293, 3T3-L1, and Caco-2 cells were purchased from ATCC (HB-8065, CRL-1573, CL-173, and HTB-37, respectively). BMDMs were cultured by the laboratory of Dr. Amanda Doran. Bone marrow progenitors were obtained from 8-12-week-old C57BL6/J mice. These progenitors were cultured using a previously published method to yield the bone marrow-derived macrophages (BMDM).[52] The base cell media for all cell assays was Dulbecco's modified eagle media (DMEM) with 4.5 g/L glucose, 1 mM sodium pyruvate, and 4 mM L-glutamine. For the growth of HEK-293 and 3T3-L1 cells, phenol red and 10% (v/v) heat-inactivated fetal bovine serum (HI-FBS) were added to base media. For Caco-2 cell growth, phenol red and 20% (v/v) HI-FBS were added to base media.

*4.6.3.2 Activity Assays*

For the assay, all cells were plated at 20,000 cells/well in clear-bottom, black-walled, tissue culture-treated, 96-well plates; negative control wells had no cells added. After the cells reached ~90% confluency, the growth media was removed and 100 µL/well of treatment media (see below) added, incubated for 1 h at 37 °C, then 5 µL of

84 µM PED-A1 or flame-NAPE in Tris-HCl/ethanol/DMSO (60:32:8 v/v/v) added to each of the wells (4 µM final).

For the initial HepG2 cell studies, the treatment media was base media with either NAPE-PLD inhibitor Bith (15 µM final), the pan-serine hydrolase lipase inhibitor THL (10 µM final), both, or vehicle (DMSO); all contained 0.71% v/v DMSO final. For the subsequent HepG2 cell study the treatment media was base media with either 15 µM Bith, 33 µM LEI-401 (Cayman Chemicals), 33 µM VU0643006 (Life Chemicals), a combination, or vehicle (DMSO); all contained 1.7% v/v DMSO final. For assays with HEK-293, 3T3-L1, BMDM, or Caco-2 cells, the inhibitor media was base media with either bithionol (15 µM final), or vehicle (DMSO); with the concentration of DMSO in all assays being 0.016% v/v final.

For all cellular experiments, fluorescence (ex/em 488/530 nm) was measured at 1-minute intervals in a BioTek Synergy H1 plate reader at 37 °C. After the initial study in HepG2 cells, subsequent studies used the fluorescence values at 10 min for analysis. Final values were reported as substrate-normalized cellular fluorescence. To calculate this value, cellular fluorescence was first calculated as the fluorescence in the well measured at 10 min minus the average fluorescence of the wells with the appropriate substrate, but no cells (background fluorescence) measured at 10 min. This cellular fluorescence value was then normalized by dividing this value by the average cellular fluorescence value for vehicle (DMSO only) treated cells and multiplying by 100%. Each experiment was carried out on at least two separate days and the normalized values from separate days combined.

For HepG2 cells, background fluorescence at 10 min for PED-A1 and flame-NAPE were typically 12% and 21%, respectively, of the raw fluorescence for vehicle-treated HepG2 cells. At the 10 min timepoint, the average raw fluorescence measured in vehicle-treated HepG2 cells with flame-NAPE was 66% that of similarly treated cells with PED-A1. For HEK-293, 3T3-L1, BMDM, and Caco-2 cells where PED-A1 was used substrate, the average background fluorescence (wells without cells) at the 10 min endpoint was 20%, 23%, 23%, and 19%, respectively, of the raw fluorescence of vehicle-treated cells. For HEK-293, 3T3-L1, BMDM, and Caco-2 cells where flame-

NAPE was used as substrate, the background fluorescence (wells without cells) at the 10 min endpoint was 24%, 34%, 33%, and 22%, respectively, of total raw fluorescence of vehicle-treated cells. The average raw fluorescence at 10 min endpoint for vehicle-treated HEK-293, 3T3-L1, BMDM, and Caco-2 cells when 4 µM flame-NAPE was used as substrate was 89%, 94%, 76%, and 92%, respectively, of the raw fluorescence when 4 µM PED-A1 was used as substrate.

### 4.6.3.3 Cytotoxicity Assay

A methylthiazoletetrazolium (MTT) assay was used to measure cytotoxicity, using a previously reported method.[126] The method was modified as follows: treatments were conducted in 96-well plates instead of 24-well plates to avoid unnecessary fluid transfers, 100 µL of 0.3 mg/mL MTT solution was added after 24 h of treatment, this was removed after 3 h of incubation and replaced with 0.1M HCl in isopropanol, absorbance at 10 nm intervals from 520-600 nm was read, and absorbance at 560 nm (the peak) was used for analysis.

### 4.6.3.4 siRNA Silencing of NAPE-PLD

NAPE-PLD and control siRNAs were obtained from Origene (SR326044). siRNA transfections were performed using Lipofectamine 3000 Transfection Reagent, according to manufacturer specifications (Invitrogen L3000015). Cells were treated with siRNA for 24 h before the siRNA-containing media was removed and replaced with NAPE-PLD modulator treatments. siRNA transfection controls were TYE 563 RNA (Origene) and they were used alongside NAPE-PLD siRNA in every plate. Transfection efficiency was measured as fluorescence (ex/em 540/570 nm) using a Biotek Synergy H1 plate reader.

# CHAPTER 5

## **Effects of NAPE-PLD Activators in Cells**

This chapter is adapted from Small Molecule Activation of NAPE-PLD Enhances Efferocytosis by Macrophages, published in bioRxiv, and has been reproduced with the permission of the publisher.[127] Authors: Jonah E. Zarrow, Abdul-Musawwir Alli-Oluwafuyi, Cristina M. Youwakim, Kwangho Kim, Andrew N. Jenkins, Isabelle C. Suero, Margaret R. Jones, Zahra Mashhadi, Kenneth P. Mackie, Alex G. Waterson, Amanda C. Doran, Gary A. Sulikowski, and Sean S. Davies. Author contributions: JEZ performed the majority of the experiments, he also performed NAPE synthesis, analyzed data, created figures, interpreted results, and assisted in writing of the initial manuscript. AMAO extracted and cultured BMDMs, assisted with efferocytosis studies, and assisted with HEK-293 cell experiments. CMY performed efferocytosis studies and analysis of efferocytosis data. ANJ assisted in the development of LC/MS assays. ZM assisted with conception of the project, LC/MS assays, and cell culture studies. ICS assisted with cellular and LC/MS assays. KM supervised the husbandry of *Napepld$^{-/-}$* and control mice and femur extraction and provided guidance on Nape-pld biology to the project. AGW edited the manuscript. ACD assisted in conception of the project, supervised and performed efferocytosis assays, provided guidance on macrophage biology to the project, created figures, and assisted in writing the initial manuscript. GAS assisted with the conception of the project, provided guidance of the project, obtained financial support, and edited the manuscript. SSD conceived and guided the overall project, supervised various studies, obtained financial support, oversaw interpretation of the data, created figures, and wrote the manuscript.

LC/MS experiments were conducted at the Vanderbilt Mass Spectrometry Research Core, with assistance from Dr. M. Wade Calcutt and Brian Hachey. Allison Pickens also assisted with LC/MS assay development. The laboratory of Dr. Amanda Doran assisted with BMDM and Jurkat culturing. The original stocks of RAW 264.7 cells were provided by Dr. Claus Schneider.

**5.1 Cytotoxicity**

We wanted to determine whether the BT-PSPs would activate NAPE-PLD in live cells, as that would make them more useful in research and clinical settings. Prior to administering them to cells, however, we had to determine whether they would be toxic to those cells. So, we conducted cellular viability assays. We used RAW 264.7 cells, as they are a macrophage cell model, and our primary biological phenomenon of interest was the effect of NAPE-PLD modulation on macrophage efferocytosis capacity. We also used HepG2 cells because NAFLD has been linked to NAPE-PLD activity and because hepatotoxicity of a compound and/or its metabolites (which are typically formed in the liver) is an important consideration for any lead drug molecule.

5.1.1 Cytotoxicity: RAW 264.7

Before testing the cytotoxicity of all of our compounds, I performed a pilot assay on 13 of them. If most of the compounds were substantially cytotoxic, we would have had to perform extensive medicinal chemistry to find/create non-toxic BT-PSPs. Fortunately, I observed that >75% of cells survived when treated with most of the compounds, and >50% survived when treated with the others (data not shown). One compound, VU0934205, had only ~30% cell survival, so it was eliminated from future cytotoxicity and cellular activity experiments in RAW 264.7 cells.

Following this pilot experiment, I conducted a cytotoxicity screening on all but two of our BT-PSPs (all at 30 µM). 13 of the 20 compounds tested had favorable cell survival (≥75%), five had moderate cell survival (50-75%) and only two had poor cell survival (<50%) relative to vehicle controls (Figure 38 A). From these results, we concluded that the BT-PSPs were sufficiently non-toxic towards RAW 264.7 cells for them to be used in our own and others' research endeavors. The two compounds excluded from this assay were VU0934205 and VU0506534. The former was excluded because it showed toxicity in both the RAW 264.7 and HepG2 pilot assays. The latter was excluded from this assay because I instead performed a full cytotoxicity CRC on it, as it was our top hit.
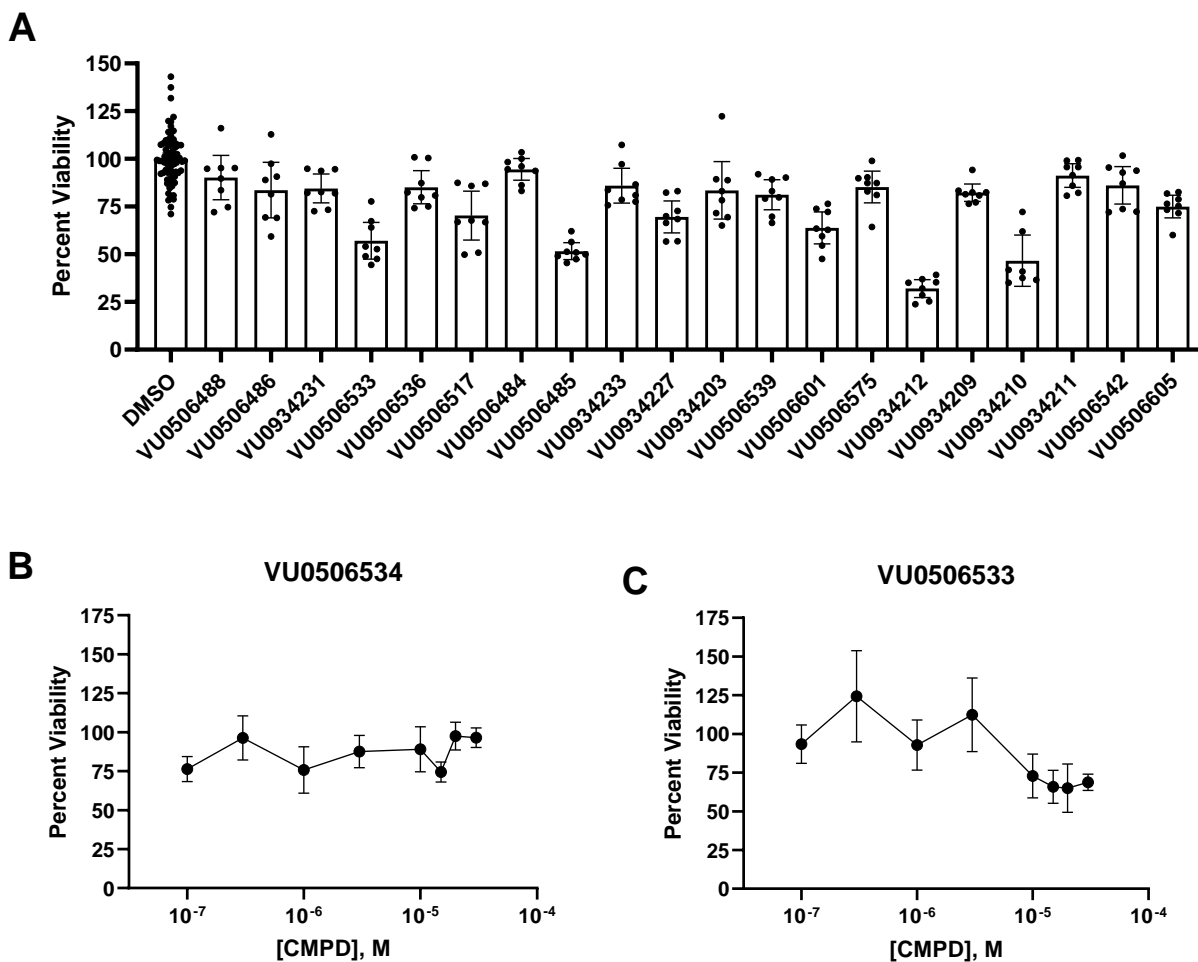
**Figure 38.** BT-PSPs lack severe cytotoxicity in RAW 264.7 cells. **A.** Cell viability at 30 µM for BT-PSPs, normalized to vehicle (DMSO) controls. Mean ± 95% CI shown. **B.** Cytotoxicity CRC for VU0506534, normalized to vehicle controls. Points are mean ± SD from n = 8 technical replicates. **C.** Cytotoxicity CRC for VU0506533, normalized to vehicle controls. Points are mean ± SD from n = 7-8 technical replicates.

The cytotoxicity CRC for VU0506534 showed that the compound lacked substantial cytotoxicity at any of the doses tested (Figure 38 B). This meant that VU0506534 remained in place as the most promising research tool among the BT-PSPs. I also performed a cytotoxicity CRC on VU0506533 because it was among our strongest activators, and in the cytotoxicity screening it only showed 57% cell survival. The full cytotoxicity CRC for VU0506533 showed that at doses above 10 µM, ~65% of the cells survived, and at 10 µM, cell survival was 73% (Figure 38 C). The 10 µM dose was important because it was the dose at which we tested all cellular (and many *in*

*vitro*) activities. We deemed VU0506533's level of cytotoxicity at 10 μM to be acceptable for our assays.

### 5.1.2 Cytotoxicity: HepG2

Once again, before testing the cytotoxicity of all of our compounds, I performed a pilot assay on the eight that we expected would be cytotoxic based on the pilot assay in RAW 264.7 cells. Most of the compounds did not cause meaningful cytotoxicity (data not shown). Only VU0934205 did (~41% cell survival), so it was eliminated from future cytotoxicity and cellular activity experiments in HepG2 cells.

Following the pilot experiment, I conducted a cytotoxicity screening on all but two of our BT-PSPs in HepG2 cells (all at 30 μM). I observed that 17 of the 20 compounds tested had favorable cell survival (≥75%), three had moderate cell survival (50-75%) and none had poor cell survival (<50%) relative to vehicle controls (Figure 39 A). From these results, we concluded that the BT-PSPs were sufficiently non-toxic towards HepG2 cells for them to be used in our and others' research studies. The two compounds that were excluded from this assay were VU0934205 and VU0506534. I excluded VU0934205 because it showed toxicity in both the RAW 264.7 and HepG2 pilot assays. I excluded VU0506534 from this assay because I instead performed a full cytotoxicity CRC on it, as it was our top hit.

**A**
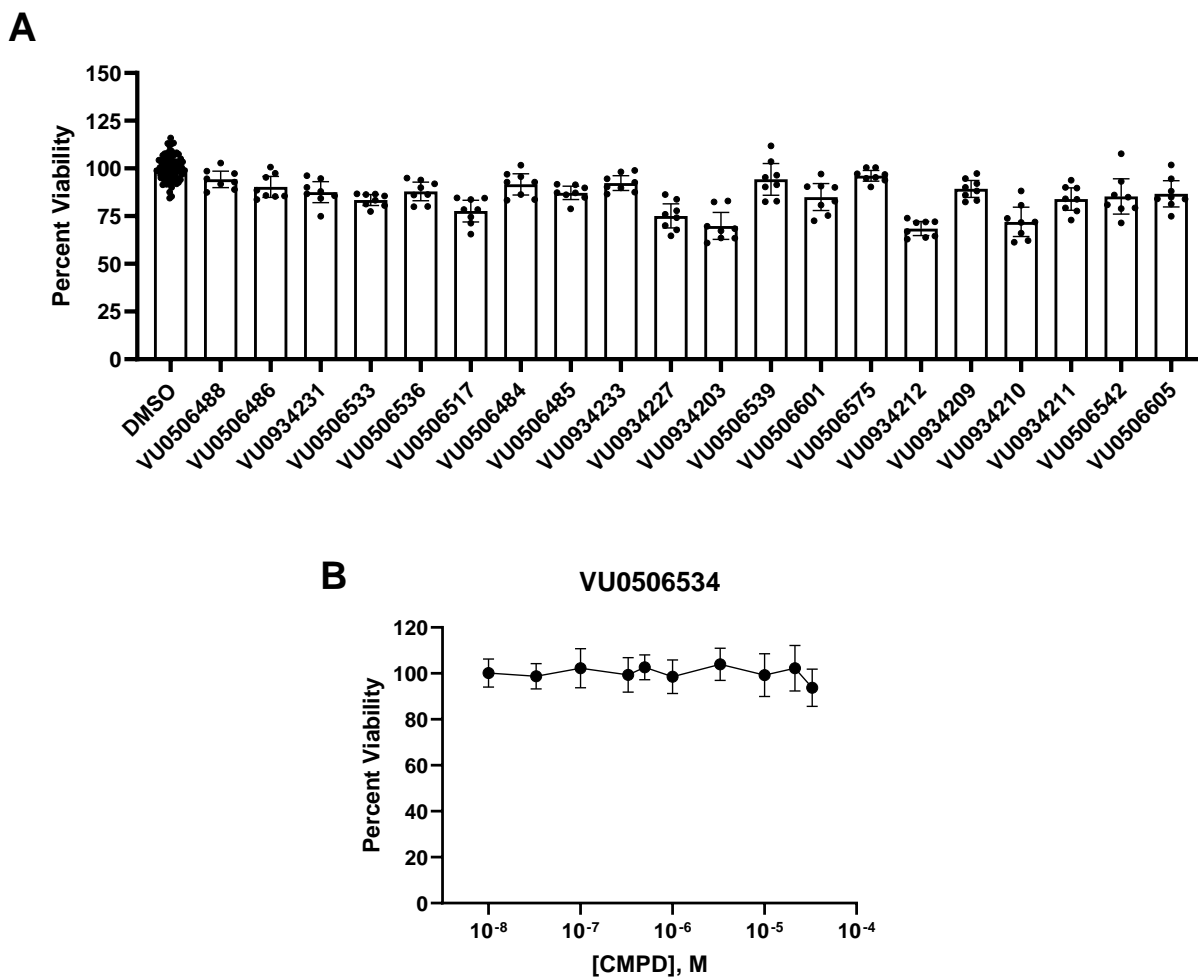


**B** VU0506534

**Figure 39.** BT-PSPs lack severe cytotoxicity in HepG2 cells. **A.** Cell viability at 30 µM for BT-PSPs, normalized to vehicle (DMSO) controls. Mean ± 95% CI shown. **B.** Cytotoxicity CRC for VU0506534, normalized to vehicle controls. Points are mean ± SD from n = 12 technical replicates.

The cytotoxicity CRC for VU0506534 in HepG2 cells showed that it lacked substantial cytotoxicity at any of the doses tested (Figure 39 B). This meant that VU0506534 remained in place as the most promising research tool among the BT-PSPs. Given the combined results of the cytotoxicity assays in RAW 264.7 and HepG2 cells, we concluded that the BT-PSPs would be safe to use by other researchers in at least the two cell types that we tested, and likely more.

**5.2 Cellular NAPE-PLD Activity**

Having established that the compounds were acceptably non-toxic to cells, we were then able to test whether they would modulate NAPE-PLD in cells. This was an important test because the intended use of the compounds is to modulate NAPE-PLD in biological settings. The method used for these assays was the fluorescence-based NAPE-PLD activity assay developed in our laboratory,[133] which was detailed in Chapter 4.

5.2.1 Cellular NAPE-PLD Modulation: RAW 264.7

*5.2.1.1 Single-Dose RAW 264.7 Nape-pld Modulation*

As a pilot experiment to determine if the BT-PSPs were likely to modulate Nape-pld activity in RAW 264.7 cells, I first tested two of our top compounds: VU0506534 and VU0934209. I also tested Bith, because we knew that it consistently modulated NAPE-PLD in many cell types in the past.[126, 133] For simplicity, I only tested them at one dose, 10 µM, as that was 10x the *in vitro* $EC_{50}$ of most of the BT-PSPs. From these results (Figure A10 in Appendix), I saw that VU0506534, VU0934209, and Bith were all able to modulate Nape-pld activity in RAW 264.7 cells. Therefore, I proceeded with testing all of the BT-PSPs for Nape-pld modulation in RAW 264.7 cells.

*5.2.1.2 RAW 264.7 Nape-pld Modulation CRCs*

Almost all of the BT-PSPs dose-dependently increased Nape-pld activity in RAW 264.7 cells (Figure 40 A), indicating their utility for studying the role of NAPE-PLD in cells generally, and in macrophages specifically. Most BT-PSP compounds that increased the activity of recombinant mouse Nape-pld also significantly increased Nape-pld activity in RAW 264.7 cells, with a robust correlation between their efficacy in the two settings (Figure 40 B). This indicated that the effects of the BT-PSPs were robust enough to translate from *in vitro* to cells. PED-A1 was used in the assays in RAW 264.7 cells due to a lack of available flame-NAPE, and PED-A1's poor selectivity was overcome by the coadministration of Orlistat to inhibit enzymes with $PLA_1$ activity. In

addition to those 5-point CRCs, I also conducted more extensive CRCs on several of the top BT-PSPs (Figure 40 C-G). Compounds that showed minimal activity in the limited CRCs (VU0506605 and VU0934233) also showed minimal activity in this assay, while the opposite was true for compounds that showed strong activity in the initial CRCs. These results demonstrated a robust dose-dependence for BT-PSP activation of Nape-pld in RAW 264.7 cells. At 10 µM, VU0506534 and VU0506533 increased Nape-pld activity by 1.5- and 2.2-fold, respectively, while VU0934233 caused no significant increase in activity.
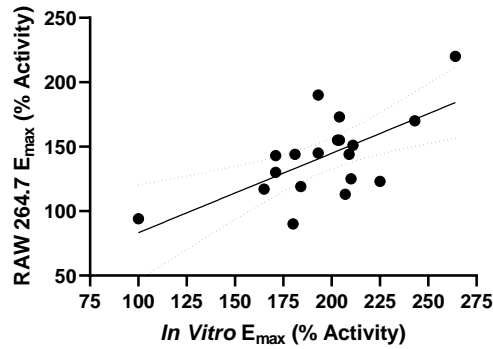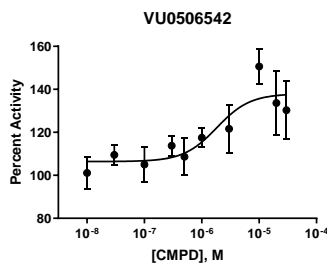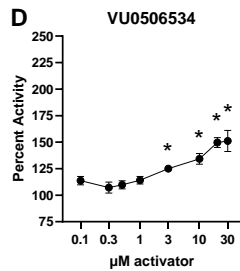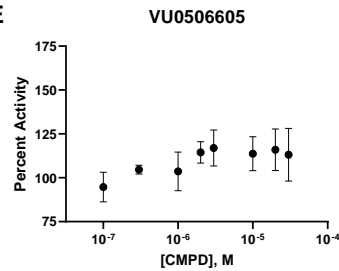
**A**
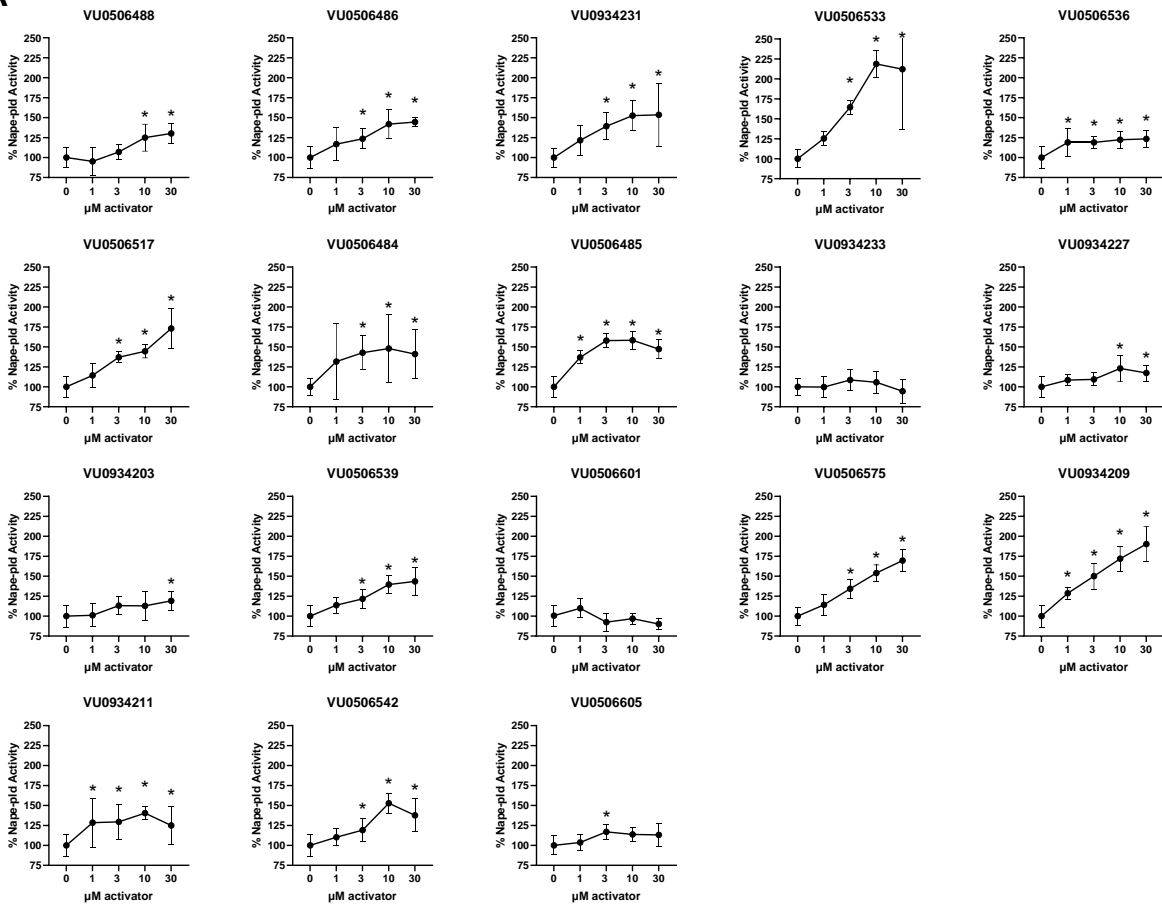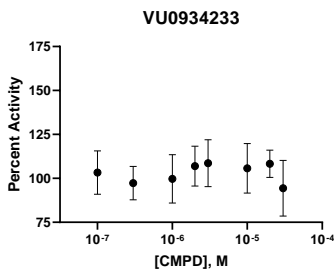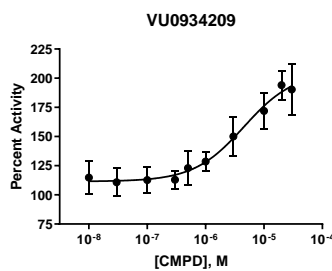
**Figure 40.** BT-PSPs dose-dependently increase Nape-pld activity in RAW 264.7 cells. **A.** Limited concentration-response curves of 18 BT-PSPs for Nape-pld activity, using PED-A1. Each compound was tested on at least two separate days and the individual replicates from each day normalized to vehicle controls and then combined (mean ± SD, n = 4-6). Ordinary one-way ANOVAs for each, $p < 0.05$, except for VU0506601 and VU0934233. *$p < 0.05$ vs. vehicle controls, Dunnett's multiple comparisons test. **B.** Correlation between maximal efficacy of 19 BT-PSPs and analogs in the recombinant Nape-pld assay and their efficacy at 30 µM in cultured RAW 264.7 cells. Maximal efficacy ($E_{max}$) is expressed as a percent relative to vehicle-treated controls. Simple linear regression (solid line) with 95% confidence intervals (dotted lines). Slope = 0.5455, $R^2$ = 0.3394, $p$ = 0.0089 for slope significantly non-zero. **C-G.** Extended CRCs for BT-PSPs. Effect of graded concentrations of VU0506542, VU0506534, VU0506605, VU0934233, and VU0934209 (respectively) on Nape-pld activity in RAW 264.7 cells, measured using PED-A1. Each compound was tested on at least two separate days and the individual replicates from each day normalized to vehicle controls and then combined (mean ± SD, n = 4-6). Best-fit curves were generated using log(agonist) vs. response, variable slope (four parameters) non-linear fits.

<u>5.2.2 Cellular NAPE-PLD Modulation: HepG2</u>

Next, to see if these effects translated to a different type of cell, from a tissue of biological significance, and in cells derived from humans, I performed activity assays in HepG2 cells.

*5.2.2.1 Single-Dose HepG2 NAPE-PLD Modulation*

As with the RAW 264.7 cells, I performed a pilot test to demonstrate BT-PSP activity in HepG2 cells before performing more extensive assays. The results of this experiment showed that the BT-PSPs could modulate NAPE-PLD activity in HepG2 cells (Figure A11 in Appendix). Therefore, I proceeded with further testing.

*5.2.2.2 HepG2 NAPE-PLD Modulation CRCs*

I next performed CRCs in HepG2 cells with some of the most promising BT-PSPs (Figure 41 A-G). The $EC_{50}$ of VU0506534 and VU0506533 were 1.5 µM (95% CI 0.6 to 2.8 µM) and 3.0 µM (95% CI 1.4 to 1.7 µM), respectively. The $E_{max}$ of VU0506534 and VU0506533 were 1.6-fold increase (95% CI 1.5 to 1.8) and 1.6-fold (95% CI 1.5 to 1.8), respectively. This experiment demonstrated that the BT-PSPs dose-dependently modulate NAPE-PLD activity in HepG2 cells, indicating their utility in research using human-derived cells. In addition to being in a different cell type and one derived from a different species than in the RAW 264.7 assays, for graphs A-E I used a different fluorogenic substrate (flame-NAPE in place of PED-A1). This was a way to further demonstrate the reliability of the effects of the BT-PSPs. All tested compounds except for VU0934231 and VU0506575 demonstrated similar activity in HepG2 and RAW 264.7 cells. For VU0934231, this may have been due to differences between the two cell types, as it demonstrated activity in both mouse and human NAPE-PLD *in vitro*. For VU0506575, this effect may have been due to the choice of substrate, as shown by its contrasting activities in Figure 41 D and G.
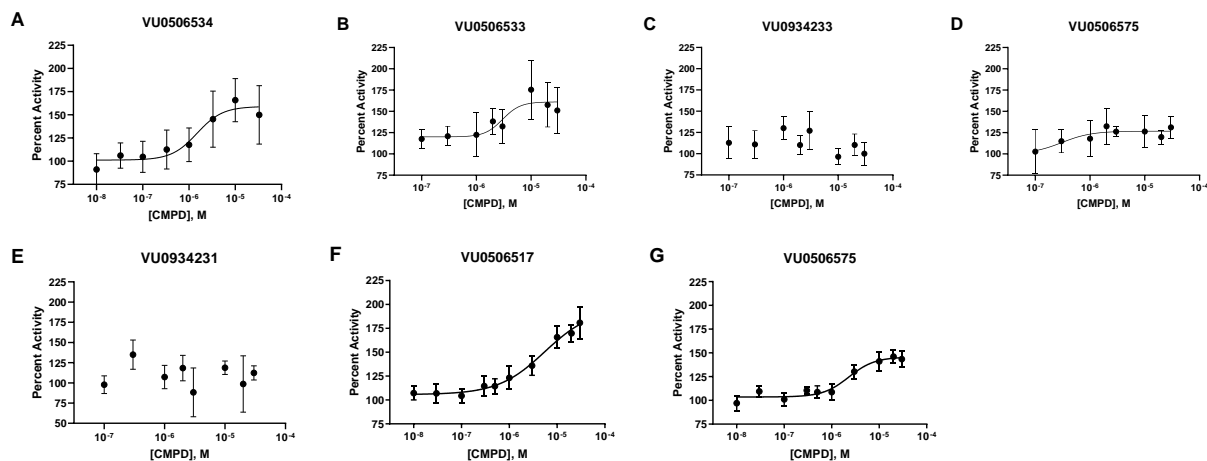
**Figure 41.** BT-PSPs dose-dependently increase NAPE-PLD activity in HepG2 cells. Effects of graded concentrations of VU0506534 (**A**), VU0506535 (**B**), VU0934233 (**C**), VU0506575 (**D**), and VU0934231 (**E**) on NAPE-PLD activity in HepG2 cells, measured using flame-NAPE. Effect of graded concentrations of VU0506517 (**F**) and VU0506575 (**G**) on NAPE-PLD activity in HepG2 cells, measured using PED-A1. Each compound was tested on at least two separate days and the individual replicates from each day normalized to vehicle controls and then combined (mean ± SD, n = 5-14). Best-fit curves were generated using log(agonist) vs. response, variable slope (four parameters).

## 5.2.3 Cellular NAPE-PLD Modulation: Other Cell Types

In addition to testing for NAPE-PLD modulation in RAW 264.7s and HepG2s, I performed modulation experiments in BMDMs and Caco-2s. While the experiments that we performed using those cells were not as extensive, they impacted the course of the research project.

### 5.2.3.1 BMDMs

While the Doran Lab and I were determining the optimal method for testing the modulators' effects on efferocytosis, I performed an activity assay in parallel to ensure that the compounds would maintain modulatory efficacy under the conditions used. At the time, we were determining how long we would treat the BMDMs with our compounds before commencing the efferocytosis, and the times we tested were 5 h and 24 h. The effects of both positive and negative NAPE-PLD modulators were more pronounced at 5 h than at 24 h (Figure 42), indicating that the 5 h incubation time was the best for observing Nape-pld activity-induced changes. This experiment was also the

first demonstration that two of our main compounds of interest (VU0506534 and Bith) modulated Nape-pld activity in primary macrophages.
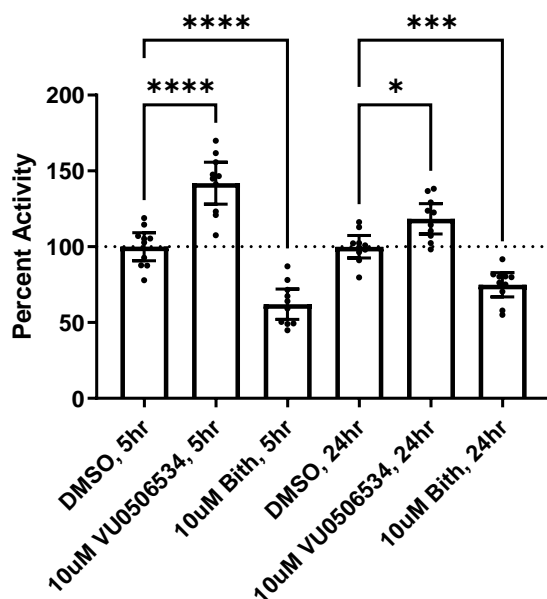


**Figure 42.** Nape-pld modulators effective in BMDMs. Effects of compounds on BMDM Nape-pld activity, with different incubation times, as measured by PED-A1 hydrolysis. Each compound treatment is normalized to its same-time controls (DMSO). Mean ± 95% CI and individual results shown, assay performed once. Ordinary one-way ANOVA $p<0.0001$. Šídák's multiple comparisons test results: *$p=0.0191$, ***$p=0.0007$, ****$p<0.0001$.

*5.2.3.2 Caco-2s*

Early on in the development of the cellular NAPE-PLD activity assay, I performed three assays of the effects of various compounds on NAPE-PLD activity in Caco-2 cells. Caco-2 cells were used because they are a model of human intestinal epithelial cells, which is a tissue of interest in NAPE-PLD research.[11, 99, 184, 185] In the first experiment, I failed to see any treatment effects because there was strong location-dependent variability in all of the treatment groups, particularly the vehicle controls (Figure A12 A in appendix). In the second experiment, severe location-agnostic variability was seen (Figure A12 B in Appendix), again masking any true variations in activity. Given these results and the fact that intestinal epithelial cells transport molecules rapidly across the cell membrane,[184, 185] in my next experiment I attempted to avoid this problem by incubating the cells with the compounds for only 1 min instead of 1 h. In this third

experiment, the inhibitor (Bith) controls that I included had no effect on NAPE-PLD activity (Figure A12 C in Appendix). After performing all three of these experiments, I concluded that something about the assay method was not working. Eventually, Isabelle Paz and I found that the media itself was interfering with our fluorescence signals. We never returned to Caco-2s to measure the activity of the BT-PSPs in them, but that will be a simple yet effective way of further assessing the utility of the BT-PSPs.

## 5.3 Cellular NAPE-PLD Modulation Validations

Having established that the compounds modulate the hydrolysis of fluorogenic NAPE-PLD substrates in various cell types, we attempted to determine whether or not this effect was due to true modulation of NAPE-PLD.

### 5.3.1 Cellular LC/MS Assay

In addition to the conclusive data verifying that BT-PSPs modulate Nape-pld hydrolysis of NAPEs *in vitro* (section 3.1.3), Dr. Alli-Oluwafuyi and I obtained preliminary data indicating that VU0506534 modulates NAPE-PLD activity in live cells. I administered 1,2-dihexanoyl-*sn*-glycero-3-phosphoethanolamine-*N*-oleoyl and 1,2-dihexanoyl-*sn*-glycero-3-phosphoethanolamine-*N*-palmitoyl to HEK-293 cells that he had transfected with either empty vector (pcDNA3.1, Invitrogen) or *NAPEPLD* overexpression plasmid. We used transfected cells as previous experiments had shown that non-transfected cells could not hydrolyze NAPEs fast enough for our assay to measure it (data not shown). Using this method, we saw that *NAPEPLD* transfection led to a large increase in NAPE hydrolysis. And we saw that 24 h treatment of the transfected cells with 20 µM VU0506534 caused an increase in NAPE hydrolysis compared to vehicle. The data from this experiment are not shown because it was performed only once and there was enough variability in the data to indicate that much larger sample sizes were needed due to insufficient statistical power. However, these preliminary data suggested that VU0506534 increases NAPE-PLD hydrolysis of NAPEs in live cells.

### 5.3.2 Modulator Competition Assay in Cells

As in the *in vitro* studies (section 3.2.1), I performed a competition assay to verify whether BT-PSPs act via NAPE-PLD in cells. For this assay, I used VU0506534 as the representative NAPE-PLD activator, Bith as the representative NAPE-PLD inhibitor, and RAW 264.7 cells. When administered alone, Bith dose-dependently decreased Nape-pld activity (Figure 43 A). In the presence of VU0506534, Bith again dose-dependently decreased activity (Figure 43 A). If VU0506534 increased the fluorescence signal via a different mechanism to Bith, there would have been the same total amount of signal increase when VU0506534 was added to each dose of Bith. But that was not the case, so we concluded that the two acted via the same enzyme to alter fluorescence. As Bith has been conclusively demonstrated to modulate NAPE-PLD activity in cells (see Chapters 2 and 4), we could conclude that the compounds' shared target was NAPE-PLD. While it would have been beneficial to include conditions where Nape-pld activity was completely inhibited, I could not increase the dose of Bith past 15 µM due to cytotoxicity (Figure A8 in Appendix). When the data were re-normalized to either vehicle alone (for Bith doses without VU0506534) or to VU0506534 alone (for Bith doses with VU0506534), we could see that each dose of Bith inhibited Nape-pld activity to the same extent, with or without VU0506534 present (Figure 43 B). Together, these results verified that VU0506534 acts via NAPE-PLD to increase PED-A1 hydrolysis in cells, and that it most likely binds to a different site than Bith when doing so.
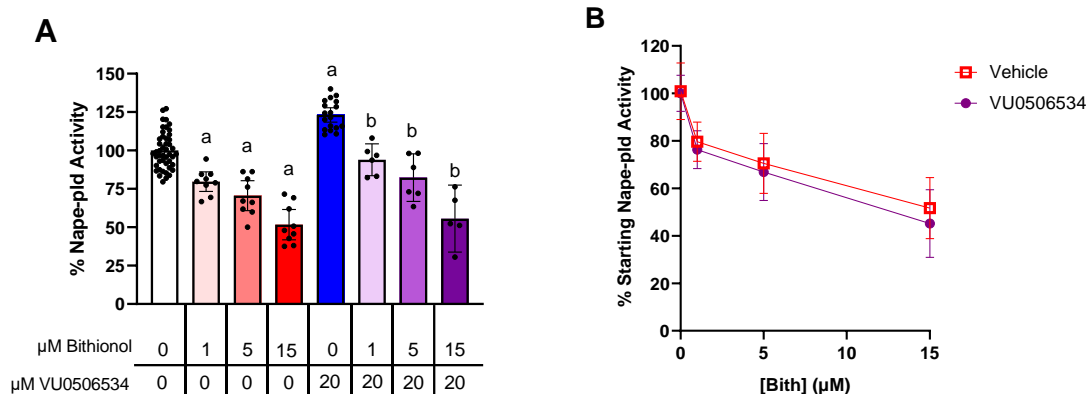
**Figure 43.** Validation of VU0506534's actions on Nape-pld in cells. **A.** Bith, a known Nape-pld inhibitor, blocks increased Nape-pld activity in RAW 264.7 cells induced by VU0506534, measured by PED-A1 hydrolysis and normalized to vehicle controls. Numbers indicate compound dose in μM. Mean ± 95% CI shown. 1-way ANOVA $p<0.0001$ Šídák's multiple comparison test, [a]$p<0.05$ vs 0 μM Bith + 0 μM VU0506534 group, [b]$p<0.05$ vs 0 μM Bith + 20 μM VU0506534 group. **B.** The same data normalized to 0 μM Bith + 0 μM VU0506534 for groups without VU0506534, or to 0 μM Bith + 20 μM VU0506534 for groups with VU0506534. Points are mean ± SD. 2-way ANOVA, Bith factor $p<0.0001$, VU0506534 factor $p=0.184$, interaction factor $p=0.8582$. Within each Bith dose, none of the vehicle-VU0506534 comparisons was significant, Šídák's multiple comparisons test.

## 5.4 Preliminary Macrophage Efferocytosis Data

As discussed in section 1.2, researchers have shown that OEA and PEA—two major products of NAPE-PLD—enhance macrophage M2 polarization, efferocytosis, and ameliorate atherosclerosis phenotypes.[53, 61] Following this lead, the Davies Lab performed preliminary studies intended to probe the influence of NAPE-PLD activity on macrophage efferocytosis capacity.

### 5.4.1 Confocal Imaging of Phagocytosis

After creating the selective PLD activity probe, flame-NAPE, we wanted to determine if it could be used to visualize areas of high NAPE-PLD activity in live cells when imaged with a confocal microscope. Since we knew that NAPE-PLD products had effects on macrophage polarization and efferocytosis, we used macrophages performing phagocytosis of apoptotic cells for this test (efferocytosis is phagocytosis of

apoptotic cells, but it must be validated with genetic markers to conclusively differentiate it from other forms of phagocytosis). As an additional benefit, this test had the potential to reveal the mechanisms by which NAPE-PLD influences efferocytosis. This experiment was performed by Dr. Amanda Doran.

When the macrophages were not performing phagocytosis, the areas with highest Nape-pld activity appeared to be the cell membrane and possibly the endoplasmic reticulum (Figure 44 A). When the macrophages were performing phagocytosis, the endoplasmic reticulum again had a higher density of Nape-pld activity. And, even more strongly, there was Nape-pld activity at the cell membranes of both the macrophage and the apoptotic cell, localized in and around the phagocytic synapse (Figure 44 B). We made two main conclusions from this experiment. The first was that flame-NAPE could, indeed, be used to visualize areas with high NAPE-PLD activity in cells. The second was that NAPE-PLD may be directly involved in the process of phagocytosis/efferocytosis, and not merely indirectly by increasing NAE levels.
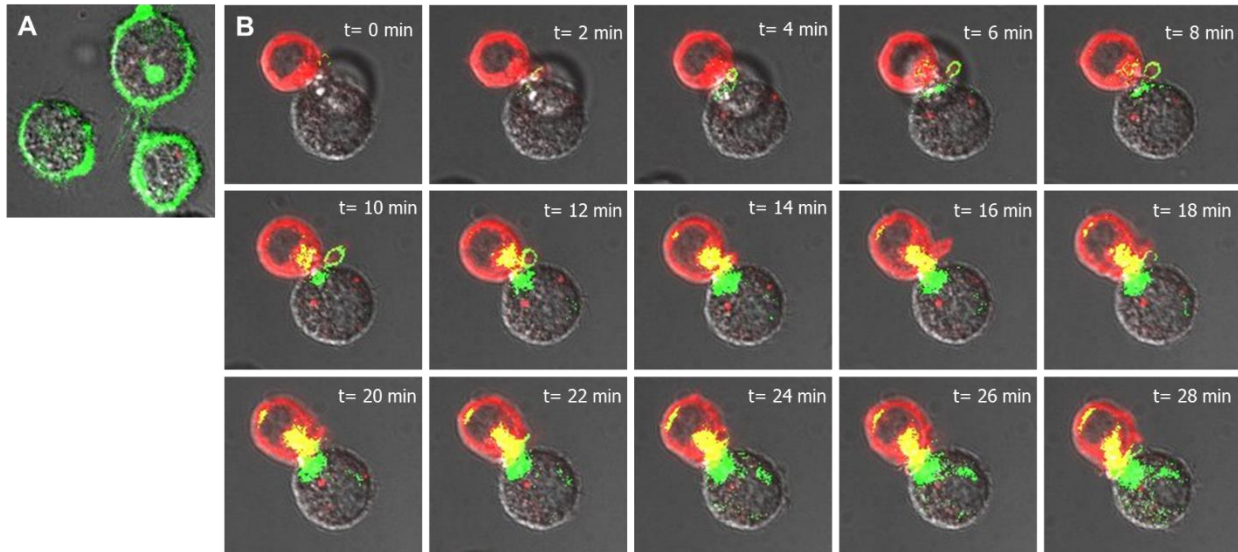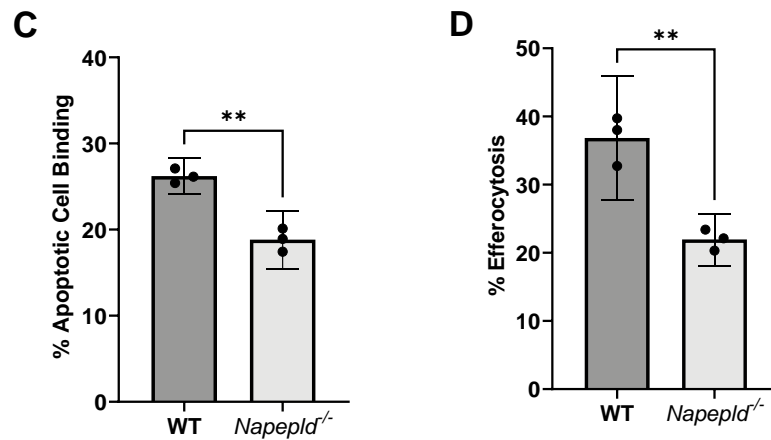
**Figure 44.** Preliminary results indicating Nape-pld's enhancement of efferocytosis. **A.** Confocal microscope image of BMDMs treated with flame-NAPE. Green produced by flame-NAPE hydrolysis product, BODIPY-PA. **B.** Confocal microscope images of BMDM (unlabeled) phagocytosing an apoptotic T cell (red cell membrane), after treatment with flame-NAPE (green, produced by BODIPY-PA). Locations where red and green overlap are yellow. Time since addition of flame-NAPE indicated in each image. **C.** Effect of *Napepld* knockout on macrophage binding to apoptotic T cells (mean ± 95% CI). Unpaired t-test, **$p$=0.0013. **D.** Effect of *Napepld* knockout on macrophage efferocytosis of apoptotic T cells (mean ± 95% CI). Unpaired t-test, **$p$=0.0029.

## 5.4.2 NAPE-PLD Knockout and Efferocytosis

Since the effects of NAPE-PLD activity on efferocytosis had only been indirectly demonstrated (via expression changes, OEA and PEA levels, and via flame-NAPE visualization), we wanted to directly demonstrate the effect of NAPE-PLD on efferocytosis. To do this, Dr. Linda May-Zhang (formerly of the Davies Lab) generated BMDMs from wild-type (WT) and *Napepld$^{-/-}$* (NPKO) mice. Then, Dr. Doran and her laboratory performed two tests of efferocytosis. The first was an assessment of macrophage binding to apoptotic cells, which is a critical initial step in the process of efferocytosis. This test showed that NPKO macrophages bound to apoptotic cells less frequently than did WT macrophages (Figure 44 C). The second test was a measurement of efferocytosis, and in this experiment, NPKO cells performed less efferocytosis than WT cells (Figure 44 D). As predicted from NAPE-PLD's products increasing efferocytosis, *Napepld* knockout decreased efferocytosis. Therefore, we concluded that we could enhance efferocytosis by increasing NAPE-PLD activity.

## 5.5 NAPE-PLD and Efferocytosis

Based on our preliminary findings that genetic knockout of *Napepld* decreased efferocytosis and that Nape-pld appeared to be directly involved in phagocytosis, and based on previous research showing that addition of NAEs hinders atherosclerosis by increasing the efferocytotic capacity of macrophages,[53, 61] we next determined whether pharmacologically activating Nape-pld would enhance efferocytosis. To do this, we used established methods for measuring efferocytosis.[52, 54] In this method, Jurkat cells (immortal T cell line) are irradiated to induce apoptosis, then they are fluorescently labelled and fed to differently labelled BMDMs. The two are co-incubated for 45 min, fixed, and then passed through a flow cytometer to count cells bearing both labels as a percentage of cells bearing only the BMDM label. All of the experiments in this section utilized this method, were designed by Dr. Davies and me, and were performed by or with the Doran Lab and Dr. Alli-Oluwafuyi.

5.5.1 Efferocytosis Modulation by BT-PSPs

Inhibition of Nape-pld with Bith (10 µM) decreased efferocytosis, while activation of Nape-pld with VU0506534 or VU0506533 (10 µM) increased efferocytosis (Figure 45 A). Treatment with VU0934233 (10 µM), which is inactive against NAPE-PLD, slightly reduced efferocytosis (Figure 45 A), indicating that the effects of VU0506534 and VU0506533 were due to their actions on NAPE-PLD and were not caused by an off-target effect shared by all BT-PSPs. These results demonstrated that Nape-pld inhibition decreases and activation increases efferocytosis, as hypothesized. And, these results showed that the BT-PSPs can be used to enhance efferocytosis in primary macrophages.
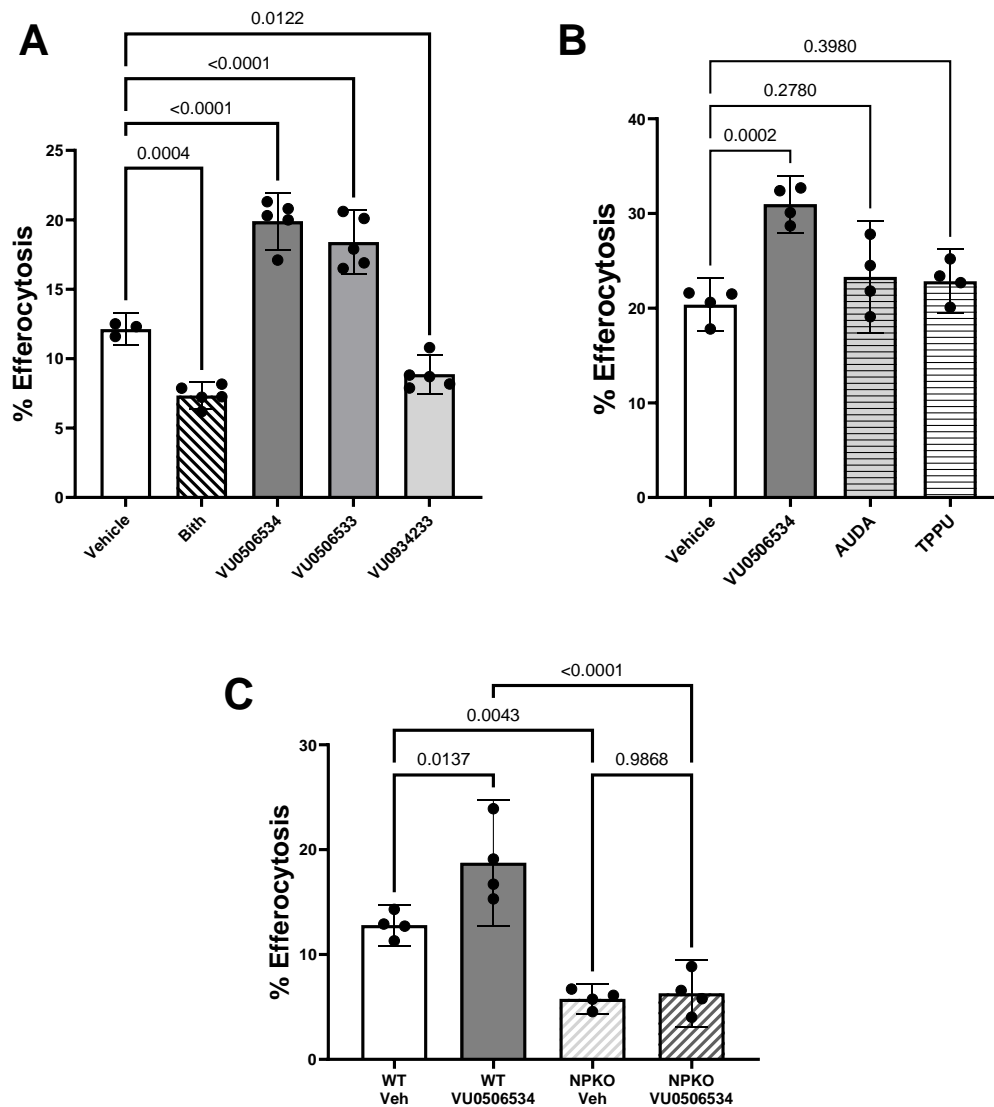
**Figure 45.** BT-PSPs enhance BMDM efferocytosis in a Nape-pld-dependent manner. **A.** BMDM from wild-type mice were treated with 10 μM VU0506534, VU0506533, VU0934233 or bithionol (Bith) for 6 h prior to initiation of efferocytosis assay. Ordinary one-way ANOVA $p$=0.0004. Dunnett's multiple comparison's test $p$ value shown for each comparison. Data shown from one representative experimental day (with mean ± 95% CI). All compounds were tested on two to six separate experimental days. **B.** BMDM from wild-type mice were treated with 10 μM VU0506534 or with sEH inhibitors AUDA (10 μM) or TPPU (10 μM) for 6 h prior to initiation of efferocytosis assay. Ordinary one-way ANOVA $p$=0.0004. Dunnett's multiple comparisons test $p$ value shown for each comparison. Data shown from one representative experimental day of two total experimental days (with mean ± 95% CI). **C.** BMDM from wild-type (WT) or *Napepld*^{-/-} (NPKO) mice were treated with vehicle (Veh) or 10 μM VU0506534 for 6 h prior to initiation of the efferocytosis assay. 1-way ANOVA $p$<0.0001, Dunnett's multiple comparison $p$ value shown for each comparison. Data shown from one representative experimental day of three total experimental days (with mean ± 95% CI).

123

## 5.5.2 Efferocytosis Modulation by sEH Inhibitors

As discussed in section 3.3.3, the BT-PSPs exhibited mild inhibition of sEH. Therefore, we needed to determine if the BT-PSPs exerted their pro-efferocytosis effects via sEH rather than Nape-pld. To do this, we used two well-characterized and potent sEH inhibitors, AUDA and TPPU (12-[[(tricyclo[3.3.1.13,7]dec-1-ylamino)carbonyl]amino]-dodecanoic acid and N-[1-(1-oxopropyl)-4-piperidinyl]-N'-[4-(trifluoromethoxy)phenyl)-urea, respectively).[146, 186, 187] When administered to BMDMs, neither AUDA nor TPPU affected efferocytosis (Figure 45 B). Therefore, we determined that the much weaker inhibition of sEH by the BT-PSPs also did not affect efferocytosis.

Additionally, sEH activity has been proposed to boost efferocytosis via the production of SPMs, but this hypothesis has never been directly tested.[59, 147] Our results in this experiment represented the first published demonstration that sEH activity does not, in fact, alter efferocytosis.[127]

## 5.5.3 Validation of NAPE-PLD Dependence

While the previous experiment demonstrated that sEH inhibition was **not** responsible for BT-PSP enhancement of efferocytosis, we still needed to validate that Nape-pld **was** responsible. To do this, we compared the effects of vehicle and VU0506534 treatment on BMDMs from WT and NPKO mice (Figure 45 C). Knocking out *Napepld* reduced efferocytosis, which was consistent with Nape-pld being a positive efferocytosis regulator. Treatment of WT macrophages with VU0506534 (10 µM) enhanced efferocytosis, matching our previous results. And, in the absence of Nape-pld, VU0506534 treatment had no effect on efferocytosis. This demonstrated that VU0506534 (and, by extension, the other BT-PSPs) enhanced efferocytosis by activating Nape-pld. Thus, we conclusively demonstrated that by activating Nape-pld in macrophages, we could pharmacologically enhance efferocytosis.

## 5.6 Conclusions

In Chapters 2 and 3, I described the discovery, validation, and characterization of the first-ever class of NAPE-PLD activators, the BT-PSPs. However, we did not know whether that activity would survive the transfer from *in vitro* to living cells. Therefore, we first developed a cell-based NAPE-PLD activity assay. I then determined whether the BT-PSPs were toxic to cells, to see if I could safely measure their effects on NAPE-PLD in cells. Upon seeing that the compounds were sufficiently non-cytotoxic, I demonstrated that they reliably and dose-dependently modulated NAPE-PLD in multiple cell lines and using two measurement methods. The combined results of cell-based competition assays, *in vitro* validation assays, and preliminary cell-based validation data demonstrated that the BT-PSPs are genuine activators of NAPE-PLD in cultured cells.

A potential role for NAPE-PLD in regulating efferocytosis was first suggested by studies showing that PEA, one of the major products of NAPE-PLD, could increase the capacity of macrophages to carry out efferocytosis.[53] Furthermore, *NAPEPLD* expression was significantly reduced in unstable atherosclerotic plaques from human coronary arteries and impaired efferocytosis has been implicated in the development of these plaques.[46, 53] Here, we showed that BMDMs derived from *Napepld*^{-/-} mice have a markedly diminished ability to carry out efferocytosis. Furthermore, we found that inhibiting Nape-pld activity using Bith phenocopied the effect of *Napepld* deletion. Importantly, treatment of wild-type BMDM with either VU0506534 or VU0506533 to increase Nape-pld activity markedly enhanced the capacity of BMDMs to carry out efferocytosis. This increase in efferocytosis required Nape-pld, as VU0506534 failed to enhance efferocytosis by *Napepld*^{-/-} BMDMs. Given previous results showing weak inhibition of sEH by the BT-PSPs, we also demonstrated that strong sEH inhibition has no effect on efferocytosis. Together, these results demonstrated that macrophage Nape-pld activity enhances efferocytosis, that modulation of macrophage Nape-pld can be used to regulate efferocytosis, and that the BT-PSPs (by activating Nape-pld) are effective pharmacological enhancers of efferocytosis.

The experiments detailed in this chapter demonstrated that the BT-PSPs are first-in-class, valid, viable, and widely usable tool compounds for studying NAPE-PLD in

live cells. Furthermore, we demonstrated that they can be used to increase efferocytosis. As dysfunctional efferocytosis and downregulation of NAPE-PLD activity contribute to the progression of many diseases, the BT-PSPs could have a substantial impact on our understanding of those diseases and, potentially, the way we treat them.

## 5.7 Methods

### 5.7.1 General

#### 5.7.1.1 Materials and Reagents

LEI-401, [$^2$H$_4$]PEA, [$^2$H$_4$]OEA, and *N*-[$^2$H$_4$]palmitoyl-dioleoyl-PE were purchased from Cayman Chemicals. *N*-palmitoyl-dioleoyl-PE was purchased from Avanti Polar Lipids. PED-A1 was purchased from ThermoFisher Scientific. Flame-NAPE was synthesized as previously described.[133] NOPE and *N*-palimtoyl-dihexanoyl-PE were synthesized using dihexanoyl-PE (Avanti Polar Lipids) and oleoyl chloride or palmitoyl chloride (Millipore-Sigma), respectively, as described previously.[127]

#### 5.7.1.2 Analyses

All statistical analyses were performed using GraphPad Prism 9 software. Unless stated otherwise, all experiments with accompanying statistical analyses were replicated two or more times on separate days, normalized to same-day controls, and combined for analysis.

#### 5.7.1.3 Cell Culture

RAW 264.7 (ATCC TIB-71), HepG2 (ATCC HB-8065), and Jurkat (ATCC TIB-152) cells were cultured according to manufacturer specifications. They were grown in Dulbecco's modified eagle medium (DMEM, Gibco 1195-065), supplemented with 10% (v/v) heat-inactivated fetal bovine serum (HI-FBS, Corning MT35011CV) and 1% (v/v) penicillin-streptomycin antibiotics (Corning, MT30002CI). Jurkats were grown in non-treated sterile petri dishes and remained in suspension. Before removing the RAW

264.7 cells from the plate, the cells were rinsed with 10mL of Dulbecco's modified phosphate buffered saline (Corning MT21031CV). Cell lifters were used to de-adhere RAW 264.7 cells, while 4 min incubation in 2 mL of 0.25% Trypsin-EDTA (Gibco 25200056) was used for HepG2 cells. When plating into assay plates, the antibiotics in the growth media were replaced with DMEM, so as to eliminate any interfering effects on the assay that they might have had. Caco-2 and HEK-293 cells were cultured following the protocols detailed in Chapter 4.

To generate BMDMs, mice were euthanized with isoflurane and hind legs were removed. Marrow was flushed from femurs and tibias using DMEM containing 4.5 g/L glucose and a 26-gauge needle. Cell suspensions were passed over a 40-μm filter, centrifuged at 500 x g, and resuspended in 50 mL of DMEM containing 4.5 g/L glucose, 20% L-cell conditioned media, 10% HI-FBS, and 1% penicillin/streptomycin. 10 mL of cell suspension was plated into each of five 100-mm dishes and incubated for four days at 37 °C and 5% $CO_2$. On day four, non-adherent cells and debris were aspirated from the plates and replaced with fresh media. After 7 days of differentiation, cells were harvested for use in experiments.

### 5.7.2 Shared Experimental Methods

#### 5.7.2.1 Cytotoxicity Assay

Cells were plated in 96-well plates and allowed to grow to appropriate confluency, then test compounds were administered in the presence of a reduced amount of serum, and then the cells were incubated with the compounds for 24 h. After 24 h, the treatment media was removed and replaced with media containing methylthiazoletetrazolium (MTT), which is a marker of mitochondrial activity and, therefore, of cellular viability. The cells were then incubated for 3 h to give time for the MTT reaction to occur, then the media was removed and replaced with a strong solvent to dissolve the crystallized, purple product of MTT's reaction in mitochondria, and finally the amount of light absorbed by this purple product was measured for each well using a Biotek Synergy H1 plate reader.

### 5.7.2.2 Cellular NAPE-PLD Activity Assay

The method used for these assays was developed in our laboratory,[133] and it is detailed in Chapter 4. Instead of phenol red-free DMEM, we used FluoroBrite DMEM (ThermoFisher A1896701), as it has superior fluorescence properties. For all assays except for those in HepG2 and Caco-2 cells, the PED-A1 + THL method was used; for the others, the flame-NAPE method was used.[133]

### 5.7.2.3 Efferocytosis Assay

Assays were performed according to previously established protocols.[52, 54] Bone marrow-derived macrophages were seeded at $0.25 \times 10^6$ cells/well in a non-tissue culture-treated 24-well plate and allowed to adhere overnight. Macrophages were treated with various compounds at a final concentration of 10 µM or DMSO as a vehicle for 6 hours prior to each experiment. Jurkat cells were exposed to ultraviolet light (254 nm) for 5 minutes to induce apoptosis and then incubated in a 37 °C incubator with 5% $CO_2$ for 2 hours. Surveillance staining of these cells routinely yields approximately 80-90% apoptosis (Annexin V$^+$) using this method. Apoptotic Jurkat cells were labeled with either CellVue Claret (Millipore Sigma) or Cell Trace Violet (Invitrogen) per the manufacturer's instructions. After staining, cells were resuspended in macrophage medium at a density of $0.75 \times 10^6$ cells/mL and 500 µL of this suspension was added to the drug-containing media on the macrophages to achieve a cell ratio of 3:1 Jurkats:macrophages. After incubating for 45 minutes at 37 °C and 5% $CO_2$, the medium was aspirated and the macrophages were gently washed twice with PBS to remove unbound apoptotic cells. Macrophages were then removed from the plate using Cell Stripper (Sigma), washed, resuspended in staining buffer consisting of 2% HI-FBS in PBS with 2 mM EDTA, and blocked with anti-mouse CD16/32 antibodies for 15 minutes on ice. After blocking, cells were pelleted and resuspended with F4/80. Cells were incubated for 45 minutes on ice in the dark, then washed and resuspended in staining buffer for analysis. Cells were analyzed using an Attune NxT cytometer (ThermoFisher) and data were analyzed using FlowJo software to quantify the proportion of F4/80$^+$ macrophages that co-stained for apoptotic cells (% efferocytosis).

### 5.7.3 Cellular LC/MS Assay

This method was the same as the *in vitro* LC/MS assay, but stably transfected HEK-293 cells were used in place of purified Nape-pld. Cells were grown as previously described. Cells were transfected with a pcDNA3.1 mammalian expression vector bearing *NAPEPLD* (Invitrogen) using Fugene 6 (Promega E2691), according to manufacturer instructions. Additional details are being spared, as no data from this experiment are shown.

### 5.7.4 Preliminary Efferocytosis Experiments

*5.7.4.1 Confocal Imaging*

To generate images of macrophages not performing efferocytosis, flame-NAPE was added to BMDMs and images were taken every minute using a confocal microscope. To generate images of macrophages performing efferocytosis, fluorescently labelled apoptotic Jurkats (see efferocytosis method for more details) were incubated with BMDMs for 45 min, and then flame-NAPE was added immediately before imaging.

*5.7.4.2 Preliminary Efferocytosis Experiments*

The methods used for to extract the BMDMSs and perform the efferocytosis experiment are the same as those described above. The method used to perform the apoptotic cell binding experiment is the same as for the efferocytosis experiment, except the BMDMs and T cells are co-incubated at 4 °C instead of 37 °C. This allows for cell binding but not engulfment.[54]

# CHAPTER 6

## <u>Conclusions and Implications</u>

Based on existing research, we predicted that modulating NAPE-PLD activity could be an effective means of both studying and treating cardiometabolic diseases, particularly due to the enzyme's proposed role in regulating efferocytosis. However, few NAPE-PLD modulators existed. Therefore, the goals of this project were to develop novel modulators of NAPE-PLD that could be used as research tools, and to then use those modulators to test the effects of NAPE-PLD modulation on efferocytosis. In the process of completing those goals, we also developed a new, PLD-selective, fluorogenic activity probe. This probe improved upon existing methods for PLD activity measurement in terms of speed, simplicity, and selectivity. By the time of this project's completion, we had characterized the first-ever pharmacological activators of NAPE-PLD and demonstrated their utility in research settings. We also demonstrated that NAPE-PLD activity enhances efferocytosis, and that NAPE-PLD modulators can be used to regulate efferocytosis. These discoveries have the potential to substantially alter the field of NAPE-PLD research and our understanding of cardiometabolic diseases.

Parts of this chapter were adapted from Small Molecule Activation of NAPE-PLD Enhances Efferocytosis by Macrophages, published in bioRxiv, and has been reproduced with the permission of the publisher.[127] Authors: Jonah E. Zarrow, Abdul-Musawwir Alli-Oluwafuyi, Cristina M. Youwakim, Kwangho Kim, Andrew N. Jenkins, Isabelle C. Suero, Margaret R. Jones, Zahra Mashhadi, Kenneth P. Mackie, Alex G. Waterson, Amanda C. Doran, Gary A. Sulikowski, and Sean S. Davies. Authors who contributed to the writing and editing of this publication: JEZ, AGW, ACD, GAS, and SSD.

## 6.1 Quality of the Activators

Our HTS efforts and subsequent compound testing revealed that molecules of the BT-PSP class activate NAPE-PLD. This represented the first discovery of a pharmacological NAPE-PLD activator. On top of that, the BT-PSPs were proven to be potent and efficacious modulators. They activated Nape-pld with single-micromolar $EC_{50}$s and they increased Nape-pld activity by 1.6- to 2.6-fold, which is a biologically meaningful amount.[188-191] Our subsequent experiments using the BT-PSPs demonstrated that they are suitable tools for researching NAPE-PLD and its actions.

6.1.1 *In Vitro* Activity

*6.1.1.1 Validation and Characterization*

Using a combination of competition assays and LC/MS-based assays, we verified that the BT-PSPs modulate Nape-pld's ability to hydrolyze its natural substrates as well as activity probes. We also demonstrated that they are positive allosteric modulators of NAPE-PLD and gained insights into their potential binding sites. These experiments validated our claim that the BT-PSPs are genuine allosteric activators of NAPE-PLD.

*6.1.1.2 Selectivity*

I demonstrated that the compounds' activities extended from mouse Nape-pld to human NAPE-PLD, which showed us that the compounds can be used in human-directed research and were not mouse-specific. I also demonstrated that the compounds had only mild off-target effects on FAAH and sEH. Those effects can be reduced or eliminated by medicinal chemistry efforts, and we later demonstrated that their inhibition of sEH was not responsible for the compounds' effects on efferocytosis. These were all important tests of BT-PSP quality *in vitro*, but the majority of NAPE-PLD research is conducted in cell and animal models.

*6.1.2.1 Cytotoxicity*

Before testing the effects of the BT-PSPs on NAPE-PLD activity in cells, I assessed whether they were cytotoxic. I found that the BT-PSPs were predominantly non-toxic to cell types of interest, thereby allowing me to proceed with testing in those cells. Additionally, the overall lack of BT-PSP cytotoxicity indicated that they can be used other research studies, should they prove effective.

*6.1.2.2 Cellular NAPE-PLD Modulation*

The BT-PSPs proved to be efficacious and acceptably potent NAPE-PLD activators in cultured cells. This was demonstrated in a macrophage cell line and a hepatocyte line, which are crucial cells in the regulation of atherosclerosis, NAFLD, immune responses, and drug metabolism. Because the BT-PSPs were effective activators of cellular NAPE-PLD activity, they can be used by researchers to uncover the many roles of NAPE-PLD in biological systems.

*6.1.2.3 Efferocytosis Modulation*

Finally, we showed that NAPE-PLD activators increase the efferocytosis of apoptotic cells by macrophages. We confirmed that this was not a result of off-target inhibition of sEH, or an effect of the BT-PSP structure independent of any NAPE-PLD-modulating properties. And we confirmed that the top BT-PSP's (VU0506534) activation of Nape-pld was responsible for its enhancement of efferocytosis. These results established the BT-PSPs as a new class of efferocytosis-enhancing molecules. Additionally, we showed that both genetic knockout and pharmacological inhibition of Nape-pld in macrophages reduced efferocytosis capacity, confirming our finding that NAPE-PLD is a positive regulator of efferocytosis.

**6.2 Research Implications**

The immediate intended use of our compounds is as probes in research settings. Flame-NAPE will allow for more accurate measurement of NAPE-PLD activity. And as

no pharmacological NAPE-PLD activators existed prior to the BT-PSPs, their discovery allows entirely new scientific questions to be answered.

### 6.2.1 NAPE-PLD Research

*6.2.1.1 flame-NAPE*

Flame-NAPE represents an opportunity for PLD researchers. Prior to its creation, researchers who wanted to measure PLD activity—especially NAPE hydrolysis—without interference from other phospholipases needed to use more cumbersome and costly methods like TLC and LC/MS. But with flame-NAPE, they can now rapidly and selectively measure PLD activity, even measuring its change over time with kinetic assays. Furthermore, the successful use of PED6 to image $PLA_2$ activity *in vivo* and our own use of flame-NAPE to image NAPE-PLD activity in cultured cells indicate that flame-NAPE can be used to selectively image PLD activity *in vivo*.[161, 183] The creation of this basic but specialized tool will greatly aid research into PLD activity.

*6.2.1.2 BT-PSPs*

Prior to our characterization of the BT-PSPs, the only way to investigate the effects of increased NAPE-PLD activity were by using permanent or inducible increases in *NAPEPLD* expression. While this method is useful and can answer questions about NAPE-PLD's many roles, it also causes changes in cells and throughout the body that do not arise after pharmacological treatment.[11, 62] Additionally, utilizing pharmacological activators enables more versatile, less expensive, more tightly-controlled, faster, and simpler experiments than genetic modification does. Lastly, evidence suggests that increasing NAPE-PLD activity could help to combat a number of diseases (see Chapter 1). The BT-PSPs will allow researchers to determine whether or not that is the case.

### 6.2.2 NAE Research

Similar to NAPE-PLD, NAEs have been linked to the biochemistry of a wide variety of healthy and diseased tissues, typically in a protective role. With the advent of

the BT-PSPs, we can now test those linkages without having to overcome the poor pharmacokinetic properties of NAEs. Also, by using BT-PSPs in combination with the small-molecule modulators of NAE synthesis and degradation that already exist, researchers can now completely control NAE levels in biological settings and so learn much more about the roles of NAEs.

### 6.2.3 Efferocytosis Research

The BT-PSPs represent a new way of pharmacologically enhancing efferocytosis. Several such mechanisms exist, but none act via NAPE-PLD. And as NAPE-PLD was only recently implicated in the regulation of efferocytosis,[53, 61] the details of its role have not been thoroughly explored. With the advent of the BT-PSPs, that gap in knowledge can be filled more easily. Additionally, the dysregulation of efferocytosis contributes to the development of a number of diseases,[47] so the advent of a new tool for enhancing efferocytosis will aid in the characterization of those diseases.

### 6.3 Disease Implications

The BT-PSPs represent a new opportunity for both treating and understanding all of the diseases in which NAPE-PLD and NAEs have been implicated. Because each disease develops through different (though often linked) mechanisms, the way in which BT-PSPs could help alleviate them is different; but shared by all of them is the opportunity to deepen our scientific understanding of NAPE-PLD. Having a first-in-class tool to study a rarely explored but often-implicated enzyme has the potential to transform our understanding of each disease in which it is involved.

### 6.3.1 Atherosclerosis

One of the critical points in the development of atherosclerosis is the failure of resident macrophages to perform efferocytosis.[45-48, 51, 52] That failure transforms a fatty streak to a necrotizing, inflamed plaque in the artery wall.[45-47, 49, 51, 52] There are several

other points in the development of atherosclerosis where the lesion is relatively stable until a certain threshold is passed. While the other failure points have drugs designed to target and prevent them, the failure of macrophage efferocytosis capacity does not.[40]

We have demonstrated that the BT-PSPs can be used to pharmacologically enhance efferocytosis. Previous trials administering OEA, PEA, or NAE-boosting bacteria decreased the size of necrotic cores within atherosclerotic lesions.[53, 65, 192] However, the poor pharmacokinetic properties of OEA and PEA have greatly hampered their clinical use, while engineered bacteria that produce these bioactive lipids *in situ* still face significant regulatory hurdles for use in humans. While still at an early stage, our work demonstrated that the BT-PSPs represent a potential alternative strategy for raising NAE levels, thereby achieving the same effects on atherosclerosis. As atherosclerosis underlies the top two causes of death worldwide,[32, 37] this potential utility of the BT-PSPs is highly impactful.

### 6.3.2 NAFLD

When NAFLD is still mild, lifestyle changes and some medications are effective at inhibiting its progression.[16, 28, 29] Once the disease worsens, however, more extreme treatments like chemotherapy and liver transplantation become necessary.[10, 27] As previously discussed, NAPE-PLD, via its creation of NAEs, has been shown to protect against NAFLD by reducing lipid accumulation and inflammation in the liver. Therefore, if their effects successfully translate into animal models, BT-PSPs could be used as treatments for NAFLD.

### 6.3.3 Type 2 Diabetes

Current research indicates that NAPE-PLD activity could combat the development of T2D by enhancing GLP-1 signaling, and that it could help to rescue the impaired wound healing that is typical of diabetics by enhancing macrophage efferocytosis capacity. While there are many drugs that effectively combat the

development of diabetes, far fewer aid in proper wound healing.[121, 122] Because the BT-PSPs enhance macrophage efferocytosis capacity, they are likely able to rescue this latter phenotype.[56, 122, 123] The Davies Laboratory intends to investigate the effects of topical administration of BT-PSPs to the wounds of diabetic animals.

### 6.3.4 Obesity

Based on the large amount of existing research, it is apparent that increasing NAPE-PLD activity will decrease obesity—both by decreasing food intake and by reducing adipogenesis. Therefore, the BT-PSPs have great potential in building our understanding of the rise and rescue of obesity, and as anti-obesity medications. While the BT-PSPs are unlikely to prevent obesity entirely, they are likely to help many people and to do so via an as yet unused mechanism.

### 6.3.5 Healing from Injuries

When the body is injured, pain is signaled to the brain, inflammation is started at the injury site, infections can enter the body, cells around the wound are strengthened to prevent the damage from spreading, damaged cells are repaired, dead cells are metabolized, and new cells are grown. NAPE-PLD has been shown to contribute to the regulation of each of those responses in order to help the body heal from injuries (detailed in Chapter 1). Therefore, by activating NAPE-PLD, BT-PSPs have immense therapeutic potential. However, as NAPE-PLD's precise role in those processes is not yet fully elucidated, flame-NAPE and the BT-PSPs can first assist in developing our understanding of NAPE-PLD's roles in the healing process.

### 6.3.6 Other Conditions

NAPE-PLD contributes to the regulation of several other diseases like colitis,[73, 81-83] celiac disease,[84] arthritis,[73] and certain cancers.[74, 76, 78-80] Much like the healing process, the role of NAPE-PLD in these diseases is poorly understood. However, as

discussed above, flame-NAPE and the BT-PSPs will greatly aid in determining exactly how NAPE-PLD is involved in each of those diseases.

## 6.4 Future Development of the Compounds

The next steps for this project will be to develop the NAPE-PLD modulators for use in research and clinical settings.

### 6.4.1 Inhibitors

While we focused our research efforts on the NAPE-PLD activators identified by the HTS, we also identified several NAPE-PLD inhibitors. While a few NAPE-PLD inhibitors already exist,[124-126] it is still beneficial to have increased options for several reasons. It allows researchers to confirm their results using multiple different inhibitors, some compounds may work better in certain settings than others, and some compounds may fail in clinical settings while others succeed. For all of these reasons, developing the NAPE-PLD inhibitors into more potent, validated, and safe compounds will be beneficial. The way that we would do this is to first apply the assays that we performed on the activators to the inhibitors—ideally with an even more expansive SAR component to enhance our odds of finding stronger compounds—and then to continue development in the same manner as we will do for the activators.

### 6.4.2 Activators

There are several avenues of research around the activators that will be important to their development as research and clinical tools.

#### 6.4.2.1 SAR

Additional structural-activity relationship studies around the BT-PSP scaffold are needed. We will test new BT-PSP compounds for *in vitro* activity, cytotoxicity, and cellular activity. Through these studies, we will be able to learn more about the

structural bases for BT-PSP activity, and we are likely to discover even better NAPE-PLD activators. These SAR studies have already begun and are being conducted by a consortium of researchers at Vanderbilt University including the Davies Lab, Dr. Alex Waterson, the SynCore, and the HTS Core.

*6.4.2.2 Target Engagement*

As discussed in Chapter 3, many of the experiments intended to demonstrate BT-PSP engagement of NAPE-PLD failed due to unforeseen experimental problems. At the conclusion of those experiments, two directions remained promising: thermal shift assays and mutagenesis. In order to make the thermal shift assays work with NAPE-PLD, many experiments of varying the assay components and setup are needed. These include isolating intact NAPE-PLD within our gross preparation from its truncated forms, determining what detergents would best stabilize the protein without interfering with the assay, and ensuring with each step that NAPE-PLD and our chosen activator are still active in the modified preparation.

As for mutagenesis, the next steps are simpler. First, we need to express and purify Δ47 NAPE-PLD using the same bacteria and plasmid that were used to obtain its crystal structure.[68] If this form of NAPE-PLD is catalytically active, our next steps would be to perform site-directed mutagenesis on the plasmid to introduce our planned mutations, express the resulting proteins, and then test the effects of our mutations on NAPE-PLD catalytic activity both with and without BT-PSPs present. This will show us the effects of the mutations themselves, whether the BT-PSPs bind to the predicted site, how they bind to that site, and confirm that they bind directly to NAPE-PLD.

*6.4.2.3 Mechanisms of Efferocytosis Modulation*

Some mechanisms by which increased NAPE-PLD activity could enhance efferocytosis have been proposed. In one, PEA acts via G protein-coupled receptor 55 to increase the expression of MerTK.[53] MerTK is a receptor that helps macrophages recognize and bind to apoptotic cells,[47, 193] and deletion of MerTK in macrophages markedly enhances necrotic core expansion in mice with atherosclerosis.[194] In another,

OEA acts via PPAR-α to increase the expression of several macrophage M2 phenotype markers, which is associated with enhanced efferocytosis.[192]

A more complete elucidation of how NAPE-PLD regulates efferocytosis will require a variety of approaches including the use of both NAPE-PLD inhibitors and activators. Efferocytosis is a complex process involving macrophage recognition of so-called "find me" and "eat me" signals, and requires the binding, internalization, and controlled degradation of apoptotic cells, followed by the export of their constituent components like cholesterol.[47, 193, 195] The effects of NAPE-PLD modulation on each of those steps needs to be examined. NAPEs exert membrane-stabilizing effects[196, 197] and facilitate the lateral diffusion of cholesterol,[198] while phosphatidic acids exert membrane-bending effects.[199] Therefore, the effect of increased NAPE-PLD activity on membrane topology as a mechanism to enhance efferocytosis also needs to be examined.

### 6.4.2.4 Selectivity

The scope of the present project did not include extensive selectivity testing. While we focused on three of the most important enzymes to test, many others were omitted. Those enzymes include the main human phospholipase D enzymes, PLD1 and PLD2,[76] as well as PLDs from other species like *Streptomyces chromofuscus*, mice, rats, and non-human primates. We should also test BT-PSP effects on enzymes in the NAPE-to-NAE biosynthesis pathways, including ABHD4, SHIP1, the PLAATs, GDE1, GDE4, GDE7, and PTPN22. Testing for effects on another common NAE-degrading enzyme, *N*-acylethanolamine acid amide hydrolase, would be informative. The compounds could also affect enzymes with similar structures to NAPE-PLD, such as those in metallo β-lactamase class B family and carbonic anhydrase.[66, 126] We should test their effects on enzymes that participate in the regulation of efferocytosis, lipid metabolism, and satiety signaling. Finally, we should test for any effects on enzymes that are crucial for life, like ATP synthase, Krebs cycle enzymes, and DNA polymerases. By determining whether the BT-PSPs have any dangerous or efficacy-limiting off-target effects on these enzymes, and performing SAR to eliminate any such effects, we will ensure that the BT-PSPs are strong candidates for *in vivo* research.

*6.4.2.5 In Vivo Studies*

       Because of the many roles that NAPE-PLD plays in biochemical disease regulation, we will want to test the effects of BT-PSP treatment on disease progression. Initial *in vivo* studies of the BT-PSPs will include drug metabolism and pharmacokinetic profiling, toxicology studies, and longevity studies. If those studies yield favorable results, we will assess the efficacy of the BT-PSPs at improving symptoms in diseases that have been linked to NAPE-PLD activity. These include atherosclerosis, NAFLD, T2D, and obesity. If successful in animal models of disease, the compounds will proceed through formulation and safety trials for use in humans, and eventually clinical trials. If successful, the BT-PSPs have tremendous therapeutic potential. But even if they fail at any of the stages listed above, they still represent immensely useful and unprecedented research tools.

# REFERENCES

(1) Organization, W. H. *Obesity and Overweight*. 2021. https://www.who.int/news-room/fact-sheets/detail/obesity-and-overweight (accessed 2022 12/06/2022).

(2) Bank, T. W. *Obesity: Health and Economic Consequences of an Impending Global Challenge*. 2020. https://www.worldbank.org/en/topic/nutrition/publication/obesity-health-and-economic-consequences-of-an-impending-global-challenge (accessed 2022 12/06/2022).

(3) Federation, W. O. *The Economic Impact of Overweight & Obesity*. 2022. https://data.worldobesity.org/publications/WOF-Economic-Impacts-2-V2.pdf (accessed 12/06/2022).

(4) Srivastava, G.; Apovian, C. Future Pharmacotherapy for Obesity: New Anti-obesity Drugs on the Horizon. *Curr Obes Rep* **2018**, *7* (2), 147-161. DOI: 10.1007/s13679-018-0300-4  From NLM Medline.

(5) Bessesen, D. H.; Van Gaal, L. F. Progress and challenges in anti-obesity pharmacotherapy. *Lancet Diabetes Endocrinol* **2018**, *6* (3), 237-248. DOI: 10.1016/S2213-8587(17)30236-X  From NLM Medline.

(6) Fildes, A.; Charlton, J.; Rudisill, C.; Littlejohns, P.; Prevost, A. T.; Gulliford, M. C. Probability of an Obese Person Attaining Normal Body Weight: Cohort Study Using Electronic Health Records. *Am J Public Health* **2015**, *105* (9), e54-59. DOI: 10.2105/AJPH.2015.302773  From NLM Medline.

(7) Puzziferri, N.; Roshek, T. B., 3rd; Mayo, H. G.; Gallagher, R.; Belle, S. H.; Livingston, E. H. Long-term follow-up after bariatric surgery: a systematic review. *JAMA* **2014**, *312* (9), 934-942. DOI: 10.1001/jama.2014.10706  From NLM Medline.

(8) Sarwer, D. B.; Polonsky, H. M. The Psychosocial Burden of Obesity. *Endocrinol Metab Clin North Am* **2016**, *45* (3), 677-688. DOI: 10.1016/j.ecl.2016.04.016  From NLM Medline.

(9) Quinn, D. M.; Puhl, R. M.; Reinka, M. A. Trying again (and again): Weight cycling and depressive symptoms in U.S. adults. *PLoS One* **2020**, *15* (9), e0239004. DOI: 10.1371/journal.pone.0239004  From NLM Medline.

(10) Younossi, Z.; Anstee, Q. M.; Marietti, M.; Hardy, T.; Henry, L.; Eslam, M.; George, J.; Bugianesi, E. Global burden of NAFLD and NASH: trends, predictions, risk factors and prevention. *Nat Rev Gastroenterol Hepatol* **2018**, *15* (1), 11-20. DOI: 10.1038/nrgastro.2017.109  From NLM Medline.

(11) Everard, A.; Plovier, H.; Rastelli, M.; Van Hul, M.; de Wouters d'Oplinter, A.; Geurts, L.; Druart, C.; Robine, S.; Delzenne, N. M.; Muccioli, G. G.; et al. Intestinal epithelial N-acylphosphatidylethanolamine phospholipase D links dietary fat to metabolic adaptations in obesity and steatosis. *Nat Commun* **2019**, *10* (1), 457. DOI: 10.1038/s41467-018-08051-7.

(12) Khan, M. A. B.; Hashim, M. J.; King, J. K.; Govender, R. D.; Mustafa, H.; Al Kaabi, J. Epidemiology of Type 2 Diabetes - Global Burden of Disease and Forecasted Trends. *J Epidemiol Glob Health* **2020**, *10* (1), 107-111. DOI: 10.2991/jegh.k.191028.001  From NLM Medline.

(13) Federation, I. D. *Type 2 Diabetes*. 2020. https://www.idf.org/aboutdiabetes/type-2-diabetes.html (accessed 2022 12/06/2022).

(14) Virani, S. S.; Alonso, A.; Aparicio, H. J.; Benjamin, E. J.; Bittencourt, M. S.; Callaway, C. W.; Carson, A. P.; Chamberlain, A. M.; Cheng, S.; Delling, F. N.; et al. Heart Disease and Stroke Statistics-2021 Update: A Report From the American Heart Association. *Circulation* **2021**, *143* (8), e254-e743. DOI: 10.1161/CIR.0000000000000950  From NLM Medline.

(15) Le, M. H.; Yeo, Y. H.; Li, X.; Li, J.; Zou, B.; Wu, Y.; Ye, Q.; Huang, D. Q.; Zhao, C.; Zhang, J.; et al. 2019 Global NAFLD Prevalence: A Systematic Review and Meta-analysis. *Clin Gastroenterol Hepatol* **2022**, *20* (12), 2809-2817 e2828. DOI: 10.1016/j.cgh.2021.12.002  From NLM Medline.

(16) Lazarus, J. V.; Mark, H. E.; Anstee, Q. M.; Arab, J. P.; Batterham, R. L.; Castera, L.; Cortez-Pinto, H.; Crespo, J.; Cusi, K.; Dirac, M. A.; et al. Advancing the global public health agenda for NAFLD: a consensus statement. *Nat Rev Gastroenterol Hepatol* **2022**, *19* (1), 60-78. DOI: 10.1038/s41575-021-00523-4  From NLM Medline.

(17) Einarson, T. R.; Acs, A.; Ludwig, C.; Panton, U. H. Economic Burden of Cardiovascular Disease in Type 2 Diabetes: A Systematic Review. *Value Health* **2018**, *21* (7), 881-890. DOI: 10.1016/j.jval.2017.12.019  From NLM Medline.

(18) Dinh, T.; Elder, S.; Veves, A. Delayed wound healing in diabetes: considering future treatments. *Diabetes Management* **2011**, *1* (5), 509-519. DOI: 10.2217/dmt.11.44.

(19) Maffi, P.; Secchi, A. The Burden of Diabetes: Emerging Data. *Dev Ophthalmol* **2017**, *60*, 1-5. DOI: 10.1159/000459641  From NLM Medline.

(20) Clinic, M. *Type 2 Diabetes*. 2022. https://www.mayoclinic.org/diseases-conditions/type-2-diabetes/symptoms-causes/syc-20351193 (accessed 2022 12/06/2022).

(21) UK, D. *Reversing Type 2 Diabetes*. 2022. https://www.diabetes.org.uk/diabetes-the-basics/type-2-reverse (accessed 2022 12/06/2022).

(22) Reed, J.; Bain, S.; Kanamarlapudi, V. A Review of Current Trends with Type 2 Diabetes Epidemiology, Aetiology, Pathogenesis, Treatments and Future Perspectives. *Diabetes Metab Syndr Obes* **2021**, *14*, 3567-3602. DOI: 10.2147/DMSO.S319895  From NLM PubMed-not-MEDLINE.

(23) Hays, N. P.; Galassetti, P. R.; Coker, R. H. Prevention and treatment of type 2 diabetes: current role of lifestyle, natural product, and pharmacological interventions. *Pharmacol Ther* **2008**, *118* (2), 181-191. DOI: 10.1016/j.pharmthera.2008.02.003  From NLM Medline.

(24) Hill-Briggs, F.; Adler, N. E.; Berkowitz, S. A.; Chin, M. H.; Gary-Webb, T. L.; Navas-Acien, A.; Thornton, P. L.; Haire-Joshu, D. Social Determinants of Health and Diabetes: A Scientific Review. *Diabetes Care* **2020**, *44* (1), 258-279. DOI: 10.2337/dci20-0053  From NLM Publisher.

(25) Riazi, K.; Azhari, H.; Charette, J. H.; Underwood, F. E.; King, J. A.; Afshar, E. E.; Swain, M. G.; Congly, S. E.; Kaplan, G. G.; Shaheen, A. A. The prevalence and incidence of NAFLD worldwide: a systematic review and meta-analysis. *Lancet Gastroenterol Hepatol* **2022**, *7* (9), 851-861. DOI: 10.1016/S2468-1253(22)00165-0  From NLM Medline.

(26) Wu, W.; Feng, A.; Ma, W.; Li, D.; Zheng, S.; Xu, F.; Han, D.; Lyu, J. Worldwide long-term trends in the incidence of nonalcoholic fatty liver disease during 1990-2019: A

joinpoint and age-period-cohort analysis. *Front Cardiovasc Med* **2022**, *9*, 891963. DOI: 10.3389/fcvm.2022.891963  From NLM PubMed-not-MEDLINE.

(27) UCSF. *Fatty Liver Disease (Nonalcoholic Steatohepatitis)*. UCSF Department of Transplant Surgery, 2014. https://transplantsurgery.ucsf.edu/conditions--procedures/fatty-liver-disease-(nonalcoholic-steatohepatitis).aspx (accessed 2022 12/06/2022).

(28) Corey, K. E.; Rinella, M. E. Medical and Surgical Treatment Options for Nonalcoholic Steatohepatitis. *Dig Dis Sci* **2016**, *61* (5), 1387-1397. DOI: 10.1007/s10620-016-4083-8  From NLM Medline.

(29) Osaka, T.; Hashimoto, Y.; Hamaguchi, M.; Kojima, T.; Obora, A.; Fukui, M. Nonalcoholic fatty liver disease remission in men through regular exercise. *J Clin Biochem Nutr* **2018**, *62* (3), 242-246. DOI: 10.3164/jcbn.17-115  From NLM PubMed-not-MEDLINE.

(30) NIDDK. *The Liver Transplant Process*. 2017. https://www.niddk.nih.gov/health-information/liver-disease/liver-transplant/preparing-transplant (accessed 2022 12/06/2022).

(31) Zezos, P.; Renner, E. L. Liver transplantation and non-alcoholic fatty liver disease. *World J Gastroenterol* **2014**, *20* (42), 15532-15538. DOI: 10.3748/wjg.v20.i42.15532  From NLM Medline.

(32) Feigin, V. L.; Brainin, M.; Norrving, B.; Martins, S.; Sacco, R. L.; Hacke, W.; Fisher, M.; Pandian, J.; Lindsay, P. World Stroke Organization (WSO): Global Stroke Fact Sheet 2022. *Int J Stroke* **2022**, *17* (1), 18-29. DOI: 10.1177/17474930211065917  From NLM Medline.

(33) Saini, V.; Guada, L.; Yavagal, D. R. Global Epidemiology of Stroke and Access to Acute Ischemic Stroke Interventions. *Neurology* **2021**, *97* (20 Suppl 2), S6-S16. DOI: 10.1212/WNL.0000000000012781  From NLM Medline.

(34) Prevention, C. f. D. C. a. *Treat and Recover from Stroke*. 2022. https://www.cdc.gov/stroke/treatments.htm (accessed 2022 12/06/2022).

(35) Organization, W. S. *Global Stroke Fact Sheet 2022*. 2022. https://www.world-stroke.org/assets/downloads/WSO_Global_Stroke_Fact_Sheet.pdf (accessed 2022 12/06/2022).

(36) Stroke, N. I. o. N. D. a. *Post-Stroke Rehabilitation Fact Sheet*. 2022. https://www.ninds.nih.gov/post-stroke-rehabilitation-fact-sheet (accessed 2022 12/06/2022).

(37) Khan, M. A.; Hashim, M. J.; Mustafa, H.; Baniyas, M. Y.; Al Suwaidi, S.; AlKatheeri, R.; Alblooshi, F. M. K.; Almatrooshi, M.; Alzaabi, M. E. H.; Al Darmaki, R. S.; et al. Global Epidemiology of Ischemic Heart Disease: Results from the Global Burden of Disease Study. *Cureus* **2020**, *12* (7), e9349. DOI: 10.7759/cureus.9349  From NLM PubMed-not-MEDLINE.

(38) Kirk, E. P.; Klein, S. Pathogenesis and pathophysiology of the cardiometabolic syndrome. *J Clin Hypertens (Greenwich)* **2009**, *11* (12), 761-765. DOI: 10.1111/j.1559-4572.2009.00054.x  From NLM Medline.

(39) Duggan, J. P.; Peters, A. S.; Trachiotis, G. D.; Antevil, J. L. Epidemiology of Coronary Artery Disease. *Surg Clin North Am* **2022**, *102* (3), 499-516. DOI: 10.1016/j.suc.2022.01.007  From NLM Medline.

(40) Malakar, A. K.; Choudhury, D.; Halder, B.; Paul, P.; Uddin, A.; Chakraborty, S. A review on coronary artery disease, its risk factors, and therapeutics. *J Cell Physiol* **2019**, *234* (10), 16812-16823. DOI: 10.1002/jcp.28350  From NLM Medline.

(41) Association, A. H. *Atherosclerosis*. 2020. https://www.heart.org/en/health-topics/cholesterol/about-cholesterol/atherosclerosis (accessed 2020 11/25/2020).

(42) NHLBI. *Atherosclerosis*. 2020. https://www.nhlbi.nih.gov/health-topics/atherosclerosis (accessed 2020 08/24/2020).

(43) Wang, Y. X.; Ulu, A.; Zhang, L. N.; Hammock, B. Soluble epoxide hydrolase in atherosclerosis. *Curr Atheroscler Rep* **2010**, *12* (3), 174-183. DOI: 10.1007/s11883-010-0108-5.

(44) Li, Y.; He, P. P.; Zhang, D. W.; Zheng, X. L.; Cayabyab, F. S.; Yin, W. D.; Tang, C. K. Lipoprotein lipase: from gene to atherosclerosis. *Atherosclerosis* **2014**, *237* (2), 597-608. DOI: 10.1016/j.atherosclerosis.2014.10.016  From NLM.

(45) Linton, M. F.; Babaev, V. R.; Huang, J.; Linton, E. F.; Tao, H.; Yancey, P. G. Macrophage Apoptosis and Efferocytosis in the Pathogenesis of Atherosclerosis. *Circ J* **2016**, *80* (11), 2259-2268. DOI: 10.1253/circj.CJ-16-0924.

(46) Yurdagul, A., Jr.; Doran, A. C.; Cai, B.; Fredman, G.; Tabas, I. A. Mechanisms and Consequences of Defective Efferocytosis in Atherosclerosis. *Front Cardiovasc Med* **2017**, *4*, 86. DOI: 10.3389/fcvm.2017.00086.

(47) Doran, A. C.; Yurdagul, A., Jr.; Tabas, I. Efferocytosis in health and disease. *Nat Rev Immunol* **2020**, *20* (4), 254-267. DOI: 10.1038/s41577-019-0240-6.

(48) He, P. P.; Jiang, T.; OuYang, X. P.; Liang, Y. Q.; Zou, J. Q.; Wang, Y.; Shen, Q. Q.; Liao, L.; Zheng, X. L. Lipoprotein lipase: Biosynthesis, regulatory factors, and its role in atherosclerosis and other diseases. *Clinica chimica acta; international journal of clinical chemistry* **2018**, *480*, 126-137. DOI: 10.1016/j.cca.2018.02.006  From NLM.

(49) Gui, Y.; Zheng, H.; Cao, R. Y. Foam Cells in Atherosclerosis: Novel Insights Into Its Origins, Consequences, and Molecular Mechanisms. *Front Cardiovasc Med* **2022**, *9*, 845942. DOI: 10.3389/fcvm.2022.845942  From NLM PubMed-not-MEDLINE.

(50) Kojima, Y.; Weissman, I. L.; Leeper, N. J. The Role of Efferocytosis in Atherosclerosis. *Circulation* **2017**, *135* (5), 476-489. DOI: 10.1161/CIRCULATIONAHA.116.025684.

(51) Basatemur, G. L.; Jorgensen, H. F.; Clarke, M. C. H.; Bennett, M. R.; Mallat, Z. Vascular smooth muscle cells in atherosclerosis. *Nat Rev Cardiol* **2019**, *16* (12), 727-744. DOI: 10.1038/s41569-019-0227-9  From NLM Medline.

(52) Doran, A. C.; Ozcan, L.; Cai, B.; Zheng, Z.; Fredman, G.; Rymond, C. C.; Dorweiler, B.; Sluimer, J. C.; Hsieh, J.; Kuriakose, G.; et al. CAMKIIgamma suppresses an efferocytosis pathway in macrophages and promotes atherosclerotic plaque necrosis. *J Clin Invest* **2017**, *127* (11), 4075-4089. DOI: 10.1172/JCI94735.

(53) Rinne, P.; Guillamat-Prats, R.; Rami, M.; Bindila, L.; Ring, L.; Lyytikainen, L. P.; Raitoharju, E.; Oksala, N.; Lehtimaki, T.; Weber, C.; et al. Palmitoylethanolamide Promotes a Proresolving Macrophage Phenotype and Attenuates Atherosclerotic Plaque Formation. *Arterioscler Thromb Vasc Biol* **2018**, *38* (11), 2562-2575. DOI: 10.1161/ATVBAHA.118.311185.

(54) Proto, J. D.; Doran, A. C.; Gusarova, G.; Yurdagul, A., Jr.; Sozen, E.; Subramanian, M.; Islam, M. N.; Rymond, C. C.; Du, J.; Hook, J.; et al. Regulatory T

Cells Promote Macrophage Efferocytosis during Inflammation Resolution. *Immunity* **2018**, *49* (4), 666-677 e666. DOI: 10.1016/j.immuni.2018.07.015.

(55) McShane, L.; Tabas, I.; Lemke, G.; Kurowska-Stolarska, M.; Maffia, P. TAM receptors in cardiovascular disease. *Cardiovasc Res* **2019**, *115* (8), 1286-1295. DOI: 10.1093/cvr/cvz100  From NLM Medline.

(56) Korns, D.; Frasch, S. C.; Fernandez-Boyanapalli, R.; Henson, P. M.; Bratton, D. L. Modulation of macrophage efferocytosis in inflammation. *Front Immunol* **2011**, *2*, 57. DOI: 10.3389/fimmu.2011.00057.

(57) Boada-Romero, E.; Martinez, J.; Heckmann, B. L.; Green, D. R. The clearance of dead cells by efferocytosis. *Nat Rev Mol Cell Biol* **2020**, *21* (7), 398-414. DOI: 10.1038/s41580-020-0232-1  From NLM Medline.

(58) Dalli, J.; Serhan, C. N. Pro-Resolving Mediators in Regulating and Conferring Macrophage Function. *Front Immunol* **2017**, *8*, 1400. DOI: 10.3389/fimmu.2017.01400 From NLM PubMed-not-MEDLINE.

(59) Deng, B.; Wang, C. W.; Arnardottir, H. H.; Li, Y.; Cheng, C. Y.; Dalli, J.; Serhan, C. N. Maresin biosynthesis and identification of maresin 2, a new anti-inflammatory and pro-resolving mediator from human macrophages. *PLoS One* **2014**, *9* (7), e102362. DOI: 10.1371/journal.pone.0102362.

(60) Schebb, N. H.; Kuhn, H.; Kahnt, A. S.; Rund, K. M.; O'Donnell, V. B.; Flamand, N.; Peters-Golden, M.; Jakobsson, P. J.; Weylandt, K. H.; Rohwer, N.; et al. Formation, Signaling and Occurrence of Specialized Pro-Resolving Lipid Mediators-What is the Evidence so far? *Front Pharmacol* **2022**, *13*, 838782. DOI: 10.3389/fphar.2022.838782 From NLM PubMed-not-MEDLINE.

(61) Chen, Z.; Zhuo, R.; Zhao, Y.; Yang, L.; Zhou, Y.; Cheng, X.; Peng, L.; Jin, X.; Wang, Y. Oleoylethanolamide stabilizes atherosclerotic plaque through regulating macrophage polarization via AMPK-PPARalpha pathway. *Biochem Biophys Res Commun* **2020**, *524* (2), 308-316. DOI: 10.1016/j.bbrc.2020.01.103.

(62) Hussain, Z.; Uyama, T.; Tsuboi, K.; Ueda, N. Mammalian enzymes responsible for the biosynthesis of N-acylethanolamines. *Biochim Biophys Acta Mol Cell Biol Lipids* **2017**, *1862* (12), 1546-1561. DOI: 10.1016/j.bbalip.2017.08.006.

(63) Leung, D.; Saghatelian, A.; Simon, G. M.; Cravatt, B. F. Inactivation of N-acyl phosphatidylethanolamine phospholipase D reveals multiple mechanisms for the biosynthesis of endocannabinoids. *Biochemistry* **2006**, *45* (15), 4720-4726. DOI: 10.1021/bi060163l.

(64) Simon, G. M.; Cravatt, B. F. Characterization of mice lacking candidate N-acyl ethanolamine biosynthetic enzymes provides evidence for multiple pathways that contribute to endocannabinoid production in vivo. *Mol Biosyst* **2010**, *6* (8), 1411-1418. DOI: 10.1039/c000237b.

(65) May-Zhang, L. S.; Chen, Z.; Dosoky, N. S.; Yancey, P. G.; Boyd, K. L.; Hasty, A. H.; Linton, M. F.; Davies, S. S. Administration of N-Acyl-Phosphatidylethanolamine Expressing Bacteria to Low Density Lipoprotein Receptor(-/-) Mice Improves Indices of Cardiometabolic Disease. *Sci Rep* **2019**, *9* (1), 420. DOI: 10.1038/s41598-018-37373-1.

(66) Pettinati, I.; Brem, J.; Lee, S. Y.; McHugh, P. J.; Schofield, C. J. The Chemical Biology of Human Metallo-beta-Lactamase Fold Proteins. *Trends Biochem Sci* **2016**, *41* (4), 338-355. DOI: 10.1016/j.tibs.2015.12.007.

(67) Wang, J.; Okamoto, Y.; Morishita, J.; Tsuboi, K.; Miyatake, A.; Ueda, N. Functional analysis of the purified anandamide-generating phospholipase D as a member of the metallo-beta-lactamase family. *J Biol Chem* **2006**, *281* (18), 12325-12335. DOI: 10.1074/jbc.M512359200.
(68) Magotti, P.; Bauer, I.; Igarashi, M.; Babagoli, M.; Marotta, R.; Piomelli, D.; Garau, G. Structure of human N-acylphosphatidylethanolamine-hydrolyzing phospholipase D: regulation of fatty acid ethanolamide biosynthesis by bile acids. *Structure* **2015**, *23* (3), 598-604. DOI: 10.1016/j.str.2014.12.018.
(69) Margheritis, E.; Castellani, B.; Magotti, P.; Peruzzi, S.; Romeo, E.; Natali, F.; Mostarda, S.; Gioiello, A.; Piomelli, D.; Garau, G. Bile Acid Recognition by NAPE-PLD. *ACS Chem Biol* **2016**, *11* (10), 2908-2914. DOI: 10.1021/acschembio.6b00624.
(70) Okamoto, Y.; Morishita, J.; Tsuboi, K.; Tonai, T.; Ueda, N. Molecular characterization of a phospholipase D generating anandamide and its congeners. *J Biol Chem* **2004**, *279* (7), 5298-5305. DOI: 10.1074/jbc.M306642200.
(71) Elphick, M. R.; Egertová, M. The Phylogenetic Distribution and Evolutionary Origins of Endocannabinoid Signalling. In *Cannabinoids*, Pertwee, R. G. Ed.; Springer Berlin Heidelberg, 2005; pp 283-297.
(72) Blancaflor, E. B.; Kilaru, A.; Keereetaweep, J.; Khan, B. R.; Faure, L.; Chapman, K. D. N-Acylethanolamines: lipid metabolites with functions in plant growth and development. *Plant J* **2014**, *79* (4), 568-583. DOI: 10.1111/tpj.12427.
(73) Pontis, S.; Ribeiro, A.; Sasso, O.; Piomelli, D. Macrophage-derived lipid agonists of PPAR-alpha as intrinsic controllers of inflammation. *Crit Rev Biochem Mol Biol* **2016**, *51* (1), 7-14. DOI: 10.3109/10409238.2015.1092944.
(74) Coulon, D.; Faure, L.; Salmon, M.; Wattelet, V.; Bessoule, J. J. Occurrence, biosynthesis and functions of N-acylphosphatidylethanolamines (NAPE): not just precursors of N-acylethanolamines (NAE). *Biochimie* **2012**, *94* (1), 75-85. DOI: 10.1016/j.biochi.2011.04.023.
(75) Ueda, N.; Okamoto, Y.; Tsuboi, K. Endocannabinoid-related enzymes as drug targets with special reference to N-acylphosphatidylethanolamine-hydrolyzing phospholipase D. *Curr Med Chem* **2005**, *12* (12), 1413-1422. DOI: 10.2174/0929867054020918.
(76) Scott, S. A.; Spencer, C. T.; O'Reilly, M. C.; Brown, K. A.; Lavieri, R. R.; Cho, C. H.; Jung, D. I.; Larock, R. C.; Brown, H. A.; Lindsley, C. W. Discovery of desketoraloxifene analogues as inhibitors of mammalian, Pseudomonas aeruginosa, and NAPE phospholipase D enzymes. *ACS Chem Biol* **2015**, *10* (2), 421-432. DOI: 10.1021/cb500828m.
(77) Palese, F.; Pontis, S.; Realini, N.; Piomelli, D. A protective role for N-acylphosphatidylethanolamine phospholipase D in 6-OHDA-induced neurodegeneration. *Sci Rep* **2019**, *9* (1), 15927. DOI: 10.1038/s41598-019-51799-1.
(78) Brown, H. A.; Thomas, P. G.; Lindsley, C. W. Targeting phospholipase D in cancer, infection and neurodegenerative disorders. *Nat Rev Drug Discov* **2017**, *16* (5), 351-367. DOI: 10.1038/nrd.2016.252.
(79) Ayakannu, T.; Taylor, A. H.; Bari, M.; Mastrangelo, N.; Maccarrone, M.; Konje, J. C. Expression and Function of the Endocannabinoid Modulating Enzymes Fatty Acid Amide Hydrolase and N-Acylphosphatidylethanolamine-Specific Phospholipase D in Endometrial Carcinoma. *Front Oncol* **2019**, *9*, 1363. DOI: 10.3389/fonc.2019.01363.

(80) Wu, X.; Han, L.; Zhang, X.; Li, L.; Jiang, C.; Qiu, Y.; Huang, R.; Xie, B.; Lin, Z.; Ren, J.; et al. Alteration of endocannabinoid system in human gliomas. *J Neurochem* **2012**, *120* (5), 842-849. DOI: 10.1111/j.1471-4159.2011.07625.x.

(81) Salaga, M.; Binienda, A.; Piscitelli, F.; Mokrowiecka, A.; Cygankiewicz, A. I.; Verde, R.; Malecka-Panas, E.; Kordek, R.; Krajewska, W. M.; Di Marzo, V.; et al. Systemic administration of serotonin exacerbates abdominal pain and colitis via interaction with the endocannabinoid system. *Biochem Pharmacol* **2019**, *161*, 37-51. DOI: 10.1016/j.bcp.2019.01.001.

(82) Marquez, L.; Suarez, J.; Iglesias, M.; Bermudez-Silva, F. J.; Rodriguez de Fonseca, F.; Andreu, M. Ulcerative colitis induces changes on the expression of the endocannabinoid system in the human colonic tissue. *PLoS One* **2009**, *4* (9), e6893. DOI: 10.1371/journal.pone.0006893.

(83) Suarez, J.; Romero-Zerbo, Y.; Marquez, L.; Rivera, P.; Iglesias, M.; Bermudez-Silva, F. J.; Andreu, M.; Rodriguez de Fonseca, F. Ulcerative colitis impairs the acylethanolamide-based anti-inflammatory system reversal by 5-aminosalicylic acid and glucocorticoids. *PLoS One* **2012**, *7* (5), e37729. DOI: 10.1371/journal.pone.0037729.

(84) Battista, N.; Di Sabatino, A.; Di Tommaso, M.; Biancheri, P.; Rapino, C.; Vidali, F.; Papadia, C.; Montana, C.; Pasini, A.; Lanzini, A.; et al. Abnormal anandamide metabolism in celiac disease. *J Nutr Biochem* **2012**, *23* (10), 1245-1248. DOI: 10.1016/j.jnutbio.2011.06.017.

(85) Paterniti, I.; Di Paola, R.; Campolo, M.; Siracusa, R.; Cordaro, M.; Bruschetta, G.; Tremolada, G.; Maestroni, A.; Bandello, F.; Esposito, E.; et al. Palmitoylethanolamide treatment reduces retinal inflammation in streptozotocin-induced diabetic rats. *Eur J Pharmacol* **2015**, *769*, 313-323. DOI: 10.1016/j.ejphar.2015.11.035.

(86) Lo Verme, J.; Fu, J.; Astarita, G.; La Rana, G.; Russo, R.; Calignano, A.; Piomelli, D. The nuclear receptor peroxisome proliferator-activated receptor-alpha mediates the anti-inflammatory actions of palmitoylethanolamide. *Mol Pharmacol* **2005**, *67* (1), 15-19. DOI: 10.1124/mol.104.006353.

(87) Dosoky, N. S.; Guo, L.; Chen, Z.; Feigley, A. V.; Davies, S. S. Dietary Fatty Acids Control the Species of N-Acyl-Phosphatidylethanolamines Synthesized by Therapeutically Modified Bacteria in the Intestinal Tract. *ACS Infect Dis* **2018**, *4* (1), 3-13. DOI: 10.1021/acsinfecdis.7b00127.

(88) Artmann, A.; Petersen, G.; Hellgren, L. I.; Boberg, J.; Skonberg, C.; Nellemann, C.; Hansen, S. H.; Hansen, H. S. Influence of dietary fatty acids on endocannabinoid and N-acylethanolamine levels in rat brain, liver and small intestine. *Biochim Biophys Acta* **2008**, *1781* (4), 200-212. DOI: 10.1016/j.bbalip.2008.01.006.

(89) Thabuis, C.; Tissot-Favre, D.; Bezelgues, J. B.; Martin, J. C.; Cruz-Hernandez, C.; Dionisi, F.; Destaillats, F. Biological functions and metabolism of oleoylethanolamide. *Lipids* **2008**, *43* (10), 887-894. DOI: 10.1007/s11745-008-3217-y.

(90) Nielsen, J. E.; Rolland, A. D.; Rajpert-De Meyts, E.; Janfelt, C.; Jorgensen, A.; Winge, S. B.; Kristensen, D. M.; Juul, A.; Chalmel, F.; Jegou, B.; et al. Characterisation and localisation of the endocannabinoid system components in the adult human testis. *Sci Rep* **2019**, *9* (1), 12866. DOI: 10.1038/s41598-019-49177-y.

(91) Notarstefano, V.; Gioacchini, G.; Giorgini, E.; Montik, N.; Ciavattini, A.; Polidori, A. R.; Candela, F. A.; Vaccari, L.; Cignitti, M.; Carnevali, O. The Impact of Controlled

Ovarian Stimulation Hormones on the Metabolic State and Endocannabinoid System of Human Cumulus Cells. *Int J Mol Sci* **2020**, *21* (19). DOI: 10.3390/ijms21197124.

(92) Lewis, S. E.; Rapino, C.; Di Tommaso, M.; Pucci, M.; Battista, N.; Paro, R.; Simon, L.; Lutton, D.; Maccarrone, M. Differences in the endocannabinoid system of sperm from fertile and infertile men. *PLoS One* **2012**, *7* (10), e47704. DOI: 10.1371/journal.pone.0047704.

(93) Trabucco, E.; Acone, G.; Marenna, A.; Pierantoni, R.; Cacciola, G.; Chioccarelli, T.; Mackie, K.; Fasano, S.; Colacurci, N.; Meccariello, R.; et al. Endocannabinoid system in first trimester placenta: low FAAH and high CB1 expression characterize spontaneous miscarriage. *Placenta* **2009**, *30* (6), 516-522. DOI: 10.1016/j.placenta.2009.03.015.

(94) Taylor, A. H.; Finney, M.; Lam, P. M.; Konje, J. C. Modulation of the endocannabinoid system in viable and non-viable first trimester pregnancies by pregnancy-related hormones. *Reprod Biol Endocrinol* **2011**, *9*, 152. DOI: 10.1186/1477-7827-9-152.

(95) Godlewski, G.; Offertaler, L.; Wagner, J. A.; Kunos, G. Receptors for acylethanolamides-GPR55 and GPR119. *Prostaglandins Other Lipid Mediat* **2009**, *89* (3-4), 105-111. DOI: 10.1016/j.prostaglandins.2009.07.001.

(96) Chen, Z.; Zhang, Y.; Guo, L.; Dosoky, N.; de Ferra, L.; Peters, S.; Niswender, K. D.; Davies, S. S. Leptogenic effects of NAPE require activity of NAPE-hydrolyzing phospholipase D. *J Lipid Res* **2017**, *58* (8), 1624-1635. DOI: 10.1194/jlr.M076513.

(97) Chen, Z.; Guo, L.; Zhang, Y.; Walzem, R. L.; Pendergast, J. S.; Printz, R. L.; Morris, L. C.; Matafonova, E.; Stien, X.; Kang, L.; et al. Incorporation of therapeutically modified bacteria into gut microbiota inhibits obesity. *J Clin Invest* **2014**, *124* (8), 3391-3406. DOI: 10.1172/JCI72517.

(98) Gillum, M. P.; Zhang, D.; Zhang, X. M.; Erion, D. M.; Jamison, R. A.; Choi, C.; Dong, J.; Shanabrough, M.; Duenas, H. R.; Frederick, D. W.; et al. N-acylphosphatidylethanolamine, a gut- derived circulating factor induced by fat ingestion, inhibits food intake. *Cell* **2008**, *135* (5), 813-824. DOI: 10.1016/j.cell.2008.10.043.

(99) Piomelli, D. A fatty gut feeling. *Trends Endocrinol Metab* **2013**, *24* (7), 332-341. DOI: 10.1016/j.tem.2013.03.001.

(100) Igarashi, M.; DiPatrizio, N. V.; Narayanaswami, V.; Piomelli, D. Feeding-induced oleoylethanolamide mobilization is disrupted in the gut of diet-induced obese rodents. *Biochim Biophys Acta* **2015**, *1851* (9), 1218-1226. DOI: 10.1016/j.bbalip.2015.05.006.

(101) Fu, J.; Astarita, G.; Gaetani, S.; Kim, J.; Cravatt, B. F.; Mackie, K.; Piomelli, D. Food intake regulates oleoylethanolamide formation and degradation in the proximal small intestine. *J Biol Chem* **2007**, *282* (2), 1518-1528. DOI: 10.1074/jbc.M607809200.

(102) Fu, J.; Gaetani, S.; Oveisi, F.; Lo Verme, J.; Serrano, A.; Rodriguez De Fonseca, F.; Rosengarth, A.; Luecke, H.; Di Giacomo, B.; Tarzia, G.; et al. Oleylethanolamide regulates feeding and body weight through activation of the nuclear receptor PPAR-alpha. *Nature* **2003**, *425* (6953), 90-93. DOI: 10.1038/nature01921.

(103) Guzman, M.; Lo Verme, J.; Fu, J.; Oveisi, F.; Blazquez, C.; Piomelli, D. Oleoylethanolamide stimulates lipolysis by activating the nuclear receptor peroxisome proliferator-activated receptor alpha (PPAR-alpha). *J Biol Chem* **2004**, *279* (27), 27849-27854. DOI: 10.1074/jbc.M404087200.

(104) Lo Verme, J.; Gaetani, S.; Fu, J.; Oveisi, F.; Burton, K.; Piomelli, D. Regulation of food intake by oleoylethanolamide. *Cell Mol Life Sci* **2005**, *62* (6), 708-716. DOI: 10.1007/s00018-004-4494-0.

(105) Fu, J.; Kim, J.; Oveisi, F.; Astarita, G.; Piomelli, D. Targeted enhancement of oleoylethanolamide production in proximal small intestine induces across-meal satiety in rats. *Am J Physiol Regul Integr Comp Physiol* **2008**, *295* (1), R45-50. DOI: 10.1152/ajpregu.00126.2008.

(106) Gaetani, S.; Fu, J.; Cassano, T.; Dipasquale, P.; Romano, A.; Righetti, L.; Cianci, S.; Laconca, L.; Giannini, E.; Scaccianoce, S.; et al. The fat-induced satiety factor oleoylethanolamide suppresses feeding through central release of oxytocin. *J Neurosci* **2010**, *30* (24), 8096-8101. DOI: 10.1523/JNEUROSCI.0036-10.2010.

(107) Rodriguez de Fonseca, F.; Navarro, M.; Gomez, R.; Escuredo, L.; Nava, F.; Fu, J.; Murillo-Rodriguez, E.; Giuffrida, A.; LoVerme, J.; Gaetani, S.; et al. An anorexic lipid mediator regulated by feeding. *Nature* **2001**, *414* (6860), 209-212. DOI: 10.1038/35102582.

(108) Oveisi, F.; Gaetani, S.; Eng, K. T.; Piomelli, D. Oleoylethanolamide inhibits food intake in free-feeding rats after oral administration. *Pharmacol Res* **2004**, *49* (5), 461-466. DOI: 10.1016/j.phrs.2003.12.006.

(109) Romano, A.; Tempesta, B.; Provensi, G.; Passani, M. B.; Gaetani, S. Central mechanisms mediating the hypophagic effects of oleoylethanolamide and N-acylphosphatidylethanolamines: different lipid signals? *Front Pharmacol* **2015**, *6*, 137. DOI: 10.3389/fphar.2015.00137.

(110) Diep, T. A.; Madsen, A. N.; Holst, B.; Kristiansen, M. M.; Wellner, N.; Hansen, S. H.; Hansen, H. S. Dietary fat decreases intestinal levels of the anorectic lipids through a fat sensor. *FASEB J* **2011**, *25* (2), 765-774. DOI: 10.1096/fj.10-166595.

(111) Igarashi, M.; Narayanaswami, V.; Kimonis, V.; Galassetti, P. M.; Oveisi, F.; Jung, K. M.; Piomelli, D. Dysfunctional oleoylethanolamide signaling in a mouse model of Prader-Willi syndrome. *Pharmacol Res* **2017**, *117*, 75-81. DOI: 10.1016/j.phrs.2016.12.024.

(112) Geurts, L.; Everard, A.; Van Hul, M.; Essaghir, A.; Duparc, T.; Matamoros, S.; Plovier, H.; Castel, J.; Denis, R. G.; Bergiers, M.; et al. Adipose tissue NAPE-PLD controls fat mass development by altering the browning process and gut microbiota. *Nat Commun* **2015**, *6*, 6495. DOI: 10.1038/ncomms7495.

(113) Li, L.; Li, L.; Chen, L.; Lin, X.; Xu, Y.; Ren, J.; Fu, J.; Qiu, Y. Effect of oleoylethanolamide on diet-induced nonalcoholic fatty liver in rats. *J Pharmacol Sci* **2015**, *127* (3), 244-250. DOI: 10.1016/j.jphs.2014.12.001.

(114) Tutunchi, H.; Ostadrahimi, A.; Saghafi-Asl, M.; Maleki, V. The effects of oleoylethanolamide, an endogenous PPAR-alpha agonist, on risk factors for NAFLD: A systematic review. *Obes Rev* **2019**, *20* (7), 1057-1069. DOI: 10.1111/obr.12853.

(115) Daynes, R. A.; Jones, D. C. Emerging roles of PPARs in inflammation and immunity. *Nat Rev Immunol* **2002**, *2* (10), 748-759. DOI: 10.1038/nri912.

(116) Tsuboi, K.; Ikematsu, N.; Uyama, T.; Deutsch, D. G.; Tokumura, A.; Ueda, N. Biosynthetic pathways of bioactive N-acylethanolamines in brain. *CNS Neurol Disord Drug Targets* **2013**, *12* (1), 7-16. DOI: 10.2174/1871527311312010005.

(117) Guo, L.; Gragg, S. D.; Chen, Z.; Zhang, Y.; Amarnath, V.; Davies, S. S. Isolevuglandin-modified phosphatidylethanolamine is metabolized by NAPE-hydrolyzing phospholipase D. *J Lipid Res* **2013**, *54* (11), 3151-3157. DOI: 10.1194/jlr.M042556.

(118) Okamoto, Y.; Wang, J.; Morishita, J.; Ueda, N. Biosynthetic pathways of the endocannabinoid anandamide. *Chem Biodivers* **2007**, *4* (8), 1842-1857. DOI: 10.1002/cbdv.200790155.

(119) Uyama, T.; Ikematsu, N.; Inoue, M.; Shinohara, N.; Jin, X. H.; Tsuboi, K.; Tonai, T.; Tokumura, A.; Ueda, N. Generation of N-acylphosphatidylethanolamine by members of the phospholipase A/acyltransferase (PLA/AT) family. *J Biol Chem* **2012**, *287* (38), 31905-31919. DOI: 10.1074/jbc.M112.368712.

(120) Cheng, Y. H.; Ho, M. S.; Huang, W. T.; Chou, Y. T.; King, K. Modulation of Glucagon-like Peptide-1 (GLP-1) Potency by Endocannabinoid-like Lipids Represents a Novel Mode of Regulating GLP-1 Receptor Signaling. *J Biol Chem* **2015**, *290* (23), 14302-14313. DOI: 10.1074/jbc.M115.655662.

(121) Burgess, J. L.; Wyant, W. A.; Abdo Abujamra, B.; Kirsner, R. S.; Jozic, I. Diabetic Wound-Healing Science. *Medicina (Kaunas)* **2021**, *57* (10). DOI: 10.3390/medicina57101072  From NLM Medline.

(122) Khanna, S.; Biswas, S.; Shang, Y.; Collard, E.; Azad, A.; Kauh, C.; Bhasker, V.; Gordillo, G. M.; Sen, C. K.; Roy, S. Macrophage dysfunction impairs resolution of inflammation in the wounds of diabetic mice. *PLoS One* **2010**, *5* (3), e9539. DOI: 10.1371/journal.pone.0009539.

(123) Louiselle, A. E.; Niemiec, S. M.; Zgheib, C.; Liechty, K. W. Macrophage polarization and diabetic wound healing. *Transl Res* **2021**, *236*, 109-116. DOI: 10.1016/j.trsl.2021.05.006  From NLM Medline.

(124) Castellani, B.; Diamanti, E.; Pizzirani, D.; Tardia, P.; Maccesi, M.; Realini, N.; Magotti, P.; Garau, G.; Bakkum, T.; Rivara, S.; et al. Synthesis and characterization of the first inhibitor of N-acylphosphatidylethanolamine phospholipase D (NAPE-PLD). *Chem Commun (Camb)* **2017**, *53* (95), 12814-12817. DOI: 10.1039/c7cc07582k.

(125) Mock, E. D.; Mustafa, M.; Gunduz-Cinar, O.; Cinar, R.; Petrie, G. N.; Kantae, V.; Di, X.; Ogasawara, D.; Varga, Z. V.; Paloczi, J.; et al. Discovery of a NAPE-PLD inhibitor that modulates emotional behavior in mice. *Nat Chem Biol* **2020**, *16* (6), 667-675. DOI: 10.1038/s41589-020-0528-7.

(126) Aggarwal, G.; Zarrow, J. E.; Mashhadi, Z.; Flynn, C. R.; Vinson, P.; Weaver, C. D.; Davies, S. S. Symmetrically substituted dichlorophenes inhibit N-acyl-phosphatidylethanolamine phospholipase D. *J Biol Chem* **2020**, *295* (21), 7289-7300. DOI: 10.1074/jbc.RA120.013362.

(127) Zarrow, J. E.; Alli-Oluwafuyi, A.-M.; Youwakim, C. M.; Kim, K.; Jenkins, A. N.; Suero, I. C.; Jones, M. R.; Mashhadi, Z.; Mackie, K. P.; Waterson, A. G.; et al. Small Molecule Activation of NAPE-PLD Enhances Efferocytosis by Macrophages. *bioRxiv* **2023**, 2023.2001.2025.525554. DOI: 10.1101/2023.01.25.525554.

(128) Miceli, M.; Casati, S.; Ottria, R.; Di Leo, S.; Eberini, I.; Palazzolo, L.; Parravicini, C.; Ciuffreda, P. Set-Up and Validation of a High Throughput Screening Method for Human Monoacylglycerol Lipase (MAGL) Based on a New Red Fluorescent Probe. *Molecules* **2019**, *24* (12). DOI: 10.3390/molecules24122241  From NLM Medline.

(129) Mitnaul, L. J.; Tian, J.; Burton, C.; Lam, M. H.; Zhu, Y.; Olson, S. H.; Schneeweis, J. E.; Zuck, P.; Pandit, S.; Anderson, M.; et al. Fluorogenic substrates for high-

throughput measurements of endothelial lipase activity. *J Lipid Res* **2007**, *48* (2), 472-482. DOI: 10.1194/jlr.D600041-JLR200  From NLM Medline.

(130) Darrow, A. L.; Olson, M. W.; Xin, H.; Burke, S. L.; Smith, C.; Schalk-Hihi, C.; Williams, R.; Bayoumy, S. S.; Deckman, I. C.; Todd, M. J.; et al. A novel fluorogenic substrate for the measurement of endothelial lipase activity. *J Lipid Res* **2011**, *52* (2), 374-382. DOI: 10.1194/jlr.D007971  From NLM Medline.

(131) Zhang, J. H.; Chung, T. D.; Oldenburg, K. R. A Simple Statistical Parameter for Use in Evaluation and Validation of High Throughput Screening Assays. *J Biomol Screen* **1999**, *4* (2), 67-73. DOI: 10.1177/108705719900400206  From NLM Publisher.

(132) Brideau, C.; Gunter, B.; Pikounis, B.; Liaw, A. Improved statistical methods for hit selection in high-throughput screening. *J Biomol Screen* **2003**, *8* (6), 634-647. DOI: 10.1177/1087057103258285.

(133) Zarrow, J. E.; Tian, J.; Dutter, B.; Kim, K.; Doran, A. C.; Sulikowski, G. A.; Davies, S. S. Selective measurement of NAPE-PLD activity via a PLA1/2-resistant fluorogenic N-acyl-phosphatidylethanolamine analog. *J Lipid Res* **2022**, *63* (1), 100156. DOI: 10.1016/j.jlr.2021.100156.

(134) Zolnik, B. S.; Stern, S. T.; Kaiser, J. M.; Heakal, Y.; Clogston, J. D.; Kester, M.; McNeil, S. E. Rapid distribution of liposomal short-chain ceramide in vitro and in vivo. *Drug Metab Dispos* **2008**, *36* (8), 1709-1715. DOI: 10.1124/dmd.107.019679.

(135) Ohyama, N.; Hamano, T.; Hamakawa, N.; Inagaki, K.; Nakanishi, M. Membrane fluidity and lipid hapten structure of liposomes affect calcium signals in antigen-specific B cells. *Biochemistry* **1991**, *30* (46), 11154-11156. DOI: 10.1021/bi00110a019.

(136) Rebecchi, M. J.; Eberhardt, R.; Delaney, T.; Ali, S.; Bittman, R. Hydrolysis of short acyl chain inositol lipids by phospholipase C-delta 1. *Journal of Biological Chemistry* **1993**, *268* (3), 1735-1741. DOI: 10.1016/s0021-9258(18)53914-4.

(137) Futerman, A. H.; Pagano, R. E. Use of N-([1-14C]hexanoyl)-D-erythro-sphingolipids to assay sphingolipid metabolism. *Methods in enzymology* **1992**, *209*, 437-446. DOI: 10.1016/0076-6879(92)09054-7  From NLM.

(138) Majd, H.; King, M. S.; Palmer, S. M.; Smith, A. C.; Elbourne, L. D.; Paulsen, I. T.; Sharples, D.; Henderson, P. J.; Kunji, E. R. Screening of candidate substrates and coupling ions of transporters by thermostability shift assays. *Elife* **2018**, *7*. DOI: 10.7554/eLife.38821.

(139) Gonzalez-Rivera, C.; Gangwer, K. A.; McClain, M. S.; Eli, I. M.; Chambers, M. G.; Ohi, M. D.; Lacy, D. B.; Cover, T. L. Reconstitution of Helicobacter pylori VacA toxin from purified components. *Biochemistry* **2010**, *49* (27), 5743-5752. DOI: 10.1021/bi100618g  From NLM Medline.

(140) Dallakyan, S.; Olson, A. J. Small-molecule library screening by docking with PyRx. *Methods Mol Biol* **2015**, *1263*, 243-250. DOI: 10.1007/978-1-4939-2269-7_19  From NLM Medline.

(141) Bedouelle, H.; Duplay, P. Production in Escherichia coli and one-step purification of bifunctional hybrid proteins which bind maltose. Export of the Klenow polymerase into the periplasmic space. *Eur J Biochem* **1988**, *171* (3), 541-549. DOI: 10.1111/j.1432-1033.1988.tb13823.x.

(142) Kapust, R. B.; Waugh, D. S. Escherichia coli maltose-binding protein is uncommonly effective at promoting the solubility of polypeptides to which it is fused. *Protein Sci* **1999**, *8* (8), 1668-1674. DOI: 10.1110/ps.8.8.1668.

(143) Guha, R.; Dexheimer, T. S.; Kestranek, A. N.; Jadhav, A.; Chervenak, A. M.; Ford, M. G.; Simeonov, A.; Roth, G. P.; Thomas, C. J. Exploratory analysis of kinetic solubility measurements of a small molecule library. *Bioorg Med Chem* **2011**, *19* (13), 4127-4134. DOI: 10.1016/j.bmc.2011.05.005  From NLM Medline.

(144) Ishikawa, M.; Hashimoto, Y. Improvement in aqueous solubility in small molecule drug discovery programs by disruption of molecular planarity and symmetry. *J Med Chem* **2011**, *54* (6), 1539-1554. DOI: 10.1021/jm101356p  From NLM Medline.

(145) Wilt, S.; Kodani, S.; Le, T. N. H.; Nguyen, L.; Vo, N.; Ly, T.; Rodriguez, M.; Hudson, P. K.; Morisseau, C.; Hammock, B. D.; et al. Development of multitarget inhibitors for the treatment of pain: Design, synthesis, biological evaluation and molecular modeling studies. *Bioorg Chem* **2020**, *103*, 104165. DOI: 10.1016/j.bioorg.2020.104165.

(146) Das Mahapatra, A.; Choubey, R.; Datta, B. Small Molecule Soluble Epoxide Hydrolase Inhibitors in Multitarget and Combination Therapies for Inflammation and Cancer. *Molecules* **2020**, *25* (23). DOI: 10.3390/molecules25235488.

(147) Gilroy, D. W.; Edin, M. L.; De Maeyer, R. P.; Bystrom, J.; Newson, J.; Lih, F. B.; Stables, M.; Zeldin, D. C.; Bishop-Bailey, D. CYP450-derived oxylipins mediate inflammatory resolution. *Proc Natl Acad Sci U S A* **2016**, *113* (23), E3240-3249. DOI: 10.1073/pnas.1521453113.

(148) Khadir, A.; Kavalakatt, S.; Madhu, D.; Cherian, P.; Al-Mulla, F.; Abubaker, J.; Tiss, A. Soluble Epoxide Hydrolase 2 Expression Is Elevated in Obese Humans and Decreased by Physical Activity. *Int J Mol Sci* **2020**, *21* (6). DOI: 10.3390/ijms21062056.

(149) Guo, L.; Amarnath, V.; Davies, S. S. A liquid chromatography-tandem mass spectrometry method for measurement of N-modified phosphatidylethanolamines. *Analytical biochemistry* **2010**, *405* (2), 236-245. DOI: 10.1016/j.ab.2010.06.027.

(150) Jo, S.; Kim, T.; Iyer, V. G.; Im, W. CHARMM-GUI: a web-based graphical user interface for CHARMM. *J Comput Chem* **2008**, *29* (11), 1859-1865. DOI: 10.1002/jcc.20945  From NLM Medline.

(151) Lee, J.; Hitzenberger, M.; Rieger, M.; Kern, N. R.; Zacharias, M.; Im, W. CHARMM-GUI supports the Amber force fields. *J Chem Phys* **2020**, *153* (3), 035103. DOI: 10.1063/5.0012280  From NLM Medline.

(152) Roe, D. R.; Cheatham, T. E., 3rd. PTRAJ and CPPTRAJ: Software for Processing and Analysis of Molecular Dynamics Trajectory Data. *J Chem Theory Comput* **2013**, *9* (7), 3084-3095. DOI: 10.1021/ct400341p  From NLM PubMed-not-MEDLINE.

(153) Petersen, G.; Hansen, H. S. N-acylphosphatidylethanolamine-hydrolysing phospholipase D lacks the ability to transphosphatidylate. *FEBS Lett* **1999**, *455* (1-2), 41-44. DOI: 10.1016/s0014-5793(99)00861-3.

(154) Tsuboi, K.; Okamoto, Y.; Rahman, I. A.; Uyama, T.; Inoue, T.; Tokumura, A.; Ueda, N. Glycerophosphodiesterase GDE4 as a novel lysophospholipase D: a possible involvement in bioactive N-acylethanolamine biosynthesis. *Biochim Biophys Acta* **2015**, *1851* (5), 537-548. DOI: 10.1016/j.bbalip.2015.01.002.

(155) Simon, G. M.; Cravatt, B. F. Anandamide biosynthesis catalyzed by the phosphodiesterase GDE1 and detection of glycerophospho-N-acyl ethanolamine precursors in mouse brain. *J Biol Chem* **2008**, *283* (14), 9341-9349. DOI: 10.1074/jbc.M707807200.

(156) Petersen, G.; Pedersen, A. H.; Pickering, D. S.; Begtrup, M.; Hansen, H. S. Effect of synthetic and natural phospholipids on N-acylphosphatidylethanolamine-hydrolyzing phospholipase D activity. *Chem Phys Lipids* **2009**, *162* (1-2), 53-61. DOI: 10.1016/j.chemphyslip.2009.08.005.

(157) Simon, G. M.; Cravatt, B. F. Endocannabinoid biosynthesis proceeding through glycerophospho-N-acyl ethanolamine and a role for alpha/beta-hydrolase 4 in this pathway. *J Biol Chem* **2006**, *281* (36), 26465-26472. DOI: 10.1074/jbc.M604660200.

(158) Zhu, C.; Solorzano, C.; Sahar, S.; Realini, N.; Fung, E.; Sassone-Corsi, P.; Piomelli, D. Proinflammatory stimuli control N-acylphosphatidylethanolamine-specific phospholipase D expression in macrophages. *Mol Pharmacol* **2011**, *79* (4), 786-792. DOI: 10.1124/mol.110.070201.

(159) Hendrickson, H. S.; Hendrickson, E. K.; Johnson, I. D.; Farber, S. A. Intramolecularly Quenched BODIPY-Labeled Phospholipid Analogs in Phospholipase A2 and Platelet-Activating Factor Acetylhydrolase Assays and in Vivo Fluorescence Imaging. *Analytical Biochemistry* **1999**, *276* (1), 27-35. DOI: https://doi.org/10.1006/abio.1999.4280.

(160) Leu, B. H.; Schmidt, J. T. Arachidonic acid as a retrograde signal controlling growth and dynamics of retinotectal arbors. *Dev Neurobiol* **2008**, *68* (1), 18-30. DOI: 10.1002/dneu.20561  From NLM.

(161) Hama, K.; Provost, E.; Baranowski, T. C.; Rubinstein, A. L.; Anderson, J. L.; Leach, S. D.; Farber, S. A. In vivo imaging of zebrafish digestive organ function using multiple quenched fluorescent reporters. *Am J Physiol Gastrointest Liver Physiol* **2009**, *296* (2), G445-453. DOI: 10.1152/ajpgi.90513.2008.

(162) Mock, E. D.; Kotsogianni, I.; Driever, W. P. F.; Fonseca, C. S.; Vooijs, J. M.; den Dulk, H.; van Boeckel, C. A. A.; van der Stelt, M. Structure-Activity Relationship Studies of Pyrimidine-4-Carboxamides as Inhibitors of N-Acylphosphatidylethanolamine Phospholipase D. *J Med Chem* **2021**, *64* (1), 481-515. DOI: 10.1021/acs.jmedchem.0c01441.

(163) Pasternack, S. M.; von Kugelgen, I.; Muller, M.; Oji, V.; Traupe, H.; Sprecher, E.; Nothen, M. M.; Janecke, A. R.; Betz, R. C. In vitro analysis of LIPH mutations causing hypotrichosis simplex: evidence confirming the role of lipase H and lysophosphatidic acid in hair growth. *J Invest Dermatol* **2009**, *129* (12), 2772-2776. DOI: 10.1038/jid.2009.154.

(164) Asano, A.; Nelson-Harrington, J. L.; Travis, A. J. Phospholipase B is activated in response to sterol removal and stimulates acrosome exocytosis in murine sperm. *J Biol Chem* **2013**, *288* (39), 28104-28115. DOI: 10.1074/jbc.M113.450981.

(165) Kuge, H.; Akahori, K.; Yagyu, K. I.; Honke, K. Functional compartmentalization of the plasma membrane of neurons by a unique acyl chain composition of phospholipids. *J Biol Chem* **2014**, *289* (39), 26783-26793. DOI: 10.1074/jbc.M114.571075.

(166) Hauptman, J. B.; Jeunet, F. S.; Hartmann, D. Initial studies in humans with the novel gastrointestinal lipase inhibitor Ro 18-0647 (tetrahydrolipstatin). *Am J Clin Nutr* **1992**, *55* (1 Suppl), 309S-313S. DOI: 10.1093/ajcn/55.1.309s.

(167) Fernandez, E.; Borgstrom, B. Effects of tetrahydrolipstatin, a lipase inhibitor, on absorption of fat from the intestine of the rat. *Biochim Biophys Acta* **1989**, *1001* (3), 249-255. DOI: 10.1016/0005-2760(89)90107-0.

(168) Hogan, S.; Fleury, A.; Hadvary, P.; Lengsfeld, H.; Meier, M. K.; Triscari, J.; Sullivan, A. C. Studies on the antiobesity activity of tetrahydrolipstatin, a potent and selective inhibitor of pancreatic lipase. *International journal of obesity* **1987**, *11 Suppl 3*, 35-42.  From NLM.

(169) Tatematsu, S.; Francis, S. A.; Natarajan, P.; Rader, D. J.; Saghatelian, A.; Brown, J. D.; Michel, T.; Plutzky, J. Endothelial lipase is a critical determinant of high-density lipoprotein-stimulated sphingosine 1-phosphate-dependent signaling in vascular endothelium. *Arteriosclerosis, thrombosis, and vascular biology* **2013**, *33* (8), 1788-1794. DOI: 10.1161/ATVBAHA.113.301300 PubMed.

(170) Rinninger, F.; Mann, W. A.; Kaiser, T.; Ahle, S.; Meyer, N.; Greten, H. Hepatic lipase mediates an increase in selective uptake of high-density lipoprotein-associated cholesteryl esters by human Hep 3B hepatoma cells in culture. *Atherosclerosis* **1998**, *141* (2), 273-285. DOI: 10.1016/s0021-9150(98)00181-6  From NLM.

(171) Yun, C. C.; Kumar, A. Diverse roles of LPA signaling in the intestinal epithelium. *Exp Cell Res* **2015**, *333* (2), 201-207. DOI: 10.1016/j.yexcr.2014.11.013.

(172) Richmond, G. S.; Smith, T. K. Phospholipases A(1). *Int J Mol Sci* **2011**, *12* (1), 588-612. DOI: 10.3390/ijms12010588.

(173) Lopategi, A.; Lopez-Vicario, C.; Alcaraz-Quiles, J.; Garcia-Alonso, V.; Rius, B.; Titos, E.; Claria, J. Role of bioactive lipid mediators in obese adipose tissue inflammation and endocrine dysfunction. *Mol Cell Endocrinol* **2016**, *419*, 44-59. DOI: 10.1016/j.mce.2015.09.033.

(174) Lee, J. H.; Kim, D.; Oh, Y. S.; Jun, H. S. Lysophosphatidic Acid Signaling in Diabetic Nephropathy. *Int J Mol Sci* **2019**, *20* (11). DOI: 10.3390/ijms20112850.

(175) Moran, B. M.; Abdel-Wahab, Y. H.; Flatt, P. R.; McKillop, A. M. Activation of GPR119 by fatty acid agonists augments insulin release from clonal beta-cells and isolated pancreatic islets and improves glucose tolerance in mice. *Biol Chem* **2014**, *395* (4), 453-464. DOI: 10.1515/hsz-2013-0255.

(176) Ning, Y.; O'Neill, K.; Lan, H.; Pang, L.; Shan, L. X.; Hawes, B. E.; Hedrick, J. A. Endogenous and synthetic agonists of GPR119 differ in signalling pathways and their effects on insulin secretion in MIN6c4 insulinoma cells. *Br J Pharmacol* **2008**, *155* (7), 1056-1065. DOI: 10.1038/bjp.2008.337.

(177) Di Paola, R.; Impellizzeri, D.; Mondello, P.; Velardi, E.; Aloisi, C.; Cappellani, A.; Esposito, E.; Cuzzocrea, S. Palmitoylethanolamide reduces early renal dysfunction and injury caused by experimental ischemia and reperfusion in mice. *Shock* **2012**, *38* (4), 356-366. DOI: 10.1097/SHK.0b013e318267bbb9.

(178) Corcoran, L.; Roche, M.; Finn, D. P. The Role of the Brain's Endocannabinoid System in Pain and Its Modulation by Stress. *Int Rev Neurobiol* **2015**, *125*, 203-255. DOI: 10.1016/bs.irn.2015.10.003.

(179) Simon, G. M.; Cravatt, B. F. Endocannabinoid Biosynthesis Proceeding through Glycerophospho-N-acyl Ethanolamine and a Role for α/β-Hydrolase 4 in This Pathway*. *Journal of Biological Chemistry* **2006**, *281* (36), 26465-26472. DOI: https://doi.org/10.1074/jbc.M604660200.

(180) Liu, J.; Wang, L.; Harvey-White, J.; Osei-Hyiaman, D.; Razdan, R.; Gong, Q.; Chan, A. C.; Zhou, Z.; Huang, B. X.; Kim, H.-Y.; et al. A biosynthetic pathway for anandamide. *Proceedings of the National Academy of Sciences* **2006**, *103* (36), 13345-13350. DOI: 10.1073/pnas.0601832103.

(181) Aoki, J.; Inoue, A.; Makide, K.; Saiki, N.; Arai, H. Structure and function of extracellular phospholipase A1 belonging to the pancreatic lipase gene family. *Biochimie* **2007**, *89* (2), 197-204. DOI: 10.1016/j.biochi.2006.09.021  From NLM.

(182) Uyama, T.; Ikematsu, N.; Inoue, M.; Shinohara, N.; Jin, X.-H.; Tsuboi, K.; Tonai, T.; Tokumura, A.; Ueda, N. Generation of N-Acylphosphatidylethanolamine by Members of the Phospholipase A/Acyltransferase (PLA/AT) Family*. *Journal of Biological Chemistry* **2012**, *287* (38), 31905-31919. DOI: https://doi.org/10.1074/jbc.M112.368712.

(183) Farber, S. A.; Pack, M.; Ho, S.-Y.; Johnson, I. D.; Wagner, D. S.; Dosch, R.; Mullins, M. C.; Hendrickson, H. S.; Hendrickson, E. K.; Halpern, M. E. Genetic Analysis of Digestive Physiology Using Fluorescent Phospholipid Reporters. *Science* **2001**, *292* (5520), 1385-1388. DOI: 10.1126/science.1060418.

(184) Hidalgo, I. J.; Raub, T. J.; Borchardt, R. T. Characterization of the Human-Colon Carcinoma Cell-Line (Caco-2) as a Model System for Intestinal Epithelial Permeability. *Gastroenterology* **1989**, *96* (3), 736-749. DOI: 10.1016/S0016-5085(89)80072-1 (acccessed 2019/07/12).

(185) Meunier, V.; Bourrie, M.; Berger, Y.; Fabre, G. The human intestinal epithelial cell line Caco-2; pharmacological and pharmacokinetic applications. *Cell Biol Toxicol* **1995**, *11* (3-4), 187-194, journal article. DOI: 10.1007/BF00756522.

(186) Morisseau, C.; Goodrow, M. H.; Newman, J. W.; Wheelock, C. E.; Dowdy, D. L.; Hammock, B. D. Structural refinement of inhibitors of urea-based soluble epoxide hydrolases. *Biochem Pharmacol* **2002**, *63* (9), 1599-1608. DOI: 10.1016/s0006-2952(02)00952-8.

(187) Rose, T. E.; Morisseau, C.; Liu, J. Y.; Inceoglu, B.; Jones, P. D.; Sanborn, J. R.; Hammock, B. D. 1-Aryl-3-(1-acylpiperidin-4-yl)urea inhibitors of human and murine soluble epoxide hydrolase: structure-activity relationships, pharmacokinetics, and reduction of inflammatory pain. *J Med Chem* **2010**, *53* (19), 7067-7075. DOI: 10.1021/jm100691c  From NLM Medline.

(188) Okamoto, Y.; Morishita, J.; Wang, J.; Schmid, P. C.; Krebsbach, R. J.; Schmid, H. H.; Ueda, N. Mammalian cells stably overexpressing N-acylphosphatidylethanolamine-hydrolysing phospholipase D exhibit significantly decreased levels of N-acylphosphatidylethanolamines. *Biochem J* **2005**, *389* (Pt 1), 241-247. DOI: 10.1042/BJ20041790  From NLM Medline.

(189) Jee Kim, M.; Tanioka, M.; Woo Um, S.; Hong, S. K.; Hwan Lee, B. Analgesic effects of FAAH inhibitor in the insular cortex of nerve-injured rats. *Mol Pain* **2018**, *14*, 1744806918814345. DOI: 10.1177/1744806918814345.

(190) Duncan, R. S.; Riordan, S. M.; Hall, C. W.; Payne, A. J.; Chapman, K. D.; Koulen, P. N-acylethanolamide metabolizing enzymes are upregulated in human neural progenitor-derived neurons exposed to sub-lethal oxidative stress. *Front Cell Neurosci* **2022**, *16*, 902278. DOI: 10.3389/fncel.2022.902278.

(191) Ayakannu, T.; Taylor, A. H.; Marczylo, T. H.; Konje, J. C. New Insights of Uterine Leiomyoma Pathogenesis: Endocannabinoid System. *Med Sci Monit Basic Res* **2019**, *25*, 76-87. DOI: 10.12659/MSMBR.914019.

(192) Chen, Z.; Zhuo, R.; Zhao, Y.; Yang, L.; Zhou, Y.; Cheng, X.; Peng, L.; Jin, X.; Wang, Y. Oleoylethanolamide stabilizes atherosclerotic plaque through regulating macrophage polarization via AMPK-PPARα pathway. *Biochem Biophys Res Commun* **2020**, *524* (2), 308-316. DOI: 10.1016/j.bbrc.2020.01.103  From NLM.

(193) Boada-Romero, E.; Martinez, J.; Heckmann, B. L.; Green, D. R. The clearance of dead cells by efferocytosis. *Nature Reviews Molecular Cell Biology* **2020**, *21* (7), 398-414. DOI: 10.1038/s41580-020-0232-1.

(194) Thorp, E.; Cui, D.; Schrijvers, D. M.; Kuriakose, G.; Tabas, I. Mertk receptor mutation reduces efferocytosis efficiency and promotes apoptotic cell accumulation and plaque necrosis in atherosclerotic lesions of apoe-/- mice. *Arterioscler Thromb Vasc Biol* **2008**, *28* (8), 1421-1428. DOI: 10.1161/atvbaha.108.167197  From NLM.

(195) Elliott, M. R.; Koster, K. M.; Murphy, P. S. Efferocytosis Signaling in the Regulation of Macrophage Inflammatory Responses. *J Immunol* **2017**, *198* (4), 1387-1394. DOI: 10.4049/jimmunol.1601520  From NLM.

(196) Domingo, J. C.; Mora, M.; Africa de Madariaga, M. Incorporation of N-acylethanolamine phospholipids into egg phosphatidylcholine vesicles: characterization and permeability properties of the binary systems. *Biochimica et Biophysica Acta (BBA) - Biomembranes* **1993**, *1148* (2), 308-316. DOI: https://doi.org/10.1016/0005-2736(93)90144-O.

(197) Mora, M.; Mir, F.; de Madariaga, M. A.; Sagristá, M. L. Aggregation and fusion of vesicles composed of N-palmitoyl derivatives of membrane phospholipids. *Lipids* **2000**, *35* (5), 513-524. DOI: 10.1007/s11745-000-551-9  From NLM.

(198) Térová, B.; Petersen, G.; Hansen, H. S.; Slotte, J. P. N-acyl phosphatidylethanolamines affect the lateral distribution of cholesterol in membranes. *Biochim Biophys Acta* **2005**, *1715* (1), 49-56. DOI: 10.1016/j.bbamem.2005.07.004  From NLM.

(199) Kooijman, E. E.; Chupin, V.; de Kruijff, B.; Burger, K. N. Modulation of membrane curvature by phosphatidic acid and lysophosphatidic acid. *Traffic (Copenhagen, Denmark)* **2003**, *4* (3), 162-174. DOI: 10.1034/j.1600-0854.2003.00086.x  From NLM.

## Supplemental Figures and Tables
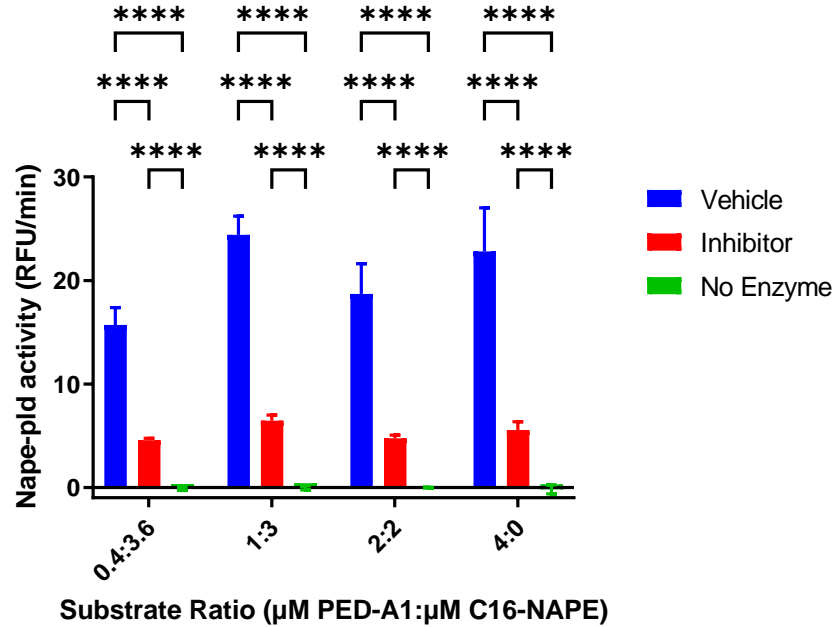


**Figure A1.** Signals can still be distinguished using diluted PED-A1. Conditions were Nape-pld treated with DMSO (vehicle, blue) or 100 µM LCA (inhibitor, red), and enzyme-free treatments (green). To those were administered 4 doses of PED-A1 + C16-NAPE. Mean + 95% CI is shown for each treatment, n = 3 replicate wells. Ordinary two-way analysis of variance (ANOVA), $p<0.0001$ for all factors. Tukey's multiple comparisons test within substrate groups, $p<0.0001$ for all comparisons.
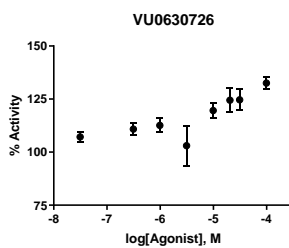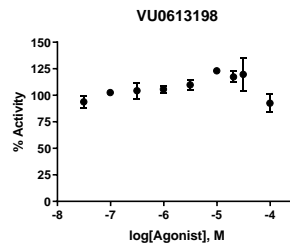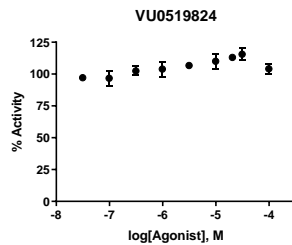
**Figure A2.** Results of initial Nape-pld CRCs. Individual points are mean ± SD from 3 replicate wells. Inhibitor curves were generally calculated using log(inhibitor) vs. normalized response, variable slope in GraphPad Prism 9. Activator curves were generally calculated using log(agonist) vs. response, variable slope (four parameters) in GraphPad Prism 9. Graphs with flat or no curves did not show sufficient dose-dependent activity changes to generate a well-fitting curve.
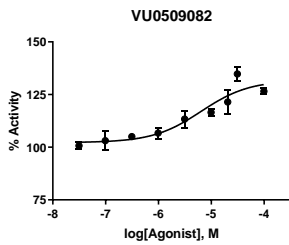
161
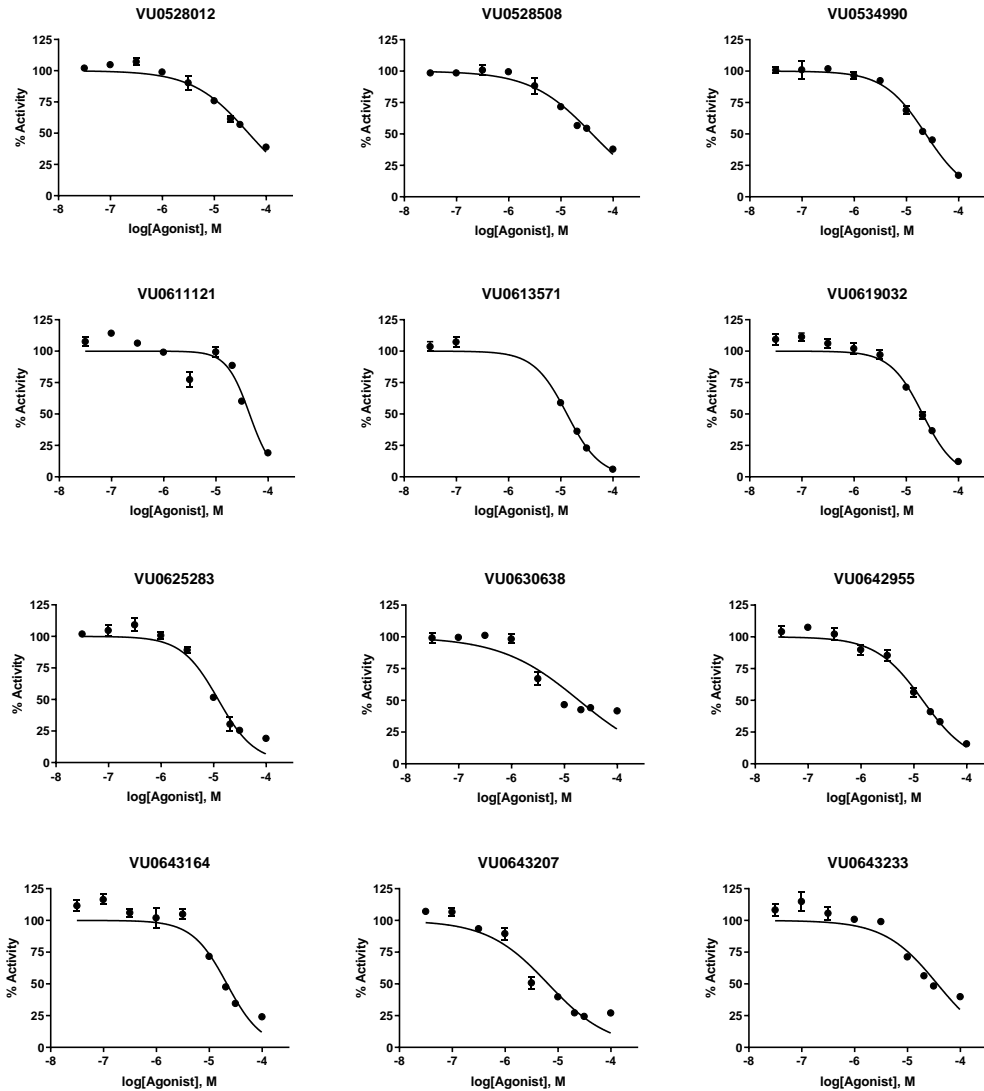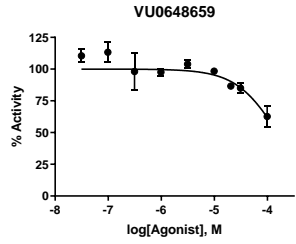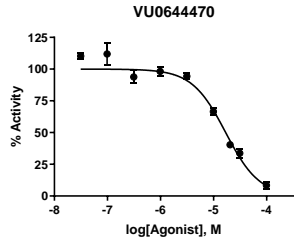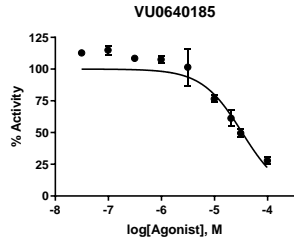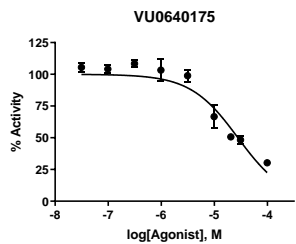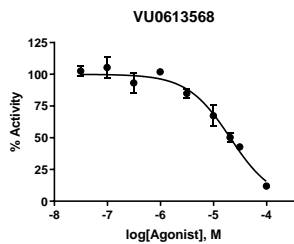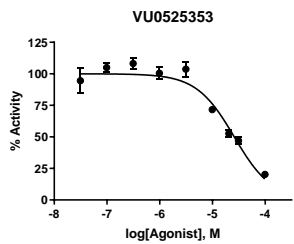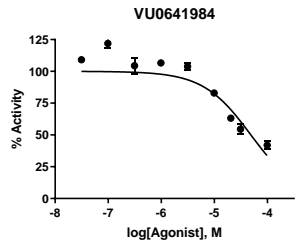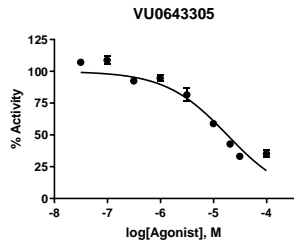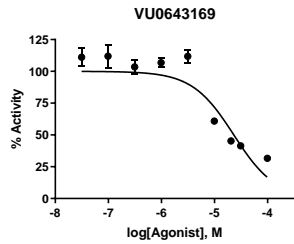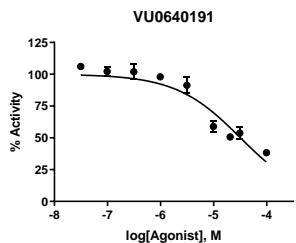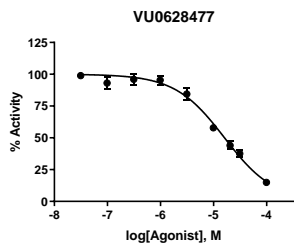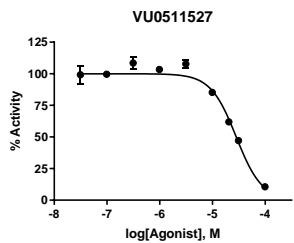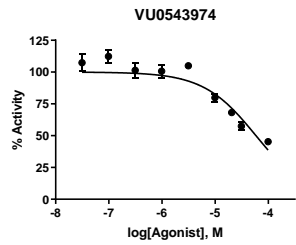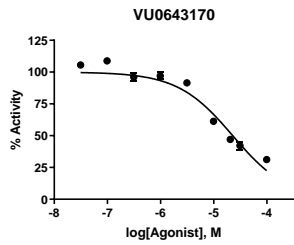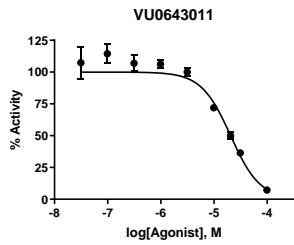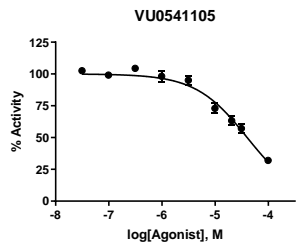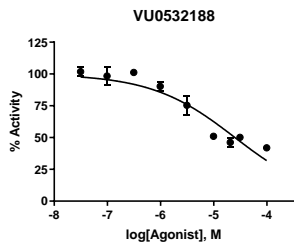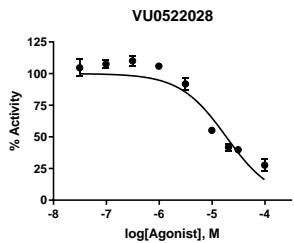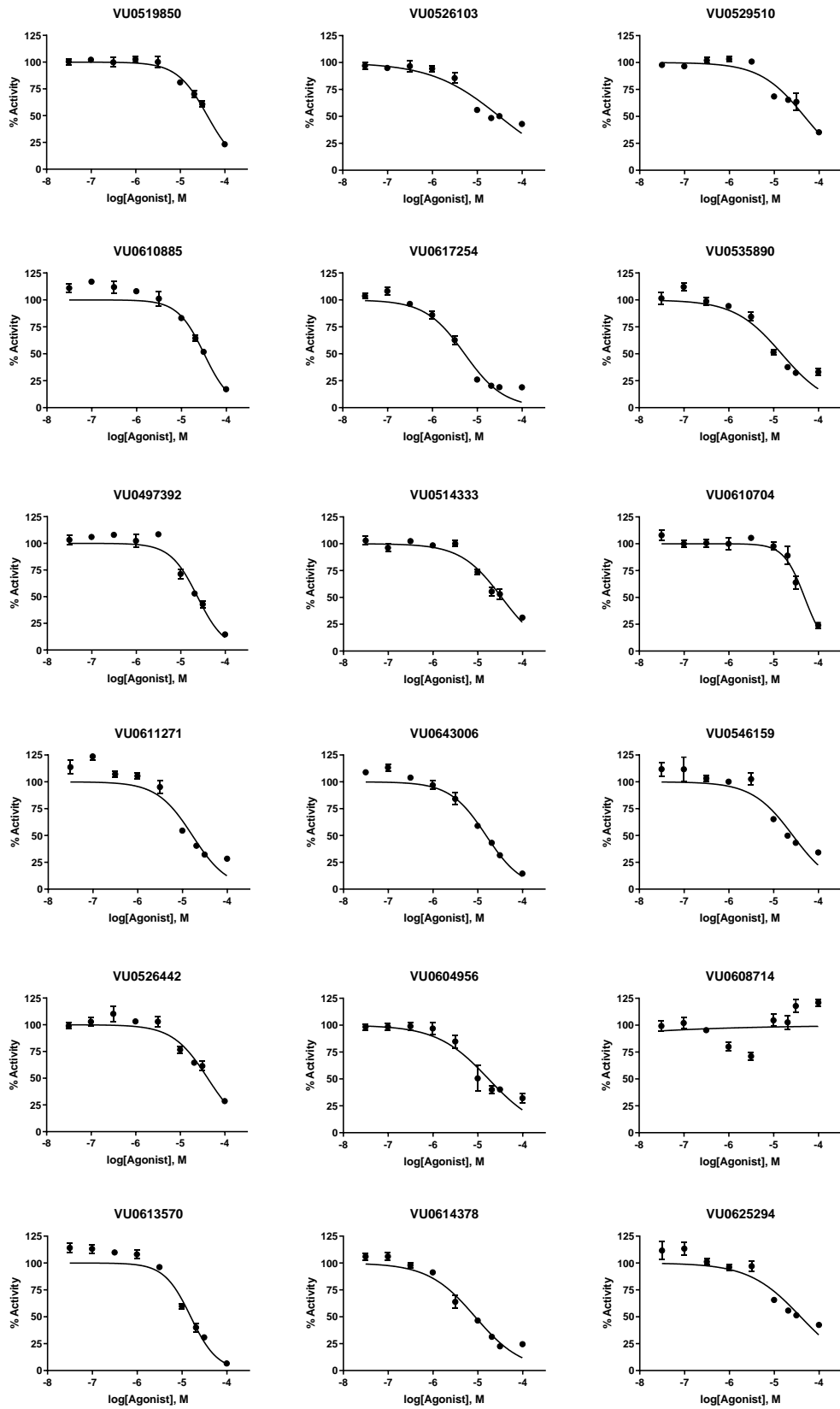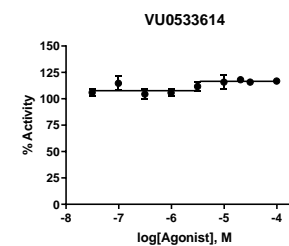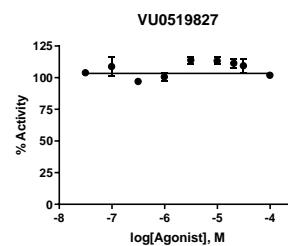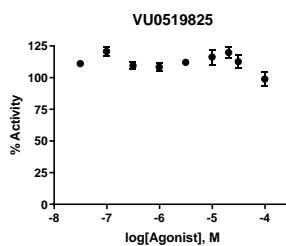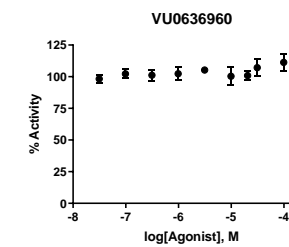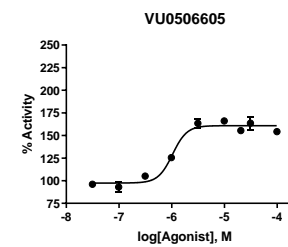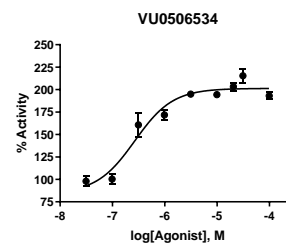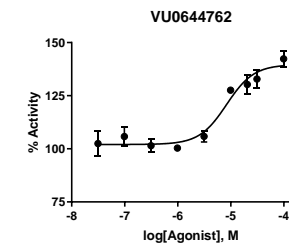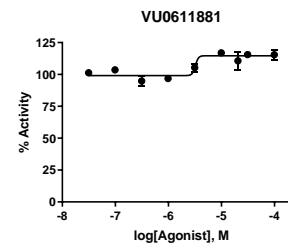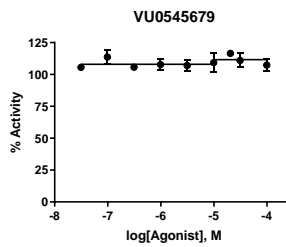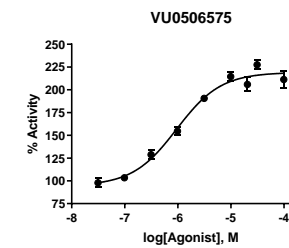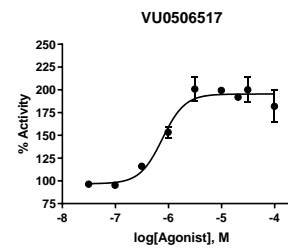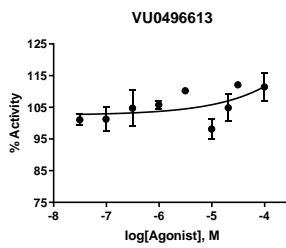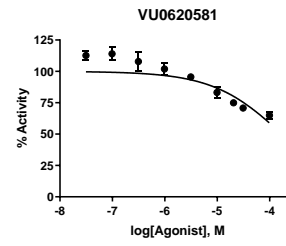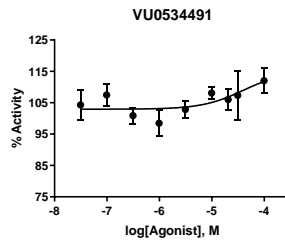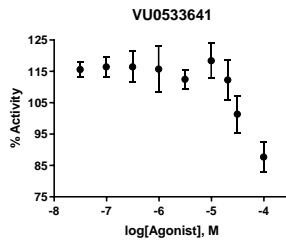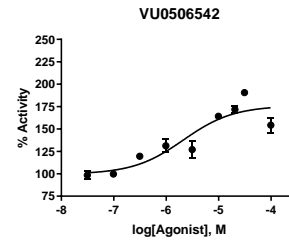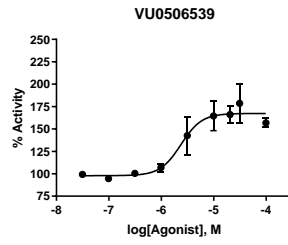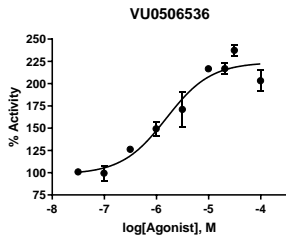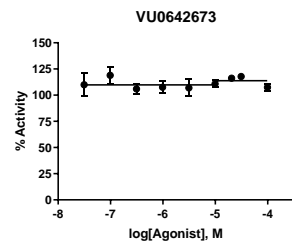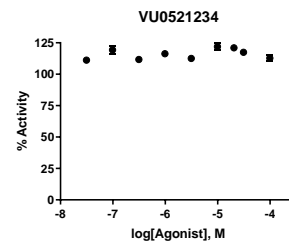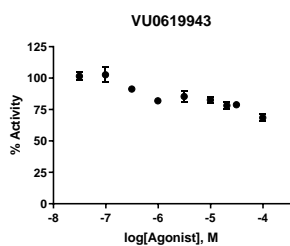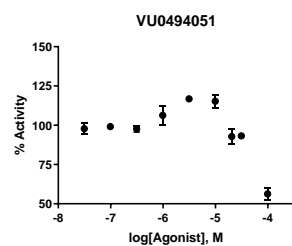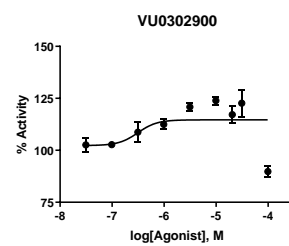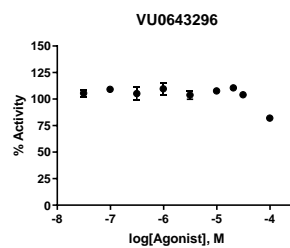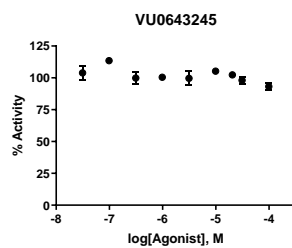
**Figure A3.** Results of follow-up Nape-pld CRCs. Individual points are mean ± SD from 3 replicate wells. Inhibitor curve was calculated using log(inhibitor) vs. normalized response, variable slope in GraphPad Prism 9. Activator curves were calculated using log(agonist) vs. response, variable slope (four parameters) in GraphPad Prism 9. Graphs with no curves did not show sufficient dose-dependent activity changes to generate a well-fitting curve.
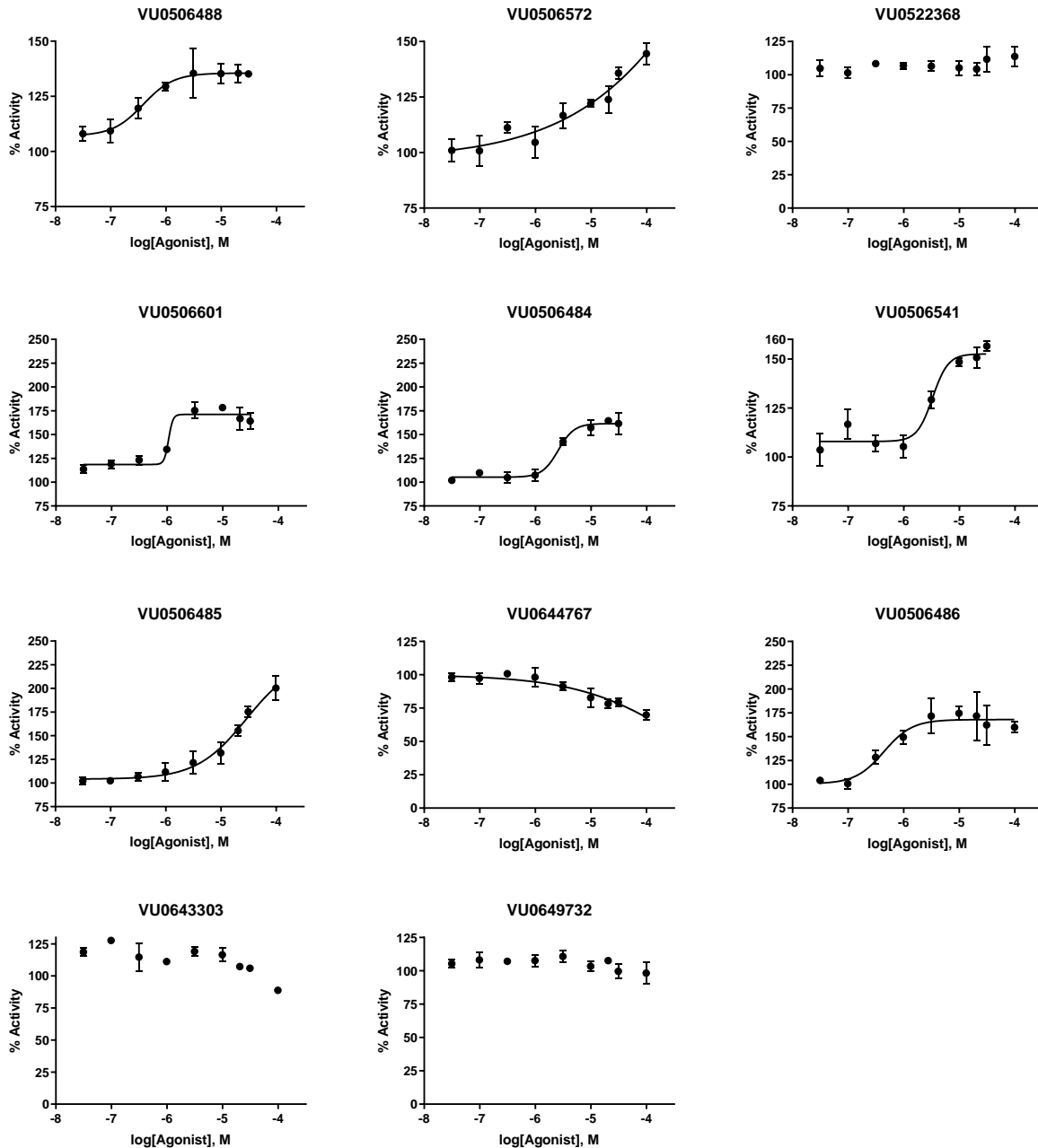
**Figure A4.** Results of BT-PSP Nape-pld CRCs. The activity of purified recombinant Nape-pld in the presence of graded concentrations of each entry in the series of BT-PSP compounds in Table 6 was measured using PED-A1 and normalized as % activity, with 100% activity being the average activity without compound (vehicle-only). Each compound was tested in triplicate on two or more separate days. Each replicate was normalized to the average of adjacent vehicle-only wells, and the three replicates from each day were averaged together. Then these normalized means ($\pm$ SD) for each experimental day were plotted together on a single graph and the nonlinear curve fit with variable slope (four parameters) generated to determine the $EC_{50}$ and $E_{max}$.

VU0506484  VU0506485  VU0506486  VU0506488

VU0506539  VU0506542  VU0506517  VU0506534

VU0506533  VU0506536  VU0506575  VU0506601

VU0506605  VU0934231  VU0934205  VU0934212

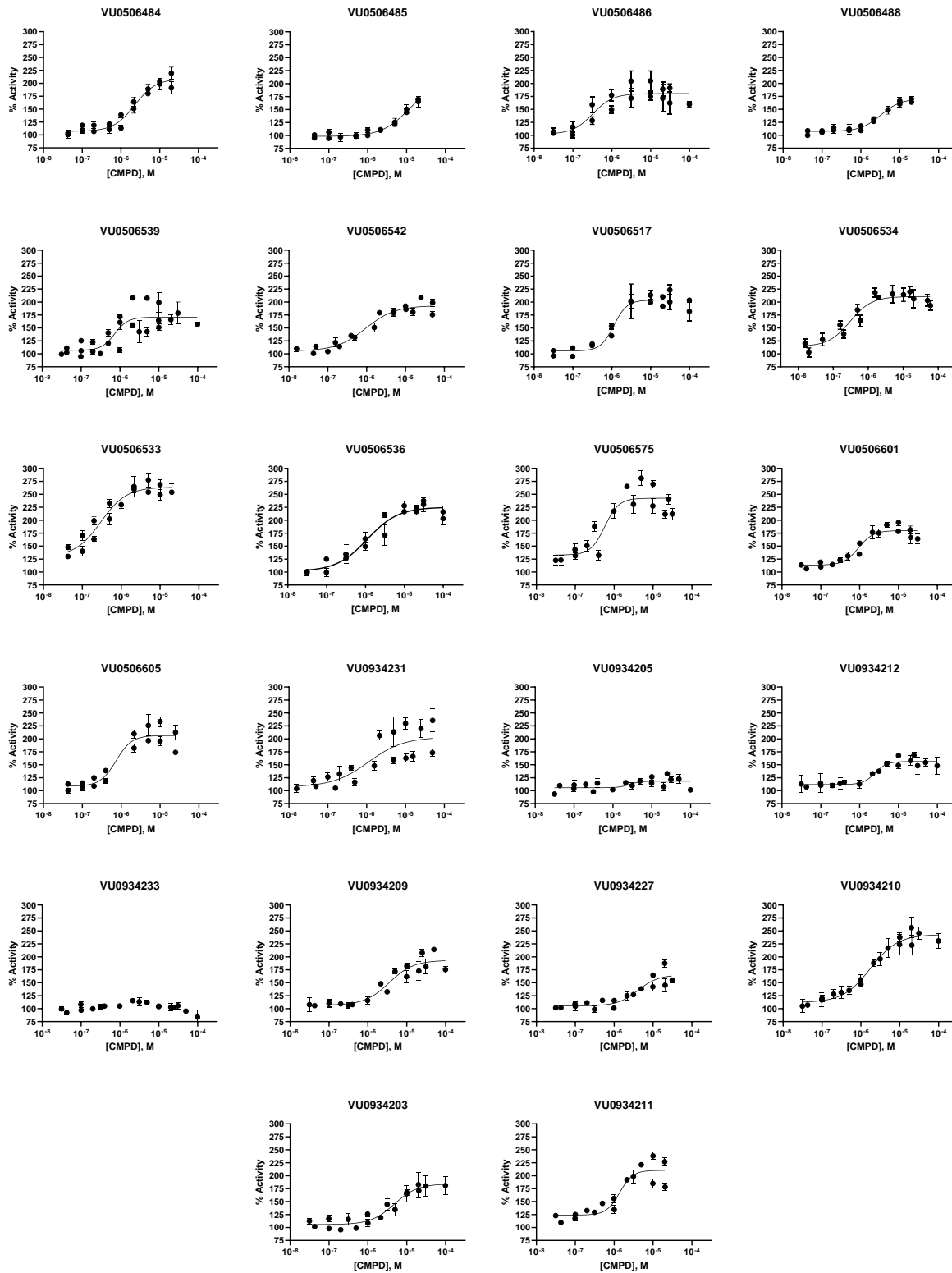VU0934233  VU0934209  VU0934227  VU0934210

VU0934203  VU0934211

**Figure A5.** Effects of deoxycholic acid (DCA) on Nape-pld activity and modulation. Because DCA altered the shape of the fluorescence kinetics curves, new metrics of Nape-pld activity are shown. **A.** Nape-pld activity represented as highest slope achieved during the full 50 min read time (high value means rapid hydrolysis). Technical replicates, mean, and 95% CI are shown. Two-way ANOVA interaction factor $p$=0.0003, row and column factors $p$<0.0001. Results of Dunnett's multiple comparisons test shown. **$p$=0.0067, ****$p$<0.0001. **B.** Nape-pld activity during the same experiment represented as the amount of time it took for each experimental reaction to reach peak fluorescence (low value means rapid hydrolysis). Technical replicates, mean, and 95% CI are shown. Two-way ANOVA interaction factor $p$=0.0009, row and column factors $p$<0.0001. Results of Dunnett's multiple comparisons test shown. *$p$<0.03, **$p$=0.002, ****$p$<0.0001.
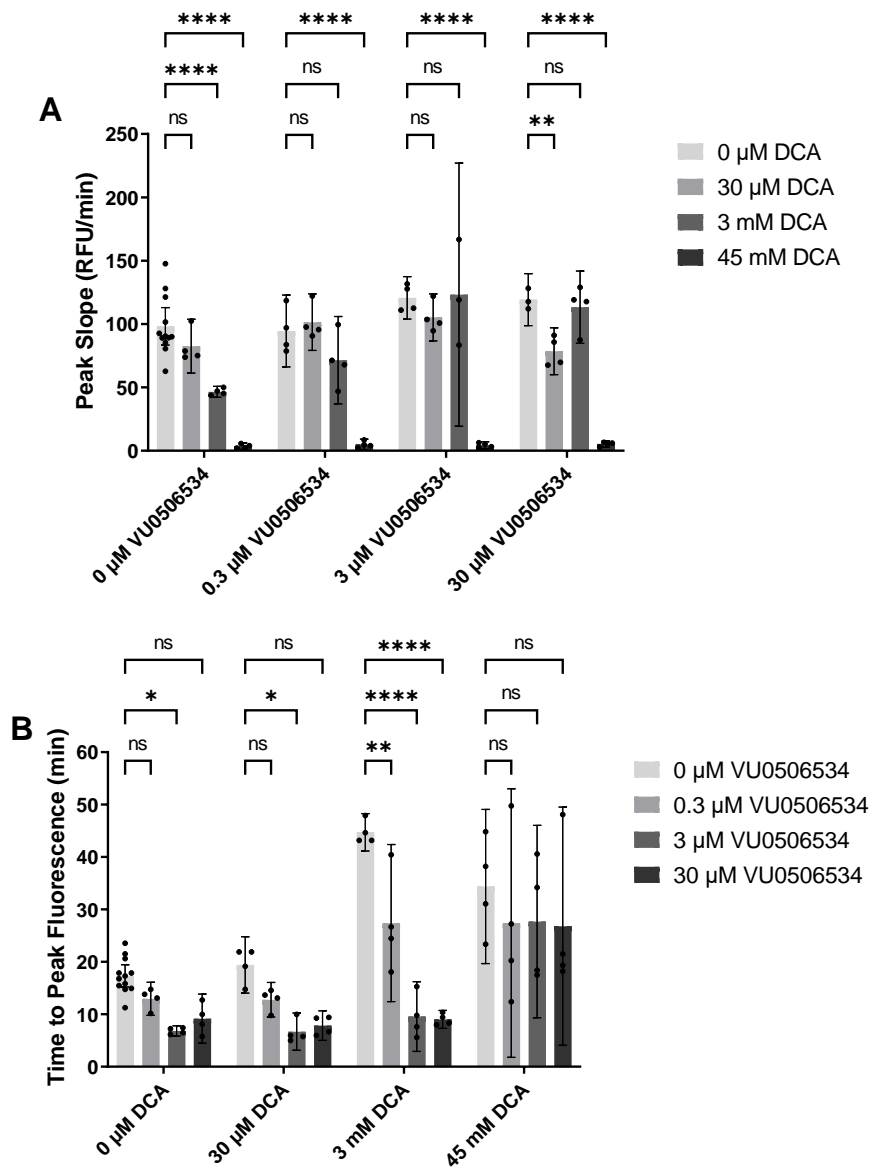
**Figure A6.** Protein binding not elucidated in Native gel. VU0506534 ("VU534") and VU0506533 ("VU533") binding in non-denaturing (Native) PAGE, Coomassie stain blot. Labels above gel indicate treatment. Labelled bands are the ladder, with molecular weights (kDa) indicated.
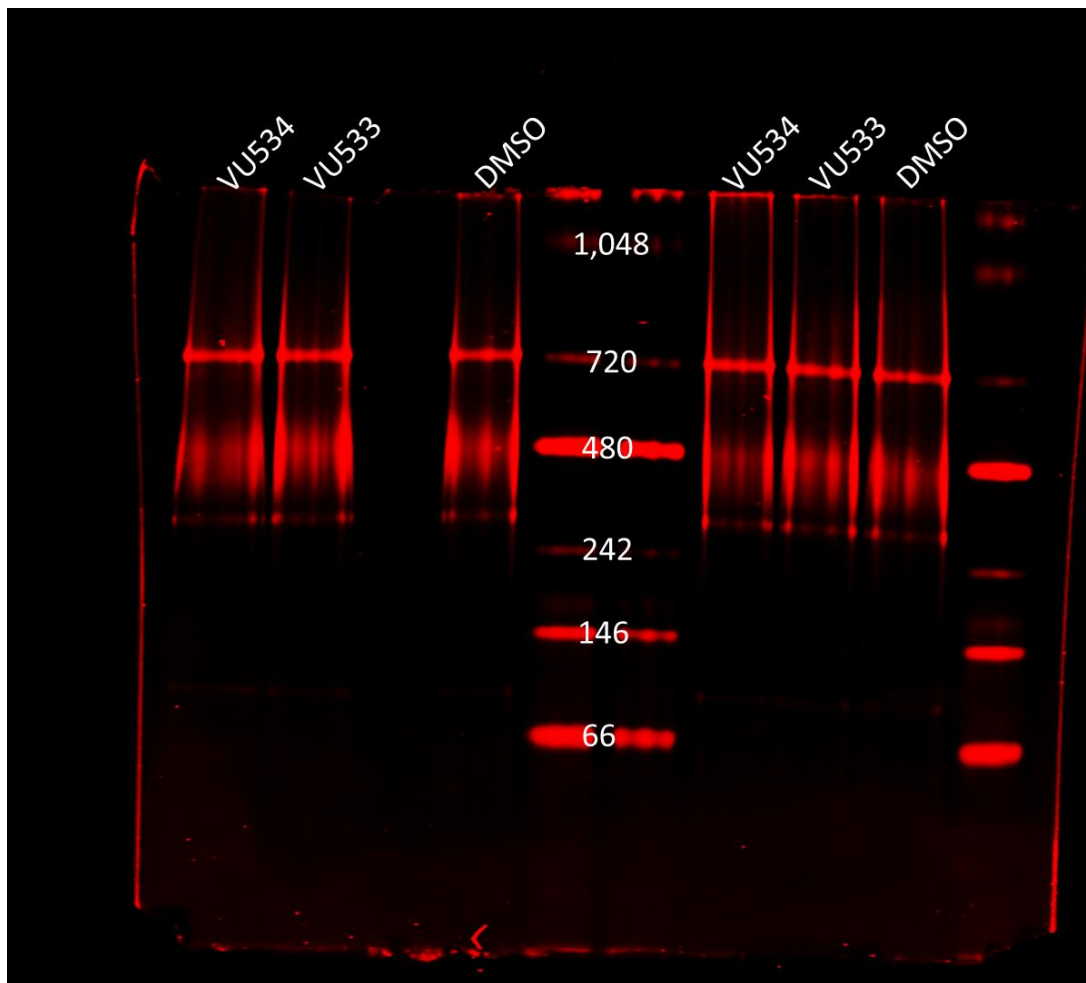
**Table AT1.** Summary of potential binding interactions between VU0506534 and NAPE-PLD at predicted binding site. Binding site is at the interface of the NAPE-PLD homodimer, meaning that there are two mirrored binding sites in one homodimer. To help delineate the interactions, only one binding site is summarized here, and one monomer is labelled as A and the other as B. Top section contains interactions identified in the final pose of the MD simulation, bottom section contains interactions identified in the initial pose of the MD simulation. "fnl" = functional.

| Monomer | Residue Number | Residue | Atom Involved | Distance | Atom on VU0506534 Involved |
|---|---|---|---|---|---|
| B | 106 | Serine | fnl group O | 1.9 | Benzothiazole NH |
| A | 100 | Arginine | fnl group NH2 | 2.2 | Bridge amide O |
| A | 99 | Arginine | fnl group NH2 | 4.1 | Benzothiazole S |
| A | 99 | Arginine | fnl group NH2 | 4.1 | Bridge amide O |
| A | 99 | Arginine | fnl group NH2 | 4.3 | Bridge amide N |
| A | 30 | Lysine | fnl group carbons | 3 | Benzothiazole 6-membered ring |
| B | 101 | Serine | fnl group OH | 5.2 | Fluorine |
|  |  |  |  |  |  |
| B | 106 | Serine | fnl group OH | 2 | Bridge amide O |
| B | 106 | Serine | backbone NH | 2 | Bridge amide O |
| A | 85 | Serine | fnl group OH | 2.1 | Sulfa O |
| A | 85 | Serine | backbone NH | 4.6 | Fluorine |
| B | 84 | Serine | fnl group OH | 4 | Pi system on phenyl |

**Figure A7.** Δ47 NAPE-PLD lacks catalytic activity. Shown is PED-A1 hydrolysis (measured by fluorescence, ex/em 488/530 nm) measured every minute for 50 min. Full-length human NAPE-PLD shown as blue circles, Δ47 human NAPE-PLD as red squares. Points are mean ± SD for six technical replicates. Both types of NAPE-PLD were administered at 0.1 µM.

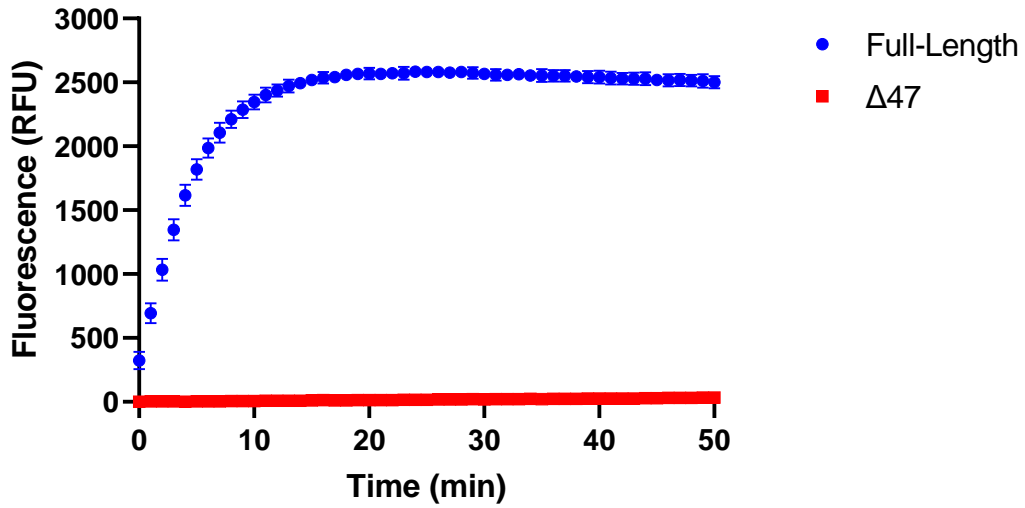**Figure A8.** Cytotoxicity of Bith for HepG2 cells. HepG2 cells were cultured for 24 h in the presence of various concentrations of Bith and cell viability measured using MTT. All values were normalized to vehicle-only controls. Mean ± 95% CI shown. Ordinary one-way ANOVA $p<0.0001$, Tukey's multiple comparisons test, ****$p<0.0001$ compared to 0 μM concentration.
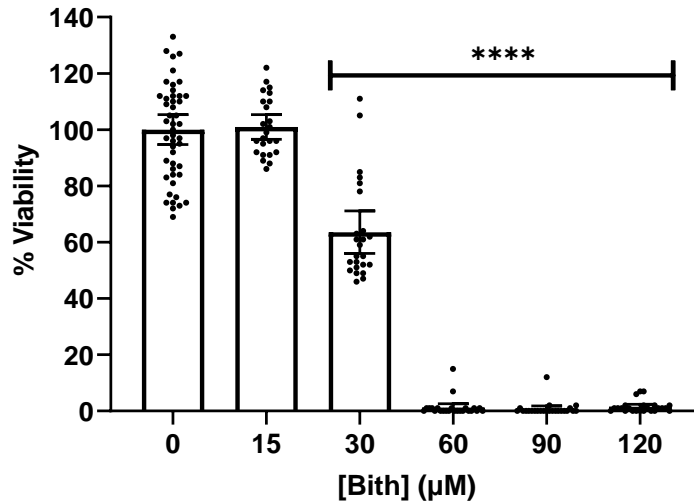


**Figure A9.** Variable siRNA transfection efficiency. Transfection efficiency of fluorescently labelled control siRNA during four different NAPE-PLD siRNA experiments, as measured by fluorescence (ex/em 540/570 nm) and normalized to the average for that experiment. Each set of symbols represents the technical replicates from one experiment.
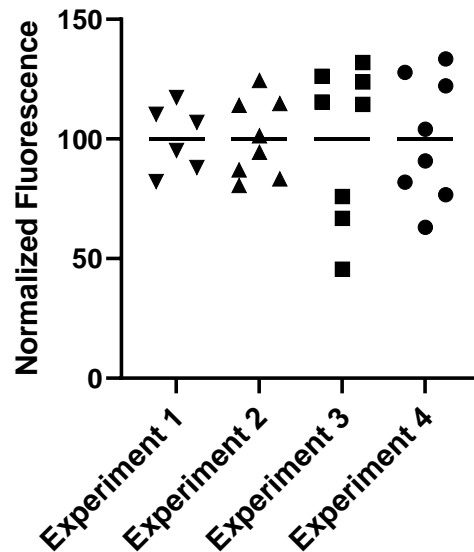
**Figure A10.** Pilot BT-PSP Nape-pld modulation test in RAW 264.7 cells. Effects of compounds (10 µM) on Nape-pld activity, as measured by PED-A1 hydrolysis, normalized to vehicle (DMSO) controls. Bith included as control with known efficacy in this assay. Mean ± 95% CI and individual results shown, assay performed once. Ordinary one-way ANOVA $p<0.0001$. Dunnett's multiple comparisons test results: **$p=0.0033$, ***$p=0.0002$, ****$p<0.0001$ vs. DMSO controls.
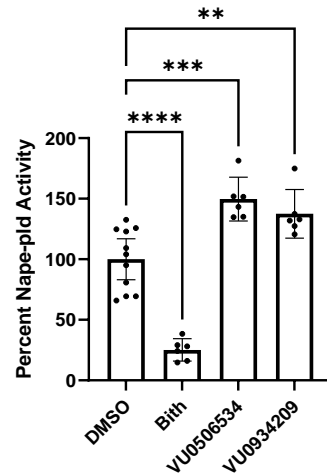


**Figure A11.** Pilot BT-PSP NAPE-PLD modulation test in HepG2 cells. Effects of compounds (10 µM) on NAPE-PLD activity, as measured by PED-A1 hydrolysis, normalized to vehicle (DMSO) controls. Mean ± 95% CI and individual results shown, assay performed once. Ordinary one-way ANOVA $p<0.0001$. Dunnett's multiple comparisons test results: *$p=0.0435$, ****$p<0.0001$, all other comparisons did not significantly differ from DMSO controls.
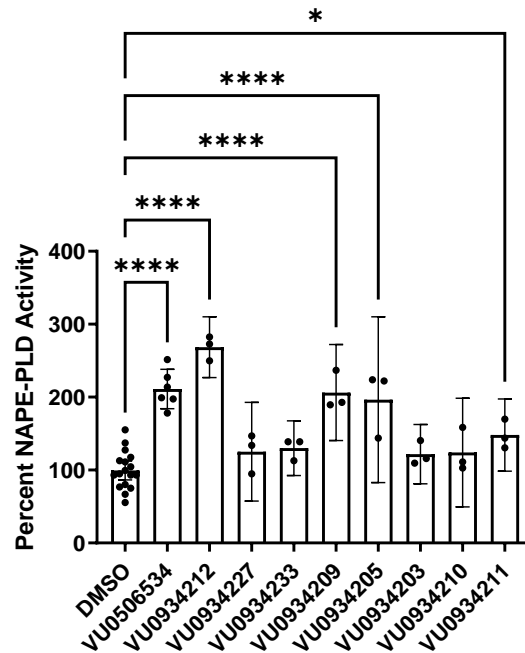
**Figure A12.** Caco-2 NAPE-PLD activity assays. **A.** Effects of plate location on NAPE-PLD activity, measured by flame-NAPE hydrolysis. Columns received identical treatments. Single run. Individual values, mean, and 95% CI shown. Unpaired t-test, ***$p$=0.0002. **B.** Effects of NAPE-PLD modulator treatments on Caco-2s, NAPE-PLD activity measured by flame-NAPE hydrolysis. Single run. Individual values and mean shown, SD shown to highlight variability. **C.** Effects of 1 min Bith incubation on NAPE-PLD activity, measured by flame-NAPE hydrolysis. Single run. Individual values, mean and 95% CI shown. Unpaired t-test, $p$=0.7793.